Molecular Dynamics of Mechanosensing and Mechanotransduction at the Focal Adhesions

By

Javad Golji

A dissertation submitted in partial satisfaction of the

requirements for the degree of

Joint Doctor of Philosophy

with University of California San Francisco

in

Bioengineering

in the

Graduate Division

of the

University of California, Berkeley

Committee in charge:

Professor Mohammad R. K. Mofrad, Chair

Professor Valerie Weaver

Professor Ahmet Yildiz

Fall 2011

Abstract

Molecular Dynamics of Mechanosensing and Mechanotransduction at the Focal Adhesions

by

Javad Golji

Joint Doctor of Philosophy with University of California, San Francisco
in Bioengineering

University of California, Berkeley

Professor Mohammad R. K. Mofrad, Chair

Focal adhesions are critical to cellular processes such as cell migration and cell-substrate adhesion. Focal adhesion formation can be mechanically regulated: forces either from outside the cell or from contracting actin filaments can induce rapid growth and maturation of the focal adhesions. One hypothesis explored here contends that force-induced focal adhesion formation results from mechanosensing by individual protein components. Molecular dynamics computational simulations are developed to evaluate mechanosensing by talin and vinculin. In Part 1 of this dissertation, two force-induced conformational changes are suggested for talin's activation: (i) the cryptic vinculin-binding sites (VBS) can be activated by stretch of an individual talin rod domain, and (ii) talin can adopt multiple dimer orientations in response to forces applied from outside the cell. The mechanisms of vinculin activation are then explored in Part 2. The trajectory of a vinculin conformational changes that would render it activated is predicted along with the structure of an activated vinculin. Domain 1 (D1) is predicted to separate from the vinculin tail (Vt) during activation. In this context, the PIP2 from the cell membrane is shown to preferentially bind basic residues on the vinculin surface and recruit vinculin to membrane proximal regions, potentially allowing for vinculin phosphorylation. The impact of phosphorylation on the vinculin structure is simulated and it is suggested that phosphorylation could prime vinculin for activation by reducing the strength of inter-domain interactions stabilizing the auto-inhibited vinculin conformation. In Part 3 of this dissertation, the interaction of activated vinculin with its binding partners is simulated. It is demonstrated that a talin VBS can only link vinculin prior to activation but can completely bind vinculin following activation. Vinculin activation by movement at D1 is shown to be necessary and sufficient for linking vinculin to actin filaments. Furthermore, simulation of F-actin capping by vinculin suggests that a second vinculin conformational change, releasing Vt from all vinculin head domains, facilitates effective capping of the actin filament. Three vinculin-binding sites on F-actin are predicted. These simulations demonstrate that indeed both talin and vinculin can exhibit molecular mechanosensing.

To My Mother and Father

Table of Contents

Acknowledgements

Support, fruitful discussion, critical evaluation, and helpful contribution from the following are gratefully acknowledged:

Mohammad Mofrad
Johnny Lam
Robert Collins
Tim Wendorff
Anwaar Al-Zireeni
Yusof Jamali
Alejandro Schuler
Amer Abdullah
Kevin Sohail Kolahi
Hengameh Shams
Mehrdad Mehrbod
Mohammad Azimi
Ruhollah Moussavi Baygi
Amir Golji
Kristina Maryam Golji

Introduction

Introduction: Cellular Mechanotransduction

Mechanotransduction involves the translation of mechanical information into cellular processes. A major site of mechanotransduction within the cell is the focal adhesion. The focal adhesion is a dynamic structure whose initial formation and subsequent maturation is highly regulated by the forces within its environment. Both forces originating from within the cell and forces imposed on the cell from its surroundings can impact the development of the focal adhesion. Upon force-induced growth and maturation the focal adhesion alters biochemical pathways leading to changes in the cells gene expression. The focal adhesion also directly alters the physical landscape of the cell. The physical changes that correlate with focal adhesion maturation include rearrangement of the actin cytoskeleton, the formation of large molecular clusters at the focal adhesions themselves, and rearrangement of the interface between the cell and its surrounding: the cell membrane bound integrin molecules. These physical changes alter the cells mechanical properties, increasing the strength of the linkage between the cell and its surrounding, and increasing the tension the cell can exert on its surroundings via traction forces. These changes in the mechanical properties of the cell are a significant component of the cells mechanotransduction response. One suggested underlying mechanism to the focal adhesion's mechanotransduction is the concerted actions of individual molecules acting as molecular mechanosensors, or as molecular reinforcing agents. Molecules such as integrin, talin, and vinculin are suggested to lie at the heart of the focal adhesion.

The cell can respond to a variety of inputs from its surroundings (65). Both biochemical cues and mechanical cues are interpreted readily by the cell and can impact the cell behavior (169). The cellular response to biochemical cues from the environment has been studied extensively and is reviewed elsewhere (see (51)). The cellular response to mechanical cues is of particular interest as it is intricately involved in a number of cellular processes including cell migration, stem cell development and specialization, wound healing, and cancer cell metastasis (27) (121) (65) (198) (95). The cell also responds to mechanical cues generated by the cell itself, for example during cell migration (111). The interpretation of mechanical cues and the subsequent translation of these cues into altered cellular behavior are known as mechanotransduction (97).

The cell forms structures known as focal adhesions at its interface with the extracellular matrix (ECM) (17). It is these focal adhesions that are implicated as the mechanotransduction site of the cell (107). The focal adhesions can be characterized as a physical hub of molecules that act as a molecular glue binding to each other, to ECM bound integrins, and to the cytoskeleton (65) (Fig. 1). The focal adhesions can also be characterized as biochemical hub with a number of kinases and phosphorylation substrates that together can alter gene expression and such cellular functions as myosin II contraction (143). The biochemical factors seen at focal adhesions include focal adhesion kinase (FAK) (130), cyclin-dependent protein kinase 5 (Cdk5) (86), and Rho family kinases (149). The activity of these and other

biochemical factors active in the mechanotransduction machinery of the focal adhesion are interested and reviewed elsewhere (see (143)(91)). The focus of this article is the function of the focal adhesion as a physical hub linking the ECM to the cytoskeleton.

The focal adhesion is linked to a number of cellular processes. Most prominently, it is linked to cell migration (160) and cancer cell metastasis (121). In both processes, the focal adhesion is the site at which the cell mechanically interacts with its ECM, exerting forces on its surroundings and interpreting the mechanical cues from the ECM. The focal adhesion is also a dynamic structure, maturing from smaller more transient structures known as nascent adhesions (63) (203). The maturation, the dynamics, and the structure of the focal adhesion are all features that can be regulated by external forces, and cell generated forces.

At the heart of focal adhesions lie molecules (221). The focal adhesion forming molecules can be as complex in their response to mechanical cues as the focal adhesion itself. The behavior of the focal adhesion can be described as the combined behavior of the individual focal adhesion forming molecules. It is hypothesized that for the focal adhesion to exhibit its mechanotransduction, there should exists molecules that act as the molecular mechanosensors of the focal adhesions (197). These molecules, such as integrin (67) and talin (84), would alter their structure and function in response to the mechanical cues they are exposed to. Other molecules, such as vinculin (229), could act as molecular reinforcing agents, increasing the strength of the link between the ECM and the cytoskeleton in response to strong mechanical stimulation.

Focal adhesions and mechanotransduction

A well-studied and interesting feature of the cell is its ability to adhere to its surroundings. Cells immersed in 3D ECM form links to the many ECM fibers in their immediate vicinity (52). Similarly, cells grown on a 2D substrate form stable linkages and adhesions to the ECM on the substrate (65). These adhesion linkages play a critical role in a number of cellular processes, including cell migration and wound healing (72). The primary structure associated with the link between the ECM and the cell is the focal adhesion (221). The primary function of the focal adhesion is to mechanically link ECM bound integrins (92) on the cell membrane to actin filaments (154) that make up the cells cytoskeleton.

The smallest actin integrin link is the nascent adhesion. Its existence is transient, but it can mature into a focal complex, which can later mature into a focal adhesion. The smallest nascent adhesion would be a connection between integrin, talin, and actin. (183) (176) Although such a small nascent adhesion would be relatively weak, the strength of its adhesion could increase as it matures. The focal complex is often characterized by the presence of zyxin (219). The mature focal adhesion is often characterized by the presence of α-actinin (38), and forms connections to the cell's stress fibers (4). Nascent adhesions are small, usually ~100nm in diameter,

although nascent adhesions as small as 30nm have been reported (174) (175). They exhibit a turnover of 60 seconds and are thus considered short-lived. Focal complexes are larger, ~1um in diameter, with a turnover reported as several minutes. And mature focal adhesions are ~2um wide and ~3-10um long (230) with a typical half-life of 3 minutes, although some can persist for as long as 10 minutes (32).

A related structure, known as fibrillar adhesions (53), display similar structural features as the focal complexes and focal adhesions, yet they are not present in migrating cells. These structures are seen almost exclusively in fibroblast cells grown on fibronectin. The fibrillar adhesions are characterized by their long life spans and super elongated structure.

Different cell types exhibit different types of adhesion structures. Neutrophils and macrophages exhibit small, dynamic nascent adhesions and focal complexes. Fibroblasts, endothelial cells, and smooth muscle cells have larger more stable focal complexes and focal adhesions. Their larger adhesion structures correlated with these cell types consistently undergoing larger mechanical loads, suggesting a mechanical role for the adhesion structure (see below). Although focal adhesions formation and disassembly has been mainly studied in fibroblasts, the principles governing both processes apply to other cell types including mesenchymal, epithelial, endothelial, and neuronal cells. (204)

A number of molecules have been characterized as being a part of the focal adhesion structure (165). The most prominent of these molecules within focal adhesion are the following: talin, vinculin, alpha-actinin, paxillin, and filamin (24, 43). The size, strength, and number of focal adhesions have been shown to correlate with exposure of the focal adhesion to a mechanical load (104) (59, 64, 196) (17) (34). Often, the source of the mechanical load can be internal, from the contraction of actin filaments by myosin II or from the retrograde flow of actin filaments near the growing focal adhesion (see below); both processes are associated with cell migration.

Cell migration

The migrating cell adopts a unique shape that gives it directionality (144) (144)(Fig. 2). The cell spans itself towards the direction of movement into a broad thin shape characterized by protrusion of the cell membrane. This thin, broad, protruding end of the cell in the direction of movement is termed the leading edge (144). At the other end, the cell contracts into a sharp pointed shape, termed the trailing edge, which is characterized by the presence of very mature and large focal adhesions. Connected to the large focal adhesions at the trailing edge of the cell are thick cytoskeletal actin fibers, termed stress fibers(28). The stress fibers run the length of the cell and together with numerous myosin II (13) molecular motors attached to them function in the migrating cell to contract the cell body and relocate it towards the leading edge (144). At the leading edge the smallest protrusion of the cell

membrane in the general direction of movement are termed the filopodium. The filopodium are absence of adhesion structures and are not sites of cellular traction (210). Directly behind the filopodium is the lamellipodium, characterized by the presence of many branched actin fibers (137). The initial adhesion structures, the nascent adhesions, form in the lamellipodium (144). Most nascent adhesions are transient and undergo rapid turnover, while some mature into focal adhesions. Behind the lamellipodium is the lamellum, characterized by parallel actin fibers and the presence of the more mature focal adhesions (193, 194). These parallel actin fibers are also under contraction by myosin II during cell migration.

In order to achieve its movement, the migrating cell undergoes a cycle of events that produce relocation of the cell mass in the direction of movement. First, at the filopodium and lamellipodium cell protrusion occurs – the cell membrane is pushed outwards in the direction of movement. Second, cellular traction is produced between the cell and the substrate it is migrating on. These traction forces are generated at the ends of the stress-fibers via the focal adhesions (68). Third, the stress fibers contract, via myosin II molecular motor activity, and the cell body is relocated in the direction of cell movement. And finally, the focal adhesion at the trailing edge of the cell are disassembled and the relocation of the cell body is completed (68, 144). The entire cycle repeats as the cell continues its movement. Throughout this cycle, both the mechanical linkage between the ECM and the cell and the biochemical pathways controlling the cell migration processes are coupled to each step of the cycle (198).

In the lamellipodium, actin is organized into a branched structure and is undergoing polymerization. The polymerizing actin fibers grow towards the leading edge and produce the cell protrusion necessary for cell movement. This polymerization of the actin fibers also results in the retrograde flow of the actin fibers away from the front end of the cell. (154) (189) Retrograde flow of actin fibers in the lamellipodium is suggested as one of the causes of mechanical stress that can lead to the maturation of nascent adhesions into focal adhesions (see below). One indicator that the retrograde flow of actin filaments is linked to nascent adhesion maturation into focal adhesions is the dependence of the rate of nascent adhesion growth on the rate of actin polymerization in the lamellipodium. (3)

The nascent adhesions in the lamellipodium can undergo slippage (100, 129). Some of the actin filaments in the lamellipodium are linked to ECM via nascent adhesions. When these actin filaments undergo retrograde flow they pull against the nascent adhesions and potentially can dislodge the nascent adhesions from their link to the ECM. When this occurs the nascent adhesion can either disassemble due to its transient nature, or it can reattach to the ECM soon after being detached. The reattached nascent adhesion has moved towards the cell body during its slippage (100, 129). One hypothesis concerning the role of the nascent adhesion during the slippage event suggests that the nascent adhesion acts as a molecular clutch (100, 129). As a clutch, the nascent adhesions would link the moving actin filaments to the stationary ECM substrate through friction and a slippage bond. Nascent adhesions

functioning in this way would be exposed to mechanical force and could thereby mature into focal adhesions.

The mechanical and physical properties the ECM have an effect on the efficiency with which a cell can migrate. Several studies have demonstrated that the rigidity of the ECM directly affects the speed of cellular migration within that ECM (151, 159). Cells migrating in more rigid ECM can move faster and more efficiently than cells migrating in soft matrices. The cell protrusions caused by the polymerization of actin filaments in the lamellipodium can physically interact with the ECM. In the case of rigid ECM the resistance to protrusion enhances the retrograde flow of actin filaments, a process suggested to cause nascent adhesion maturation (see below). Cell protrusion in soft matrices would encounter less resistance to protrusion, slower retrograde flow of actin filaments, and likely slower maturation of the nascent adhesions. Considering the critical importance of focal adhesions to establishing traction between the stress fibers and the substrate prior to cell body relocation, this reduced maturation of the nascent adhesions can slow cell mobility. A similar phenomenon can be seen in cells migrating after immersion into a 3D substrate matrix. These cells exhibit the same migration patterns as cells migrating on soft ECM substrates (2, 45).

The final step in cellular migration is focal adhesion disassembly at the trailing edge. Focal adhesion disassembly can result from either the depolymerization of actin filaments near the focal adhesion, or the cleavage of key molecular constituents of the focal adhesion. Although the process of focal adhesion disassembly has yet to be truly investigated, some studies suggest that focal adhesion disassembly occurs at the boundary between the lamellum and the lamellipodium due to the depolymerization of branched actin filaments from the lamellipodium (25). Other studies of have shown focal adhesion disassembly via cleavage of the molecules within the focal adheison linkage suggested cleavage contributes to nascent adhesion slippage (11). At these nascent adhesions, the connection between integrin and the focal adhesion forming molecule talin is likely cleaved (49). One well studied protease likely involved in cleavage of focal adhesions is calpain (57). It has been shown that calpain will truncate the interaction between talin and integrin leading to the rapid disassembly of focal adhesions (58).

The cell's internal source of mechanical force

Integral to cell motility are the processes of actin polymerization causing membrane protrusion at the leading edge, and myosin II contraction causing cell body relocation (192). Both processes are also the cell's own internal source of mechanical force that could lead to focal adhesion formation (65). For a mature focal adhesion to form, its predecessor, the transient nascent adhesion, must first mature into a focal complex, which can then mature into the focal adhesion. Both steps of the maturation can be explained as force dependent processes.

Actin filaments exist in both the lamellipodium and the lamellum (see above), but with different arrangements. In the lamellipodium they form a branched, non-uniform arrangement, while in the lamellum they form a parallel uniform arrangement (155). This contrast extends to the mechanical load on the two variants of the actin cytoskeleton. Both the distributed actin filaments in the lamellipodium and the parallel actin filaments in the lamellum are under load from myosin II contractile forces but with different magnitudes; The parallel actin fibers are under much higher load (106, 112, 150). However, the actin filaments in the lamellipodium are moving towards the center of the cell – retrograde flow – with much higher velocity than the movement of the parallel actin fibers of the lamellum, even with less myosin II load (41, 189, 190)(Fig. 3). The source of the added velocity of these actin filaments is the actin filaments themselves: lamellipodum actin filaments are under constant polymerization near the leading edge (23). The polymerization serves to push the cell membrane and develop the needed cell protrusions, but because the cell protrusions do not develop as fast as actin polymerizes, the actin filaments are pushed away from the leading edge by the polymerization (3). The resulting retrograde flow of actin filaments can brush against the developing nascent adhesions in the lamellipodium, driving their maturation to focal complexes (3). The subsequent development of the focal complex into a mature focal adhesion likely occurs at the transition form the lamellipodium to the lamellum (65), where the developing focal complex is exposed more directly to the pull of myosin II on the parallel actin fibers (38).

It seems then, that the smaller mechanical perturbations cause by the brushing of moving actin filaments against nascent adhesions can provide the necessary force to drive their maturation. To test this, Alexandrova et al. (3) prevented the movement of actin filaments within the lamellipodium. The results from their work support the proposition that actin filament movement is the source of mechanical force to the nascent focal adhesions: the transient structures failed to mature into focal complexes in the absence of actin filament flow.

The maturation of focal complexes into focal adhesion results from the contraction of the parallel actin fibers by myosin II (38). To confirm this notion, Choi et al. (38) eliminated expression of myosin IIA. Cells grown without the myosin IIA failed to show formation of mature focal adhesions. They were able to rescue some focal adhesion formation with a myosin IIA mutant lacking molecular motor capacity. To achieve complete focal adhesion formation however, the cell requires contraction of the cytoskeleton by myosin II.

An interesting effect resulting from the formation of mature focal adhesion only in the lamellum, where the focal adhesions bind to parallel actin filaments under load, is the movement of a noticeable boundary between the lamellum and the lamellipodium. The focal complexes mature into focal adhesions at this junction. A nascent adhesion that matures into a focal adhesion moves the boundary to include itself (3). The boundary is characterized by the arrangement of actin filaments not focal adhesions. The newly maturing focal adhesion correlates with rearrangement

of the actin filaments, so that they too are more 'matured', that is, organized into parallel arrangements and likely exposed to greater load from myosin II. In this way the maturation of the focal adhesion correlates with the formation of parallel actin filaments in the regions near to it.

Force induced focal adhesion formation

Aside form the forces generated by the cell itself, the focal adhesion in the adherent cell can be exposed to several other mechanical stimulations. For example, the movement of fluid across the cell membrane could directly apply a shear stress to the focal adhesions (186). More likely, the ECM can mechanically stimulate the cell (64) (17) (34). In this case, the source of the force would be whatever mechanical load is applied to the tissue in which this cell resides.

One way to simulate the external load on a cell in vitro would be the use of optical tweezers to apply a force directly to the cell surface (Fig. 4). In fact, Galbraith et al. (59) have achieved this feat in their foundational work in cellular mechanotransduction. Using optical tweezers to constrain and thereafter move micro sized beads nearby focal complexes, they were able to exert a local force on the focal complex. The beads were coated with ECM proteins that can readily bind integrin (19). Once bound to integrin, the optical tweezers were used to exert a force on the focal complex via integrin. As a result of the externally applied force, the focal complexes matured into focal adhesions. These newly formed focal adhesions appear at the same site of the application of external force, suggesting that the external force is indeed causing the formation of the focal adhesions. Combined with other evidence showing that existing focal adhesions grow and mature when exposed to external force (162), this points to the understanding that focal adhesions are regulated by force.

This assertion is consistent with the location of focal adhesions in adherent cells. Focal adhesion can form at the interface between the cell membrane and rigid surfaces, but not at sites of interaction between the membrane and soluble ligands; traction forces result from the adhesion of the cell to rigid surfaces, and the traction is necessary for focal adhesion formation. The presence of tension from rigid ECM results in reinforcement of the cellular adhesion by the growth and maturation of focal adhesions (39) (162). The importance of ECM rigidity is further highlighted by studies focused on the mechanotransduction of cancerous cells (see below).

External forces can interact with the cellular machinery either directly or indirectly. External shear stress induced from the movement of fluid across the surface of a cell interacts directly with the mechanotransduction molecular machinery (186), whereas stress impacting connective or bone tissue interacts with the cell indirectly via the ECM.

Not only can the focal adhesions be mechanically perturbed by their surrounding environment, but they too can mechanically perturb the ECM. In fact, it follows from

the contraction of the cells' cytoskeleton during cell motility (see above) that the cells should be exerting a force on their surroundings during migration. Indeed, Balaban et al. (10) have shown the existence of forces exerted on the ECM by adherent cells. They used a micro-patterned elastomer substrate to measure the traction forces exerted on the surface by living cells. In addition, using GFP-labeled vinculin, they fluorescently traced the formation of focal adhesions and were able to correlate the exerted traction forces with formation of focal adhesions. The traction force measured was linearly dependent on the intensity of fluorescence from the focal adhesions. Disruption of focal adhesions correlated with the reduction in traction forces. Furthermore, the focal adhesions would form within seconds of the application of traction forces by actin-myosin contraction. The cell is able to exert ~10pN of traction force on its substrate at each site of focal adhesion formation.

The ECM is comprised mainly of collagen, fibronectin, laminin, glycosaminoglycans, and tenascin. The distribution of each type of ECM protein characteristically differs between various tissue types and helps to determine the mechanical properties of that tissue. The specific ECM of each tissue determines not only the elastic properties of the tissue, but also the type of mechanical load the tissue would best withstand, e.g. tension, compression, or shear. (148, 157, 201)

Cell mechanics

The mechanical properties of an individual cell impact the extent to which that cell can exhibit mechanotransduction. Cells characterized by less stiffness and rigidity are likely to undergo more strain when exposed to an external force. This larger strain can in turn result in direct impact of the external force on a larger number of molecules. (98) Measurements of individual cells show a cell's stiffness can range from 0.1 kPa to 40kPa. (119) This range is similar to range of stiffness for soft tissue.

Actin filaments and not microtubules mainly determine the elasticity of the cell. (180) (123) The network of actin filaments is arranged to allow diffusion of macromolecules and micelles through the network. Crosslinkers such as filamin and alpha-actinin hold the actin network together (110). Although numerous in vitro actin networks have been created and characterized (177) (139), the precise rheological properties of the intracellular actin networks remain under study (123). One clear rheological feature of the cytoskeleton is that the cell changes its stiffness drastically when exposed to an external force. (54) Cell stiffness is also heterogeneous, increases in spatially distinct regions near externally applied force. (98)

Focal adhesions and the cancerous cell

The mechanical properties of the cell's environment have a significant impact on the cell's ability to adhere to the ECM or to migrate. This becomes especially important in the discussion of cancerous cells. In order for a cancerous cell to metastasize it must be able to migrate effectively (202). To achieve effective migration, the

cancerous cells will reorganize their surrounding tissue to increase its rigidity. By producing a rigid environment, the cancerous cell will more easily be able to migrate and metastasize (121).

The rigidity of the ECM environment also has an impact on developing cells. The developing cell differentiates and undergoes specialization in response to both chemical cues from its environment and mechanical cues from its environment (134). Environmental mechanical properties such as ECM rigidity affect the specialization of the developing cell (108). The most rigid of the tissues is bone with an elastic modulus of 15,000 – 30,000 nN/μm^2, then arteries and connective tissue with an elastic modulus of 100 - 1,000 nN/μm^2, then muscle with an elastic modulus of 10 - 100 nN/μm^2, and the softest tissue is brain tissue with an elastic modulus of 0.1 – 10 nN/μm^2 (134). The developing stem cell will differentiate into an osteoblast, an endothelial cell, an epithelial cell, a myoblast, or a neuron depending on the rigidity of the tissue it develops in (134). The importance of ECM rigidity is further highlighted by pathological conditions that correlate with disruption of ECM mechanical properties, including atherosclerosis, osteoporosis, or fibrosis. (94)

The metastasizing cancer cell utilizes a unique cellular feature to facilitate its movement through tissue: the invadopodia (216). These filopodia like extensions secrete proteases into the ECM to degrade the existing ECM architecture and rebuild the ECM to be more rigid and conducive to cell movement (113). The newly formed ECM is organized such that it contains tracks that the metastasizing cell can use to swiftly migrate through the tissue (207). The importance of these tracts is highlighted removing the protease activity of the invadopodia; cancerous cells whose ECM protease activity has been blocked fail to metastasize (208).

Structure of Focal adhesions

Each focal adhesion is large in size, reported to be several μm in diameter (223), and composed of more than 160 different molecules (221). Together these molecules bind several integrins and multiple actin filaments. Initially, it would appear that this mass of molecules would form a single, large, continuous macrostructure – at least that is what is seen from microscopy images of the several μm structure. Recently, Patla et al. (147) were able to reveal the architecture and layout of this large complex structure at much higher resolution (Fig. 5). To achieve this, they used a clever combination of fluorescence microscopy and cryo-electron tomography. (128) Surprisingly, they found that when viewed at a sub-micron resolution, the focal adhesion is not a single large continuous μm sized macrostructure, but rather a dense conglomerate of many small nm sized structures. These nano-structures, termed focal-adhesion associated particles, are doughnut shaped with a typical diameter of 20-30nm. They exist within the focal adhesions at a high density of ~170 doughnut shaped particles per μm^2, and outside the focal adhesions (and nearby) at a density of ~8 doughnut shaped particles per μm^2. The typical distance between each doughnut shaped particle is

about 43nm.

Three immediate concerns arise from considering this novel suggestion that focal adhesions are a network of small 20-30nm sized particles rather than a single μm sized continuous macrostructure. First, what molecules comprise these doughnut shaped nanostructures, and how can all 160 different focal adhesion-forming molecules be accounted for within this suggested architecture? Second, these particles were mainly seen in tomographic slices taken 30-70nm above the cell membrane interacting with ECM but not in the regions directly about the ECM (due to imaging limitations, the architecture of this region was not well imaged); are these particles also present in the regions near to integrins or does this architecture only represent the focal adhesion forming molecules in the juxtamembrane regions (see below)? And third, is the formation of the doughnut shaped particles force-dependent in the same way focal adhesion formation is force-dependent? Patla et al. (147) addressed some of these concerns, but together the concerns call for future investigation. To address the first concern, Patla at al. demonstrated a high association of vinculin with the doughnut shaped particles. However, no other biochemical characterization of the doughnut shaped rings has been presented. One possibility we suggest is that perhaps the doughnut shaped rings are actually α-actinin molecules, which are also ~30nm in length (120), exhibit bending flexibility (75), are highly associated with vinculin (20), and crosslink two parallel actin filaments near focal adhesions (140).

To address the second concern supplemental slices of a region near the membrane are presented showing the presence of the doughnut shaped ring near the membrane, but the distribution and density of these particles in the regions nearby the cell membrane require further study.

Finally, to address the third concern, Patla et al. (147) demonstrate a significant reduction in the size of the particles after inhibition of myosin II contraction of actin filaments. Although not feasible given the lack of temporal resolution in cryoelectron tomography, an investigation of the dynamics of the doughnut shaped particles, especially in the presence of mechanical force, would be very convincing. The suggestion of a particulate nano-architecture for focal adhesions is novel and will likely impact investigations of focal adhesion structure for years to come.

The focal adhesion is made up of well over 180 proteins (220), each of which can potentially interact with a multitude of binding partners (Fig. 6). Nevertheless, there exist credible suggestions of a focal adhesion nano-architecture in which the focal adhesions are in fact a high-density collection of many particles. (147) How can so many proteins possible arrange themselves into such small particles? One possibility, presented by Zaidel-Bar and Geiger (220), is that not every focal adhesion-associating molecule is present at every focal adhesion, or, by extension, in every nano-particle. Each of the focal adhesion forming molecules can be modified, either by phosphorylation (87, 141, 164, 200, 222), by interaction with a

phospholipid (171, 191), or by interaction with an external force (47, 116, 131). The modification can alter the binding affinity of the molecule, either increasing its incorporation into focal adhesions or focal adhesion particles, or reducing its affinity for the other focal adhesion forming molecules. Furthermore, many of the focal adhesion forming molecules compete for similar binding sites (221). The incorporation of one competing molecule into a focal adhesion nano-particle renders the other competing molecule excluded. The combined effect of modification by phosphorylation, modification by binding to phospholipids, modification by an external force, and competition with other focal adhesion forming molecules is a mechanism for regulating the biochemical identity of each focal adhesion nano-particle, or from a macroscopic perspective, of each focal adhesion. The idea of differential incorporation into focal adhesions accounts for the large number of molecules known to associate with focal adhesions. More importantly, it defines a mechanism with which a diversity of focal adhesion nano-particles can be assembled, even within a single focal adhesion. The future research efforts should aim to characterize each of the distinct nano-particles seen at focal adhesions (147), and define distinct modification or competition pathways towards the assembly of that nano-particle.

Are focal adhesions formed in 3D matrices?

Focal adhesions are readily recognized in cells grown on 2D surfaces. They are also seen in cells grown in 3D matrices, but with much smaller size and frequency. (45, 46, 124, 125) Similarly, cells studied in vivo show few or no focal adhesion structures when living in 3D matrices. (152) Of course it is possible that focal adhesion like structures are forming in 3D matrices and are not recognizable with modern microscopy techniques. If so, these focal adhesion like structures would be much smaller, less than 0.3 μm in diameter, and much more transient, lasting no more than 1s, than focal adhesion found in cells grown on 2D surfaces. (55)

The speed and efficiency of cell migration in 2D is regulated by the size and strength of focal adhesions. In contrast, cell migration in 3D is regulated differently, by pseudopodia activity and by matrix deformation. Interestingly, the same molecules that form focal adhesions when the cell is on a 2D surface, function to regulate the speed of cell migration in 3D. Farley et al. (55) investigated the impact of focal adhesion forming molecules on cell motility in 3D matrices. Using RNA interference (RNAi) they were able to deplete the following molecules from cells completely immersed in a 3D matrix: vinculin, talin, α-actinin, paxillin, zyxin, FAK, p130Cas, and vasodilator-stimulated phosphoprotein (VASP). Depletion of these molecules impacted the speed at which the cells would migrate in both 2D and 3D matrices, but with different mechanisms. Depletion of p130Cas would increase cell motility on 2D surfaces, but would decrease cell motility in a 3D matrix. Zyxin would have no effect on cell motility on 2D surfaces, but would increase cell motility in a 3D matrix. One molecule consistently needed for motility both on a 2D surface and in a 3D matrix was integrin. (55) These results suggest that cell motility is fundamentally different in 3D matrices.

The speed of cell motility on 2D surfaces is regulated by three things: (1) the traction force exerted by actin-myosin contraction, (2) the formation of focal adhesion near the leading edge, and (3) the assembly of actin filaments near the lamellipodium. (111, 161). In 3D matrices, the cell produces what are referred to as pseudopodia (55), which are thinner, narrower, and longer than the lamellipodium formed on 2D surfaces. It is the rate of formation of and the number of these pseudopodia that is regulated by talin, vinculin, α-actinin, paxillin, zyxin, p130Cas, VASP, and FAK. These molecules also regulate the size and persistence of the pseudopodia, but neither seems to impact the speed of migration.

The pseudopodia seem to function as trailblazers for the cell, allowing the larger cell to navigate through the 3D matrix. The cells migrate through a 3d matrix by pulling on the matrix fibers. (55) Each pseudopodium briefly applies pulling forces on the ECM fibers near to it. The movement of the cell becomes a net result form the many brief pulls of multiple pseudopodia. In this way, regulation of the cell migration speed is not dependent on the length or persistence of each pseudopodium as much as the number of pseudopodia.

Dynamics of Focal adhesions

Focal adhesions are dynamic structures. The molecules that make up focal adhesions undergo rapid exchange with their cytoplasmic equivalents. A single focal adhesion is characterized by the presence of a multitude of focal adhesion forming molecules throughout its several minute existence, but each of these individual molecules do not necessarily persist in the focal adhesion throughout its existence. Several studies have demonstrated that that the focal adhesion molecules undergo exchange and are readily replaced by other molecules. (26, 33, 40, 49, 50, 56, 66, 73, 81, 85, 117, 199) One study (209) is of particular interest in that it provides a combination of in vitro measurements and in silico computations to produce a model capturing both the distribution of focal adhesion forming molecules and the distribution of exchange events around the focal complex (Fig. 7). Their model suggests that focal adhesion can be categorized into three spatially distinct layers: (1) the focal adhesion itself, (2) the juxtamembrane region near the focal adhesion, and (3) the cytoplasm. Each layer, or domain, has its own distinct dynamic properties. The focal adhesion domain contains one population of fixed molecules not undergoing exchange or diffusion. These molecules form the core of the focal adhesion, and are likely integrins bound tightly to the ECM. Bound to them are molecules undergoing exchange but not diffusion. These molecules lie at the cytoplasmic surface of the focal adhesion. The juxtamembrane domain contains molecules undergoing both exchange and diffusion. The molecular dynamics within this domain are gradient. Molecules near the focal adhesion domain are less mobile and molecules closer to the cytoplasm domain are more mobile. Additionally, these molecules are in higher density in regions closer to the focal adhesion domain and in lower density in regions closer to the cytoplasm domain. The juxtamembrane domain also extends laterally, and integrins show intermediate dynamics in regions near the focal adhesion edge. Here it is likely that integrins are not fixed as they are

in the focal adhesion domain, but still maintain significant interaction with the focal adhesion forming molecules. The cyptoplasm domain, predictably, is characterized by diffusion but not exchange. The notion of a juxtamembrane domain is novel and captures an important feature of focal adhesion dynamics.

The modern advanced fluorescence speckle microscopy technique allows for investigation of individual molecular movement in vivo. (101, 155) Using fluorescence speckle microscopy Hu et al. (85) investigated the movement of focal adhesion forming molecules within the lamellipodium of migrating cells. One set of fluorescent probes was used to track the movement of actin filaments, while other fluorescent probes were used to track the movement of focal adhesion forming molecules. The movements of the different molecules were then correlated and reported. Several focal adhesion forming molecules were probed, including integrin, paxillin, zyxin, FAK, α-actinin, vinculin, and talin. Of these, integrin showed the least movement overall, confirming the notion that integrin lies at the heart of focal adhesions and is relatively fixed. (209) Several of the focal adhesion forming molecules showed movement, but not movement correlated with the movement of the actin filaments. These semi-stationary molecules included zyxin, FAK, and paxillin. None of these molecules have been suggested to interact with actin filaments directly (181) (15) (168) (185). Their movements are likely due to exchange dynamics within the individual focal adhesions. The molecules that are known to interact with actin directly (127) (105) (62) (103) include vinculin, talin, and alpha-actinin. Their motions were reported to correlate with the motions of actin filaments, but to differing degrees. α-Actinin is an actin filament crosslinker (18) and would be expected to demonstrate movement highly correlated with actin filaments. The results reported by Hu et al. (85) confirm α-actinin to have the highest correlation in movement with the actin filaments. Both talin and vinculin have actin filament binding sites, but are both primarily associated with focal adhesions. The results show vinculin to have much more movement than talin. The movement of vinculin and the talin molecules that did show movement are both correlated with actin filament motions. Considering the numerous vinculin binding sites on talin, it is possible that those talin molecules with numerous vinculin molecules crosslinking them to actin filaments would dissociate form integrin and move along with the contracting actin filaments, while those talin molecules lacking numerous vinculin crosslinks to the actin filaments would dissociate from the contracting actin filament.

It had previously been shown that some focal adhesions in the lamellipodium undergo slippage during migration. (100, 129) These focal adhesion would disassemble during actin filament contraction, and reform again soon after. The FSM single molecule tracking results from Hu et al. (85) suggest one mechanism for this slippage. They report that soon before the slippage event vinculin molecules start movement correlated with the contracting actin filaments. The vinculin molecule continue movement throughout the slippage of the focal adhesion and again, soon before the focal adhesion is reformed, the vinculin molecules stop their correlated movement. This suggests a mechanism for focal adhesion slippage during cell

migration: the contraction of actin filaments detaches vinculin molecules from the focal adhesion. Once vinculin is removed, the focal adhesion loses its strength and begins to disassemble. Upon breakage of the vinculin actin bond, which persisted throughout part of the slippage and resulted in the correlated movement of vinculin with the contracting actin filaments, the vinculin can re-associate with the focal adhesions and the focal adhesion can reform. The dual role of vinculin and talin as both moving with the contracting actin filaments and at times dissociating from them has led to the idea of vinculin and talin acting as a molecular clutch during cell migration. (85) This thought provoking concept needs further study and investigation.

The molecular mechanosensor

The focal adhesion forms in response to a mechanical stimulation, either from forces originating in the cell's own processes of myosin II contraction and actin polymerization, or from forces originating from outside the cell and likely transmitted by the ECM. But what machinery within the focal adhesion itself provides the capacity for sensing mechanical stimulation and responding to it, through growth and maturation? Focal adhesions are the mechanotransduction structure of the cell. A complete understanding of cell mechanotransduction requires understanding the mechanically induced molecular events at the focal adhesion.

The most prominent hypothesis accounting for mechanical sensation at focal adhesions suggests that there exist individual molecules that act as molecular mechanosensors (104) (196). These molecules alter their structure when exposed to a mechanical stimulation. Once their structure undergoes some kind of conformational change the molecules can function differently. The most often suggested mechanosensors are talin and integrin (65, 76, 115, 116, 158). Both molecules lie at the heart of focal adhesions (156) (5, 14, 220, 224). Integrin is the only molecule that can link a nascent adhesion or a mature focal adhesion to the ECM. Talin is crucial to the formation of nascent adhesions (224), and persists throughout maturation of the nascent adhesion into a mature focal adhesion.

Other molecules suggested to be molecular mechanosensors include p130Cas (167, 222), filamin (36, 61, 110), FAK (173), and mechanosensitive calcium channels (83). Potential mechanosensation by any of these molecules is plausible but needs further study and investigation.

A number of investigations have addressed the two suggested molecular mechanosensors reviewed here, talin and integrin (170) (44) (12). The role of talin in the development of focal adhesions has been studied with genetically modified fibroblasts (156). In these fibroblast cells talin1 expression had been eliminated, yet nascent adhesions and focal adhesion developed. The likely reason for the persistence of nascent adhesions in the absence of talin1 was the overexpression of talin2 (132). To fully understand the role of talin in nascent adhesion formation

both talin1 and talin2 would need to be eliminated from the cell. To do this, Zhang et al. (224) used the genetically modified fibroblasts not expressing talin1 and blocked talin2 expression with talin 2 short interfering RNA (siRNA). In these cells, the nascent adhesions failed to form and the cellular morphology changed drastically as compared to the wild type fibroblast cells. Talin's presence is essential to the formation of a stable nascent adhesion that can later mature into a focal adhesion.

In their study removing both talin1 and talin2 from fibroblast cells, Zhang et al. (224) also reported that the talin-null cells failed to produce significant traction forces. This should not be surprising considering the correlation between focal adhesion formation and the generation of cellular traction forces (10). However, it does highlight the critical importance of talin to the mechanosensation of focal adhesions. The work of Jiang et al. (103) builds on these results to demonstrate the critical importance of talin to the adhesive strength of focal adhesions. Jiang et al. report that a slip-bond (197) exists between the ECM and the nascent adhesion with an adhesive strength of 2pN. Removal of talin from the cells eliminates this transient 2pN slip bond. Similarly, removal of β3-integrin from the cells eliminates this transient 2pN slip bond. The talin and integrin molecules are necessary for formation of nascent adhesions, for formation of stable traction forces from those nascent adhesions, and for the formation of the initial slip-bond between the ECM and the cytoskeleton.

Integrin structure

As the pivotal molecule in the nascent adhesion and focal adhesion (7, 82), integrin is a transmembrane protein, with the bulk of its mass residing outside the cell. The molecule has three domains, and intercellular domain, a transmembrane domain, and an ectodomain (90, 114, 226, 227). The cytoplasmic domain is known to bind the focal adhesion forming molecules (90). Molecules suggested to bing the cytoplasmic domain of integrin include talin, kindling, alpha-actinin, filamin, and FAK (12). The ectodomain binds the ECM, and the transmembrane domain is suggested to structural govern the conformation of integrin as either active or inactive (225).

Integrin is a heterodimer with an □ and a □ subunit (Fig. 8). There are 18 □ and 8 □ subunits that are known. The □ subunit has a larger cytoplasmic domain and a larger transmembrane domain, while the □ subunit has a larger ectodomain (114, 227). Binding of the □ cytoplasmic domain to intracellular molecules is suggested to be involved in integrin activation (71). Both subunits bind the ECM with their ectodomains, however binding of the □ ectodomain to ECM is suggested to have more specificity (227).

Recently, studies have determined the structure of all three domains of the integrin molecule (114, 226, 227). Of particular importance is the solved structure of the transmembrane domain as it represents the first instance of a solved structure for a transmembrane heterodimer (114). The solved structure of the transmembrane

domain shows a unique structure in which a longer □ subunit is associating with a smaller □ subunit within a phospholipid bilayer. This is made possible by two sets of interactions stabilizing the dimer: the outer membrane clasp (OMC) and the inter membrane clasp (IMC). The OMC comprises of a packing interaction between three glysine residues. The IMC comprises a hydrophobic contact between two nearby hydrophobic residues, and an electrostatic bridge between nearby charged residues. The IMC clasp is likely stronger and more stabilizing due to its electrostatic character. The OMC is likely the site of specificity between the many types of integrin heterodimers. To confirm the importance of the IMC and the OMC to integrin cellular function, Lau et al. (114) complemented their NMR investigation of integrin transmembrane domain structure with structure based site directed mutagenesis. They selectively mutated the residues suggested to form either the IMC or the OMC. The results showed reduced packing between the □ and the □ subunit whenever the interactions near either IMC or OMC were disturbed. Notably, the mutation of residues near the OMC could also reduce packing if the newly introduced leucine residue displaces an existing glycine from the hydrophobic packing and the strength of the OMC is reduced. Taken together, the mutagenesis results further implicate both the OMC and the IMC as critical to maintaining a strong association between the integrin subunits.

The integrin ectodomain adopts either an extended conformation or an bent conformation. Numerous recent studies have solved structures for the ectodomains, including structure of the bent conformation (213-215) (227), structures of the extended conformation (163, 218), and structures of the extended conformation bound to ligand (211). Together these structures describe several key features of the ectodomain. Both the ectodomains of the □ and the □ subunits contain a head domain, and two leg domains with a knee domain in between them (Fig. 9). In the bent conformation, the head domains are adjacent and near the cell membrane. The leg domains are collapsed, and the knee domain is the main point of bending to achieve the collapsed conformation. In the extended conformation, the head domain is extended away from the cell membrane. The leg domains are extended, and the knee domain is no longer bent. The □ subunit is suggested to cross the □ subunit upon extension (227).

The extension of the ectodomain is suggested to correlate with conformational change in the transmembrane domain (12). Insight from the recent structural investigation of the integrin transmembrane domain structure (114) suggests the transmembrane domains of the □ and □ subunits dissociate and separate upon extension of the ectodomain. Such a conformational change requires breakage of the IMC and the OMC, a molecular event associated with integrin activation.

Integrin activation

The entire integrin molecule, including its ectodomain, its transmembrane domain, and its cytoplasmic domain, can adopt an active or and inactive conformation (5, 12). In its inactive conformation the transmembrane α and β subunits are in close

association, the ectodomain is in a bent conformation, and both the OMC and the IMC are intact. In its active conformation the transmembrane α and β subunits are separated, the ectodomain is in an extended conformation, and both the OMC and the IMC are broken. Some studies contend that the extension of the ectodomain causes activation (1, 163, 211, 218, 227) while others contend that the dissociation of the transmembrane domain drives integrin activation (88, 109, 118, 145, 225). Similarly, two descriptions of the integrin activation exist: outside-in integrin activation (122), and inside-out integrin activation (6).

The outside-in integrin activation hypothesis suggests that an interaction between ECM ligand and the ectodomain of integrin drives ectodomain extension that in turn drives separation of the transmembrane domains and activation of integrin (5). Support for this hypothesis comes from the strong affinity between the integrin ectodomains and their ligands (12).

In order for integrin to be activated by an outside-in activation mechanism the ectodomain needs to transition its conformation from a bent conformation to an extended conformation. Two hypothesis have been proposed concerning the mechanisms by which integrin would undergo this transition: (1) the ectodomain would necessarily need to undergo a large-scale conformational shift (16, 179), or (2) a small yet critical conformational shift is sufficient to lead to activation (212). The second theory, the deadbolt theory, suggests that several critical interactions exist stabilizing the bent conformation, and disruption of these interactions is sufficient to lead to extension of the ectodomain. Both theories suggest that interaction with ligand is likely the driving force for the conformational switch.

To investigate the outside-in hypothesis directly in vitro, Askari et al. (8) used a fluorescent pair attached to integrin to assay the conformational changes of the integrin ectodomain. The loss in the Forster Resonance Energy Transfer (FRET) between the paired fluorescent probes signifies an increase in distance between the probes (80), effectively assaying a stretch of the ectodomain. The FRET results from their assay demonstrate that integrin adopts an extended conformation mainly at sites of focal adhesions. To illustrate the impact of this extension on the function of focal adhesions in mechanotransduction Asakri et al. prevented the elongation of the ectodomain by introducing a disulfide bond between the α and β leg domains in a membrane proximal region – the α and β subunits would need to separate in the membrane proximal regions just as the transmembrane domains would need to separate in the membrane. Introduction of the disulfide bridge prevented both the extension of the ectodomain (as reported by the FRET signal) and the migration of the cell. The extension of the ectodomain of integrin is necessary for complete focal adhesion mechanotransduction.

Using a molecular dynamics approach (153) another group investigated the possibility of integrin ectodomain extension being a force-regulated process (37) (Fig. 10). The structure of the integrin ectodomain in its bent conformation was used. The bent integrin dimer was simulated in with an external force applied to its

ligand binding domains, or directly to a ligand bound to the integrin dimer. The integrin ectodomain was able to undergo extension with the exposure to external force. The final extended conformation of integrin is similar to the solved structures of an extended integrin ectodomain (163, 218). During extension integrin adopts a partially extended conformation. If the force is removed while the integrin ectodomain is in the partially extended conformation the integrin will retract to its initial bent conformation. Once the integrin ectodomain is extended beyond a threshold then it maintains an extended conformation.

Both recent works by Askari et al. (8) and Chen et al. (37) support integrin as a candidate molecular mechanosensor. Nascent adhesions respond to external force by maturing into focal complexes and then into focal adhesions. Focal adhesions, in turn, respond to external force by growing in size strengthening the adhesion between the ECM and the cytoskeleton. The focal adhesion response to external force is to increase its load-bearing capacity. A focal adhesion molecular mechanosensor would need to trigger this increased load-bearing capacity. By extending its ectodomain during exposure to load, integrin becomes activated. Once activated, integrin can recruit talin and a multitude of other focal adhesion associated molecules to reinforce the link between the ECM and the cytoskeleton, increasing the load-bearing capacity of the focal adhesion. The presence of a threshold above which integrin extension becomes irreversible signifies an additional feature of this mechanosensor. The focal adhesion response can be regulated based on the extent of the mechanical load. Smaller loads could extend the ectodomain partially, temporarily activating integrin for binding to talin and formation of a nascent adhesion, while large loads could extend the ectodomain completely, more persistently activating integrin for prolonged binding of talin and other molecules leading to the formation of a mature focal adhesion. Integrin then, is a mechanosensor with a feature for showing a gradient response.

Inside-out activation

The cytoplasmic domain of integrin contains a short helical β domain and a short α subunit (90, 114). The β domain will bind cytoplasmic molecules that contain a FERM like domain (71). Two prominent molecules known to contain FERM like domains and bind the β subdomain of integrin are talin and Kindlin. The inside-out activation hypothesis suggests that the binding of either talin or kindling to the cytoplasmic domain of integrin can cause integrin activation. According to this hypothesis, the binding of the cytoplasmic β domain to a FERM like domain would precede extension of the integrin extodomain.

Talin contains at least one FERM like domain that can bind the β subdomain at its cytoplasmic residues (30, 60, 71, 146, 217). It has been demonstrated that binding of the talin FERM like domain to integrin is sufficient to activate integrin (31, 178, 182). Several other molecules have been shown to bind the β cytoplasmic domain of integrin, only talin binding to the β subunit, however, has led to integrin activation (178, 182). One plausible theory has arisen which suggests that in addition to

binding the β cytoplasmic domain with its FERM domain, talin forms another critical interaction with the integrin dimer that uniquely influences integrin activation (187, 195). It is suggested that talin might interact with residues near the transmembrane domain of integrin during inside-out activation.

Structural evidence has emerged supporting a second critical interaction between talin and integrin (205). Other structural studies have documented the interaction of the talin FERM domain with the β subunit of integrin (29, 60), but Wegener et al. (205) conclusively demonstrate that in addition to binding via the FERM like domain, talin interacts with a membrane proximal region of integrin. The interaction of talin with this membrane proximal region interrupts the IMC of the integrin transmembrane domain, releasing the α and β subunits (114). Once the association between the α and β subunits is removed, they are able to move apart from each other, causing the integrin ectodomain to respond by undergoing extension. This sequence of events can account for inside-out activation of integrin by talin.

Kindlins are the other molecule suggested to bind the integrin cytoplasmic domain and contribute to inside-out activation (138). The kindlin molecules contain FERM like domains and are known to bind integrin. Kindlins are suggested to contribute to integrin inside-out activation synergistically through cooperative binding to the integrin with talin (78, 133). Kindlin binds integrin at a distinct site from talin and can increase integrin's binding affinity for talin once bound (138). There exist three types of kindlin: kindlin-1, kindlin-2, kindlin-3 (184, 188, 206). All three are known to bind the β subunit of integrin, and all three are suggested to cooperate in the activation of integrin (188). Kindlin-3 is unique in that it is expressed exclusively in hematopoietic cells and contributes to the formation of blood clots and platelet aggregates (136). One indication that kindlins are critical to in vivo focal adhesion mechanotransduction comes from the knockout of kindlin-3 in mice (136). These mice died within one week due to severe hemorrhages throughout multiple tissues.

It is clear that both talin and kindlins contribute significantly to the activation of integrin via inside-out activation. But is inside-out activation of integrin a mechanosensitive process in the same way as outside-in activation? One possibility is that the activation of talin for binding to integrin is a mechanically regulated process. If so, then integrin inside-out activation could also be interpreted as part of its features as a mechanosensor.

Structure of talin

There are two talin isoforms, talin 1 and talin 2 (132). Both talin isomers exist as a dimer within the cell (48). Each talin monomer has a head domain and a tail domain connected by a flexible linker (44). It is suggested that during focal adhesion turnover a protease, calpain 2, dissociated the talin head and tail domains (58). The head domain contains, most notably, a FERM domain for binding to integrin (71)(Fig. 11). The head domain also contains an actin bindng domain (44), and

potentially a FAK binding domain (221). The tail domain of talin is much larger and contains numerous binding sites. The tail domain contains as many as eleven vinculin-binding sites (228), two actin-binding sites (44), and potentially an additional integrin-binding site (71).

The FERM domain in the talin head consists of three subdomains: F1, F2, and F3 (135). The F3 subdomain is the domain responsible for binding to the β subdomain of integrin. The talin tail has a binding site for the residues in the F3 subdomain (74). The association of the tail with the talin head at the site of integrin binding prevents the binding of the talin head to integrin, rendering talin auto-inhibited. The activation of talin for binding of the head domain to integrin requires removal of this auto-inhibitory interaction. One possibility is that an interaction between the head domain of talin and phosphotidylinositol-4,5-bisphosphate (PtdIns(4,5)P2) would cause a conformational change in the head domain (126). This conformational change could release the talin tail domain allowing for binding of the talin head domain to the β subunit of integrin. Alternatively, the binding of talin to (PtdIns(4,5)P2) could alter the conformation of the head domain such that there is higher affinity for the integrin β subunit than for the residues in the talin rod domain. Or perhaps the activation of talin is a mechanically regulated process. Perhaps a stretching force is needed to pull the talin rod domain apart from its head domain. Such a mechanism would support inside-out activation as being a mechanically regulated process. These suggestions seem plausible but require further investigation.

The c-terminus of talin contains an actin-binding domain suggested to be similar to a THATCH (talin/HIP1R/Sla2p actin tethering C-terminal homology) domain. The THATCH-like domain modulated binding of talin to actin, and is nearby to the regions of the talin rod suggested to be involved in talin dimerization. (172) Gingras et al. (70) have solved the structure of this region of the talin rod domain (Fig. 12). The revealed structural details highlight a number of significant differences between the THATCH domain and the actin-binding domain found in the talin rod. The most important difference is the necessity of talin dimerization to actin binding. Another notable difference between the THATCH domains and the c-terminus of the talin rod is the presence of a flexible linker between helices in the c-terminus of the talin rod. A helical bundle containing the actin-binding residues and an attached dimerization helix characterizes the structure of the c-terminus region of the talin rod domain. When talin is not dimerized, the dimerization helix can bind the helical bundle and prevent actin binding, that rendering dimerization necessary for actin binding to the c-terminus of the talin rod domain.

The dimerization of talin involves the formation of a coiled-coil between the two adjacent dimerization helices from each monomer (70). The coiled-coil interaction is stabilized by both a series of electrostatic salt-bridges and the formation of a hydrophobic contact between the two dimerization helices. One feature of this dimerization region of talin that requires further investigation is the orientation of the two dimers relative to each other. The structure of this region of talin suggests

that the dimer can form with at least three potential orientations: (1) a parallel orientation, (2) a V-shaped orientation, or (3) an extended dimer. It is possible that the talin dimer can adopt all three orientations. In this case, the orientation of the talin dimer could signify the level of stress that the talin is exposed to. Under high mechanical stress, the talin dimer would react with strain and adopt the extended orientation. Under less mechanical load, the talin dimer could react and form the V-shaped orientation, and under no mechanical load the talin dimer could adopt the parallel dimer orientation. This suggestion is thought provoking but requires further investigation.

If the talin dimer does exhibit a load-dependent orientation, then its suggested role as a molecular mechanosensor would be further supported. As a mechanosensor, the talin dimer would likely alter the number of focal adhesion forming binding partners it can form depending on the extent of the mechanical load. For example, when at a nascent adhesion and under less mechanical load, the talin dimer could adopt the V-shaped orientation and bind fewer actin filaments, or vinculin molecules. When the same nascent adhesion matures into a focal adhesion the talin dimer could adopt an extended orientation, increasing the number possible interactions with vinculin and actin filaments.

The talin vinculin-binding site

The talin rod domain contains many vinculin-binding sites (VBS) (89). A number of these vinculin-binding sites have been suggested to be cryptic and not exposed to solvent (116). The vinculin-binding sites are highly conserved and hydrophobic in nature. The likely mechanism of their cryptic conformation is the formation of a hydrophobic core with the VBS and the hydrophobic residues of the nearby helical domains. The structure of the VBS containing regions of the talin rod domain is highly helical and supports such a mechanism (70, 142). In order for these VBS regions to bind vinculin in a maturing focal adhesion they need to become exposed to solvent and removed from their hydrophobic cores (116). This process, termed talin VBS activation, has been studied extensively (44). The likely mechanism for VBS activation is mechanical perturbation; VBS becomes exposed to solvent for binding to vinculin after exposure of the talin rod to a stretching force (93).

The notion of a force-activated VBS was first introduced in a molecular dynamic investigation (116)(Fig. 13). Using the molecular dynamics simulation technique, Lee et al. (116) exposed a region of the talin rod domain that contains a cryptic VBS to a stretching force. The stretching force was designed to replicate the theorized stretching of the talin rod domain during force-induced talin VBS activation. The results from the simulation showed that cryptic VBS does indeed become activated for binding to vinculin upon exposure to the stretching force. The trajectory for VBS activation involves the rotation of the VBS residues out of the hydrophobic core from the talin rod domain. The stretching force is translated into a torsional force by a series of hydrogen bonds and salt-bridges between talin rod domain helices and VBS. After rotation out of the hydrophobic core, the VBS residues show a marked

increase in exposure to solvent, and are likely activated for binding to vinculin. Other molecular dynamics simulations have addressed talin VBS activation in a similar way (93). Taken together, the series of molecular dynamics simulations support a force-induced activation of talin VBS.

Recently, using a combination of FRET and optical tweezers, Del Rio et al. (47) have been able to experimentally confirm the suggestion of Lee et al. (116) that talin VBS is a force activated process. In their approach, a pair of fluorescent markers were used to report the binding of vinculin to talin VBS. A region of the talin rod domain was attached to substrate at one end and attached to a bead the other end. The optical tweezers were then used to stretch the talin rod domain by moving the bead away from the substrate. Upon stretch, the vinculin molecules were able to bind the then exposed VBS. Although the conformational changes predicted by Lee et al. could not be confirmed directly with this experiment, the overall suggestion from Lee et al. (116) of a force activated talin VBS was confirmed.

The experimental evidence combined with the computational simulations of talin VBS strongly support talin as a candidate molecular mechanosensor. Talin is initially recruited to the nascent adhesion (103) before exposure of the nascent adhesion to tension from myosin II. At this stage, talin is likely not under any stretching force and its cryptic VBS remain cryptic. As the nascent adhesion matures, the link to more load bearing actin filaments is strengthened exposing the talin rod domain to an increasing amount of tension and stretch. As the rod domain stretches, each of cryptic VBS are activated and vinculin molecules are recruited to the growing focal complex. Once mature, all talin VBS are likely activated and bound to vinculin. In this way talin can function as a molecular mechanosensor.

Comparing the features of integrin to those of talin a distinction can be made between the two focal adhesion molecular mechanosensors. Integrin exhibits its force-induced responses at the initial stages of forming the nascent adhesion. Its ectodomain undergoes an initial force induced stretch to bind ECM. As the nascent adhesion matures to a focal complex the integrin ectodomain increases its stretch until it eventually passes a threshold after which it remains in an active conformation (see above). Talin exhibits its force-induced response at later stages in the maturation of the nascent adhesion to a focal adhesion. The talin dimer adopts a parallel orientation initially at the nascent adhesion but shifts into a V-shaped orientation as the nascent adhesion matures into a focal complex. Once the focal complex begins to gain exposure to the higher tension from myosin II contraction it beings mature into a focal adhesion. At this stage the talin dimer adopts an extended conformation while the individual cryptic VBS residues become activated by the stretch of the talin rod. The final stage in this suggested pathway to focal adhesion mechanotransduction is the recruitment of vinculin to the exposed VBS residues. Vinculin is recruited to the maturing adhesion once the VBS residues are exposed (115, 116), and it functions as a reinforcing agent to further strengthen the maturing focal adhesion.

The reinforcing agent

The recruitment of vinculin to focal adhesions is correlated with exposure of the focal adhesion to an external force (59)(Fig. 14). Furthermore, vinculin-null cells show markedly smaller focal adhesions (166). These cells also exert reduced cellular traction forces (102). These results suggest that vinculin is recruited to growing focal adhesions as a reinforcing agent. With the presence of vinculin, focal adhesions have a higher load-bearing capacity. These more mature focal adhesions are also able to exert higher traction forces on their environments.

Before it can function as a reinforcing agent, vinculin needs to undergo a conformational change removing its auto-inhibition (96). Vinculin has five domains, four head domains (D1-D4) and a single tail domain (Vt) (9)(Fig. 15). The vinculin tail is connected to the four head domains via a flexible proline rich linker region. In its native conformation, Vt is in close association with all four head domains, including D1. Vt is also the site of the actin binding domains on vinculin (99). Numerous other molecules are suggested to bind vinculin, including talin, α-actinin, paxillin, and PIP2 (229). Of these, the binding of talin to vinculin is of particular significance given its role as a suggested focal adhesion molecular mechanosensor (see above). Talin VBS binds vinculin at residues in D1. The hydrophobic VBS is suggested to insert itself into the hydrophobic core of D1, a helical subdomain (115). The close association of Vt with D1 and the other head domain regions prevents the binding of VBS to D1, rendering vinculin auto-inhibited (76). The auto-inhibited conformation is stabilized by a number of salt-bridges between Vt and D1-D4, and the presence of a hydrophobic surface between D1 and Vt (22). Vinculin activation would require disruption of these stabilizing interactions. The auto-inhibitory conformation prevents the binding of Vt to actin filaments (99) and likely also prevents binding of talin to VBS (76).

A number of biochemical investigations have addressed vinculin activation (42). Bois et al. (21) investigated activation of vinculin by interaction with VBS. Vinculin was captured onto a gold surface and exposed to VBS from talin. Their results show that VBS is sufficient to displace the Vt and activate vinculin. In contrast, Chen et al. (35) demonstrated that in vitro vinculin is only activated when both actin filaments and talin VBS are present. Chen et al. used a co-sedimentation assay and showed co-sedimentation of actin with vinculin only after both actin and VBS were introduced to the vinculin molecules. Although their results seem contrasting, taken together, they highlight the importance of VBS binding in activating vinculin.

One possibility is that the VBS and actin-binding partners of vinculin cooperate to activate vinculin by both simultaneously interacting with different regions of vinculin. If Vt is interacting with actin filaments and D1 is interacting with VBS, even if they are not bound, the result would be a molecular interaction induced stretch on vinculin. The simultaneous interactions would attract vinculin in two different directions, Vt would be attracted towards actin filaments and D1 would be attracted towards the VBS. Molecular dynamics simulations set up to replicate this scenario

demonstrate that indeed such a dual attraction could cause a significant conformational change in vinculin (77)(Fig. 16). The results from the simulations show that when D1 is attracted towards VBS and Vt is attracted towards actin filaments, the result is a separation that emerges between Vt and D1 (Fig. 17).

The auto-inhibitory conformation of vinculin resulted from the proximity of D1 to Vt, which prevented an actin filament form binding Vt without steric interaction with D1 (99). The molecular dynamics simulations using a stretch between D1 and Vt suggest that one trajectory that could eliminate this proximity would be the movement of D1 away from Vt (77). Although it had previously been suggested that Vt separation from all four head domains was likely the trajectory of vinculin activation (229), this simulation suggests that D1 separates from Vt and the other vinculin domains during activation (77).

Vinculin activation likely also has an impact on binding of vinculin to VBS. Simulation of VBS binding to D1 in the absence of Vt or other vinculin domains suggested a three-step mechanism to vinculin binding (Fig. 18): (1) insertion of VBS in between helices of D1, (2) movement of the D1 helices to accommodate VBS, and (3) rotation of VBS into the hydrophobic core of D1 (115). The trajectory of binding between VBS and D1 illustrates the similarity between VBS stability when bound to D1 and VBS stability when cryptic in the talin rod domain. In both instances, the VBS joins the hydrophobic core created by the helical bundle of either D1 or the talin rod domain.

The trajectory of VBS binding to vinculin D1 without the other vinculin domains can be compared to the trajectory of vinculin binding to D1 with the other domains attached in either the open or the closed conformation (76). These molecular dynamics simulations demonstrate that the VBS is only able to insert into D1 as it did before (115) after vinculin activation. In its auto-inhibited conformation vinculin fails to accommodate a VBS insertion into the D1 hydrophobic core. The proximity of Vt to D1 prevents the necessary conformational changes in D1. After activation however, D1 is able to undergo the needed conformational changes and VBS is able to fully bind vinculin. The results from this study indicate that a cooperative binding is likely. VBS is able to attract D1 without binding while vinculin is in its auto-inhibited conformation, just as actin filaments are able to attract Vt without binding, and the simultaneous attraction could produce an activated vinculin.

If vinculin can be activated by a stretch induced by the simultaneous interaction of two binding partners at two separate vinculin domains, could the activation also be induced by an external mechanical force, or by the mechanical stretch of vinculin? One possibility is that vinculin would be activated by the cooperative binding mechanism, but the affinity of vinculin for its binding partners would be greatly enhanced by exposure of the complex to tension. According to this hypothesis, vinculin would undergo a gradient activation. One conformational change would result from the cooperative binding of vinculin with its binding partners, and a second conformational change would follow after exposure to an external force. No

gradient activation mechanism has been demonstrated in experiment or simulation, but should be the topic of future investigations.

A recent experimental investigation of vinculin in vivo (79) supports the notion that vinculin could be under load while reinforcing the maturing focal adhesion. Having produced an elastic polymer with a FRET pair incorporated into the structure, and having calibrated the produced elastic polymer FRET signal to specific stress values needed to cause a given loss in FRET signal between the pair of fluorescent probes built into the elastic polymer, Grashoff et al. (79) attached the FRET pair containing elastic probe to vinculin and assayed the tension across vinculin molecules in vivo. Their results suggest vinculin is under a 2.5pN tension when recruited to growing focal adhesions. This novel experimental probe supports the notion put force by the molecular dynamics simulations (77) that a possible stretch of vinculin correlates with vinculin activation.

Vinculin likely demonstrates a force induced conformational change. This conformational change either activated vinculin for binding to actin and talin (or other VBS residues), or it enhances an existing linkage. An accurate term to describe vinculin and its force-induced conformational changes would be the molecular reinforcing agent. Beyond molecular mechanosensation, the vinculin is enhancing its linkage upon exposure to an external force. The term also captures the role of vinculin recruitment to the maturing focal adhesion. Vinculin is recruited to focal complexes after the initial activation of integrin and the likely the activation of talin VBS. At this stage, the maturing focal adhesion is in need of reinforcement to increase its load-bearing capacity; the maturing focal adhesion is become exposed more directly to the tensile forces from myosin II (see above). Upon vinculin recruitment the focal complex and the resulting matured focal adhesion are reinforced and can withstand the larger load.

Focal adhesions also increase in size with vinculin recruitment. The discussion of vinculin thus far illustrates mechanisms by which vinculin reinforcement of focal adhesions can directly increase the strength of the focal adhesion, but how does vinculin recruitment correlate with an increased size in focal adhesions? One possible answer comes from the number of VBS regions in the talin rod domain. Vinculin recruitment signifies talin VBS activation. With more VBS regions activated, and more vinculin recruited, a single integrin-talin complex can expand the number of actin filaments it is attached to, by indirectly binding more actin filaments via the recruited vinculin molecules (Fig 20). The suggestion that the talin dimer can alter its orientation as the nascent adhesion matures into a focal adhesion can also provide insight in understanding how focal adhesion grow in size upon vinculin recruitment. While in its parallel orientation, the two talin monomers are likely binding the same actin filaments via their actin binding sites and via vinculin. As the dimer orientation changes with the maturation of the nascent adhesion into a mature focal adhesion and a V-shaped orientation is adopted, the number of unique actin filaments bound by the talin dimer increases, fewer actin filaments are bound to binding sites on both talin monomers. And with the full extension of the talin

dimer into an extended conformation there likely remain few actin filaments bond to both talin monomers, further increasing the number of unique actin filaments bound to the single talin-integrin complex. As the number of actin filaments bound to the growing focal complex increases the number of other focal adhesion forming molecules also increases. These additional molecules associate with the newly recruited actin filaments, and other focal adhesion forming molecules associate with these newly recruited actin filament binding molecules. Eventually, the increased density in actin filaments and focal adhesion forming molecules leads to the recruitment of more talin-integrin complexes. This positive feedback loop of subsequent molecular interactions is initiated by the molecular mechanosensors integrin and talin, and catalyzed by the molecular reinforcing agent vinculin.

Conclusion

The focal adhesion is the cell's mechanotransduction machinery. It is formed at sites of substrate adhesion and sites of cellular traction. The focal adhesion begins as a nascent adhesion, characterized by a weak 2pN molecular link to the ECM, and matures into a focal adhesion that can bear a traction force of more than 10pN. Throughout the maturation of the nascent adhesion into a focal adhesion individual molecular mechanosensors talin and integrin undergo significant conformational changes. Integrin becomes activated either by an outside-in or an inside-out mechanism at initiation of the nascent adhesion formation and possibly extents its ectodomain further into ECM during maturation into a more persistent focal adhesions. Talin is either recruited to an activated integrin or is activated itself and subsequently activates integrin. Once part of the initial nascent adhesion, the talin dimer can possibly undergo extension and adopt a dimer orientation that introduces each talin monomer to more unique actin filaments. Each talin monomer can also undergo specific conformational changes activating the rod domain for binding to vinculin. As the nascent adhesion matures into a focal adhesion, the molecular reinforcing agent vinculin is recruited and the load-bearing capacity of the focal adhesion is expanded. The entire process of mechanically regulated focal adhesion maturation and growth is likely a torrent of individual molecular mechanosensor and reinforcing agent functions.

The discussed suggestion of molecular events leading to the maturation of nascent adhesions into mature focal adhesions is thought provoking but is in need of more investigation. Can the talin dimer extend and form a different orientation upon exposure to a stretching force? Does the integrin ectodomain become mechanically extended in vivo leading to outside-in integrin activation? Is vinculin activation a gradient conformational change, and is the linkage between vinculin and its binding partners enhanced upon vinculin stretch? These are some of the critical questions raised by the theories discussed here. As these molecular events are investigated more thoroughly in vivo and in silico, the possibility, or impossibility, of the molecular mechanosensors talin and integrin, and the molecular reinforcing agent vinculin becomes more evident.

References

1. Adair BD, Xiong J-P, Maddock C, Goodman SL, Arnaout MA, and Yeager M. Three-dimensional EM structure of the ectodomain of integrin {alpha}V{beta}3 in a complex with fibronectin. J Cell Biol 168: 1109-1118, 2005.
2. Albiges-Rizo C, Destaing O, Fourcade B, Planus E, and Block MR. Actin machinery and mechanosensitivity in invadopodia, podosomes and focal adhesions. Journal of cell science 122: 3037-3049, 2009.
3. Alexandrova AY, Arnold K, Schaub S, Vasiliev JM, Meister J-J, Bershadsky AD, and Verkhovsky AB. Comparative dynamics of retrograde actin flow and focal adhesions: formation of nascent adhesions triggers transition from fast to slow flow. PLoS ONE 3: e3234, 2008.
4. Amano M, Chihara K, Kimura K, Fukata Y, Nakamura N, Matsuura Y, and Kaibuchi K. Formation of actin stress fibers and focal adhesions enhanced by Rho-kinase. Science 275: 1308-1311, 1997.
5. Anthis NJ and Campbell ID. The tail of integrin activation. Trends in biochemical sciences, 2011.
6. Arnaout MA, Mahalingam B, and Xiong J-P. Integrin structure, allostery, and bidirectional signaling. Annu Rev Cell Dev Biol 21: 381-410, 2005.
7. Askari JA, Buckley PA, Mould AP, and Humphries MJ. Linking integrin conformation to function. Journal of cell science 122: 165-170, 2009.
8. Askari JA, Tynan CJ, Webb SED, Martin-Fernandez ML, Ballestrem C, and Humphries MJ. Focal adhesions are sites of integrin extension. J Cell Biol 188: 891-903, 2010.
9. Bakolitsa C, Cohen D, Bankston L, and Bobkov A. Structural basis for vinculin activation at sites of cell adhesion. Nature, 2004.
10. Balaban NQ, Schwarz US, Riveline D, Goichberg P, Tzur G, Sabanay I, Mahalu D, Safran S, Bershadsky A, Addadi L, and Geiger B. Force and focal adhesion assembly: a close relationship studied using elastic micropatterned substrates. Nat Cell Biol 3: 466-472, 2001.
11. Ballestrem C, Hinz B, Imhof BA, and Wehrle-Haller B. Marching at the front and dragging behind: differential alphaVbeta3-integrin turnover regulates focal adhesion behavior. J Cell Biol 155: 1319-1332, 2001.
12. Banno A and Ginsberg MH. Integrin activation. Biochem Soc Trans 36: 229-234, 2008.
13. Bárány M. ATPase activity of myosin correlated with speed of muscle shortening. The Journal of General Physiology, 1967.
14. Barczyk M, Carracedo S, and Gullberg D. Integrins. Cell Tissue Res 339: 269-280, 2010.
15. Beckerle MC. Zyxin: zinc fingers at sites of cell adhesion. Bioessays 19: 949-957, 1997.
16. Beglova N, Blacklow SC, Takagi J, and Springer TA. Cysteine-rich module structure reveals a fulcrum for integrin rearrangement upon activation. Nat Struct Biol 9: 282-287, 2002.
17. Bershadsky AD, Balaban NQ, and Geiger B. Adhesion-dependent cell mechanosensitivity. Annu Rev Cell Dev Biol 19: 677-695, 2003.

18. Blanchard A, Ohanian V, and Critchley D. The structure and function of alpha-actinin. J Muscle Res Cell Motil 10: 280-289, 1989.
19. Bloom L, Ingham KC, and Hynes RO. Fibronectin regulates assembly of actin filaments and focal contacts in cultured cells via the heparin-binding site in repeat III13. Mol Biol Cell 10: 1521-1536, 1999.
20. Bois P, Borgon R, Vonrhein C, and Izard T. Structural dynamics of alpha-actinin-vinculin interactions. Mol Cell Biol 25: 6112-6122, 2005.
21. Bois P, O'Hara B, Nietlispach D, and Kirkpatrick J. The Vinculin Binding Sites of Talin and {alpha}-Actinin Are Sufficient to Activate Vinculin. Journal of Biological Chemistry, 2006.
22. Borgon RA, Vonrhein C, Bricogne G, Bois PRJ, and Izard T. Crystal structure of human vinculin. Structure 12: 1189-1197, 2004.
23. Borisy GG and Svitkina TM. Actin machinery: pushing the envelope. Current Opinion in Cell Biology 12: 104-112, 2000.
24. Brakebusch C and Fässler R. The integrin-actin connection, an eternal love affair. EMBO J 22: 2324-2333, 2003.
25. Broussard JA, Webb DJ, and Kaverina I. Asymmetric focal adhesion disassembly in motile cells. Current Opinion in Cell Biology 20: 85-90, 2008.
26. Brown CM, Hebert B, Kolin DL, Zareno J, Whitmore L, Horwitz AR, and Wiseman PW. Probing the integrin-actin linkage using high-resolution protein velocity mapping. Journal of cell science 119: 5204-5214, 2006.
27. Butcher DT, Alliston T, and Weaver VM. A tense situation: forcing tumour progression. Nat Rev Cancer 9: 108-122, 2009.
28. Byers HR and Fujiwara K. Stress fibers in cells in situ: immunofluorescence visualization with antiactin, antimyosin, and anti-alpha-actinin. J Cell Biol 93: 804-811, 1982.
29. Calderwood DA, Fujioka Y, de Pereda JM, García-Alvarez B, Nakamoto T, Margolis B, McGlade CJ, Liddington RC, and Ginsberg MH. Integrin beta cytoplasmic domain interactions with phosphotyrosine-binding domains: a structural prototype for diversity in integrin signaling. Proc Natl Acad Sci USA 100: 2272-2277, 2003.
30. Calderwood DA, Zent R, Grant R, Rees DJ, Hynes RO, and Ginsberg MH. The Talin head domain binds to integrin beta subunit cytoplasmic tails and regulates integrin activation. J Biol Chem 274: 28071-28074, 1999.
31. Campbell ID and Ginsberg MH. The talin-tail interaction places integrin activation on FERM ground. Trends in biochemical sciences 29: 429-435, 2004.
32. Carman CV and Springer TA. Integrin avidity regulation: are changes in affinity and conformation underemphasized? Current Opinion in Cell Biology 15: 547-556, 2003.
33. Chandrasekar I, Stradal TEB, Holt MR, Entschladen F, Jockusch BM, and Ziegler WH. Vinculin acts as a sensor in lipid regulation of adhesion-site turnover. Journal of cell science 118: 1461-1472, 2005.
34. Chen CS. Mechanotransduction - a field pulling together? Journal of cell science 121: 3285-3292, 2008.
35. Chen H, Choudhury D, and Craig S. Coincidence of Actin Filaments and Talin Is Required to Activate Vinculin. Journal of Biological Chemistry, 2006.

36. Chen HS, Kolahi KS, and Mofrad MRK. Phosphorylation facilitates the integrin binding of filamin under force. Biophys J 97: 3095-3104, 2009.
37. Chen W, Lou J, Hsin J, and Schulten… K. Molecular Dynamics Simulations of Forced Unbending of Integrin α V β 3. PLoS Computational …, 2011.
38. Choi CK, Vicente-Manzanares M, Zareno J, Whitmore LA, Mogilner A, and Horwitz AR. Actin and alpha-actinin orchestrate the assembly and maturation of nascent adhesions in a myosin II motor-independent manner. Nat Cell Biol, 2008.
39. Choquet D, Felsenfeld DP, and Sheetz MP. Extracellular matrix rigidity causes strengthening of integrin-cytoskeleton linkages. Cell 88: 39-48, 1997.
40. Cluzel C, Saltel F, Lussi J, Paulhe F, Imhof BA, and Wehrle-Haller B. The mechanisms and dynamics of (alpha)v(beta)3 integrin clustering in living cells. J Cell Biol 171: 383-392, 2005.
41. Cramer LP. Molecular mechanism of actin-dependent retrograde flow in lamellipodia of motile cells. Front Biosci 2: d260-270, 1997.
42. Critchley DR. Cytoskeletal proteins talin and vinculin in integrin-mediated adhesion. Biochem Soc Trans 32: 831-836, 2004.
43. Critchley DR. Focal adhesions - the cytoskeletal connection. Current Opinion in Cell Biology 12: 133-139, 2000.
44. Critchley DR and Gingras AR. Talin at a glance. Journal of cell science 121: 1345-1347, 2008.
45. Cukierman E, Pankov R, Stevens DR, and Yamada KM. Taking cell-matrix adhesions to the third dimension. Science 294: 1708-1712, 2001.
46. Cukierman E, Pankov R, and Yamada KM. Cell interactions with three-dimensional matrices. Current Opinion in Cell Biology 14: 633-639, 2002.
47. Del Rio A, Perez-Jimenez R, Liu R, Roca-Cusachs P, Fernandez J, and Sheetz M. Stretching single talin rod molecules activates vinculin binding. Science's STKE 323: 638, 2009.
48. Devenport D, Bunch TA, Bloor JW, Brower DL, and Brown NH. Mutations in the Drosophila alphaPS2 integrin subunit uncover new features of adhesion site assembly. Dev Biol 308: 294-308, 2007.
49. Digman MA, Brown CM, Horwitz AR, Mantulin WW, and Gratton E. Paxillin dynamics measured during adhesion assembly and disassembly by correlation spectroscopy. Biophys J 94: 2819-2831, 2008.
50. Edlund M, Lotano MA, and Otey CA. Dynamics of alpha-actinin in focal adhesions and stress fibers visualized with alpha-actinin-green fluorescent protein. Cell Motil Cytoskeleton 48: 190-200, 2001.
51. Etienne-Manneville S and Hall A. Rho GTPases in cell biology. Nature 420: 629-635, 2002.
52. Even-Ram S and Yamada KM. Cell migration in 3D matrix. Curr Opin Cell Biol 17: 524-532, 2005.
53. Faucheux N, Tzoneva R, Nagel M-D, and Groth T. The dependence of fibrillar adhesions in human fibroblasts on substratum chemistry. Biomaterials 27: 234-245, 2006.
54. Fernández P, Pullarkat PA, and Ott A. A master relation defines the nonlinear viscoelasticity of single fibroblasts. Biophys J 90: 3796-3805, 2006.

55. Fraley SI, Feng Y, Krishnamurthy R, Kim D-H, Celedon A, Longmore GD, and Wirtz D. A distinctive role for focal adhesion proteins in three-dimensional cell motility. Nat Cell Biol 12: 598-604, 2010.
56. Fraley T, Pereira C, Tran T, Singleton C, and Greenwood J. Phosphoinositide binding regulates alpha-actinin dynamics: mechanism for modulating cytoskeletal remodeling. J Biol Chem 280: 15479-15482, 2005.
57. Franco SJ and Huttenlocher A. Regulating cell migration: calpains make the cut. Journal of cell science 118: 3829-3838, 2005.
58. Franco SJ, Rodgers MA, Perrin BJ, Han J, Bennin DA, Critchley DR, and Huttenlocher A. Calpain-mediated proteolysis of talin regulates adhesion dynamics. Nat Cell Biol 6: 977-983, 2004.
59. Galbraith CG, Yamada KM, and Sheetz MP. The relationship between force and focal complex development. J Cell Biol 159: 695-705, 2002.
60. García-Alvarez B, de Pereda JM, Calderwood DA, Ulmer TS, Critchley D, Campbell ID, Ginsberg MH, and Liddington RC. Structural determinants of integrin recognition by talin. Molecular Cell 11: 49-58, 2003.
61. Gehler S, Baldassarre M, Lad Y, Leight JL, Wozniak MA, Riching KM, Eliceiri KW, Weaver VM, Calderwood DA, and Keely PJ. Filamin A-beta1 integrin complex tunes epithelial cell response to matrix tension. Mol Biol Cell 20: 3224-3238, 2009.
62. Geiger B. A 130K protein from chicken gizzard: its localization at the termini of microfilament bundles in cultured chicken cells. Cell 18: 193-205, 1979.
63. Geiger B and Bershadsky A. Assembly and mechanosensory function of focal contacts. Curr Opin Cell Biol 13: 584-592, 2001.
64. Geiger B and Bershadsky A. Exploring the neighborhood: adhesion-coupled cell mechanosensors. Cell 110: 139-142, 2002.
65. Geiger B, Spatz JP, and Bershadsky AD. Environmental sensing through focal adhesions. Nat Rev Mol Cell Biol 10: 21-33, 2009.
66. Geuijen CAW and Sonnenberg A. Dynamics of the alpha6beta4 integrin in keratinocytes. Mol Biol Cell 13: 3845-3858, 2002.
67. Giancotti FG and Ruoslahti E. Integrin signaling. Science 285: 1028-1032, 1999.
68. Giannone G, Dubin-Thaler BJ, Rossier O, Cai Y, Chaga O, Jiang G, Beaver W, Döbereiner H-G, Freund Y, Borisy G, and Sheetz MP. Lamellipodial actin mechanically links myosin activity with adhesion-site formation. Cell 128: 561-575, 2007.
69. Gingras AR, Bate N, Goult BT, Hazelwood L, Canestrelli I, Grossmann JG, Liu H, Putz NSM, Roberts GCK, Volkmann N, Hanein D, Barsukov IL, and Critchley DR. The structure of the C-terminal actin-binding domain of talin. EMBO J 27: 458-469, 2008.
70. Gingras AR, Bate N, Goult BT, Patel B, Kopp PM, Emsley J, Barsukov IL, Roberts GCK, and Critchley DR. Central region of talin has a unique fold that binds vinculin and actin. J Biol Chem 285: 29577-29587, 2010.
71. Gingras AR, Ziegler WH, Bobkov AA, Joyce MG, Fasci D, Himmel M, Rothemund S, Ritter A, Grossmann JG, Patel B, Bate N, Goult BT, Emsley J, Barsukov IL, Roberts GCK, Liddington RC, Ginsberg MH, and Critchley DR. Structural determinants of integrin binding to the talin rod. J Biol Chem 284: 8866-8876, 2009.

72. Ginsberg MH, Partridge A, and Shattil SJ. Integrin regulation. Current Opinion in Cell Biology 17: 509-516, 2005.
73. Goetz JG, Joshi B, Lajoie P, Strugnell SS, Scudamore T, Kojic LD, and Nabi IR. Concerted regulation of focal adhesion dynamics by galectin-3 and tyrosine-phosphorylated caveolin-1. J Cell Biol 180: 1261-1275, 2008.
74. Goksoy E, Ma Y-Q, Wang X, Kong X, Perera D, Plow EF, and Qin J. Structural basis for the autoinhibition of talin in regulating integrin activation. Molecular Cell 31: 124-133, 2008.
75. Golji J, Collins R, and Mofrad M. Molecular mechanics of the alpha-actinin rod domain: bending, torsional, and extensional behavior. PLoS Comput Biol 5: e1000389, 2009.
76. Golji J, Lam J, and Mofrad MRK. Vinculin activation is necessary for complete talin binding. Biophys J 100: 332-340, 2011.
77. Golji J and Mofrad MRK. A molecular dynamics investigation of vinculin activation. Biophys J 99: 1073-1081, 2010.
78. Goult BT, Bouaouina M, Harburger DS, Bate N, Patel B, Anthis NJ, Campbell ID, Calderwood DA, Barsukov IL, Roberts GC, and Critchley DR. The structure of the N-terminus of kindlin-1: a domain important for alphaiibbeta3 integrin activation. Journal of Molecular Biology 394: 944-956, 2009.
79. Grashoff C, Hoffman BD, Brenner MD, Zhou R, Parsons M, Yang MT, McLean MA, Sligar SG, Chen CS, Ha T, and Schwartz MA. Measuring mechanical tension across vinculin reveals regulation of focal adhesion dynamics. Nature 466: 263-266, 2010.
80. Grecco HE and Verveer PJ. FRET in Cell Biology: Still Shining in the Age of Super-Resolution? Chemphyschem 12: 484-490, 2011.
81. Hamadi A, Bouali M, Dontenwill M, Stoeckel H, Takeda K, and Rondé P. Regulation of focal adhesion dynamics and disassembly by phosphorylation of FAK at tyrosine 397. Journal of cell science 118: 4415-4425, 2005.
82. Harburger DS and Calderwood DA. Integrin signalling at a glance. Journal of cell science 122: 159-163, 2009.
83. Hayakawa K, Tatsumi H, and Sokabe M. Actin stress fibers transmit and focus force to activate mechanosensitive channels. Journal of cell science 121: 496-503, 2008.
84. Horwitz A, Duggan K, Buck C, and Beckerle… M. Interaction of plasma membrane fibronectin receptor with talin—a transmembrane linkage. naturecom, 1986.
85. Hu K, Ji L, Applegate KT, Danuser G, and Waterman-Storer CM. Differential transmission of actin motion within focal adhesions. Science 315: 111-115, 2007.
86. Huang C, Rajfur Z, Yousefi N, Chen Z, Jacobson K, and Ginsberg MH. Talin phosphorylation by Cdk5 regulates Smurf1-mediated talin head ubiquitylation and cell migration. Nat Cell Biol 11: 624-630, 2009.
87. Huang Z, Yan D-P, and Ge B-X. JNK regulates cell migration through promotion of tyrosine phosphorylation of paxillin. Cell Signal 20: 2002-2012, 2008.
88. Hughes PE, Diaz-Gonzalez F, Leong L, Wu C, McDonald JA, Shattil SJ, and Ginsberg MH. Breaking the integrin hinge. A defined structural constraint regulates integrin signaling. J Biol Chem 271: 6571-6574, 1996.

89. Humphries J, Wang P, Streuli C, and Geiger B. Vinculin controls focal adhesion formation by direct interactions with talin and actin. J Cell Biol, 2007.
90. Humphries MJ. Integrin structure. Biochem Soc Trans 28: 311-339, 2000.
91. Huveneers S and Danen EHJ. Adhesion signaling - crosstalk between integrins, Src and Rho. Journal of cell science 122: 1059-1069, 2009.
92. Hynes R. Integrins: bidirectional, allosteric signaling machines. Cell 110: 673-687, 2002.
93. Hytönen VP and Vogel V. How force might activate talin's vinculin binding sites: SMD reveals a structural mechanism. PLoS Comput Biol 4: e24, 2008.
94. Ingber D. Mechanobiology and diseases of mechanotransduction. Ann Med 35: 564-577, 2003.
95. Ingber DE. Cellular mechanotransduction: putting all the pieces together again. FASEB J 20: 811-827, 2006.
96. Izard T, Evans G, Borgon R, Rush C, Bricogne G, and Bois P. Vinculin activation by talin through helical bundle conversion. Nature 427: 171-175, 2004.
97. Jaalouk DE and Lammerding J. Mechanotransduction gone awry. Nat Rev Mol Cell Biol 10: 63-73, 2009.
98. Janmey PA and McCulloch CA. Cell mechanics: integrating cell responses to mechanical stimuli. Annu Rev Biomed Eng 9: 1-34, 2007.
99. Janssen M, Kim E, Liu H, Fujimoto L, and Bobkov A. Three-Dimensional Structure of Vinculin Bound to Actin Filaments. Molecular Cell, 2006.
100. Jay DG. The clutch hypothesis revisited: ascribing the roles of actin-associated proteins in filopodial protrusion in the nerve growth cone. J Neurobiol 44: 114-125, 2000.
101. Ji L and Danuser G. Tracking quasi-stationary flow of weak fluorescent signals by adaptive multi-frame correlation. J Microsc 220: 150-167, 2005.
102. Ji L, Lim J, and Danuser G. Fluctuations of intracellular forces during cell protrusion. Nat Cell Biol 10: 1393-1400, 2008.
103. Jiang G, Giannone G, Critchley DR, Fukumoto E, and Sheetz MP. Two-piconewton slip bond between fibronectin and the cytoskeleton depends on talin. Nature 424: 334-337, 2003.
104. Johnson CP, Tang H-Y, Carag C, Speicher DW, and Discher DE. Forced unfolding of proteins within cells. Science 317: 663-666, 2007.
105. Johnson RP and Craig SW. F-actin binding site masked by the intramolecular association of vinculin head and tail domains. Nature 373: 261-264, 1995.
106. Katoh K, Kano Y, Amano M, Onishi H, Kaibuchi K, and Fujiwara K. Rho-kinase--mediated contraction of isolated stress fibers. J Cell Biol 153: 569-584, 2001.
107. Katsumi A, Orr A, Tzima E, and Schwartz M. Integrins in Mechanotransduction. Journal of Biological Chemistry, 2004.
108. Keller R, Davidson LA, and Shook DR. How we are shaped: the biomechanics of gastrulation. Differentiation 71: 171-205, 2003.
109. Kim M, Carman CV, and Springer TA. Bidirectional transmembrane signaling by cytoplasmic domain separation in integrins. Science 301: 1720-1725, 2003.
110. Kolahi K and Mofrad M. Molecular mechanics of filamin's rod domain. Biophys J 94: 1075-1083, 2008.

111. Kole TP, Tseng Y, Jiang I, Katz JL, and Wirtz D. Intracellular mechanics of migrating fibroblasts. Mol Biol Cell 16: 328-338, 2005.
112. Kumar S, Maxwell IZ, Heisterkamp A, Polte TR, Lele TP, Salanga M, Mazur E, and Ingber DE. Viscoelastic retraction of single living stress fibers and its impact on cell shape, cytoskeletal organization, and extracellular matrix mechanics. Biophys J 90: 3762-3773, 2006.
113. Kumar S and Weaver VM. Mechanics, malignancy, and metastasis: the force journey of a tumor cell. Cancer Metastasis Rev 28: 113-127, 2009.
114. Lau T-L, Kim C, Ginsberg MH, and Ulmer TS. The structure of the integrin alphaIIbbeta3 transmembrane complex explains integrin transmembrane signalling. EMBO J 28: 1351-1361, 2009.
115. Lee S, Chunsrivirot S, Kamm R, and Mofrad M. Molecular Dynamics Study of Talin-Vinculin Binding. Biophys J, 2008.
116. Lee SE, Kamm RD, and Mofrad M. Force-induced activation of talin and its possible role in focal adhesion mechanotransduction. Journal of biomechanics 40: 2096-2106, 2007.
117. Lele TP, Pendse J, Kumar S, Salanga M, Karavitis J, and Ingber DE. Mechanical forces alter zyxin unbinding kinetics within focal adhesions of living cells. J Cell Physiol 207: 187-194, 2006.
118. Li W, Metcalf DG, Gorelik R, Li R, Mitra N, Nanda V, Law PB, Lear JD, Degrado WF, and Bennett JS. A push-pull mechanism for regulating integrin function. Proc Natl Acad Sci USA 102: 1424-1429, 2005.
119. Lieber SC, Aubry N, Pain J, Diaz G, Kim S-J, and Vatner SF. Aging increases stiffness of cardiac myocytes measured by atomic force microscopy nanoindentation. Am J Physiol Heart Circ Physiol 287: H645-651, 2004.
120. Liu J, Taylor D, and Taylor K. A 3-D reconstruction of smooth muscle alpha-actinin by CryoEm reveals two different conformations at the actin-binding region. J Mol Biol 338: 115-125, 2004.
121. Lopez JI, Mouw JK, and Weaver VM. Biomechanical regulation of cell orientation and fate. Oncogene 27: 6981-6993, 2008.
122. Luo B-H, Carman CV, and Springer TA. Structural basis of integrin regulation and signaling. Annu Rev Immunol 25: 619-647, 2007.
123. Mandadapu KK, Govindjee S, and Mofrad MRK. On the cytoskeleton and soft glassy rheology. Journal of biomechanics 41: 1467-1478, 2008.
124. Mao Y and Schwarzbauer JE. Accessibility to the fibronectin synergy site in a 3D matrix regulates engagement of alpha5beta1 versus alphavbeta3 integrin receptors. Cell Commun Adhes 13: 267-277, 2006.
125. Mao Y and Schwarzbauer JE. Fibronectin fibrillogenesis, a cell-mediated matrix assembly process. Matrix Biol 24: 389-399, 2005.
126. Martel V, Racaud-Sultan C, Dupe S, Marie C, Paulhe F, Galmiche A, Block MR, and Albiges-Rizo C. Conformation, localization, and integrin binding of talin depend on its interaction with phosphoinositides. J Biol Chem 276: 21217-21227, 2001.
127. Maruyama K and Ebashi S. Alpha-actinin, a new structural protein from striated muscle. II. Action on actin. J Biochem 58: 13-19, 1965.

128. Medalia O, Weber I, Frangakis AS, Nicastro D, Gerisch G, and Baumeister W. Macromolecular architecture in eukaryotic cells visualized by cryoelectron tomography. Science 298: 1209-1213, 2002.
129. Mitchison T and Kirschner M. Cytoskeletal dynamics and nerve growth. Neuron 1: 761-772, 1988.
130. Mitra SK, Hanson DA, and Schlaepfer DD. Focal adhesion kinase: in command and control of cell motility. Nat Rev Mol Cell Biol 6: 56-68, 2005.
131. Mofrad M, Golji J, Abdul Rahim N, and Kamm R. Force-induced unfolding of the focal adhesion targeting domain and the influence of paxillin binding. Mechanics & chemistry of biosystems : MCB 1: 253-265, 2006.
132. Monkley SJ, Pritchard CA, and Critchley DR. Analysis of the mammalian talin2 gene TLN2. Biochemical and biophysical research communications 286: 880-885, 2001.
133. Montanez E, Ussar S, Schifferer M, Bösl M, Zent R, Moser M, and Fässler R. Kindlin-2 controls bidirectional signaling of integrins. Genes Dev 22: 1325-1330, 2008.
134. Moore SW, Roca-Cusachs P, and Sheetz MP. Stretchy proteins on stretchy substrates: the important elements of integrin-mediated rigidity sensing. Dev Cell 19: 194-206, 2010.
135. Moser M, Legate KR, Zent R, and Fässler R. The tail of integrins, talin, and kindlins. Science 324: 895-899, 2009.
136. Moser M, Nieswandt B, Ussar S, Pozgajova M, and Fässler R. Kindlin-3 is essential for integrin activation and platelet aggregation. Nat Med 14: 325-330, 2008.
137. Nicholson-Dykstra S, Higgs HN, and Harris ES. Actin dynamics: growth from dendritic branches. Curr Biol 15: R346-357, 2005.
138. Nieswandt B, Varga-Szabo D, and Elvers M. Integrins in platelet activation. J Thromb Haemost 7 Suppl 1: 206-209, 2009.
139. Onck PR, Koeman T, van Dillen T, and van der Giessen E. Alternative explanation of stiffening in cross-linked semiflexible networks. Phys Rev Lett 95: 178102, 2005.
140. Otey C and Carpen O. Alpha-actinin revisited: a fresh look at an old player. Cell Motil Cytoskeleton 58: 104-111, 2004.
141. Panetti TS. Tyrosine phosphorylation of paxillin, FAK, and p130CAS: effects on cell spreading and migration. Front Biosci 7: d143-150, 2002.
142. Papagrigoriou E, Gingras AR, Barsukov IL, Bate N, Fillingham IJ, Patel B, Frank R, Ziegler WH, Roberts GCK, Critchley DR, and Emsley J. Activation of a vinculin-binding site in the talin rod involves rearrangement of a five-helix bundle. EMBO J 23: 2942-2951, 2004.
143. Parsons JT. Focal adhesion kinase: the first ten years. J Cell Sci 116: 1409-1416, 2003.
144. Parsons JT, Horwitz AR, and Schwartz MA. Cell adhesion: integrating cytoskeletal dynamics and cellular tension. Nat Rev Mol Cell Biol 11: 633-643, 2010.
145. Partridge AW, Liu S, Kim S, Bowie JU, and Ginsberg MH. Transmembrane domain helix packing stabilizes integrin alphaIIbbeta3 in the low affinity state. J Biol Chem 280: 7294-7300, 2005.

146. Patil S, Jedsadayanmata A, Wencel-Drake JD, Wang W, Knezevic I, and Lam SC. Identification of a talin-binding site in the integrin beta(3) subunit distinct from the NPLY regulatory motif of post-ligand binding functions. The talin n-terminal head domain interacts with the membrane-proximal region of the beta(3) cytoplasmic tail. J Biol Chem 274: 28575-28583, 1999.
147. Patla I, Volberg T, Elad N, Hirschfeld-Warneken V, Grashoff C, Fässler R, Spatz JP, Geiger B, and Medalia O. Dissecting the molecular architecture of integrin adhesion sites by cryo-electron tomography. Nat Cell Biol 12: 909-915, 2010.
148. Pérez-Tamayo R. Pathology of collagen degradation. A review. Am J Pathol 92: 508-566, 1978.
149. Pertz O, Hodgson L, Klemke RL, and Hahn KM. Spatiotemporal dynamics of RhoA activity in migrating cells. Nature 440: 1069-1072, 2006.
150. Peterson LJ, Rajfur Z, Maddox AS, Freel CD, Chen Y, Edlund M, Otey C, and Burridge K. Simultaneous stretching and contraction of stress fibers in vivo. Mol Biol Cell 15: 3497-3508, 2004.
151. Petrie RJ, Doyle AD, and Yamada KM. Random versus directionally persistent cell migration. Nat Rev Mol Cell Biol 10: 538-549, 2009.
152. Petroll WM, Ma L, and Jester JV. Direct correlation of collagen matrix deformation with focal adhesion dynamics in living corneal fibroblasts. Journal of cell science 116: 1481-1491, 2003.
153. Phillips J, Braun R, Wang W, and Gumbart J. Scalable molecular dynamics with NAMD. J Comput Chem, 2005.
154. Pollard TD and Borisy GG. Cellular motility driven by assembly and disassembly of actin filaments. Cell 112: 453-465, 2003.
155. Ponti A, Machacek M, Gupton SL, Waterman-Storer CM, and Danuser G. Two distinct actin networks drive the protrusion of migrating cells. Science 305: 1782-1786, 2004.
156. Priddle H, Hemmings L, Monkley S, Woods A, Patel B, Sutton D, Dunn GA, Zicha D, and Critchley DR. Disruption of the talin gene compromises focal adhesion assembly in undifferentiated but not differentiated embryonic stem cells. J Cell Biol 142: 1121-1133, 1998.
157. Provenzano PP and Vanderby R. Collagen fibril morphology and organization: implications for force transmission in ligament and tendon. Matrix Biol 25: 71-84, 2006.
158. Puklin-Faucher E, Gao M, Schulten K, and Vogel V. How the headpiece hinge angle is opened: New insights into the dynamics of integrin activation. J Cell Biol 175: 349-360, 2006.
159. Puklin-Faucher E and Sheetz MP. The mechanical integrin cycle. Journal of cell science 122: 179-186, 2009.
160. Ridley A, Schwartz M, Burridge K, and Firtel… R. Cell migration: integrating signals from front to back. Science, 2003.
161. Ridley AJ, Schwartz MA, Burridge K, Firtel RA, Ginsberg MH, Borisy G, Parsons JT, and Horwitz AR. Cell migration: integrating signals from front to back. Science 302: 1704-1709, 2003.
162. Riveline D, Zamir E, Balaban N, Schwarz U, Ishizaki T, Narumiya S, Kam Z, Geiger B, and Bershadsky A. Focal contacts as mechanosensors: externally applied

local mechanical force induces growth of focal contacts by an mDia1-dependent and ROCK-independent mechanism. J Cell Biol 153: 1175-1186, 2001.
163. Rocco M, Rosano C, Weisel JW, Horita DA, and Hantgan RR. Integrin conformational regulation: uncoupling extension/tail separation from changes in the head region by a multiresolution approach. Structure 16: 954-964, 2008.
164. Rosen MK, Yamazaki T, Gish GD, Kay CM, Pawson T, and Kay LE. Direct demonstration of an intramolecular SH2-phosphotyrosine interaction in the Crk protein. Nature 374: 477-479, 1995.
165. Sastry SK and Burridge K. Focal adhesions: a nexus for intracellular signaling and cytoskeletal dynamics. Experimental Cell Research 261: 25-36, 2000.
166. Saunders R, Holt M, Jennings L, and Sutton D. Role of vinculin in regulating focal adhesion turnover. European Journal of Cell Biology, 2006.
167. Sawada Y, Tamada M, Dubin-Thaler BJ, Cherniavskaya O, Sakai R, Tanaka S, and Sheetz MP. Force sensing by mechanical extension of the Src family kinase substrate p130Cas. Cell 127: 1015-1026, 2006.
168. Schlaepfer DD and Hunter T. Signal transduction from the extracellular matrix--a role for the focal adhesion protein-tyrosine kinase FAK. Cell Struct Funct 21: 445-450, 1996.
169. Schwartz MA. Cell biology. The force is with us. Science 323: 588-589, 2009.
170. Schwarz U, Erdmann T, and Bischofs I. Focal adhesions as mechanosensors: The two-spring model. BioSystems, 2006.
171. Sechi AS and Wehland J. The actin cytoskeleton and plasma membrane connection: PtdIns(4,5)P(2) influences cytoskeletal protein activity at the plasma membrane. Journal of cell science 113 Pt 21: 3685-3695, 2000.
172. Senetar MA, Foster SJ, and McCann RO. Intrasteric inhibition mediates the interaction of the I/LWEQ module proteins Talin1, Talin2, Hip1, and Hip12 with actin. Biochemistry 43: 15418-15428, 2004.
173. Shattil SJ, Kim C, and Ginsberg MH. The final steps of integrin activation: the end game. Nat Rev Mol Cell Biol 11: 288-300, 2010.
174. Shroff H, Galbraith CG, Galbraith JA, and Betzig E. Live-cell photoactivated localization microscopy of nanoscale adhesion dynamics. Nat Methods 5: 417-423, 2008.
175. Shroff H, Galbraith CG, Galbraith JA, White H, Gillette J, Olenych S, Davidson MW, and Betzig E. Dual-color superresolution imaging of genetically expressed probes within individual adhesion complexes. Proc Natl Acad Sci USA 104: 20308-20313, 2007.
176. Smith SJ and McCann RO. A C-terminal dimerization motif is required for focal adhesion targeting of Talin1 and the interaction of the Talin1 I/LWEQ module with F-actin. Biochemistry 46: 10886-10898, 2007.
177. Storm C, Pastore JJ, MacKintosh FC, Lubensky TC, and Janmey PA. Nonlinear elasticity in biological gels. Nature 435: 191-194, 2005.
178. Tadokoro S, Shattil SJ, Eto K, Tai V, Liddington RC, de Pereda JM, Ginsberg MH, and Calderwood DA. Talin binding to integrin beta tails: a final common step in integrin activation. Science 302: 103-106, 2003.

179. Takagi J, Petre BM, Walz T, and Springer TA. Global conformational rearrangements in integrin extracellular domains in outside-in and inside-out signaling. Cell 110: 599-511, 2002.
180. Takai E, Landesberg R, Katz RW, Hung CT, and Guo XE. Substrate modulation of osteoblast adhesion strength, focal adhesion kinase activation, and responsiveness to mechanical stimuli. Mol Cell Biomech 3: 1-12, 2006.
181. Tanaka T, Yamaguchi R, Sabe H, Sekiguchi K, and Healy JM. Paxillin association in vitro with integrin cytoplasmic domain peptides. FEBS Lett 399: 53-58, 1996.
182. Tanentzapf G and Brown NH. An interaction between integrin and the talin FERM domain mediates integrin activation but not linkage to the cytoskeleton. Nat Cell Biol 8: 601-606, 2006.
183. Tanentzapf G, Martin-Bermudo MD, Hicks MS, and Brown NH. Multiple factors contribute to integrin-talin interactions in vivo. Journal of cell science 119: 1632-1644, 2006.
184. Tu Y, Wu S, Shi X, Chen K, and Wu C. Migfilin and Mig-2 link focal adhesions to filamin and the actin cytoskeleton and function in cell shape modulation. Cell 113: 37-47, 2003.
185. Turner CE, Glenney JR, and Burridge K. Paxillin: a new vinculin-binding protein present in focal adhesions. J Cell Biol 111: 1059-1068, 1990.
186. Tzima E, Irani-Tehrani M, Kiosses WB, Dejana E, Schultz DA, Engelhardt B, Cao G, DeLisser H, and Schwartz MA. A mechanosensory complex that mediates the endothelial cell response to fluid shear stress. Nature 437: 426-431, 2005.
187. Ulmer TS, Calderwood DA, Ginsberg MH, and Campbell ID. Domain-specific interactions of talin with the membrane-proximal region of the integrin beta3 subunit. Biochemistry 42: 8307-8312, 2003.
188. Ussar S, Wang H-V, Linder S, Fässler R, and Moser M. The Kindlins: subcellular localization and expression during murine development. Experimental Cell Research 312: 3142-3151, 2006.
189. Vallotton P, Danuser G, Bohnet S, Meister J-J, and Verkhovsky AB. Tracking retrograde flow in keratocytes: news from the front. Mol Biol Cell 16: 1223-1231, 2005.
190. Vallotton P, Gupton SL, Waterman-Storer CM, and Danuser G. Simultaneous mapping of filamentous actin flow and turnover in migrating cells by quantitative fluorescent speckle microscopy. Proc Natl Acad Sci USA 101: 9660-9665, 2004.
191. van den Bout I and Divecha N. PIP5K-driven PtdIns(4,5)P2 synthesis: regulation and cellular functions. Journal of cell science 122: 3837-3850, 2009.
192. Vicente-Manzanares M, Choi CK, and Horwitz AR. Integrins in cell migration--the actin connection. Journal of cell science 122: 199-206, 2009.
193. Vicente-Manzanares M, Koach MA, Whitmore L, Lamers ML, and Horwitz AF. Segregation and activation of myosin IIB creates a rear in migrating cells. J Cell Biol 183: 543-554, 2008.
194. Vicente-Manzanares M, Ma X, Adelstein RS, and Horwitz AR. Non-muscle myosin II takes centre stage in cell adhesion and migration. Nat Rev Mol Cell Biol 10: 778-790, 2009.

195. Vinogradova O, Velyvis A, Velyviene A, Hu B, Haas T, Plow E, and Qin J. A structural mechanism of integrin alpha(IIb)beta(3) "inside-out" activation as regulated by its cytoplasmic face. Cell 110: 587-597, 2002.
196. Vogel V. Mechanotransduction involving multimodular proteins: converting force into biochemical signals. Annu Rev Biophys Biomol Struct 35: 459-488, 2006.
197. Vogel V and Sheetz M. Local force and geometry sensing regulate cell functions. Nat Rev Mol Cell Biol 7: 265-275, 2006.
198. Vogel V and Sheetz MP. Cell fate regulation by coupling mechanical cycles to biochemical signaling pathways. Current Opinion in Cell Biology 21: 38-46, 2009.
199. von Wichert G, Haimovich B, Feng G-S, and Sheetz MP. Force-dependent integrin-cytoskeleton linkage formation requires downregulation of focal complex dynamics by Shp2. EMBO J 22: 5023-5035, 2003.
200. von Wichert G, Jiang G, Kostic A, De Vos K, Sap J, and Sheetz MP. RPTP-alpha acts as a transducer of mechanical force on alphav/beta3-integrin-cytoskeleton linkages. J Cell Biol 161: 143-153, 2003.
201. Warden SJ, Hurst JA, Sanders MS, Turner CH, Burr DB, and Li J. Bone adaptation to a mechanical loading program significantly increases skeletal fatigue resistance. J Bone Miner Res 20: 809-816, 2005.
202. Weaver AM. Invadopodia: specialized cell structures for cancer invasion. Clin Exp Metastasis 23: 97-105, 2006.
203. Webb D and Parsons… J. Adhesion assembly, disassembly and turnover in migrating cells–over and over and over again. Nat Cell Biol, 2002.
204. Webb DJ, Parsons JT, and Horwitz AF. Adhesion assembly, disassembly and turnover in migrating cells -- over and over and over again. Nat Cell Biol 4: E97-100, 2002.
205. Wegener KL, Partridge AW, Han J, Pickford AR, Liddington RC, Ginsberg MH, and Campbell ID. Structural basis of integrin activation by talin. Cell 128: 171-182, 2007.
206. Weinstein EJ, Bourner M, Head R, Zakeri H, Bauer C, and Mazzarella R. URP1: a member of a novel family of PH and FERM domain-containing membrane-associated proteins is significantly over-expressed in lung and colon carcinomas. Biochim Biophys Acta 1637: 207-216, 2003.
207. Wolf K and Friedl P. Mapping proteolytic cancer cell-extracellular matrix interfaces. Clin Exp Metastasis 26: 289-298, 2009.
208. Wolf K, Wu YI, Liu Y, Geiger J, Tam E, Overall C, Stack MS, and Friedl P. Multi-step pericellular proteolysis controls the transition from individual to collective cancer cell invasion. Nat Cell Biol 9: 893-904, 2007.
209. Wolfenson H, Lubelski A, Regev T, Klafter J, Henis YI, and Geiger B. A role for the juxtamembrane cytoplasm in the molecular dynamics of focal adhesions. PLoS ONE 4: e4304, 2009.
210. Wood… W. Structures in focus--filopodia. The International Journal of Biochemistry & Cell …, 2002.
211. Xiao T, Takagi J, Coller BS, Wang J-H, and Springer TA. Structural basis for allostery in integrins and binding to fibrinogen-mimetic therapeutics. Nature 432: 59-67, 2004.

212. Xiong J, Stehle T, Goodman S, and Arnaout M. New insights into the structural basis of integrin activation. Blood 102: 1155-1159, 2003.
213. Xiong J-P, Mahalingham B, Alonso JL, Borrelli LA, Rui X, Anand S, Hyman BT, Rysiok T, Müller-Pompalla D, Goodman SL, and Arnaout MA. Crystal structure of the complete integrin alphaVbeta3 ectodomain plus an alpha/beta transmembrane fragment. J Cell Biol 186: 589-600, 2009.
214. Xiong J-P, Stehle T, Zhang R, Joachimiak A, Frech M, Goodman SL, and Arnaout MA. Crystal structure of the extracellular segment of integrin alpha Vbeta3 in complex with an Arg-Gly-Asp ligand. Science 296: 151-155, 2002.
215. Xiong JP, Stehle T, Diefenbach B, Zhang R, Dunker R, Scott DL, Joachimiak A, Goodman SL, and Arnaout MA. Crystal structure of the extracellular segment of integrin alpha Vbeta3. Science 294: 339-345, 2001.
216. Yamaguchi H, Wyckoff J, and Condeelis J. Cell migration in tumors. Current Opinion in Cell Biology 17: 559-564, 2005.
217. Yan B, Calderwood DA, Yaspan B, and Ginsberg MH. Calpain cleavage promotes talin binding to the beta 3 integrin cytoplasmic domain. J Biol Chem 276: 28164-28170, 2001.
218. Ye F, Liu J, Winkler H, and Taylor KA. Integrin alpha IIb beta 3 in a membrane environment remains the same height after Mn2+ activation when observed by cryoelectron tomography. Journal of Molecular Biology 378: 976-986, 2008.
219. Zaidel-Bar R, Ballestrem C, Kam Z, and Geiger B. Early molecular events in the assembly of matrix adhesions at the leading edge of migrating cells. Journal of cell science 116: 4605-4613, 2003.
220. Zaidel-Bar R and Geiger B. The switchable integrin adhesome. Journal of cell science 123: 1385-1388, 2010.
221. Zaidel-Bar R, Itzkovitz S, Ma'ayan A, Iyengar R, and Geiger B. Functional atlas of the integrin adhesome. Nat Cell Biol 9: 858-867, 2007.
222. Zaidel-Bar R, Milo R, Kam Z, and Geiger B. A paxillin tyrosine phosphorylation switch regulates the assembly and form of cell-matrix adhesions. Journal of cell science 120: 137-148, 2007.
223. Zamir E and Geiger B. Components of cell-matrix adhesions. Journal of cell science 114: 3577-3579, 2001.
224. Zhang X, Jiang G, Cai Y, Monkley S, Critchley D, and Sheetz M. Talin depletion reveals independence of initial cell spreading from integrin activation and traction. Nat Cell Biol, 2008.
225. Zhu J, Carman CV, Kim M, Shimaoka M, Springer TA, and Luo B-H. Requirement of alpha and beta subunit transmembrane helix separation for integrin outside-in signaling. Blood 110: 2475-2483, 2007.
226. Zhu J, Luo B-H, Barth P, Schonbrun J, Baker D, and Springer TA. The structure of a receptor with two associating transmembrane domains on the cell surface: integrin alphaIIbbeta3. Molecular Cell 34: 234-249, 2009.
227. Zhu J, Luo B-H, Xiao T, Zhang C, Nishida N, and Springer TA. Structure of a complete integrin ectodomain in a physiologic resting state and activation and deactivation by applied forces. Molecular Cell 32: 849-861, 2008.
228. Ziegler WH, Gingras AR, Critchley DR, and Emsley J. Integrin connections to the cytoskeleton through talin and vinculin. Biochem Soc Trans 36: 235-239, 2008.

229. Ziegler WH, Liddington RC, and Critchley DR. The structure and regulation of vinculin. Trends in Cell Biology 16: 453-460, 2006.
230. Zimerman B, Volberg T, and Geiger B. Early molecular events in the assembly of the focal adhesion-stress fiber complex during fibroblast spreading. Cell Motil Cytoskeleton 58: 143-159, 2004.

Figure

Figure 1. The focal adhesion functions to link the cell's cytoskeleton to the ECM. Membrane bound integrin molecules bind the ECM and numberous cyplasmic molecules. These cytoplasmic molecules bind to each other, to integrin, and to nearby actin filaments. Together the conglomerate of focal adhesion forming molecules constitute a molecular glue attaching the actin filaments to the cell's extracellular environment.

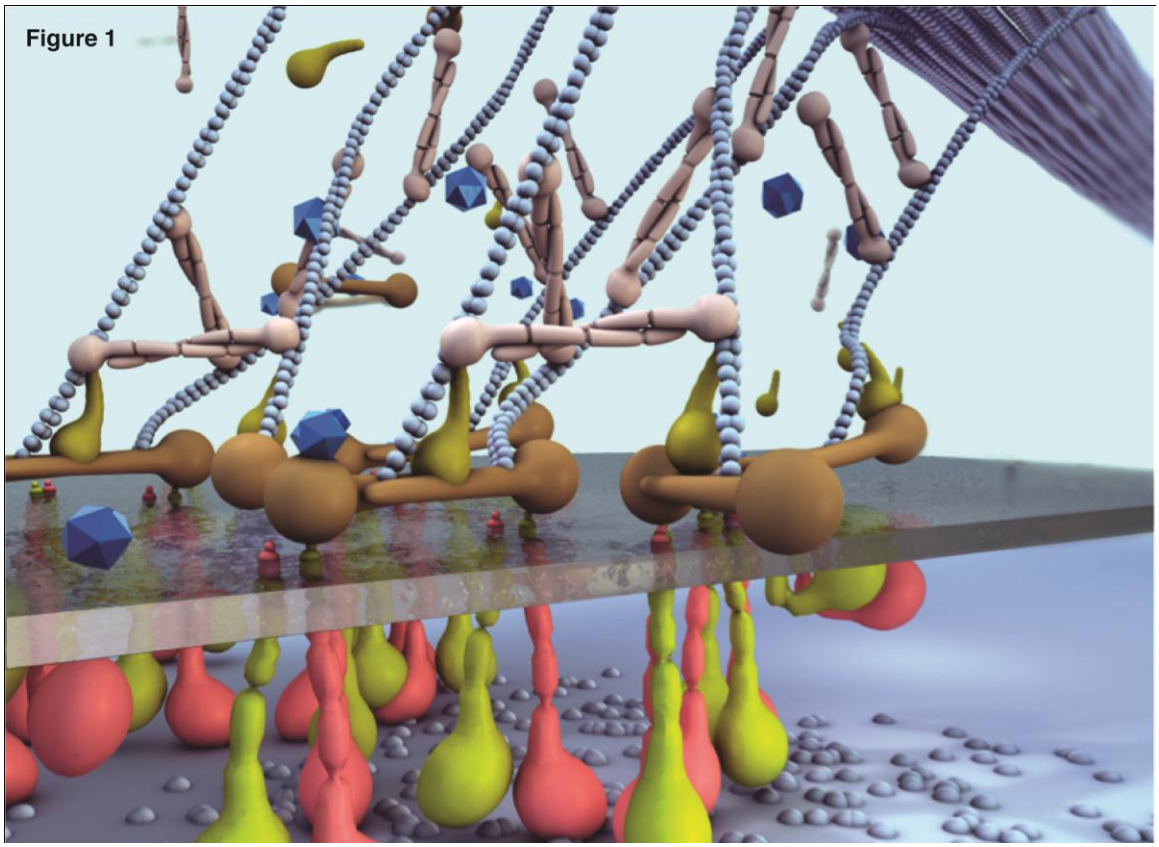

Figure 2. The migrating cell adopts a directional shape to facilitate its movement. At the front of the cell, in the direction of the cell movement, the cell forms filopodia. The migrating cell adopts a directional shape to facilitate its movement. At the front of the cell, in the direction of the cell movement, the cell forms filopodium that extend into the ECM. Behind the filopodium is that lamellipodium. The lamellipodium is the site where the cell generates it protrusions via actin polymerization. Behind the lamellipodium is the lamellum where stress fibers adhere to the front of the cell. These stress fibers also adhere to the back of the cell near the trailing edge. Nascent adhesions are formed in the lamellipodium as transient links between the polymerizing branched actin filaments. These nascent adhesions mature into focal adhesions at the lamellum, where they function to link the stress fibers to the ECM. Figure adopted from (144).

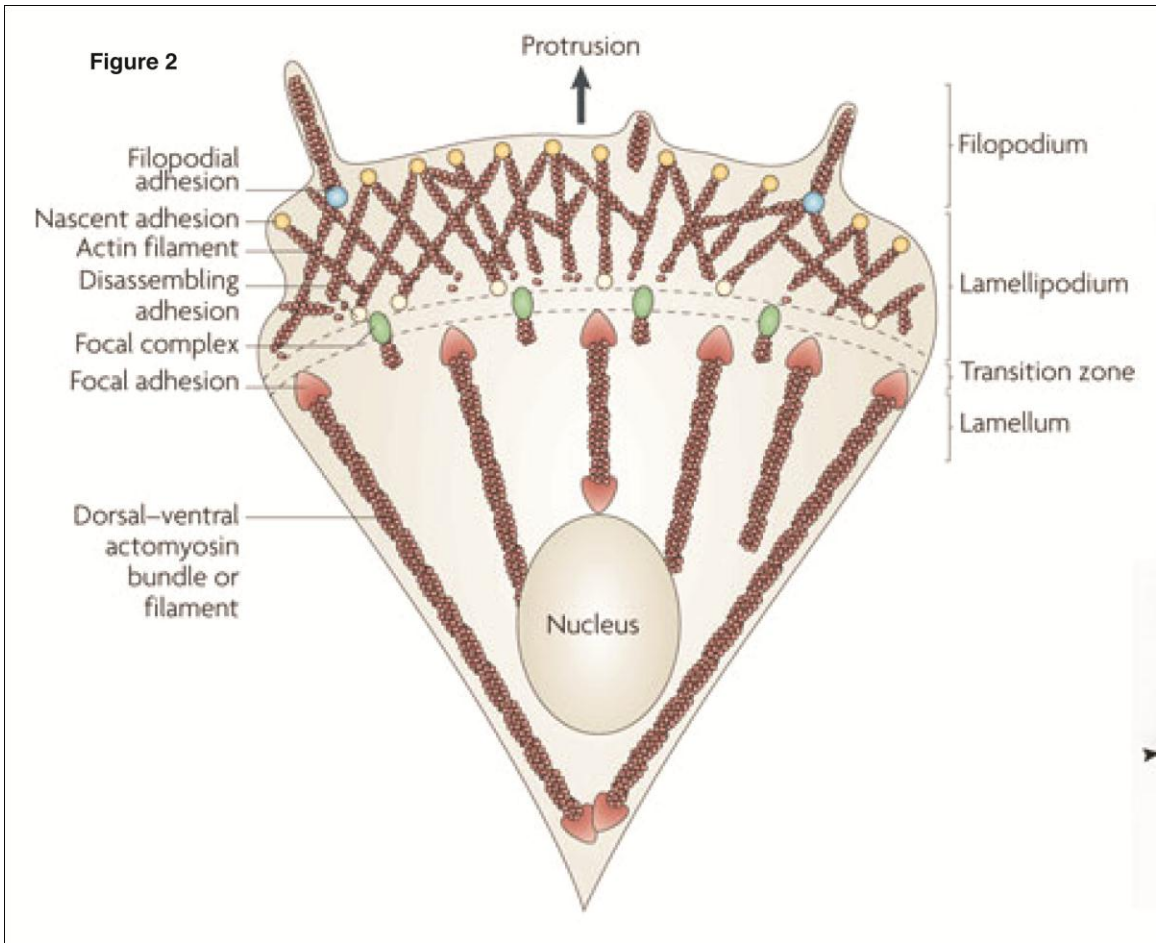

Figure 3. Nascent adhesions mature into focal adhesions at the boundary between the lamellipodium and the lamellum. The retrograde flow of actin filaments within the lamellipodium exerts a force on the nascent adhesions. This force can lead to the maturation of the nascent adhesion first to a focal complex and then to a focal adhesion. The maturation to a focal adhesion occurs upon exposure of the maturing focal complex to the contraction of myosin II on actin filaments in the lamellum. With the maturation of a nascent adhesion to a focal adhesion the boundary between the lamellum and the lamellipodium is advanced and the actin filaments near the newly formed focal adhesion reorganize into parallel fibers. Figure adopted from (3) with permission.

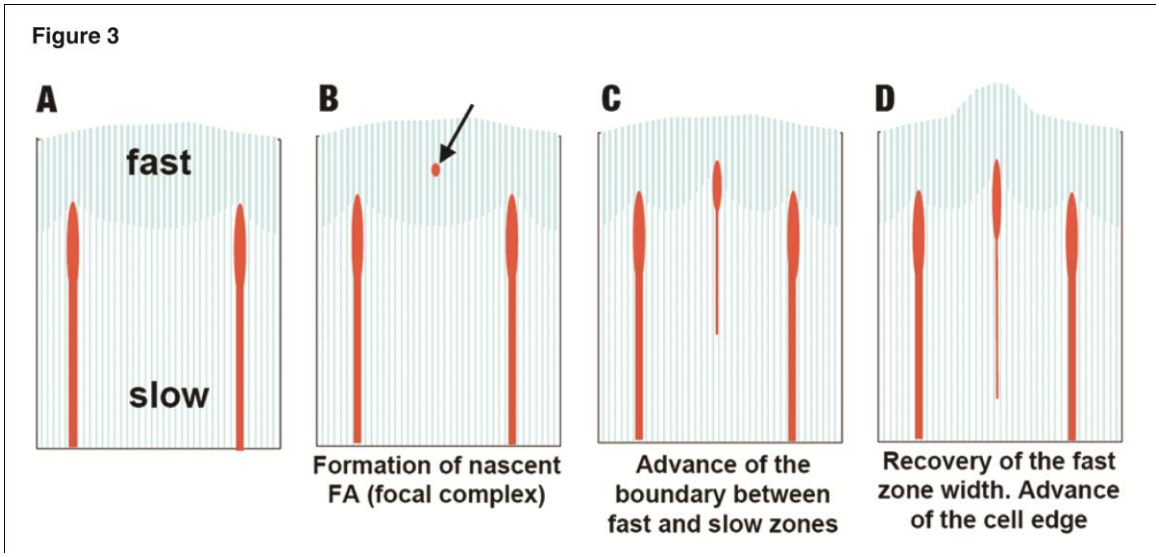

Figure 4. Focal adhesions can be induced in vitro using optical tweezers. The optical tweezers can apply an external force to ECM coated beads that in turn can apply the force to membrane bound integrins interacting with the ECM proteins. The bead initially is bound to integrin (A) and as it is moved away from integrin (A-C) a force is transmitted to the integrin. As the force is applied to integrin focal adhesions develop at the site of mechanical perturbation (right panels). Figure adopted from (59) with permission.

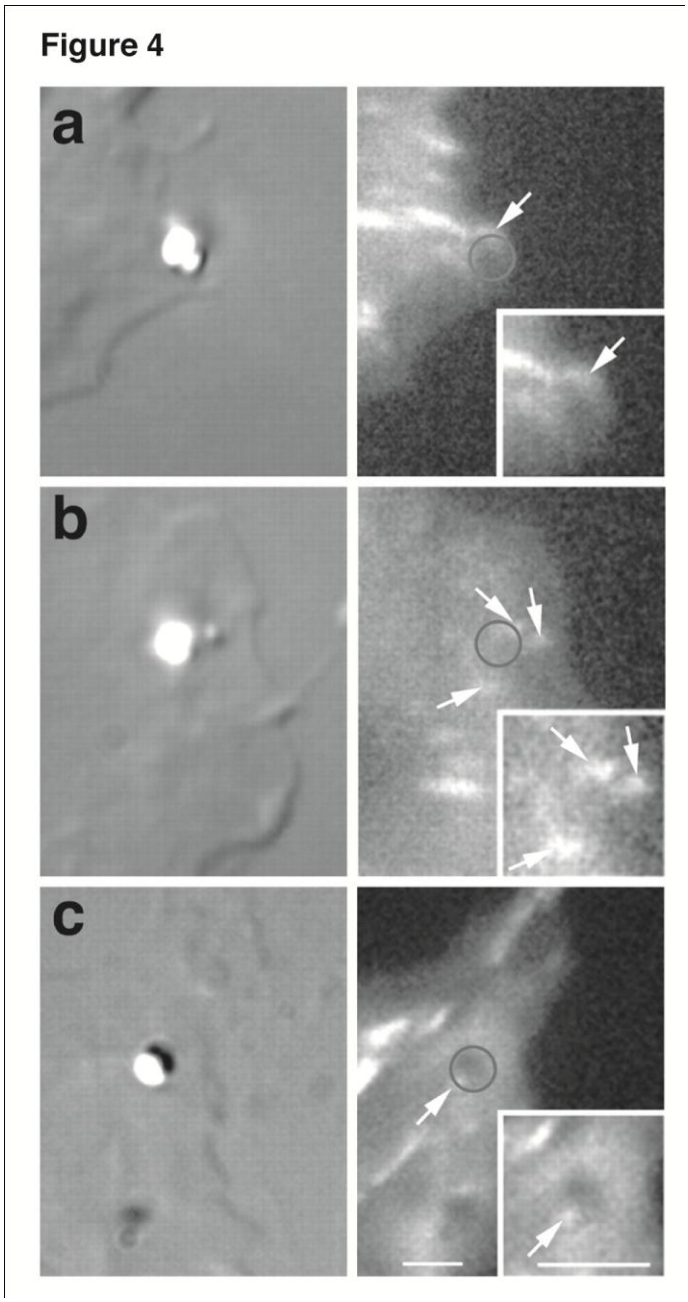

Figure 5. Focal adhesions are μm-sized structures. Reconstruction of the nano-architecture of these focal adhesions from fluorescence microscopy combined with cryo-electron tomography slices reveals the organization of focal adhesion forming molecules into many doughnut-shaped particles 20-30nm in diameter. Although the biochemical identity of these particles has yet to be determined, their existence suggests the focal adhesion is a dense collection of many nanometer sized molecular complexes and not a single μm sized continuous multi-molecule conglomerate. Figure adopted from (147).

Figure 5

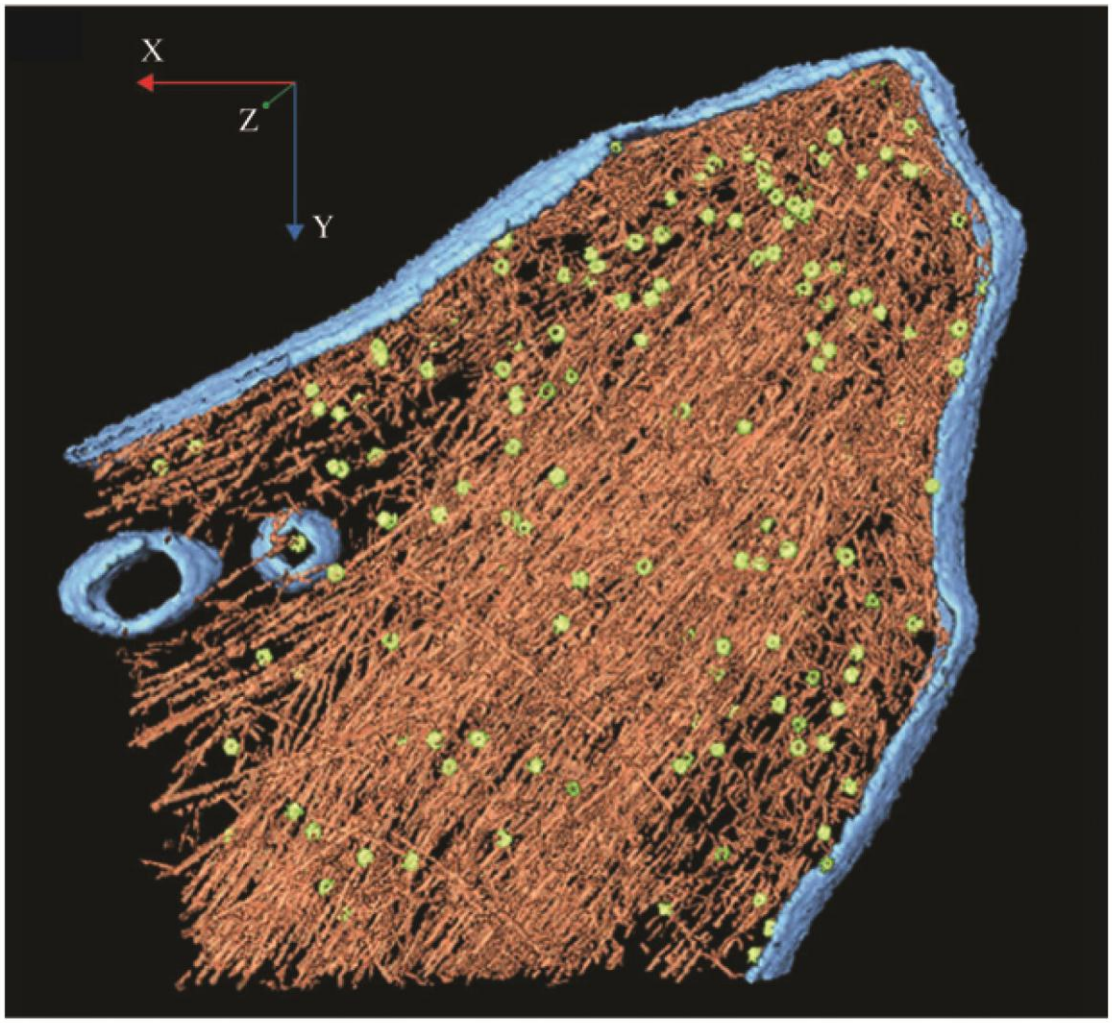

Figure 6. A multitude of molecules are known to associate with focal adhesions. One possibility is that only a select group of the many focal adhesion forming molecules are incorporated into a single maturing focal complex. This is possible given the high degree of competition between the various molecules for similar binding sites on other focal adhesion forming molecules. The multitude of focal adhesion forming molecules are shown here. Figure adopted from (220) with permission.

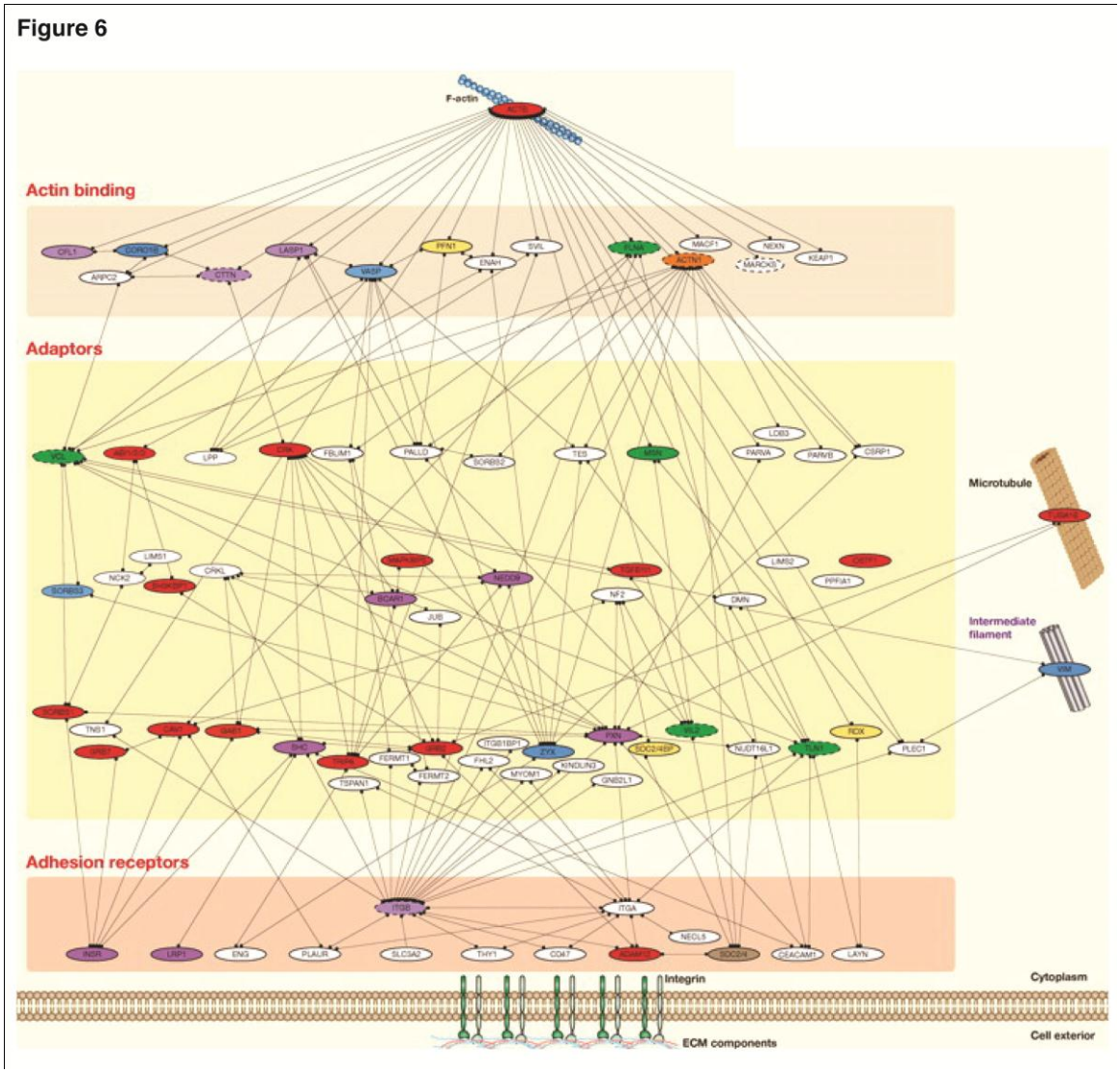

Figure 7. The dynamics of focal adhesion forming molecules are governed by either diffusion, exchange, or both. There exist three distinct domains at the focal adhesion: the focal adhesion domain, the juxtamembrane domain, and the cytoplasmic domain. Molecules in the focal adhesion domain are either fixed and not exhibiting dynamic behavior or their dynamics are governed solely by exchange. Molecules in the Juxtamembrane domain exhibit dynamic behavior governed by both exchange and diffusion. Molecules in the cytoplasmic domain exhibit behavior governed solely by diffusion. Figure adopted from (209) with permission.

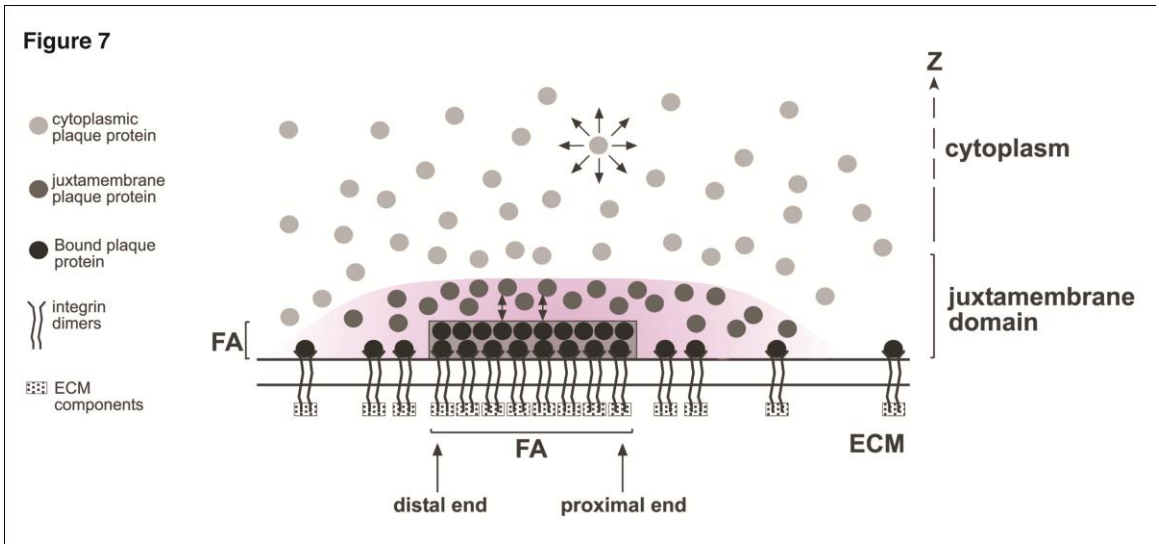

Figure 8. Integrin is a heterodimer with an α subdomain and a β subdomain. Each subdomain contains a cytoplasmic domain, a transmembrane domain, and an ectodomain. The heterodimer can adopt either an inactive or an activated conformation. Integrin activation can be caused by inside-out activation via binding of talin or kindlin to the β cytoplasmic subdomain, or by outside-in activation via binding of an agonist to the ectodomain. The activated conformation is characterized by an extended ectodomain conformation and separation of the α and β subdomains in the transmembrane region. Figure adopted from (114).

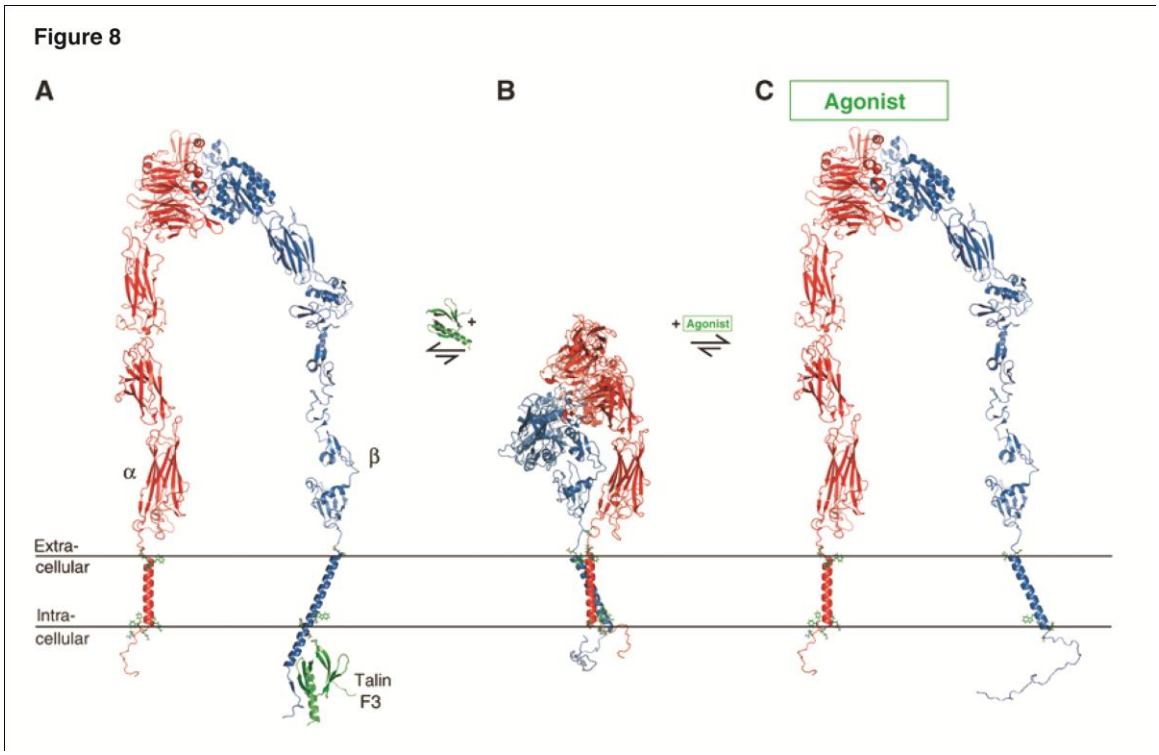

Figure 9. The integrin ectodomain contains a head domain and two leg domains separated by a knee region. In the bent conformation, the molecule is bend at the knee region between EGF1 and EGF2, bringing the upper leg domain near to the lower leg domain. Figure adopted from (227).

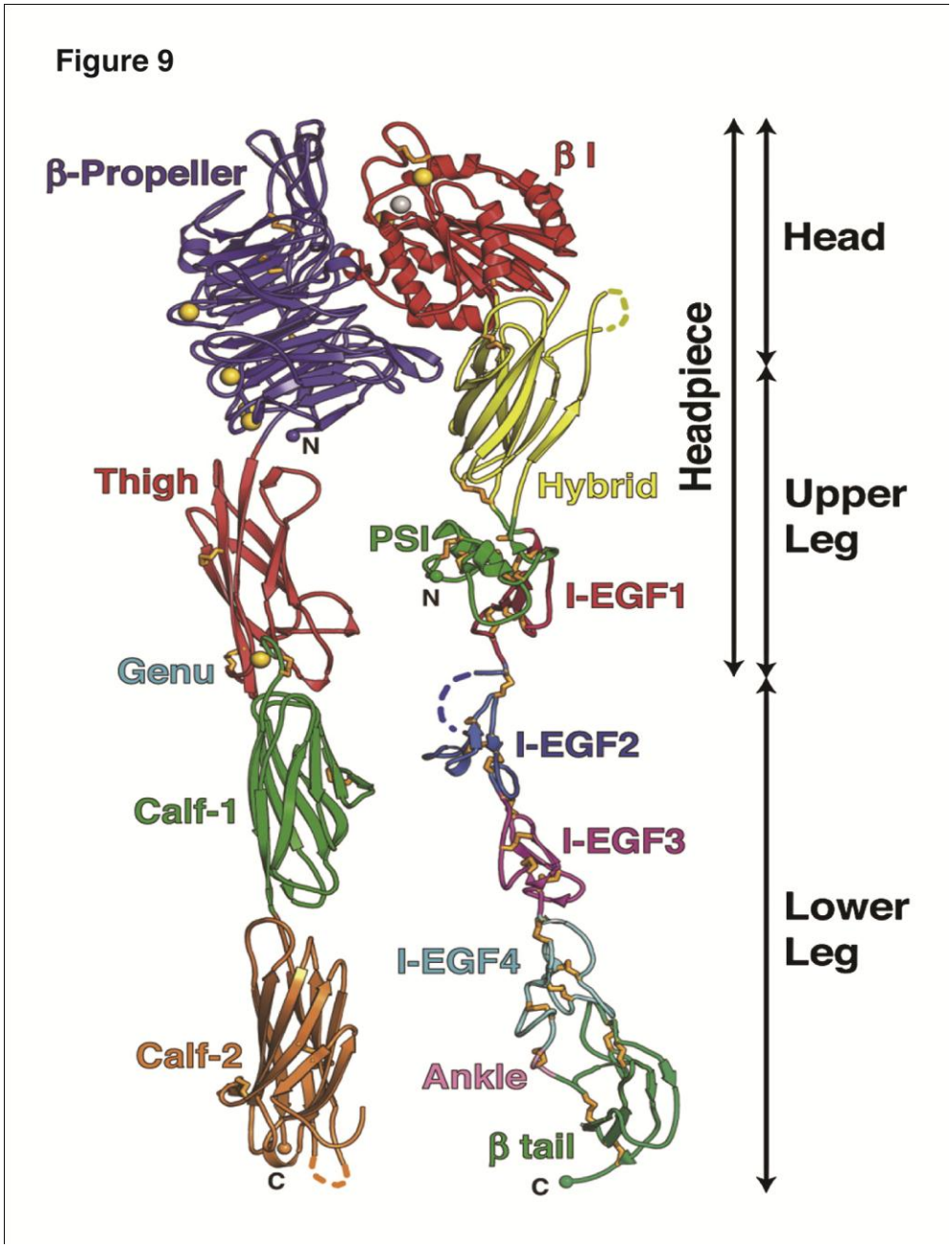

Figure 10. The integrin ectodomain can undergo transition into its extended conformation via an externally applied force in silico. (A) The molecular dynamics simulation technique was used to simulate integrin ectodomain extension. (B) Force was applied to the ectodomain in its bent conformation at residues involved in binding of integrin to the ECM. (C) The ectodomain could be extended to a partially extended conformation that would retract to the bent conformation if the force were removed, or it could be extended to a fully extended conformation that would persist even after removal of the extending force. Figure adopted from (37) with permission.

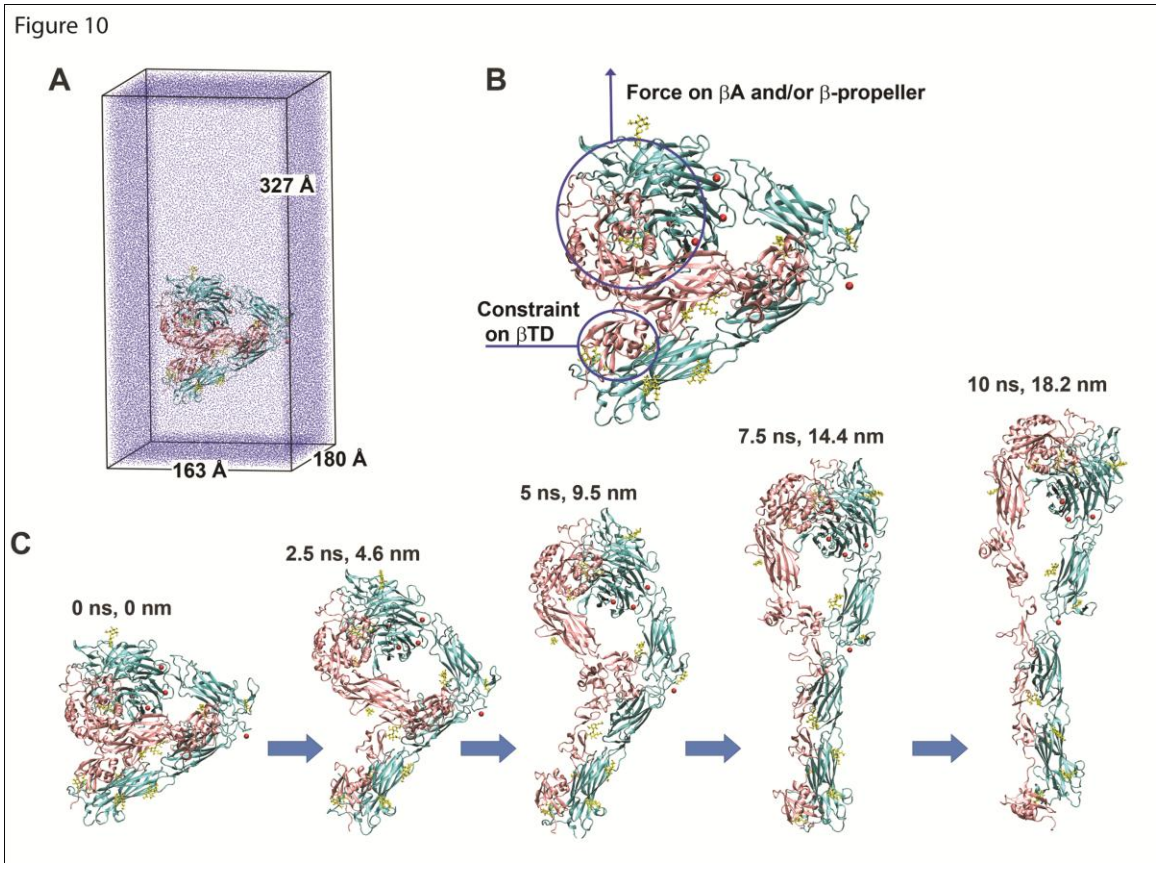

Figure 11. Talin is critical to the formation and maturation of nascent adhesions and focal adhesions. Talin has a head domain and a tail domain. Its head domain has a major binding site for the integrin β subdomain and a potential actin-binding domain. Its tail domain has many vinculin binding sites, two actin-binding domains, and potentially a second integrin-binding domain. Figure adopted from (44) with permission.

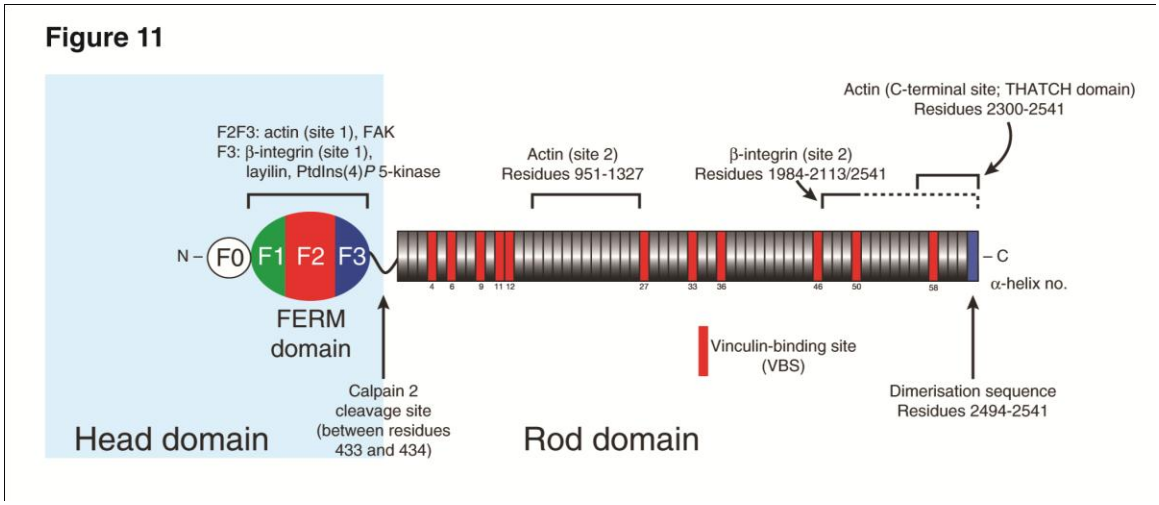

Figure 12. Talin dimerization results from the formation of a coiled-coil between the c-terminus helices of each monomer. Adjacent to the dimerization helix on each monomer is an actin-binding site. Each monomer alone cannot bind actin as the dimerization helix associated with the adjacent actin-binding region. Talin dimers, however, can bind actin filaments. The orientation of the talin dimers relative to each other is likely dynamic. The talin dimer can adopt a number of orientations including: a parallel dimer orientation, a V-shaped dimer orientation, and an extended dimer orientation. Figure adopted from (69).

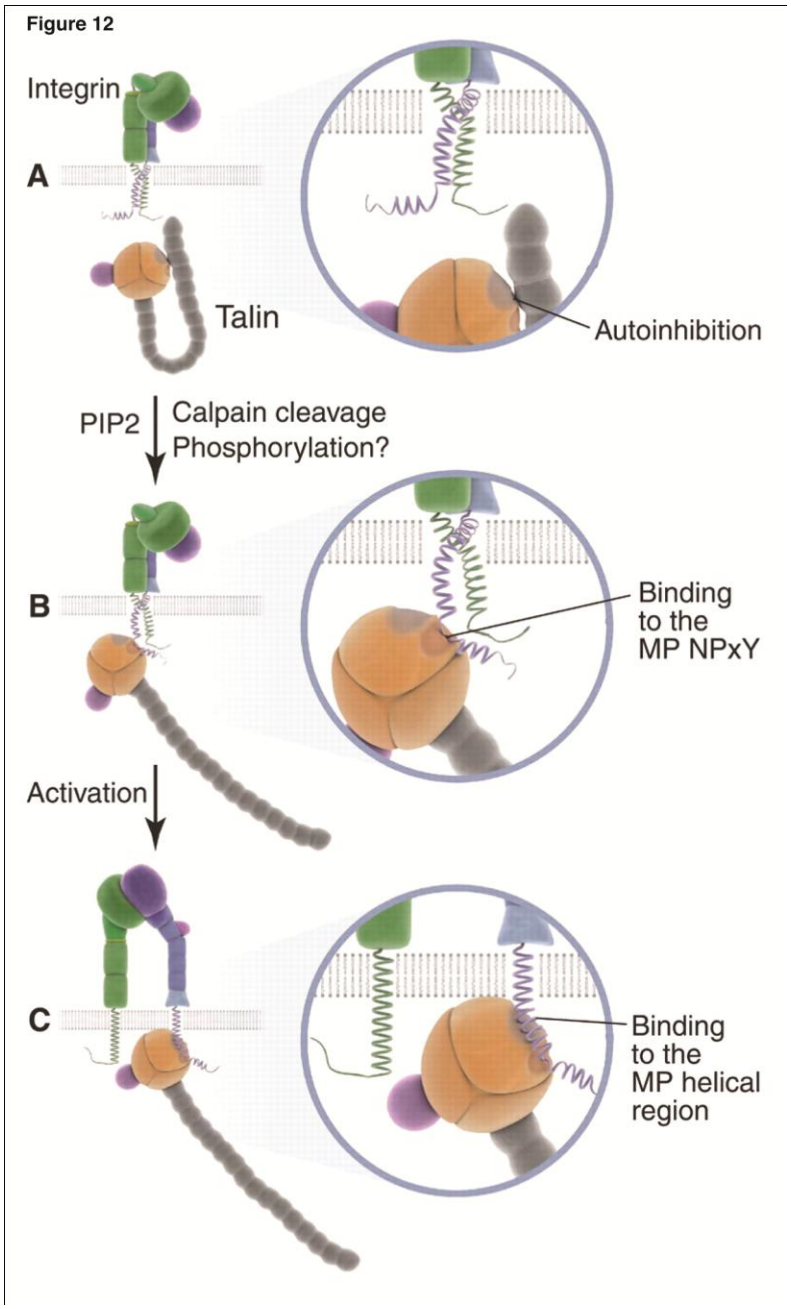

Figure 13. The talin rod domain contains many cryptic vinculin binding sites (VBS). As a suggested molecular mechanosensor talin could undergo force induced conformational changes activating these cryptic VBS regions. (A) Molecular dynamics simulations have tested the conformational response of talin rod domain exposure to force but applying a stretching force to a VBS contain region of the rod domain. (B) The VBS in this region is buried in the hydrophobic core of the talin rod domain prior to exposure to the stretching force, and (C) the VBS is rotated out of the hydrophobic core by the stretch of the talin rod. Figure adopted from (116).

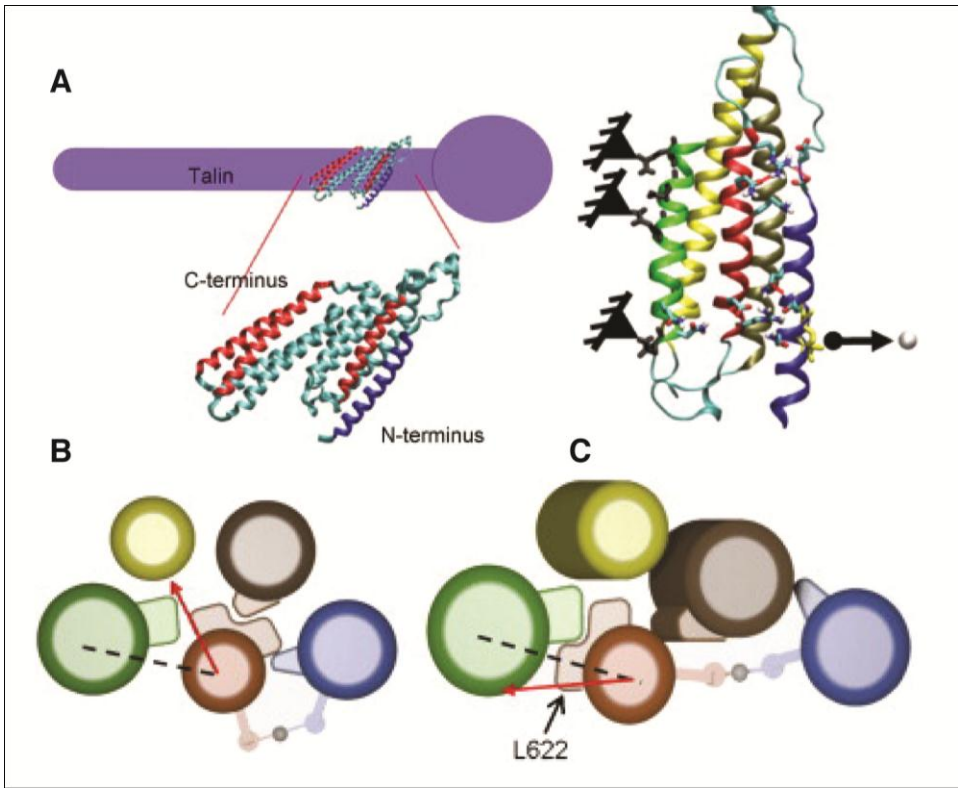

Figure 14. Vinculin is a molecular reinforcing agent. It is recruited to sites of force-induced focal adhesion formation. When optical tweezers are used to induce focal adhesion formation, fluorescently tagged vinculin molecules show recruitment to the force induced sites and correlate with the growth and maturation of the focal adhesion. Figure adopted from (59) with permission.

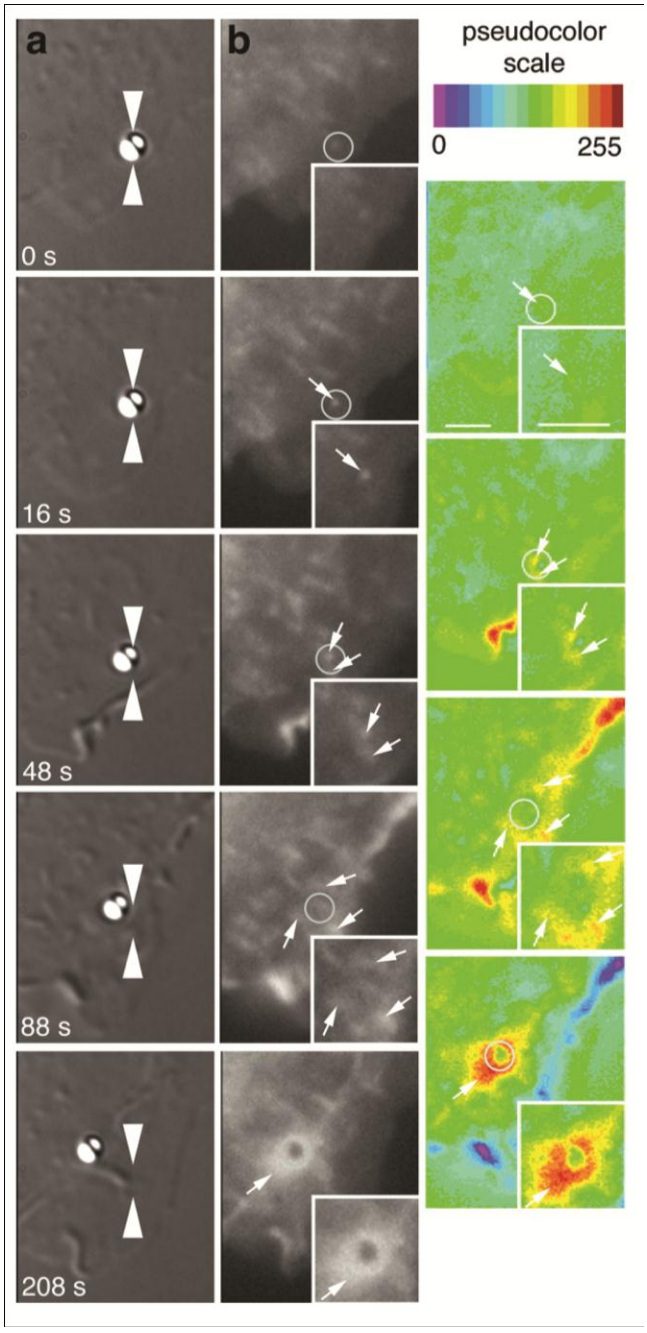

Figure 15. Vinculin is a helical bundle protein with 5 major domains: the vinculin tail (Red), domain 1 (blue), domain 2 (light blue), domain 3 (green), and domain 4 (yellow). Actin is suggested to bind at the vinculin tail while talin VBS and other VBS regions are suggested to bind at domain 1. Figure adopted from (9).

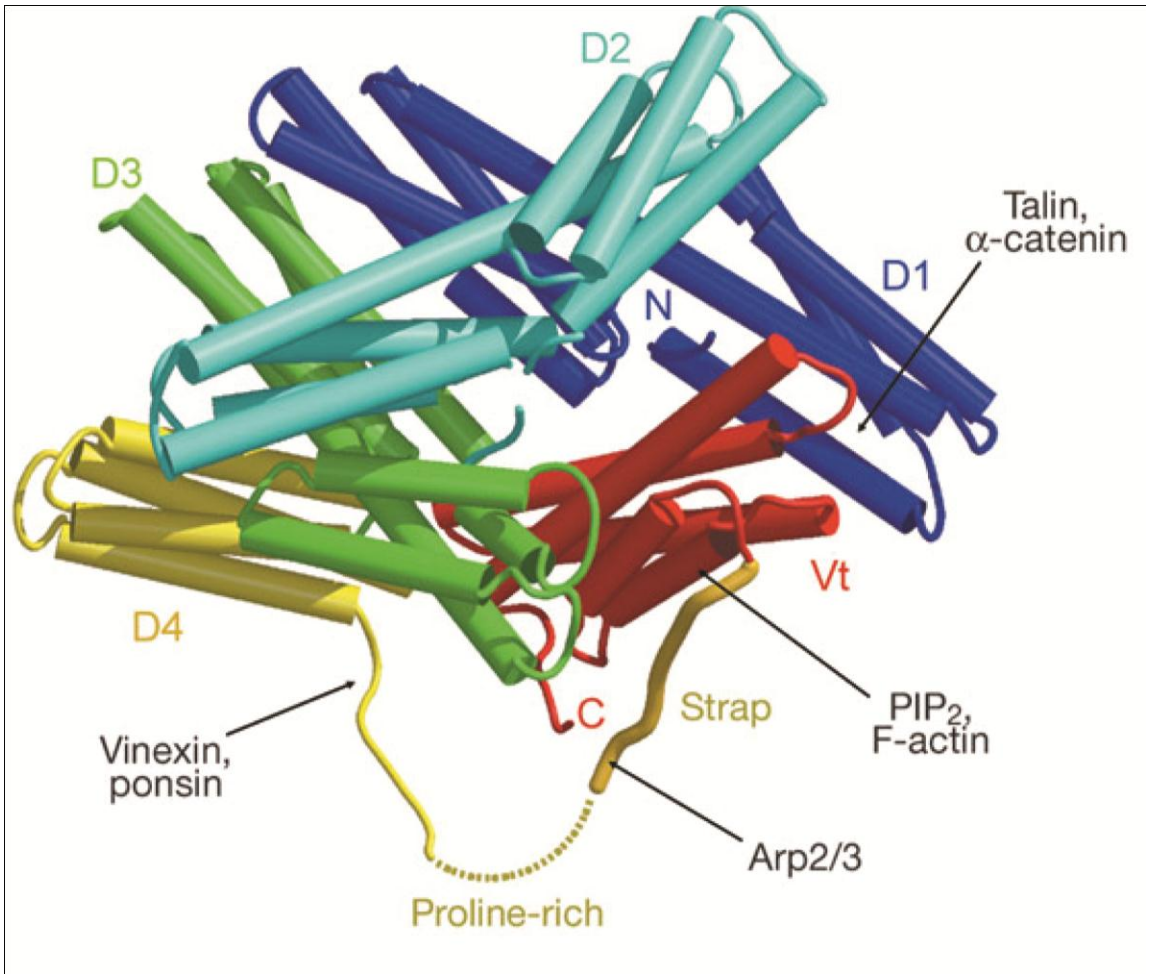

Figure 16. In its native conformation vinculin is in an auto-inhibited conformation. The proximity of D1 to Vt prevents binding of actin filaments to Vt, and the proximity of Vt to D1 potentially prevents binding of VBS to D1. Molecular dynamics simulation has been able to produce a suggested conformation for activated vinculin. It is suggested that D1 moves away from Vt during vinculin activation. Figure from (77).

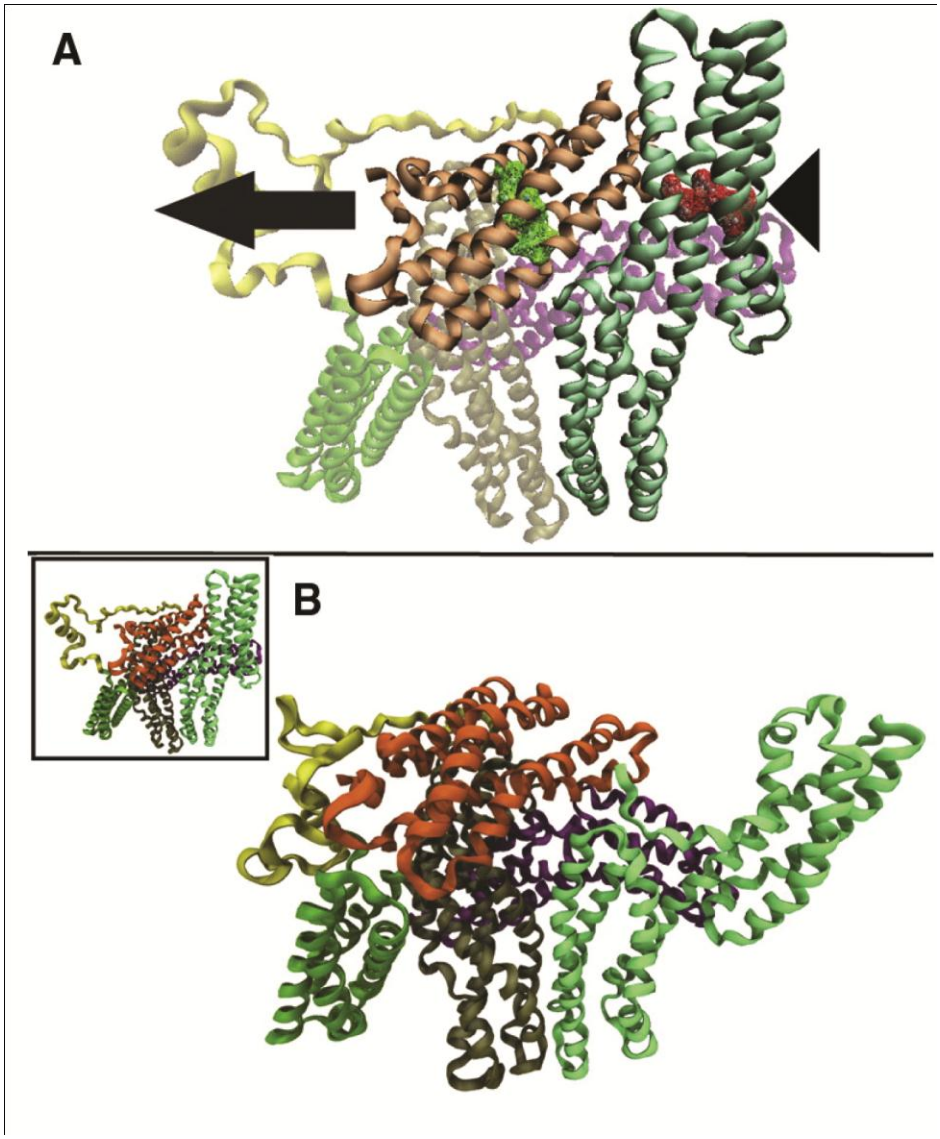

Figure 17. In order for vinculin to undergo activation D1 and Vt of vinculin need to separate. One possible mechanism by which vinculin can achieve activation is through a simultaneous binding event with its two binding partners actin and VBS. A simultaneous interaction of nearby actin filaments with Vt and nearby VBS regions with D1 would stretch vinculin; D1 would be attracted towards VBS and Vt would be attracted towards actin. The resulting stretch of vinculin could result in an activating conformational change. Figure adopted from (77).

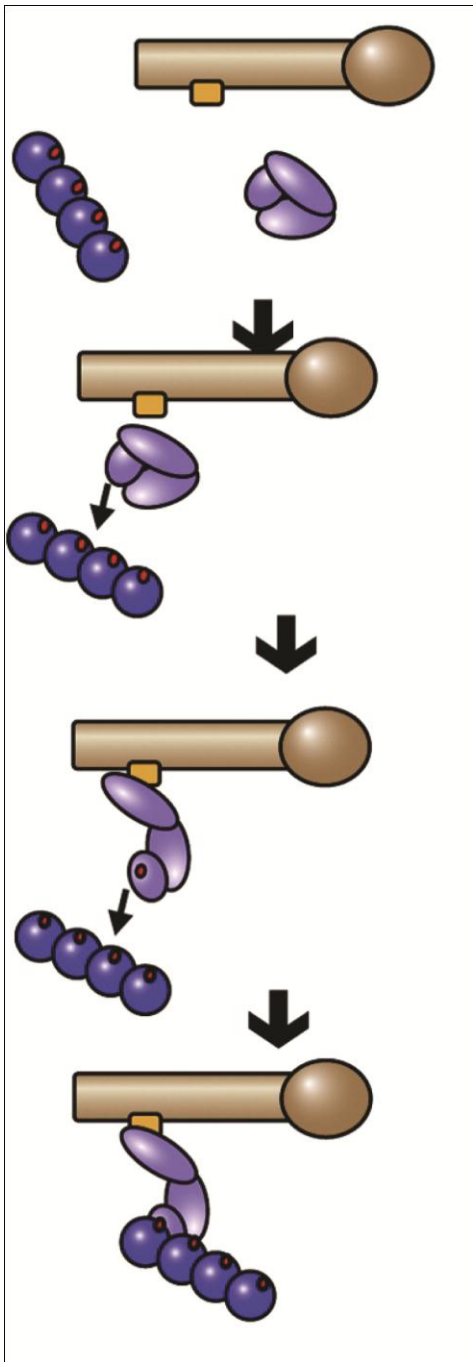

Figure 18. VBS binds vinculin by a three-step process: (1) half of VBS inserts between the helices in D1 but full insertion is not achieved without vinculin activation, (2) vinculin undergoes a stretch by the simultaneous attraction of Vt to actin and the surface interaction of D1 with the half inserted VBS, and (3) VBS fully inserts into D1 after vinculin activation. This three-step process suggests that VBS is unable to activate vinculin in the absence of a vinculin stretch. Figure adopted from (76).

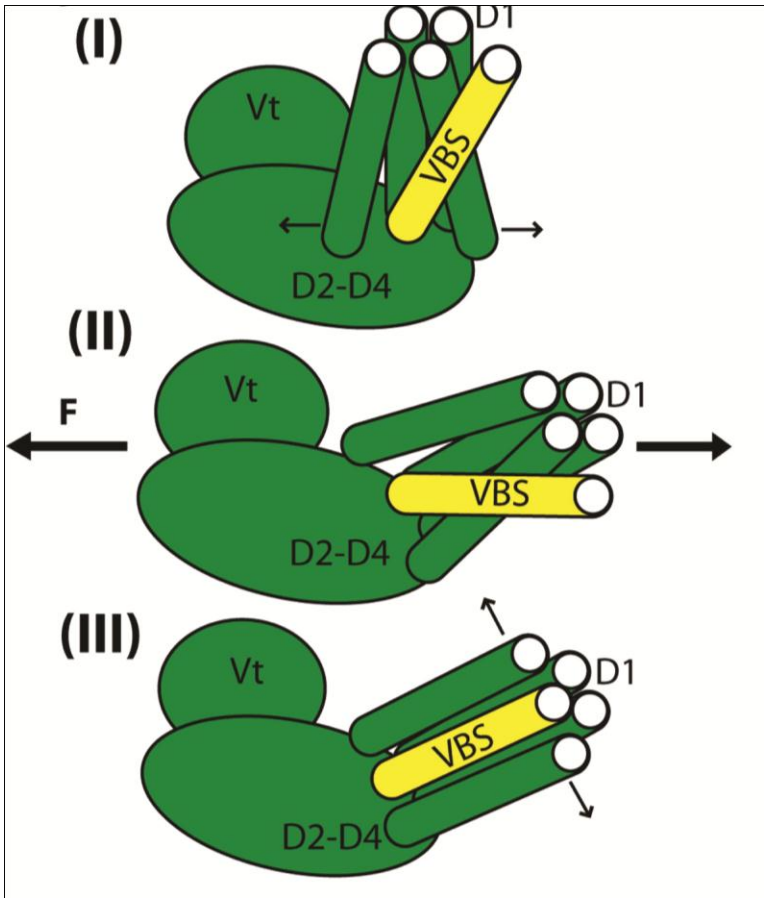

Figure 19. Integrin and talin are molecular mechanosensors, they alter their structure and function in response to their mechanical environment. One possible mechanism by which focal adhesions exhibit a mechanotransduction response is through the sequential mechanosensation of integrin and talin: (a) integrin exposure to a small force at its ectodomain causes a transient activated conformation, (b) the transiently activated integrin recruits a talin dimer in the parallel dimer orientation and a nascent adhesion is formed, (c) further exposure of the nascent adhesion to force results in the shift of the talin dimer from a parallel dimer orientation to a V-shaped dimer orientation and the nascent adhesion matures to a focal complex by binding more unique actin filaments, (d) the focal complex is exposed to larger forces that further extend the integrin ectodomain and cause a persistent activated conformation in integrin, (e) the larger forces also shift the talin dimer to an extended orientation maximizing the number of unique actin filaments it can bind and a focal adhesion is formed, (f) the recruitment of many actin filaments correlates with recruitment of many actin-binding and focal adhesion forming molecules, and (g) the recruited focal adhesion molecules recruit other integrin and talin molecular mechanosensors, further expanding the size of the maturing focal adheison.

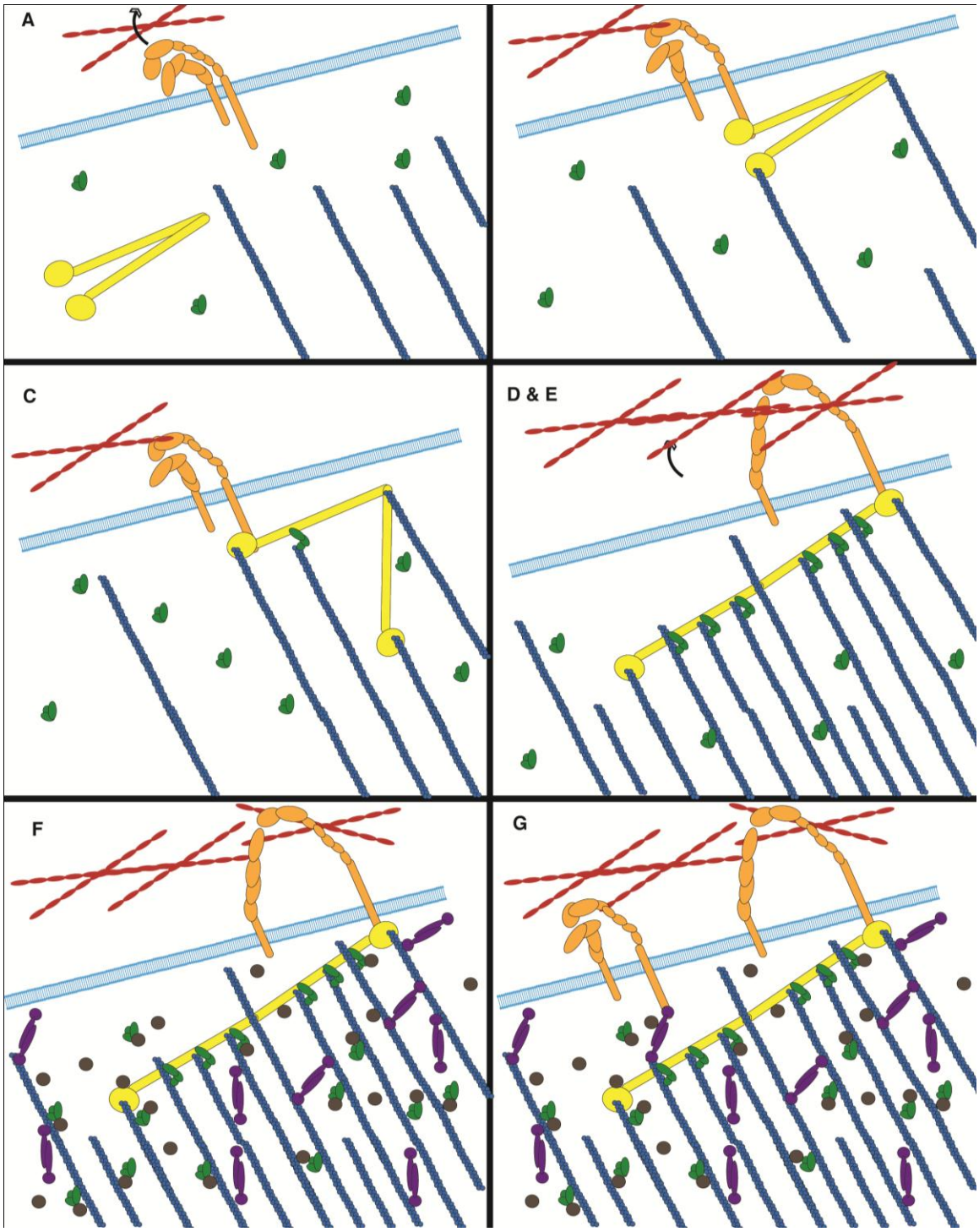
A
C
D & E
F
G

Section I:

The Mechanosensing of Talin

Mechanical Force Can Regulate Orientation of the Talin Dimer

Abstract
The formation of focal adhesions and a stable cell-substrate contact can be regulated by mechanical stimulation. Individual proteins that make up the focal adhesions, such as talin, can exhibit mechanosensing. Previously one mode of talin mechanosensing had been described in which the vinculin-binding site of talin is exposed after force induced stretch of a single talin rod domain. Presently a second mode of talin mechanosensing is described in which the talin dimer itself can adopt different orientations in response to mechanical stimulation. Using molecular dynamics, first, it is demonstrated that the C-terminus region of the talin dimer is flexible mainly at the linker between the dimerization helices and the nearby actin-binding helical bundle. Then, molecular dynamics simulation reveals two possible orientations of the talin dimer at its C-terminus. The extracellular matrix (ECM) bound integrins cross-linked by talin can be forced apart leading to an elongated orientation of the talin dimer, and the ECM bound integrins can be forced together by the ECM producing a collapse orientation of the talin dimer. Formation of the elongated orientation is shown to be more favorable. Switching between the two talin dimer orientations constitutes a mode of mechanosensing.

Introduction

A variety of cell types and cellular processes rely heavily on the formation of a stable linkage between the cell and its substrate (Hoffman et al., 2011). The linkages create a mechanical interface between the cell and its environment that can govern cellular structure and behavior, for example: cancer cell metastasis is governed by the stiffness of its extra cellular matrices (ECM) (Kumar and Weaver, 2009); stem cell differentiation is governed by the specific mechanical properties of its ECM (Discher et al., 2009); endothelial cell shape is governed by the pattern cyclic mechanical load from blood flow (Ngu et al., 2010); and cellular movement is wound healing requires mechanical interaction with its substrate (Zaidel-Bar et al., 2003). A focal adhesion structure underlies the mechanical linkage and acts to cement the ECM bound integrins (Askari et al., 2010) to cytoskeletal actin filaments (Humphries et al., 2007). One hypothesis concerning mechanically regulated focal adhesion formation asserts that individual proteins can act as molecular mechanosensors, or switches, whose structure and function can be governed by the level and source of mechanical stimulation (Moore et al., 2010).

The simplest adhesion structure that could link the cytoskeleton to ECM bound integrin would consist of merely 1 protein: talin (Jiang et al., 2003). Talin is universally recruited to focal adhesions, and even smaller nascent adhesions (Bruinsma, 2005) or weaker 3D matrix adhesions (Fraley et al., 2010). Mechanosensing by talin has previously been suggested and explored (Lee et al., 2007). Talin has an integrin-binding head domain (Critchley and Gingras, 2008), and

a rod domain consisting of: 11 vinculin-binding sites (Gingras et al., 2005), at least two actin-binding sites (Hemmings et al., 1996), and a second integrin binding site (Roberts and Critchley, 2009). Talin is suggested to exist as a dimer when bound to actin filaments (Goldmann et al., 1994). The talin dimer is anti-parallel and initial reports suggest the talin dimer to be Y-shape (Winkler et al., 1997) and also a dumbbell shape (Hemmings et al., 1996). More recent investigation suggests variability in the shape of the talin dimer (Gingras et al., 2008). Previous studies have explored at least one mode of talin mechanosensing: force induced activation of its cryptic vinculin-binding sites (del Rio et al., 2009; Golji et al., 2011; Hytönen and Vogel, 2008; Lee et al., 2008; Lee et al., 2007).

Talin is large: over 2500 residues in sequence, and about 270 Kda in mass (Roberts and Critchley, 2009). Structural investigations have solved crystal structures of multiple domains throughout talin, but not of the entire talin protein (Roberts and Critchley, 2009). The talin head domain is known to have an integrin-binding region called the FERM domain, whose structure has been approximately solved (Elliott et al., 2010). The talin rod domain consists of a multitude of helical bundles, the structure of several of which have been solved (Roberts and Critchley, 2009). Recently, the structure of the C-terminus dimerization domain along with a nearby actin-binding helical bundle – often referred to as the talin/HIP1R/Sla2p actin tethering C-terminal homology (THATCH) domain – has also been solved (Gingras et al., 2008). Throughout the rod domain, and especially between the dimerization domain and the THATCH domain are linker regions thought to be flexible. It is likely that the flexibility of the linker regions impart orientation flexibility to the talin dimer allowing it to adopt different dimer orientations.

In this study the flexibility at the C-terminus end of the talin rod domain is explored using molecular dynamics. In addition, the effect of mechanical stimulus on the specific orientation adopted by the talin dimer at its C-terminus is explored. The different mechanical loads likely experienced by talin are simulated and the predicted structures of the talin dimer at each load are predicted. A free energy profile of talin dimer orientation elongation is also produced.

Methods

Initial Structure

PDB ID 1SJW is used for the structure of the actin-binding helical bundle near the dimerization helices, and PDB ID 2QDQ was used for the structure of the dimerization helices, both from Gingras et al (Gingras et al., 2008). The missing linker region was built by homology modeling using in house code. Chimera (Pettersen et al., 2004) was used to arrange the C-terminus regions together and connect the linker to both the dimerization helix structure and the actin-binding bundle structure.

Molecular Dynamics

Simulations were carried out using NAMD (Phillips et al., 2005) and molecular visualization and analysis was carried out using VMD (Humphrey et al., 1996). Periodic boundary conditions were used. Rigid bonds to hydrogen atoms were used (Kraeutler et al., 2001) along with a 2fs timestep. Simulations were carried out using the CHARMm 27 force fields (Lazaridis and Karplus, 1999), the Langevin piston Nose-Hoover pressure control algorithm, and the Langevin damping thermostat for temperature control. Pressure was maintained at 1 atm and temperature at 310K with a damping coefficient of 5 /ps.

Five trials of the talin dimer C-terminus region were simulated at equilibrium. Each trial was initially minimized for 1000 steps using the conjugate gradient and line search algorithm implemented in NAMD (Phillips et al., 2005). Following minimization each configuration is simulated for 5ns or until equilibrium is reached. The final structures from each of the trials are compared after structural alignment in VMD (Humphrey et al., 1996). For simulation of elongation of the talin dimer a constant velocity pull of 1 m/s with a spring constant of 20 Kcal/mol*Å^2 was used. Residues 2445, 2385, 2369, and 2300 of one monomer were pulled away from the same residues on the other monomer. For simulation of collapse of the talin dimer the same constant velocity pull is applied to the same residues at both monomers while 2497 and 2529 of the dimerization domain are constrained harmonically. The direction of pull is defined as away from the center of mass of the held residues, towards the center of mass of the pulled, residues, and orthogonal to the pull used to elongate the talin dimer. Both pull simulations were run for 10ns.

Umbrella Sampling

The umbrella sampling method (Torrie and Valleau, 1977) was used to sample the free energy changes as the talin dimer (C-terminus region) is elongated. All sampling was carried out using GROMCAS (Van Der Spoel et al., 2005) and the final PMF was calculated using Grossfield's WHAM code (Kumar et al., 1992). A periodic box of 250Å by 90Å by 80Å is used along with 57800 water molecules for each simulation. The reaction coordinate is defined as the distance between residues 2445, 2385, 2369, ad 2300 of talin monomer A and 2445, 2385, 2369, and 2300 of talin monomer B. The residues at the end of monomer B are defined as the pull group and pulled away along the reaction coordinate. An umbrella of 1000 Kj/mol*nm^2 was used along with a reference step of 3 Å to produced the sampling. The α-carbon of the residues at monomer A were harmonically constrained with 1000 Kj/mol*nm^2.

Results

Residues 2300-2541 of the talin rod make up its C-terminus end (Critchley and Gingras, 2008). The structure of the dimerization domain, a single helix made up of residues 2496 to 2529, is taken from PDB ID 2QDQ (Gingras et al., 2008). The structure of the nearby actin-binding bundle (residues 2204 to 2483) containing the

THATCH domain is taken from PDB ID 1SJW (Cavasotto and Phatak, 2009; Gingras et al., 2008). The linker region between the two crystal structures is build using homology modeling (Cavasotto and Phatak, 2009). The resulting talin C-terminus structure (Figure 1) is used in simulation. The structure adopted by the C-terminus of each monomer could signal the structure of the entire dimer. Two talin monomers are held together only by the dimerization domain. The orientation of the C-terminus actin-binding bundle relative to the dimerization domain would determine the orientation of one monomer relative to the other.

Flexibility at the talin C-terminus

To determine the flexibility of the C-terminus region several trials of molecular dynamics were produced. No external constraints or forces were used in these trials. Simulation until equilibration (over 5ns) in each of the trials showed flexibility in the homology modeled linker region between the dimerization domain and the actin-binding bundle (Figure 2 and 3).

Residues 2484 to 2495 of the C-terminus end make up the flexible linker (Figure 2). These 12 residues lack an inherent structure. In one simulation two stabilizing interfaces were formed at the linker regions (Figure 2 B), but no consistent structure was formed across both linker regions and 5 trials. The flexibility at the linker region likely impacted the observed overall flexibility of the C-terminus domains.

Structural alignment of the 5 different equilibrated structures shows the C-terminus region can adopt a variety of angles between the dimerization domain and the helical bundle (Figure 3). Two orthogonal angles can be defined between the dimerization domain and the actin-binding helical bundle: the α-angle, the in-plane angle between the dimerization domain and the bundle (Figure 3), is defined by residues Q2529, D2482, and G2374; and the β-angle, the out-of-plane angle between the dimerization domain and the bundle (Figure 3 inset), is defined by Q2527, I2499, and D2482. Across the different trials, the α-angle tended to increase after equilibration (Figure S1 A) whereas the β-angle tended to decrease after equilibration (Figure S1 B). The trials showed more variability amongst the α-angle than the β-angle, suggesting more flexibility in the in-plane elongation of the talin dimer. To determine regions of flexibility the average fluctuation of each residue (RMSD per residue) is calculated for all trails (Figure 3). Two fluctuation values are reported for each structure, one for each talin monomer. The results show flexibility in the C-terminus region is demonstrated by: (i) the linker between helices in the helical bundle, and (ii) the linker region between the bundle domain and the dimerization domain. This flexibility is expected given the unstructured nature of the linker region (Figure 2). Given its flexibility any conformational change at the C-terminus region is predicted to present as changes in the angle between the bundle and the dimerization helices and perhaps stretching of the linker region.

Talin dimer conformational changes after mechanical load

The orientation that the two actin-binding bundles adopt relative to the dimerization helices at the C-terminus region could govern the orientation that the two talin monomers adopt relative to each other. The flexibility at the linker between the dimerization helix and the actin-binding bundle suggests a variety of orientations could be adopted. To determine the impact of mechanical load on the specific orientation adopted, molecular dynamics is used to simulate the force-induced conformational changes at the C-terminus.

At the focal adhesion, the talin dimer is likely crosslinking two ECM bound integrins (Lepzelter and Zaman, 2010). Forces from outside the cell could either move an integrin apart from the cross-linked integrin (Figure 4 inset) or move the two integrins towards each other (Figure 5 inset). In the case where the integrins are forced apart from each other the resultant of that force would be the stretching of the talin dimer C-terminus region. This force is simulated *in silico* by applying a force on one monomer away from the other monomer. Residues near the end of each monomer likely to form stabilizing interactions with the adjacent helical bundle on the rod domain – residues K2445, D2385, E2369, and D2300 – are the direct subjects of force at one end, and the same residues are harmonically held at the other end (Figure 4). A stretching velocity is applied at a constant rate of 1 m/s for 10ns. After stretch the C-terminus region shows little unfolding of the helical structure in either the actin-binding bundle or the dimerization helices. One α-angle is increased from 48° to 166° (Figure S2 A) and the actin-binding bundle closest to the pull has reoriented itself relative to the dimerization helices. Continued stretch would likely cause reorientation at the other actin-binding bundle as well. The flexible linker region becomes extended by the end of the simulation. The flexibility of the linker region allows the C-terminus region (and potentially the entire talin dimer) to adopt a new conformation consistent in response to the movement of the two integrins apart. A structure of the talin C-terminus after extension is suggested (Figure 4).

The movement of two integrins towards each other would result in a force at the C-terminus region on both actin-binding bundles towards each other. We simulate this force by applying a force at residues K2445, D2385, E2369, and D2300 at the ends of both bundles in a common direction. To prevent translation of the entire complex residues 2497 and 2529 at the ends of each dimerization helix are harmonically constrained. The pull direction is defined by the vector from the average of the held residues towards the average of the pulled residues. A constant velocity of 1 m/s is used to simulate the conformational changes within 10ns. The resulting conformation (Figure 5) shows the two actin-binding bundles have collapsed near to each other, the linker region has extended, and little helical structure is lost at either the actin-binding bundle or the dimerization helices. The β-angle between the dimerization helices and both actin-binding bundles is decreased from 132° to 81° and from 150° to 116°, at the two monomer (Figure S2 B). The forcing of the two

integrins towards each other is likely to cause the C-terminus region of the talin dimer crosslinking the integrins (and likely the entire talin rod domain) to collapse onto each other and adopt the conformation predicted form simulation (Figure 5). Comparison of α-angle and β-angle changes from equilibration to changes from simulation suggests both the elongation of the talin dimer from integrins forced apart and the collapse of the talin dimer from integrins forced together can be consistent with the conformational flexibility of at the C-terminus region.

Free energy profile of talin dimer elongation

To thermodynamically determine the likelihood of a talin dimer C-terminus region elongation, and more directly evaluate the impact of its flexibility, we used umbrella sampling (Torrie and Valleau, 1977) to determine the potential of mean force (PMF) to a transition of the talin dimer from our initial guessed structure (Figure 1) to the predicted elongated structure (Figure 4). Calculation of the PMF shows that there is a free energy *decrease* after elongation of the C-terminus structure of around 16 KT (Figure 6). This suggests elongation of the dimerization domain is favorable and could be adopted with only kinetic forces. Movement of two integrins bridged by a talin dimer apart would more easily result in reorientation of the talin dimer to an elongated conformation than movement of two integrins bridged by talin towards each other. This is consistent with the level of forces needed to achieve both conformational changes within 10ns of simulation (Figure S3). Although the magnitude of these forces are not useful – the rate of the conformational changes *in vivo* would be orders of magnitude slower than the rates used in this study – the different in force between the two conformational changes can be analyzed. The free energy profile and the difference in forces suggest that higher magnitude stimulation will be necessary to collapse the talin dimer than to elongate the structure.

Discussion

Molecular dynamics simulation of the dimerization domain of talin, and its nearby C-terminus region demonstrated: (i) the flexibility of the linker between the dimerization helices and the rod domain helical bundles (Figure 3), (ii) the ability of ECM-induced forces to regulate the orientation of the talin rod domains relative to the dimerization helices (Figure 4 and 5), (ii) a predicted structure of an elongated talin dimer (Figure 4), (ii) a predicted structure of a collapse talin dimer (Figure 5), and (iv) the favorability of elongation of the talin dimer (Figure 6). Taken together, the simulations establish the possibility of a second mode of talin mechanosensing: that the talin dimer could alter its orientation in response to forces from the ECM.

A number of studies have considered the possibility of talin mechanosensing (del Rio et al., 2009; Hytönen and Vogel, 2008; Lee et al., 2007). Initially, molecular dynamics simulation of a helical bundle from the talin rod showed that the cryptic vinculin-binding site can become activated after mechanical stress (Lee et al., 2007). Thereafter, experimental studies confirmed the suggestion and demonstrated that

stretching of a single talin rod domain would activate that domain for binding to vinculin (del Rio et al., 2009). Other researchers have also addressed this possibility and confirmed the suggestion further (Carragher and Frame, 2004; Critchley and Gingras, 2008; Hytönen and Vogel, 2008; Patel et al., 2006). The force that would stretch a talin rod domain would result from an actin filament (Carragher and Frame, 2004). Talin can link integrin at its head domain and link actin at the C-terminus region actin-binding bundle. Movement of the actin filament (after linking to the talin C-terminus) or contraction of the actin filament would result in stretching of a talin (Geiger et al., 2009). There are 11 cryptic vinculin-binding sites within the talin rod. The stretch of talin would activate each rod for binding the vinculin and thereby a new actin filament (Figure 7 A). This first mode of talin mechanosensing is a response to forces that are initiated from within the cell, likely by myosin contraction (Gardel et al., 2010).

The second mode of talin mechanosensing is likely to be a response to forces that are initiated from without the cell, likely from ECM movement (Figure 7 B). The talin dimer likely adopts a more elongated structure when crosslinking or bridging to ECM bound integrins (Figure 5). This notion is supported both by the PMF calculated in this study (Figure 6) and the small-angle X-ray scattering (SAXS) result from Gingras et al (Gingras et al., 2008). As two integrins are forced together the talin dimer is forced to adopt a new more compact orientation. The C-terminus region is likely to adopt a compact conformation with the two helical rod domains collapsed onto each other (Figure 4). If the other rod domain regions continue from the helical bundle in the C-terminus region, then the talin protein will adopt a conformation with the two rod domains collapse onto each other. The collapsed conformation reduces the number of actin filaments that could bind the talin dimer and vinculin-binding sites from the two monomers would be likely binding to the same actin filaments (Figure 7 B). In contrast, elongation of the talin dimer and the elongated orientation of the C-terminus region would likely allow for each vinculin-binding site (22 total in the talin dimer) to bind a unique actin filament (Figure 7 B). The second mode of talin mechanosensing, in response to forces from outside the cell, presents itself as a change in the orientation of the talin monomers relative to each other. Not only is the conformation of the rod domain near each vinculin binding site force dependent, but the orientation of the talin dimer is also force dependent.

It is interesting to consider the possible sources of a force that would move integrins apart or close together. One possibility is that an external force on the tissue itself is transduced to the integrins through the ECM of the tissue. Such a force could be experimentally controlled, either *in vivo* or *in vitro*, and the predicted talin dimer conformation could be tested. Another possibility would have the second mode of talin mechanosensing dominate mechanotransduction in endothelial cells (Pahakis et al., 2007) where shear stress on the ECM and integrins would cause reorientation of the talin dimer.

The second mode of talin mechanosensing is independent of myosin contraction. Even without actin filaments bound either the C-terminal region actin-binding site or another actin-binding site, the talin dimer will likely react by dimer reorientation in response to mechanical stimulation from outside the cell. This is of particular importance in thinking about focal adhesion like structures that are formed in a cell immersed in a 3-D matrix (Cukierman et al., 2001; Fraley et al., 2010; Kubow and Horwitz, 2011). This focal-adhesion is smaller, and is shown to form in the absence of myosin contraction (Fraley et al., 2010). Furthermore, talin is consistently recruited to these structures but vinculin is not. Vinculin plays a crucial role in connecting actin filaments to the talin rod, and has been shown previously to potentially be mechanosensing (Golji and Mofrad, 2010; Grashoff et al., 2010; Ziegler et al., 2006). In the absence of vinculin at the 3-D focal adhesions, and in the absence of myosin contraction, talin can maintain a mechanosensing role through reorientation of its dimer (Figure 7 B). This would predict then that the focal adhesions at 3-D interfaces are also mechanoresponsive.

The suggestions from the molecular dynamics presented here are consistent with a number of studies aimed at understanding the talin structure and the overall structure of the focal adhesions. In their presentation of the structures of the dimerization helices and the nearby actin-binding bundle, Gingras et al (Gingras et al., 2008) considered the orientation of the talin dimer. Their considerations suggest talin to adopt a more elongated orientation at the C-terminus region and further suggest several talin dimer orientations to be possible. The results in this study consider include a modeled structure of the linker region but confirm that the elongated dimer orientation is favorable (Figure 6). The flexibility of the linker region allows for other orientations to be adopted and for the mechanosensing response.

Other studies aimed at understanding the impact of ECM organization on focal adhesion structure suggest a separation of at most 60nm between successive RGD residues in ECM is necessary to form stable and larger focal adhesions (Massia and Hubbell, 1991; Roca-Cusachs et al., 2009; Schvartzman et al., 2011). Earlier studies also measured the talin dimer to be likely 56 +/_ 7 nm in length (Winkler et al., 1997). The length of the dimer has been shown to be dependent on the ionic strength of the solvent. The 56-60nm length corresponds to an elongated talin dimer orientation. RGC residues placed further than that are beyond the reach of even an elongated talin dimer. By crosslinking two integrins the talin dimer allows a scaffold onto which the focal adhesion can develop (Dubash et al., 2009). That the talin dimer could adopt other sizes with different ionic solvent strengths supports our notion of other talin dimer orientations, but also suggests additional structural mechanisms could be contributing to the length of the talin dimer, beyond just the orientation at the C-terminus region.

Understanding the structure and the orientation of the talin dimer can impact the outstanding understanding of focal adhesion formation. The simulations presented here suggest that multiple modes of mechanosensing exist, at least for the talin

protein. The source of the mechanical stimulation, the magnitude of the mechanical stimulation, and the direction of any force can differentiate which mode of mechanosensing is operating. In the case of a ECM based stimulus that would occur in the absence of a mechanical stretch it is likely that the talin dimer will reorient itself. In the case of a myosin induced actin filament contraction, stretch of the talin rod and activation of individual vinculin-binding sites is likely. The two modes will act together. Perhaps the talin dimer reorientation occurs initially in response to smaller activating forces from outside the cell. This would allow a foundation to be formed for focal adhesion formation on the talin dimer. Later forces across the talin dimer originating from inside the cell could contribute to recruitment of a multitude of vinculin to this scaffold. And with the recruitment of vinculin, other actin filaments, and other focal adhesion forming molecules the focal adhesion would grow and mature.

The talin structure considered in this study restricted the predictions of force-induced orientation changes to only the C-terminus residues of talin. Although a complete structure of the entire talin protein is not yet solved, a creative effort to model the missing residues, or build approximate structures (or even solve crystal structures) of the remaining regions from talin would extension of the analysis presented here to the entire talin structure. Such a simulation could expand our predictions of the force induced talin dimer orientation changes. Beyond further *in silico* studies, experimental studies are called for to test the predictions presented here and investigate the possibility of a second mode of talin mechanosensing. As our understanding of the focal adhesion mechanosensors advances we can begin to arrive at a more complete picture of the focal adhesion, of cell-substrate adhesion, and of the mechanisms by which the cell can interact with its mechanical environment.

References

Askari, J.A., Tynan, C.J., Webb, S.E., Martin-Fernandez, M.L., Ballestrem, C., and Humphries, M.J. (2010). Focal adhesions are sites of integrin extension. J Cell Biol *188*, 891-903.

Bruinsma, R. (2005). Theory of force regulation by nascent adhesion sites. Biophys J *89*, 87-94.

Carragher, N.O., and Frame, M.C. (2004). Focal adhesion and actin dynamics: a place where kinases and proteases meet to promote invasion. Trends Cell Biol *14*, 241-249.

Cavasotto, C.N., and Phatak, S.S. (2009). Homology modeling in drug discovery: current trends and applications. Drug Discov Today *14*, 676-683.

Critchley, D.R., and Gingras, A.R. (2008). Talin at a glance. J Cell Sci *121*, 1345-1347.

Cukierman, E., Pankov, R., Stevens, D.R., and Yamada, K.M. (2001). Taking cell-matrix adhesions to the third dimension. Science *294*, 1708-1712.

del Rio, A., Perez-Jimenez, R., Liu, R., Roca-Cusachs, P., Fernandez, J.M., and Sheetz, M.P. (2009). Stretching Single Talin Rod Molecules Activates Vinculin Binding. Science *323*, 638.

Discher, D.E., Mooney, D.J., and Zandstra, P.W. (2009). Growth factors, matrices, and forces combine and control stem cells. Science *324*, 1673-1677.

Dubash, A.D., Menold, M.M., Samson, T., Boulter, E., Garc a-Mata, R., Doughman, R., and Burridge, K. (2009). Focal adhesions: new angles on an old structure. International review of cell and molecular biology *277*, 1-65.

Elliott, P.R., Goult, B.T., Kopp, P.M., Bate, N., Grossmann, J.G., Roberts, G.C., Critchley, D.R., and Barsukov, I.L. (2010). The Structure of the talin head reveals a novel extended conformation of the FERM domain. Structure *18*, 1289-1299.

Fraley, S.I., Feng, Y., Krishnamurthy, R., Kim, D.-H., Celedon, A., Longmore, G.D., and Wirtz, D. (2010). A distinctive role for focal adhesion proteins in three-dimensional cell motility. Nat Cell Biol *12*, 598-604.

Gardel, M.L., Schneider, I.C., Aratyn-Schaus, Y., and Waterman, C.M. (2010). Mechanical integration of actin and adhesion dynamics in cell migration. Annu Rev Cell Dev Biol *26*, 315-333.

Geiger, B., Spatz, J.P., and Bershadsky, A.D. (2009). Environmental sensing through focal adhesions. Nat Rev Mol Cell Biol *10*, 21-33.

Gingras, A.R., Bate, N., Goult, B.T., Hazelwood, L., Canestrelli, I., Grossmann, J.G., Liu, H., Putz, N.S.M., Roberts, G.C.K., Volkmann, N.*, et al.* (2008). The structure of the C-terminal actin-binding domain of talin. EMBO J *27*, 458-469.

Gingras, A.R., Ziegler, W.H., Frank, R., Barsukov, I.L., Roberts, G.C., Critchley, D.R., and Emsley, J. (2005). Mapping and consensus sequence identification for multiple vinculin binding sites within the talin rod. J Biol Chem *280*, 37217-37224.

Goldmann, W.H., Bremer, A., Haner, M., Aebi, U., and Isenberg, G. (1994). Native talin is a dumbbell-shaped homodimer when it interacts with actin. J Struct Biol *112*, 3-10.

Golji, J., Lam, J., and Mofrad, M.R. (2011). Vinculin activation is necessary for complete talin binding. Biophys J *100*, 332-340.

Golji, J., and Mofrad, M.R. (2010). A molecular dynamics investigation of vinculin activation. Biophys J *99*, 1073-1081.

Grashoff, C., Hoffman, B.D., Brenner, M.D., Zhou, R., Parsons, M., Yang, M.T., McLean, M.A., Sligar, S.G., Chen, C.S., Ha, T.*, et al.* (2010). Measuring mechanical tension across vinculin reveals regulation of focal adhesion dynamics. Nature *466*, 263-266.

Hemmings, L., Rees, D.J., Ohanian, V., Bolton, S.J., Gilmore, A.P., Patel, B., Priddle, H., Trevithick, J.E., Hynes, R.O., and Critchley, D.R. (1996). Talin contains three actin-binding sites each of which is adjacent to a vinculin-binding site. J Cell Sci *109 (Pt 11)*, 2715-2726.

Hoffman, B.D., Grashoff, C., and Schwartz, M.A. (2011). Dynamic molecular processes mediate cellular mechanotransduction. Nature *475*, 316-323.

Humphrey, W., Dalke, A., and Schulten, K. (1996). VMD: visual molecular dynamics. J Mol Graph *14*, 33-38, 27-38.

Humphries, J.D., Wang, P., Streuli, C., Geiger, B., Humphries, M.J., and Ballestrem, C. (2007). Vinculin controls focal adhesion formation by direct interactions with talin and actin. J Cell Biol *179*, 1043-1057.

Hytönen, V.P., and Vogel, V. (2008). How force might activate talin's vinculin binding sites: SMD reveals a structural mechanism. PLoS Comput Biol *4*, e24.

Jiang, G., Giannone, G., Critchley, D.R., Fukumoto, E., and Sheetz, M.P. (2003). Two-piconewton slip bond between fibronectin and the cytoskeleton depends on talin. Nature *424*, 334-337.

Kraeutler, V., Gunsteren, W.F., and Huenenberger, P.H. (2001). A fast SHAKE algorithm to solve distance constraint equations for small molecules in molecular dynamics simulations¶. J Comput Chem *22*, 501-508.

Kubow, K.E., and Horwitz, A.R. (2011). Reducing background fluorescence reveals adhesions in 3D matrices. Nat Cell Biol *13*, 3-5; author reply 5-7.

Kumar, S., Rosenberg, J.M., Bouzida, D., Swendsen, R.H., and Kollman, P.A. (1992). THE weighted histogram analysis method for free-energy calculations on biomolecules. I. The method. Journal of Computational Chemistry *13*, 1011-1021.

Kumar, S., and Weaver, V.M. (2009). Mechanics, malignancy, and metastasis: the force journey of a tumor cell. Cancer Metastasis Rev *28*, 113-127.

Lazaridis, T., and Karplus, M. (1999). Effective energy function for proteins in solution. Proteins *35*, 133-152.

Lee, S.E., Chunsrivirot, S., Kamm, R.D., and Mofrad, M.R. (2008). Molecular dynamics study of talin-vinculin binding. Biophys J *95*, 2027-2036.

Lee, S.E., Kamm, R.D., and Mofrad, M.R. (2007). Force-induced activation of talin and its possible role in focal adhesion mechanotransduction. Journal of biomechanics *40*, 2096-2106.

Lepzelter, D., and Zaman, M.H. (2010). Clustered diffusion of integrins. Biophys J *99*, L106-108.

Massia, S.P., and Hubbell, J.A. (1991). An RGD spacing of 440 nm is sufficient for integrin alpha V beta 3-mediated fibroblast spreading and 140 nm for focal contact and stress fiber formation. J Cell Biol *114*, 1089-1100.

Moore, S.W., Roca-Cusachs, P., and Sheetz, M.P. (2010). Stretchy proteins on stretchy substrates: the important elements of integrin-mediated rigidity sensing. Dev Cell *19*, 194-206.

Ngu, H., Feng, Y., Lu, L., Oswald, S.J., Longmore, G.D., and Yin, F.C. (2010). Effect of focal adhesion proteins on endothelial cell adhesion, motility and orientation response to cyclic strain. Annals of biomedical engineering *38*, 208-222.

Pahakis, M.Y., Kosky, J.R., Dull, R.O., and Tarbell, J.M. (2007). The role of endothelial glycocalyx components in mechanotransduction of fluid shear stress. Biochem Biophys Res Commun *355*, 228-233.

Patel, B., Gingras, A.R., Bobkov, A.A., Fujimoto, L.M., Zhang, M., Liddington, R.C., Mazzeo, D., Emsley, J., Roberts, G.C.K., Barsukov, I.L., *et al.* (2006). The activity of the vinculin binding sites in talin is influenced by the stability of the helical bundles that make up the talin rod. J Biol Chem *281*, 7458-7467.

Pettersen, E.F., Goddard, T.D., Huang, C.C., Couch, G.S., Greenblatt, D.M., Meng, E.C., and Ferrin, T.E. (2004). UCSF Chimera--a visualization system for exploratory research and analysis. J Comput Chem *25*, 1605-1612.

Phillips, J.C., Braun, R., Wang, W., Gumbart, J., Tajkhorshid, E., Villa, E., Chipot, C., Skeel, R.D., Kale, L., and Schulten, K. (2005). Scalable molecular dynamics with NAMD. J Comput Chem *26*, 1781-1802.

Roberts, G.C., and Critchley, D.R. (2009). Structural and biophysical properties of the integrin-associated cytoskeletal protein talin. Biophys Rev *1*, 61-69.

Roca-Cusachs, P., Gauthier, N.C., Del Rio, A., and Sheetz, M.P. (2009). Clustering of alpha(5)beta(1) integrins determines adhesion strength whereas alpha(v)beta(3) and talin enable mechanotransduction. Proc Natl Acad Sci U S A *106*, 16245-16250.

Schvartzman, M., Palma, M., Sable, J., Abramson, J., Hu, X., Sheetz, M.P., and Wind, S.J. (2011). Nanolithographic control of the spatial organization of cellular adhesion receptors at the single-molecule level. Nano letters *11*, 1306-1312.

Torrie, G., and Valleau, J. (1977). Nonphysical sampling distributions in Monte Carlo free-energy estimation: Umbrella sampling. Journal of Computational Physics *23*, 187-199.

Van Der Spoel, D., Lindahl, E., Hess, B., Groenhof, G., Mark, A.E., and Berendsen, H.J.C. (2005). GROMACS: Fast, flexible, and free. Journal of Computational Chemistry *26*, 1701-1718.

Winkler, J., Lunsdorf, H., and Jockusch, B.M. (1997). Energy-filtered electron microscopy reveals that talin is a highly flexible protein composed of a series of globular domains. Eur J Biochem *243*, 430-436.

Zaidel-Bar, R., Ballestrem, C., Kam, Z., and Geiger, B. (2003). Early molecular events in the assembly of matrix adhesions at the leading edge of migrating cells. J Cell Sci *116*, 4605-4613.

Ziegler, W.H., Liddington, R.C., and Critchley, D.R. (2006). The structure and regulation of vinculin. Trends in Cell Biology *16*, 453-460.

Figure Legends

Figure 1. The C-terminus residues of the talin rod domain are used in molecular dynamics simulations. **(A)** Two talin monomers (blue and green) are connected at their C-terminus. The C-terminus region consists of a two helix dimerization domain connected to a nearby helical region (inset). Two viewpoints of the C-terminus region are shown with each monomer colored either green or blue. **(B)** The structure of the nearby actin-binding helical bundle is taken from PDB ID 1SJW (Gingras et al., 2008) (black) and the structure of the dimerization domain itself is taken from PDB ID 2QDQ (Gingras et al., 2008) (pink). The linker region (yellow) connecting these two segments was modeled and added to the structure.

Figure 2. (A) The modeled linker region has no intrinsic structure. There are two nonpolar patches made up of residues V2488, V2489, and V2490, and M2494 to V2495. There are 5 charged residues: K2493, E2492, K2491, E2486, and E2484. The linker is modeled using homology modeling essentially as a random coil. **(B)** The linker region adopted different conformation in each of the 5 trials. Furthermore, each of the two linkers in a single talin dimer adopted a unique conformation after equilibration. An example conformation is shown stabilized by formation of a hydrophobic patch between the two nonpolar regions, and a single salt-bridge between E2486 and K2491.

Figure 3. Five trials of the C-terminus region from the talin dimer were simulated in equilibrium with no external constraints. Shown in the top is the final structure after equilibration from each of the 5 trials after structural alignment. The α-angle describes the angle between the dimerization domain (pink) and the actin-binding

helical bundle (black) within the plane shown. Inset shows the same aligned five structures rotated 90°. The β-angle describes the angle between the dimerization helices and the bundle when moving in this rotated plane. The average fluctuations of each residue across both monomers and 5 trials are calculated and plotted (lower panel). Peaks in the RMSD represent regions undergoing high fluctuation. Each linker between helices from the helical bundle along with the larger linker between the bundle and the dimerization helices undergo the largest fluctuation and are predicted to be the flexible regions.

Figure 4. The talin dimer can potentially adopt a number of different orientations. To test the impact of mechanical load on the dimer orientation a pulling force is applied to the C-terminus region of talin to simulate the movement of an ECM-bound integrin away from another while cross-linked by talin. The resulting conformational change at the C-terminus region suggests talin adopts an elongated conformation after exposure to the stretching force. The conformational shift to an elongated conformation is a mode of talin mechanosensing. ECM forces on integrins can be translated to changes within the cell through elongation of the talin dimer. Shown in the top inset is a schematic of the source of an elongating force on talin. Shown in the bottom inset is a schematic of the impact of the elongate talin dimer structure on allowing talin to crosslink more separated integrins. Each monomer is shown in either green or blue.

Figure 5. The talin dimer can potentially adopt a collapse conformation if the two talin head domains are forced together by the ECM-bound integrins. ECM forces that would push to integrins together are simulated using molecular dynamics. The results show the C-terminus region of the talin dimer adopts a collapse conformation (bottom rendered figure). Flexibility in the C-terminus region allows the talin dimer to change its orientation in response to mechanical load. Shown in the top inset is a schematic of the source of a force moving two integrins towards each other. Shown in the bottom inset is a schematic the possible orientation of the talin dimer if two integrins move towards each other. Each monomer is shown in green or blue.

Figure 6. The potential of mean force for is calculated for the elongation of the talin dimer. The reaction coordinate is defined as the distance between the ends of each monomer's actin-binding helical bundle. The free energy difference is negative suggesting formation of an elongated conformation is favorable. It predicts that a talin C-terminus region will adopt a more elongated conformation and that forces will be needed to move the monomers towards each other.

Figure 7. Talin can have two modes of mechanosensing: **(A)** The application of a stretching force across a single monomer could result in the exposure of cryptic vinculin-binding sites (VBS). Shown here is a schematic depicting the force across a talin monomer (green) from contraction of an attached actin filament (blue) leading to exposure of a VBS (orange). **(B)** The application of a force on the talin dimer can cause reorientation of the dimer. Shown here is a schematic depicting the forcing of

an integrin away from another by the ECM and the resulting reorientation of the talin dimer to an elongated conformation. In the elongated conformation, more actin filaments can link to the talin dimer as more VBS are available for activation and linking to actin via vinculin.

Figure 1

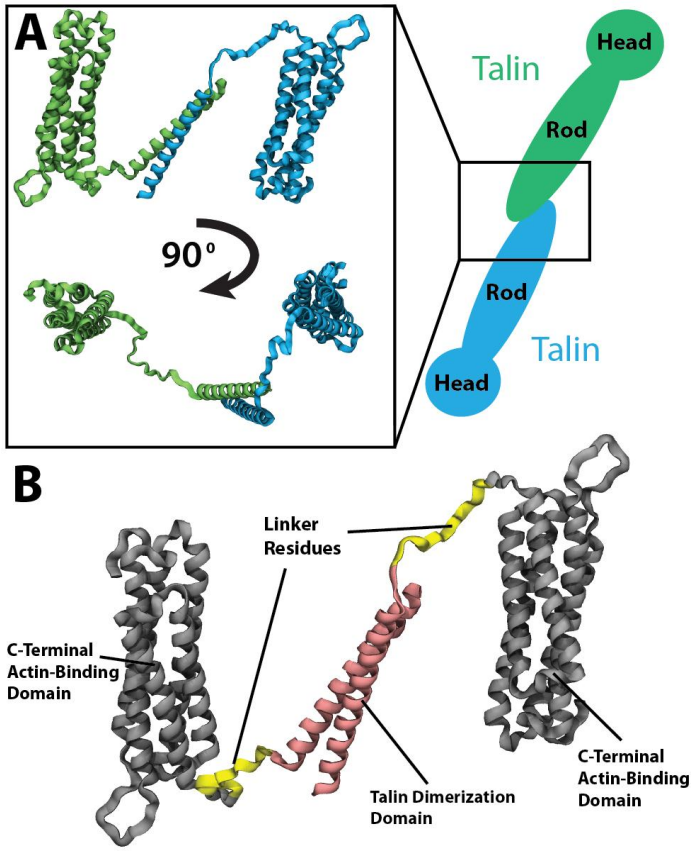
A
90°
Talin
Head
Rod
Rod
Talin
Head
B
Linker
Residues
C-Terminal
Actin-Binding
Domain
Talin Dimerization
Domain
C-Terminal
Actin-Binding
Domain

Figure 2

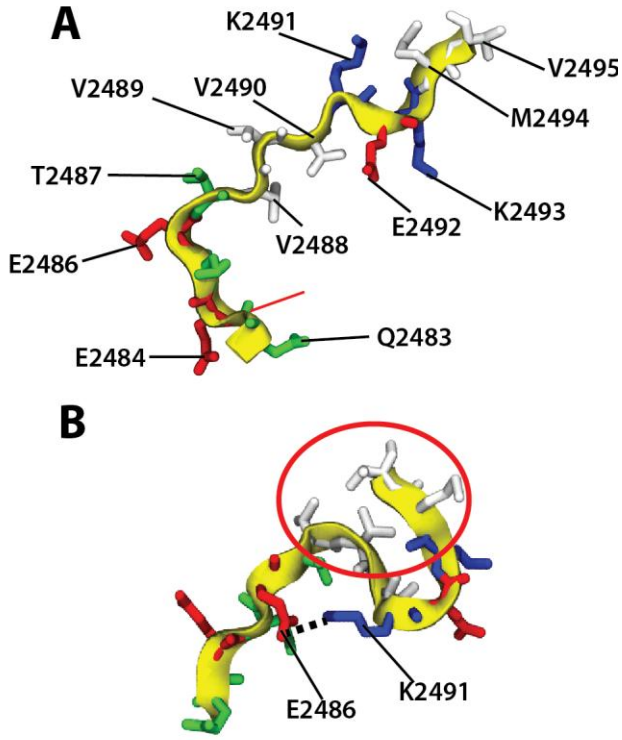
A
K2491
V2495
V2489
V2490
M2494
T2487
K2493
E2492
V2488
E2486
Q2483
E2484
B
K2491
E2486

Figure 3

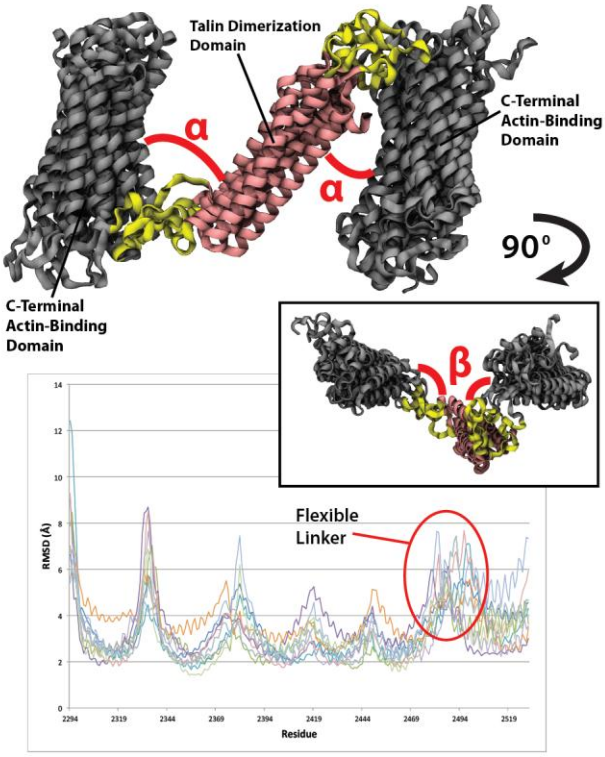
Talin Dimerization Domain
C-Terminal Actin-Binding Domain
α
α
90°
C-Terminal Actin-Binding Domain
β
Flexible Linker
RMSD (Å)
Residue
0
2
4
6
8
10
12
14
2294
2319
2344
2369
2394
2419
2444
2469
2494
2519

Figure 4

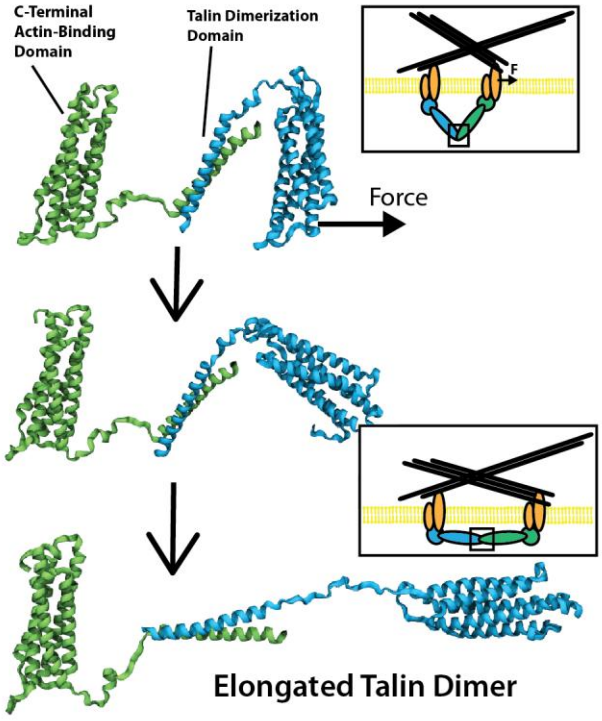
C-Terminal
Actin-Binding
Domain
Talin Dimerization
Domain
F
Force
Elongated Talin Dimer

Figure 5

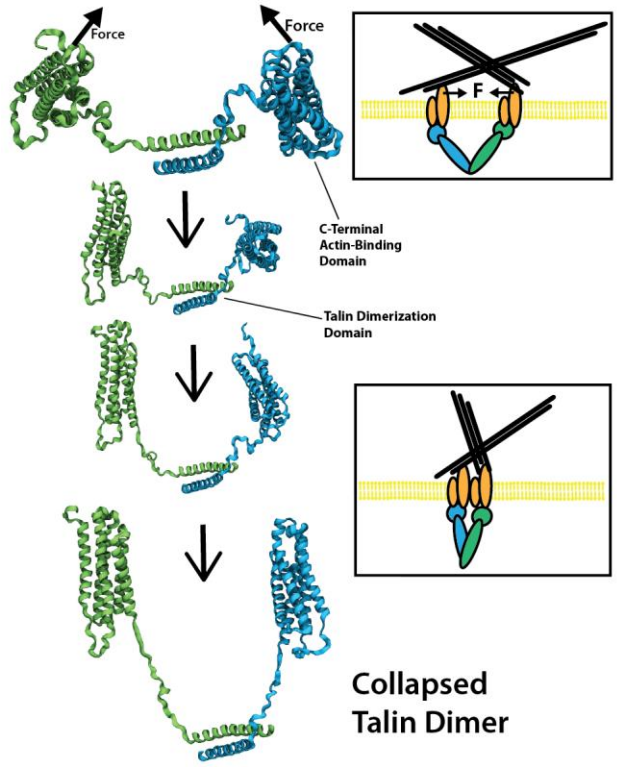
Force
Force
F
C-Terminal
Actin-Binding
Domain
Talin Dimerization
Domain
Collapsed
Talin Dimer

Figure 6

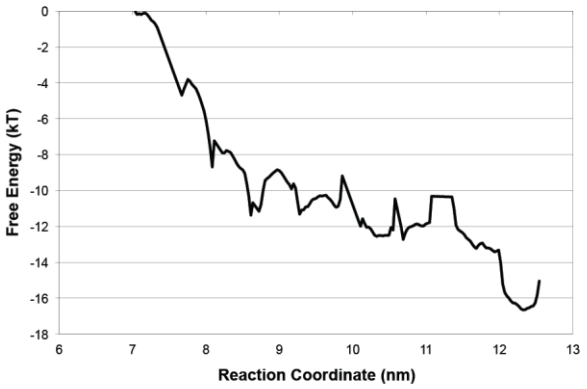
Free Energy (kT)
0
-2
-4
-6
-8
-10
-12
-14
-16
-18
6
7
8
9
10
11
12
13
Reaction Coordinate (nm)

Figure 7

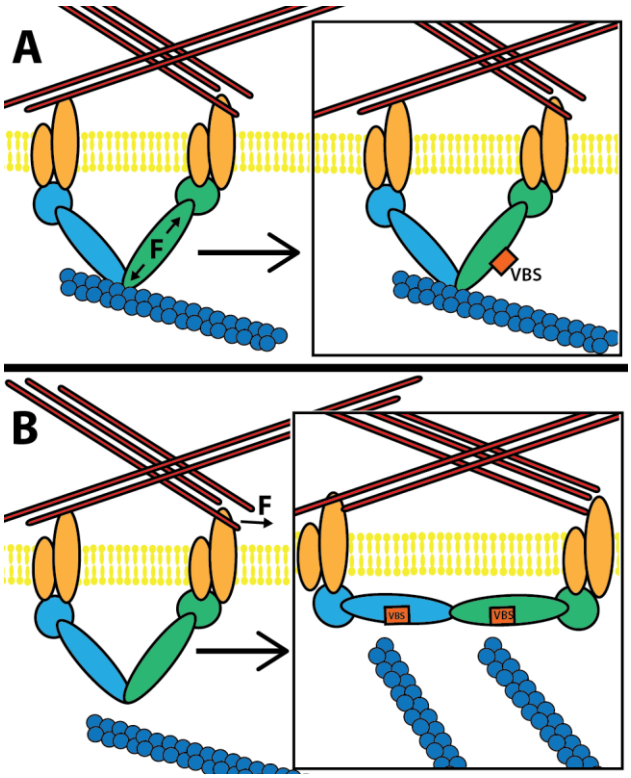

Section II:

The Activation of Vinculin

A Molecular Dynamics Investigation of Vinculin Activation

Abstract

Vinculin activation plays a critical role in focal adhesion initiation and formation. In its native state vinculin is in an auto-inhibitory conformation in which domain 1 is preventing interaction of the vinculin tail domain with actin by steric hindrance. Once activated, vinculin is able to interact with both actin and talin. Several hypotheses have been put forth addressing the mechanisms of vinculin activation. One set of studies suggests that vinculin interaction with talin is sufficient to cause activation, while another set of studies suggests that a simultaneous interaction with several binding partners is necessary to achieve vinculin activation. Using molecular dynamics simulation we investigate the mechanisms of vinculin activation and suggest both a trajectory of conformational changes leading to vinculin activation, and key structural features likely involved in stabilizing the auto-inhibited conformation. Assuming that the simultaneous interaction of vinculin with both actin and talin causes a stretching force on vinculin, and that vinculin activation results from a removal of steric hindrance blocking the actin binding sites, we simulate with molecular dynamics, the stretching and activation of vinculin. The molecular dynamics simulations are further confirmed by normal mode analysis and simulation after residue modification. Taken together, these simulations suggest that bending of the VBS binding region in vinculin away from the vinculin tail is the likely trajectory of vinculin activation.

Introduction

Cellular response to external stress involves both a passive and an active cytoskeletal rearrangement. External force is transduced through membrane bound integrin to the cytoskeleton causing both passive reinforcement via focal adhesion formation and active reinforcement via tyrosine kinase activity (1-3). Focal adhesions are formed at plasma membrane sites of external stress, and function as molecular glues cementing the actin filaments (F-actin) to external stress (4-9). The formation of focal adhesion sites is initiated by the formation of a molecular connection between talin (bound to integrin) and F-actin, and reinforced by vinculin (10-12). Once the talin-vinculin-F-actin complex is formed, other focal adhesion molecules are recruited to form the molecular glue (13, 14). Vinculin null cells can produce focal adhesions, but show significant defects in cell spreading, cell stiffness, cell shape, and regulation of apoptotic cues (15-19).

Vinculin can exist in two conformations: an auto-inhibited conformation and an activated conformation. It is in the activated conformation that vinculin is able to initiate focal adhesion site formation (20). The crystal structure of the auto-inhibited conformation shows that vinculin has five major structural domains (Figure 1A): residues 1-252 make up domain 1 (D1)(light-green), residues 253-485 make up domain 2 (D2)(purple), residues 493-717 make up domain 3 (D3)(tan),

residues 719-839 make up domain 4 (D4)(green), and residues 896-1066 make up the vinculin tail domain (Vt)(orange). Together D1, D2, D3, and D4 make up the vinculin head domain (Vh). There is also a proline-rich linker region connecting Vh to Vt (yellow) (21). Vinculin has several binding sites including one for the talin vinculin binding site (VBS) in D1 and one for F-actin in Vt (22). In its auto-inhibitory conformation, vinculin interaction with talin in the VBS binding regions (Figure 1B) is limited by the higher affinity interaction between Vt and the VBS binding region (23), while interaction with F-actin at the Vt domain is limited by steric hindrance by the VBS binding region (24) (Figure 1B). Vt is a five-helix anti-parallel bundle. All five of its helices are amphipathic with the hydrophobic regions pointed inward and the hydrophilic regions pointed outward. However, there is an exposed hydrophobic surface near the interface with domain 1 involved in stabilizing the auto-inhibited conformation(21). The Vt domain also has two positively charged regions: a basic collar near the C-terminus, and a basic ladder near the center (25) (Figure 1B). These positively charged regions have been implicated as binding sites for F-actin (24). In its activated conformation, vinculin can interact with both talin and F-actin.

Vinculin interacts critically with talin and this interaction is potentially able to activate vinculin (20). Initial studies of the vinculin binding sites in talin pinpointed three vinculin binding sites (VBSs) in the talin rod: residues 607-636, 852-876, and 1944-1969. All three VBSs are amphipathic α-helices that experimental data has suggested interact with D1 via hydrophobic residues (26). Later studies showed eight additional talin VBSs, all with similar properties as VBS1, VBS2, and VBS3 (27). The VBS regions are cryptic binding sites and only upon talin activation by external force are the VBS regions exposed for interaction with vinculin (28-31). The interaction between talin VBS and Vh is high affinity with K_d values of 14.7 nM for VBS1, 32.8 nM for VBS2, and 3.2 nM for VBS3 (32), but is kinetically slow due to local conformational changes in D1 resulting from VBS binding (33). X-ray crystallization studies have revealed the structure of VBS1 (32, 34) and VBS3 (35) with D1. The interaction is mediated by a helical bundle conversion mechanism in D1. Potential mechanisms of helical bundle conversion have been elucidated in a computational simulation of the interaction between VBS and D1: first, insertion of the VBS hydrophobic patch, second, movement of two helices in D1 away from VBS, and third, rotation of the VBS α-helix to form a hydrophobic core with D1 helices (36).

Two competing hypotheses exist to describe the mechanism of vinculin activation: talin binding to D1 is sufficient to activate vinculin (37), or, a simultaneous interaction of both talin and F-actin is necessary to achieve activation, i.e. a combinatorial mechanism is necessary for vinculin activation(23). Using a FRET probe, Chen et al. first demonstrated *in vivo* that vinculin becomes activated in focal adhesions (38), and later demonstrated *in vitro* that only after coincidence of both F-actin and talin does vinculin become activated and show cosedimentation with F-actin (23). Conversely, using vinculin captured on a gold surface, Bois et al. (37) showed that VBSs are able to bind even full length vinculin with the following affinities: VBS1 with a K_d of 78 nM, VBS2 with a K_d of 530 nM and VBS3 with a K_d of 74 nM. Taken together with previous results suggesting VBS binding involves dissociation of Vt from D1 (32), they suggest that talin VBS is sufficient to cause

activation in vinculin. Besides the question of what the mechanism of vinculin activation is, several related questions exist that likewise remain unanswered: what are the structural mechanisms of vinculin auto-inhibition? What is the trajectory of conformational changes during vinculin activation? What is the final conformation of an activated vinculin molecule?

In this study we examine the detailed structural mechanisms of vinculin activation. Using molecular dynamics simulation the likely conformational changes leading to vinculin activation are investigated with regards to both existing hypotheses for vinculin activation. We simulate what effects VBS association with full-length vinculin may have on vinculin activation, and also the activating conformational changes resulting from the stretching forces that vinculin and vinculin-VBS complex are likely to be exposed to by simultaneous interaction with F-actin and talin (Figure 2).

Methods

Homology modeling of proline-rich loop region

We used SWISSMODEL (39) to create a homology model of full-length vinculin including its proline-rich domain. The original sequence was taken from the crystal structure (PDB 1TR2) (21) and submitted to SWISSMODEL using the Swiss-Pdb Viewer DeepView (40) interface. PDB 1TR2 (21) had sequence alignment and structural information for all regions of the vinculin sequence except residues P843 to P877. The structure of the proline-rich loop region was taken from PDB 3PTE (41) because high sequence homology between 3PTE and the loop region. The final merged structure had no changes to any residues from PDB 1TR2. The total number of bad phi angle in the merged structure prior to minimization was 6. CHARMm (42) was then used to minimize the homology structure and alleviate the bad phi angles. The minimization was carried out in CHARMm by alternatively applying the Steepest Descent and Adopted Basis Newton Raphson methods for 3000 steps each.

Molecular Dynamics Simulation of Vinculin Activation

Molecular dynamics simulations were carried out to explore the molecular trajectory of vinculin activation. CHARMm (42) installed on Intel Xeon workstations were used for all molecular dynamics simulations. CHARMm simulations were setup to first load structure, topology, and parameter information, then heat and equilibrate the system, and finally simulated for response to the stretching forces. The Effective Energy Function (EEF1) (43) implicit solvent model was used to calculate solvent effects. Implicit solvent models including EEF1 are viable alternatives to computationally costly explicit solvent approximations, and have been used repeatedly in simulation (44). The model has also been compared to experimental results for validation (45). The use of the implicit solvent model is appropriate in this study, where the main consideration is the large-scale conformational change resulting from stretching force. With the implicit model significant solvent viscous effects are absent and large scale conformational changes can take place within our simulation window, whereas prohibitively longer simulation times would be necessary using an explicit solvent. One potential artifact

of using an implicit solvent model would be the lack of dielectric screening in non-bonded interactions; however these effects should not alter the large-scale conformational changes. The SHAKE method (46) was used to constrain bond lengths between heavy atoms and hydrogen atoms. All molecular dynamics simulations used the CHARMM19 force fields (47). Each simulation was first heated to 300 K for 40 ps and then equilibrated. Equilibration simulations were run until no further total RMSD was calculated indicating no further net conformational change. An average of 400 ps of simulation was sufficient to achieve equilibration. All results from the simulations were visualized in VMD (48). Trajectory data from the simulations were recorded and saved in VMD.

Forced Activation in three directions

Forces were applied to Vt in three directions: in a stretching direction to simulate simultaneous interaction of vinculin with talin and actin, and in two directions to simulate Vt complete separation from Vh. Forces were applied to the center of mass of Vt in each of the three directions. For simulation of Vt complete separation from Vh, first N193, K261, V491, and Q662 were constrained fixed and force was in the direction away from the center of mass of Vh. Then the fixation constraints were applied to: D505-D510, A560-R570. The direction of force was away from the center of those residues in domain3. For simulation of stretching of vinculin due to simultaneous interaction, the center of mass of the VBS binding region (M1 to R132) was constrained with the following residues fixed: V16, V51, V81, and I115. In all three simulations the forces were applied to the center of mass of Vt at: M926, S958, I988, and M1031. Forces were applied at 50 pN and 100 pN in the three directions for 800 ps. The force levels used here are comparable to forces used in numerous molecular dynamics simulations (49, 50), however they are significantly higher than those from *in vitro* experiments or physiology because of the faster timescales required for computational simulation (51). Molecular conformational changes, including vinculin activation, are expected to occur on a millisecond timescale *in vivo* whereas the conformational changes simulated here occur on a nanosecond timescale. Quantitatively this difference in timescale results in a difference in reported force and energy levels reported for conformational changes, and qualitatively this difference in timescale can result in significant local conformational changes such as loss of helical integrity. However, in other computational simulations the major molecular conformational changes have been shown to be consistent between nanosecond simulation and millisecond experiment. For example, the activation of talin's vinculin binding site *in silico* (28, 52)compares to its activation *in vitro* (31).

Simulation of vinculin activation with VBS bound

To investigate the effects of VBS binding to D1 on vinculin activation using molecular dynamics, a vinculin-VBS complex was formed using the crystal structure for D1 bound to VBS1 (PDB 1T01) (34) to get the structure of the D1 region with VBS bound and the full length vinculin structure (21) with a homology modeled loop region. The hybrid vinculin structure was minimized in CHARMm (42) using the Steered Descent and Adopted Basis Newton Raphson minimization techniques for

3000 steps each. Activation simulation of the vinculin-VBS complex used similar methods as activation of the vinculin molecule itself. Fixation constraints were applied to V16, V51, V81, and I115 while constant forces were applied to M926, S958, I988, and M1031. These represent the center of mass of the VBS binding region and the Vt region respectively. Forces of the following values were applied to the Vt residues for 800 ps: 50 pN, 100 pN, 125 pN, 150 pN, and 200 pN.

Residue Modification in D1

Activation of vinculin involves overcoming electrostatic interactions between Vt and the VBS binding region. To further test the role the electrostatic interactions play in stabilizing the auto-inhibited vinculin structure, residue modifications were introduced to the charged residues in D1 of the vinculin-VBS complex. Three residues were chosen and modified to GLY: E29 was modified to G29, E14 was modified to G14, R7 was modified to G7. Modification removed electrostatic interactions. The molecular dynamic simulations of activation were rerun with the modifications using 50 pN, 100 pN, and 125 pN of force.

Full-length vinculin Normal Mode Analysis

Natural vibrational frequencies of the full-length vinculin molecule were determined using the normal mode analysis software WEBnm@ (53) and ElNemo (54). The normal modes are a function of vinculin molecular structure; the normal modes show natural movements in flexible molecular regions, and little movement in rigid regions. WEBnm@ uses the MMTK (55) software internally and computes natural frequencies using Hinsen's computational methods (56), which calculates approximate normal modes by determining the eigenvectors of the matrix of second derivatives of potential energy with respect to displacement of the Cα atoms of each residue. The potential energy function used for this calculation utilizes a Hookian potential between Cα atoms within an 8 Å cutoff distance. Because NMA represents movements resulting from overall structure, the use of Cα atoms is sufficient for NMA calculations (57). WEBnm@ calculates the six lowest frequency vibrational modes, mode 7-12. These modes are then analyzed and visualized using VMD (48). Similar to WEBnm@, ElNemo uses the elastic network model (58) to determine the normal modes but can produce up to 100 of the lowest frequency modes.

Results and Discussion

Presently, the structure of activated vinculin has not been solved. Yet features of inactive vinculin structure play a critical role in auto-inhibition. Considering previous suggestions (24) that vinculin auto-inhibition results from the steric hindrance of the actin-binding domain in Vt by regions in domain 1 (Figure 1B), any conformational change in vinculin that would remove the steric hindrance would also result in activation. To investigate the two hypotheses regarding vinculin activation we devised a series of molecular dynamics simulation to induce conformational changes in vinculin removing the steric hindrance and potentially activating vinculin, and allow us to compare the two hypotheses. First, vinculin is simulated with a stretching force carefully defined to be consistent with the

simultaneous interaction hypothesis; during simultaneous interaction the actin binding domain would be attracted to actin while the talin binding domain would be attracted to VBS thus resulting in a simultaneous stretch of vinculin with those two binding domains (Vt and domain1) stretched away from each other. Second, the simulations are extended to include VBS binding and evaluate effects of talin binding on activation. Third, to control for the effects of pull direction, and to investigate other conformational changes, the simulations are repeated with several different pull directions. Finally, to confirm the validity of the structural mechanism the simulations are repeated with specific residue modifications introduces, and the vinculin normal modes are analyzed. We aim to simulate a simultaneous interaction via applying a stretching force. The use of a stretching force is a novel indirect measure of a binding interaction and can therefore have several limitations. The potential limitations of our study are discussed in the Discussion section.

Simulation of activation by simultaneous interaction. Actin interacts directly with Vt while talin VBS interacts with Vh at domain 1 (22). The interaction of talin with Vh involves hydrophobic insertion (35) and is likely to anchor vinculin to talin, even if this interaction alone is not sufficient to activate vinculin. The interaction of Vt with actin is polar, and therefore there is likely to be a strong electrostatic force attracting Vt towards actin prior to binding (24). A simultaneous interaction of vinculin with talin and actin would likely then involve anchoring of Vh to talin while Vt is attracted and pulled towards actin, resulting in a stretching force pulling Vt away from the talin binding domain (Figure 2A). The direction of force for our simulation is then chosen to simulate the stretching of vinculin during simultaneous interaction: we applied a pulling force to Vt and pulled it away from VBS binding domain (Figure 3A). The center of mass of the VBS binding domain was held fixed, as if anchored to talin during the simultaneous interaction.

The conformational change that results from stretching vinculin by constant force matches the criterion for activation, that is, removal of steric hindrance from actin binding domain (Figure 3B). In the molecular dynamics simulations of vinculin stretching with a constant force of 100 pN the significant conformational change occurs in 8 out of 9 trials, where bending of domain 1 causes the VBS binding domain to move away from the Vt domain. This movement occurs while no other regions of vinculin undergo noticeable conformational changes. Movement of the VBS binding domain away from Vt has the effect of removing the steric hindrance and therefore likely resulting in an activated conformation.

The activation trajectory entails specific structural changes. In its auto-inhibited conformation there are 3 sets of salt-bridges between Vt and the VBS binding region. When the stretching force is applied in molecular dynamics these sets of salt-bridges break sequentially (Video S1 and Figure S1). At each breakage event the strength of the connection between Vt and the VBS binding region is weakened and the distance between the VBS binding domain and Vt further increases. The first of the salt bridges to break is (3) E14 with E986, the second (2) E14 with K996, and the final (1) E29 and E31 with R945 and R1008.

The tentative result of our molecular dynamics simulation is to show that a stretching force, assumed to be from a simultaneous interaction of vinculin with

talin and actin, could result in activation by bending the VBS binding domain away from Vt. This activation trajectory is similar to the activation trajectory described by Chen et al. (59). Using a discrete molecular dynamics simulation in which three backbone beads and a single side group bead represented each residue, they suggested that vinculin activation might involve a clincher-like movement of domain 1 and 3. Both their simulations and ours suggest vinculin activation, at least from simultaneous interaction with actin and talin, involves movement in domain 1 exposing Vt.

Activation by helical bundle conversion. The other suggested mechanism of vinculin activation is that vinculin is activated sequentially (Figure 2B). First, the talin VBS inserts itself into the VBS binding domain on Vh. Second, the helices near the VBS insertion rearrange to stabilize the new hydrophobic core; this rearrangement is termed helical bundle conversion (35). Third, vinculin is activated by the helical bundle conversion, and finally, once activated, Vt interacts with actin. To investigate this hypothesis using molecular dynamics, we introduced VBS along with the suggested conformational changes from helical bundle conversion (36) into our full-length vinculin structure.

Several significant changes were introduced to the full-length vinculin structure after VBS insertion. The two helical regions from R7-E31 (H1) and from L40-T64 (H2) near the site of VBS insertion have moved further apart and H1 has moved closer to Vt (Figure 4A). The shift of H1 closer to Vt results directly in shifts in the interaction distance between three groups of salt-bridges: (1) E29 and E31 with R945 and R1008, (2) E14 with K996, and (3) E7 with E986. Specifically, the distance between charged residues in salt-bridge 3 is increased by 2.73 Å, in salt-bridge 2 is decreased by 0.23 Å, and in salt-bridge set 1 the multiple charged residues are each rearranged and shifted. E29 and R945 are now closer by 2.63 Å, E31 and R945 are now closer by 7.09 Å, E29 and R1008 are now closer by 7.64 Å, and E31 and R1008 are now further by 8.29 Å (Figure 4B-D). These shifts and rearrangements are maintained even after minimization and equilibration. After equilibration it becomes clear that the structural changes after VBS insertion have weakened salt-bridge set 3 while strengthened salt-bridge set 1 by bringing three of the four charged residues in close electrostatic contact with each other.

To compare activation in the vinculin-VBS compound with all its structural changes to activation in full-length vinculin alone, molecular dynamics simulations were run with a range of constant forces (50 pN to 200 pN) and multiple trials with a similar set up as above: the forces were applied to Vt in a direction away from the VBS binding region in domain 1. After 800 ps of simulation it appeares that the VBS insertion may increase the force necessary to cause movement of the VBS binding region away from Vt (Figure 5).

If the trajectory of vinculin activation conformational changes is assumed to be the trajectory suggested by the simulation of vinculin alone, then the hypothesis of simultaneous interaction with talin and actin is more likely. The conformational changes induced in Vh by VBS insertion make activation by movement of the VBS binding region away from Vt more costly and therefore less likely to occur.

Alternative Trajectories for Forced Induced Vinculin Activation. To discover other potential activation mechanisms using molecular dynamics both full-length vinculin and the vinculin-VBS compound were simulated with alternative force directions. Whatever the mechanisms or trajectory, one characteristic of vinculin activation is that the steric hindrance of Vt should be removed. Aside from the movements described thus far, another structural change that could remove the steric hindrance would be the complete separation of Vt from all regions of Vh. To simulate this mechanism of vinculin activation, force was used in molecular dynamics simulation with the following new parameters: force was applied to the center of mass of Vt in the direction away from the center of mass of Vh (Figure S2A).

Vt was separated from Vh using molecular dynamics in both the full-length vinculin and the vinculin-VBS compound. In both structures, forces of 50 pN and 100 pN simulated for 1ns were unable to induce significant conformational changes. The resilience of vinculin to complete separation of Vt from Vh in simulation indicated there are likely structural features that prevent the complete separation. There are 14 salt-bridges between Vt and Vh that likely lend the structural stability (Figure 1C). Of these, three are between Vt and the VBS binding region and are broken in the activation mechanism discussed above. It is the combined strength of all 14 salt-bridges that likely accounts for the resistance to complete separation of Vt form Vh in the molecular dynamics simulations. The closed conformation of vinculin is stable with a total energy of -23,380 Kcal/Mol, and is therefore not likely to become completely separated. Furthermore, any conformational change that involves breaking the 14 salt-bridges could break the three bridges between Vt and the VBS binding region first, causing activation before any further interaction between Vt and Vh is broken.

A third potential conformational change that could lead to activation of vinculin could be the movement of Vt away from the VBS binding region, as opposed to the movement of VBS away from Vt. To induce this movement, a pulling force was applied to Vt in a third direction: away from the loop region of domain 3 (Figure S2B). This direction is the only other direction to pull Vt without introducing other steric hindrances. The results from pulling both vinculin and vinculin-VBS with 50 pN and 100 pN in this third direction show no significant conformational changes. The same 14 salt-bridges that had stabilized Vt when being pulled away from the center of mass of Vh are likely also stabilizing Vt in these simulations.

Considering the structural features linking Vt to Vh, such as the 14 salt-bridges and the molecular dynamics results showing no Vt movement with forces up to 100 pN, it is not likely that a vinculin activation mechanism involves complete separation of Vt. Of course other movements are possible, but considering that any vinculin conformational change will likely first disrupt the connection between Vt and D1, shown above to be sufficient for activation, the critical movement underlying activation is the movement of the VBS binding region away from Vt. This movement is likely to occur after a simultaneous interaction between vinculin and its two binding partners F-actin and talin.

Confirmation of vinculin activation structural mechanisms. To confirm the proposed activation conformational change is consistent with all the vinculin structural

features, two computational methods were used: normal mode analysis and residue modification/mutation. Normal mode analysis involves the calculation of the lowest frequency vibrational modes using the minimized structure. Conformational changes that occur during the lowest frequency modes represent the likely movement within the local well of the energy landscape. Normal mode analysis is useful for considering the general flexibility of a molecule as a whole and cannot capture movements, such as activation, that require significant energy input (60). To consider the general flexibility of full-length vinculin an all-atom normal mode calculation would be computationally costly and unnecessary. Instead, normal modes were calculated using the elastic network model (54, 56, 58). Vibrational movements calculated using the elastic network model involved mainly movement of the linker region between domain 4 and Vt (Figure S3A). Other regions that showed significant vibrational movements consistently in both computational techniques were peripheral loop regions not near to Vt (Figure S3B). These vibrational movements suggest the most flexible region in vinculin to be the linker region between Vt and Vh. Other flexible regions include loop regions not near Vt. In none of the lowest vibrational modes was there movement of Vt or any of the regions near Vt, including the VBS binding domain. The results from normal mode analysis of vinculin-VBS showed similar structural features. Molecular dynamics results considered atomic-scale features such as salt-bridges, while the normal mode analysis considered more intuitive flexibility resulting from the general structure of vinculin, yet the structural features suggested by the normal mode analysis are consistent with results from molecular dynamics: Vt is rigidly connected to Vh and vinculin activation involving complete removal of Vt is unlikely.

To confirm the vitality of the three salt-bridges between Vt and the VBS binding region and to investigate the capacity for vinculin activation in the absence of these salt-bridges, molecular dynamics simulation was run following modification of the following charged residues at each of the three salt-bridges to glycine: E29, E14, and R7. Following modification the same molecular dynamics simulations as above were run with the modified vinculin structure. In the new simulation of modified vinculin, conformational changes indicating activation, movement of VBS binding region away from Vt, occurs with less force (within 400ps with 50pN of force). Furthermore, once the conformational change is achieved a stable intermediary structure is formed and sustained for an additional 300ps of simulation. This stable intermediary structure was present briefly in previous simulations, but due to the larger force necessary to induce conformational changes in simulation of unmodified vinculin the intermediary unfolded quickly as simulation progressed. The molecular dynamics results following modification are consistent with past experimental investigation of vinculin activation following genetic mutation (61). Cohen et al. (61) showed that modification of key polar residues between domain 1 and Vt (same residues that were modified in this molecular dynamics) reduced vinculin auto-inhibition. The simulations presented here confirm the key role of polar residues in stabilizing the auto-inhibited conformation and further suggest a trajectory for vinculin activation involving the breakage of salt-bridges and movement of the VBS binding region away from Vt.

Conclusion

Two hypothesis have been formulated regarding the mechanisms of vinculin activation: that a simultaneous interaction between vinculin and its two binding partners talin and actin is necessary for activation, or that at first an interaction of vinculin with talin causes helical bundle conversion and then after activation vinculin interacts with actin. Using molecular dynamics both hypothesis were investigated, and the results suggest that it is the simultaneous interaction between vinculin and its two binding partners causing an internal stretching force and movement of the VBS binding region away from Vt that activates vinculin. The results further suggest that insertion of talin VBS is insufficient to activate vinculin; a VBS insertion prior to a stretching event would reduce activation potential by strengthening electrostatic interactions between the VBS binding region in Vh and Vt. The results are consistent with vinculin structural features, simulated residue modification and previous experimental mutation. The results from these simulations are currently the sole suggested trajectory for vinculin activation. Although experiments have demonstrated a clear role for force induced protein conformational change in the other cytoskeletal proteins (62), our results should be considered suggestive and inviting further study.

The interaction of vinculin with its binding partners has been indirectly simulated using a stretching force. This strategy can have limitations. In addition to potentially serving as an indirect measure of biding, the use of a stretching force in these vinculin simulations can also evaluate the hypothesis that vinculin would be activated by an external force. Physiologically, can an external force regulate vinculin activation? Experimental investigation by Mierke et al. (63) has suggested that perhaps mechanical force plays a role in vinculin activation. In their work magnetic beads were used on vinculin null cells and normal cells. They found that in the absence of vinculin, cells were less responsive in reinforcement against the external force. Although far from conclusive, those experiments along with the molecular dynamics simulations indicate a possible role of mechanical force in vinculin activation.

The activation of vinculin is central to the process of focal adhesion formation and all the many processes dependent on focal adhesions, therefore some disease states associated with failure of focal adhesion formation could be linked to failure of vinculin activation. Such a link between disease states and failed molecular structure has been demonstrated in other systems (64). Several studies have also described the link between focal adhesion formation and disease(65-68).

Molecular dynamics is a valuable tool for investigating atomic scale phenomena in critical molecular processes in the cell such as vinculin activation(69-72). The results from these simulations should be used as a complement to existing experiments or to suggest future experiments. One possible experimental investigation of the suggested trajectory of vinculin activation would be to track conformational changes in vinculin during activation using contrasting vinculin constructs for FRET analysis. The vinculin conformational changes during activation could then be compared to those suggested by our molecular dynamics. Another possibility would be to force induce vinculin conformational change *in vitro* with an

optical trap and report on its activation. This study has used molecular dynamics to shed light on an important cellular process: vinculin activation. For the first time a trajectory for vinculin activation has been suggested that can be evaluated by future investigations.

References:

1. Vogel, V., and M. Sheetz. 2006. Local force and geometry sensing regulate cell functions. Nature reviews Molecular cell biology 7:265-275.
2. Jiang, G., G. Giannone, D. R. Critchley, E. Fukumoto, and M. P. Sheetz. 2003. Two-piconewton slip bond between fibronectin and the cytoskeleton depends on talin. Nature 424:334-337.
3. Giannone, G., G. Jiang, D. H. Sutton, D. R. Critchley, and M. P. Sheetz. 2003. Talin1 is critical for force-dependent reinforcement of initial integrin-cytoskeleton bonds but not tyrosine kinase activation. The Journal of cell biology 163:409-419.
4. Galbraith, C. G., K. M. Yamada, and M. P. Sheetz. 2002. The relationship between force and focal complex development. The Journal of cell biology 159:695-705.
5. Mofrad, M. R., and R. D. Kamm. 2009. Cellular Mechanotransduction: Diverse Perspectives From Molecules to Tissues. Cambridge University Press, New York.
6. Mofrad, M. R., and R. D. Kamm. 2006. Cytoskeletal Mechanics: Models and Measurements. Cambridge University Press, New York.
7. Bao, G., R. D. Kamm, W. Thomas, W. Hwang, D. A. Fletcher, A. J. Grodzinsky, C. Zhu, and M. R. Mofrad. 2010. Molecular biomechanics: the molecular basis of how forces regulate cellular function. Cellular & Molecular Bioengineering IN PRESS.
8. Kolahi, K. S., and M. R. Mofrad. 2010. Mechanotransduction: A major regulator of homeostasis and development. Wiley Interdisciplinary Reviews: Systems Biology and Medicine. IN PRESS.
9. Kamm, R. D., and M. R. Kaazempur-Mofrad. 2004. On the molecular basis for mechanotransduction. Mech Chem Biosyst 1:201-209.
10. Gallant, N. D., K. E. Michael, and A. J. Garcia. 2005. Cell adhesion strengthening: contributions of adhesive area, integrin binding, and focal adhesion assembly. Mol Biol Cell 16:4329-4340.
11. Rodriguez Fernandez, J. L., B. Geiger, D. Salomon, and A. Ben-Ze'ev. 1992. Overexpression of vinculin suppresses cell motility in BALB/c 3T3 cells. Cell Motil Cytoskeleton 22:127-134.
12. Volberg, T., B. Geiger, Z. Kam, R. Pankov, I. Simcha, H. Sabanay, J. L. Coll, E. Adamson, and A. Ben-Ze'ev. 1995. Focal adhesion formation by F9 embryonal carcinoma cells after vinculin gene disruption. J Cell Sci 108 (Pt 6):2253-2260.
13. Liu, S., D. A. Calderwood, and M. H. Ginsberg. 2000. Integrin cytoplasmic domain-binding proteins. J Cell Sci 113 (Pt 20):3563-3571.

14. Garcia-Alvarez, B., J. M. de Pereda, D. A. Calderwood, T. S. Ulmer, D. Critchley, I. D. Campbell, M. H. Ginsberg, and R. C. Liddington. 2003. Structural determinants of integrin recognition by talin. Mol Cell 11:49-58.
15. Saunders, R. M., M. R. Holt, L. Jennings, D. H. Sutton, I. L. Barsukov, A. Bobkov, R. C. Liddington, E. A. Adamson, G. A. Dunn, and D. R. Critchley. 2006. Role of vinculin in regulating focal adhesion turnover. Eur J Cell Biol 85:487-500.
16. Alenghat, F. J., B. Fabry, K. Y. Tsai, W. H. Goldmann, and D. E. Ingber. 2000. Analysis of cell mechanics in single vinculin-deficient cells using a magnetic tweezer. Biochem Biophys Res Commun 277:93-99.
17. Coll, J. L., A. Ben-Ze'ev, R. M. Ezzell, J. L. Rodriguez Fernandez, H. Baribault, R. G. Oshima, and E. D. Adamson. 1995. Targeted disruption of vinculin genes in F9 and embryonic stem cells changes cell morphology, adhesion, and locomotion. Proc Natl Acad Sci U S A 92:9161-9165.
18. DeMali, K. A., C. A. Barlow, and K. Burridge. 2002. Recruitment of the Arp2/3 complex to vinculin: coupling membrane protrusion to matrix adhesion. J Cell Biol 159:881-891.
19. Subauste, M. C., O. Pertz, E. D. Adamson, C. E. Turner, S. Junger, and K. M. Hahn. 2004. Vinculin modulation of paxillin-FAK interactions regulates ERK to control survival and motility. J Cell Biol 165:371-381.
20. Ziegler, W. H., R. C. Liddington, and D. R. Critchley. 2006. The structure and regulation of vinculin. Trends in Cell Biology 16:453-460.
21. Bakolitsa, C., D. M. Cohen, L. A. Bankston, A. A. Bobkov, G. W. Cadwell, L. Jennings, D. R. Critchley, S. W. Craig, and R. C. Liddington. 2004. Structural basis for vinculin activation at sites of cell adhesion. Nature 430:583-586.
22. Zamir, E., and B. Geiger. 2001. Components of cell-matrix adhesions. Journal of cell science 114:3577-3579.
23. Chen, H., D. M. Choudhury, and S. W. Craig. 2006. Coincidence of actin filaments and talin is required to activate vinculin. J Biol Chem 281:40389-40398.
24. Janssen, M. E., E. Kim, H. Liu, L. M. Fujimoto, A. Bobkov, N. Volkmann, and D. Hanein. 2006. Three-dimensional structure of vinculin bound to actin filaments. Mol Cell 21:271-281.
25. Bakolitsa, C., J. M. de Pereda, C. R. Bagshaw, D. R. Critchley, and R. C. Liddington. 1999. Crystal structure of the vinculin tail suggests a pathway for activation. Cell 99:603-613.
26. Bass, M. D., B. J. Smith, S. A. Prigent, and D. R. Critchley. 1999. Talin contains three similar vinculin-binding sites predicted to form an amphipathic helix. The Biochemical journal 341 (Pt 2):257-263.
27. Gingras, A. R., W. H. Ziegler, R. Frank, I. L. Barsukov, G. C. Roberts, D. R. Critchley, and J. Emsley. 2005. Mapping and consensus sequence identification for multiple vinculin binding sites within the talin rod. J Biol Chem 280:37217-37224.
28. Lee, S. E., R. D. Kamm, and M. R. Mofrad. 2007. Force-induced activation of talin and its possible role in focal adhesion mechanotransduction. Journal of biomechanics 40:2096-2106.

29. Hyt√∂nen, V. P., and V. Vogel. 2008. How force might activate talin's vinculin binding sites: SMD reveals a structural mechanism. PLoS Comput Biol 4:e24.
30. Fillingham, I., A. R. Gingras, E. Papagrigoriou, B. Patel, J. Emsley, D. R. Critchley, G. C. Roberts, and I. L. Barsukov. 2005. A vinculin binding domain from the talin rod unfolds to form a complex with the vinculin head. Structure (London, England : 1993) 13:65-74.
31. del Rio, A., R. Perez-Jimenez, R. Liu, P. Roca-Cusachs, J. M. Fernandez, and M. P. Sheetz. 2009. Stretching single talin rod molecules activates vinculin binding. Science 323:638-641.
32. Izard, T., and C. Vonrhein. 2004. Structural basis for amplifying vinculin activation by talin. J Biol Chem 279:27667-27678.
33. Bass, M. D., B. Patel, I. G. Barsukov, I. J. Fillingham, R. Mason, B. J. Smith, C. R. Bagshaw, and D. R. Critchley. 2002. Further characterization of the interaction between the cytoskeletal proteins talin and vinculin. The Biochemical journal 362:761-768.
34. Papagrigoriou, E., A. R. Gingras, I. L. Barsukov, N. Bate, I. J. Fillingham, B. Patel, R. Frank, W. H. Ziegler, G. C. Roberts, D. R. Critchley, and J. Emsley. 2004. Activation of a vinculin-binding site in the talin rod involves rearrangement of a five-helix bundle. The EMBO journal 23:2942-2951.
35. Izard, T., G. Evans, R. A. Borgon, C. L. Rush, G. Bricogne, and P. R. J. Bois. 2004. Vinculin activation by talin through helical bundle conversion. Nature 427:171-175.
36. Lee, S. E., S. Chunsrivirot, R. D. Kamm, and M. R. Mofrad. 2008. Molecular dynamics study of talin-vinculin binding. Biophys J 95:2027-2036.
37. Bois, P. R., B. P. O'Hara, D. Nietlispach, J. Kirkpatrick, and T. Izard. 2006. The vinculin binding sites of talin and alpha-actinin are sufficient to activate vinculin. J Biol Chem 281:7228-7236.
38. Chen, H., D. M. Cohen, D. M. Choudhury, N. Kioka, and S. W. Craig. 2005. Spatial distribution and functional significance of activated vinculin in living cells. The Journal of cell biology 169:459-470.
39. Arnold, K., L. Bordoli, J. Kopp, and T. Schwede. 2006. The SWISS-MODEL workspace: a web-based environment for protein structure homology modelling. Bioinformatics 22:195-201.
40. Guex, N., and M. C. Peitsch. 1997. SWISS-MODEL and the Swiss-PdbViewer: an environment for comparative protein modeling. Electrophoresis 18:2714-2723.
41. Kelly, J. A., and A. P. Kuzin. 1995. The refined crystallographic structure of a DD-peptidase penicillin-target enzyme at 1.6 A resolution. J Mol Biol 254:223-236.
42. Brooks, B. R., R. E. Bruccoleri, B. D. Olafson, D. J. States, S. Swaminathan, and M. Karplus. 1983. Charmm - a Program for Macromolecular Energy, Minimization, and Dynamics Calculations. Journal of Computational Chemistry 4:187-217.
43. Lazaridis, T. 2003. Effective energy function for proteins in lipid membranes. Proteins 52:176-192.

44. Feig, M., and C. L. Brooks, 3rd. 2004. Recent advances in the development and application of implicit solvent models in biomolecule simulations. Curr Opin Struct Biol 14:217-224.
45. Best, R. B., J. Clarke, and M. Karplus. 2005. What contributions to protein side-chain dynamics are probed by NMR experiments? A molecular dynamics simulation analysis. J Mol Biol 349:185-203.
46. Kraeutler, V., W. F. Gunsteren, and P. H. Huenenberger. 2001. A fast SHAKE algorithm to solve distance constraint equations for small molecules in molecular dynamics simulations¶. J. Comput. Chem. 22:501-508.
47. Neria, E., S. Fischer, and M. Karplus. 1996. Simulation of activation free energies in molecular systems. J. Chem. Phys. 105:1902-1921.
48. Humphrey, W., A. Dalke, and K. Schulten. 1996. VMD: visual molecular dynamics. J Mol Graph 14:33-38.
49. Isralewitz, B., J. Baudry, J. Gullingsrud, D. Kosztin, and K. Schulten. 2001. Steered molecular dynamics investigations of protein function. Journal of molecular graphics & modelling 19:13-25.
50. Karplus, M., and J. A. McCammon. 2002. Molecular dynamics simulations of biomolecules. Nature structural biology 9:646-652.
51. Sotomayor, M., and K. Schulten. 2007. Single-molecule experiments in vitro and in silico. Science (New York, NY) 316:1144-1148.
52. Hytonen, V. P., and V. Vogel. 2008. How force might activate talin's vinculin binding sites: SMD reveals a structural mechanism. PLoS Comput Biol 4:e24.
53. Hollup, S. M., G. Salensminde, and N. Reuter. 2005. WEBnm@: a web application for normal mode analyses of proteins. BMC Bioinformatics 6:52.
54. Suhre, K., and Y. H. Sanejouand. 2004. ElNemo: a normal mode web server for protein movement analysis and the generation of templates for molecular replacement. Nucleic Acids Res 32:W610-614.
55. Hinsen, K. 2000. The molecular modeling toolkit: A new approach to molecular simulations. Journal of Computational Chemistry 21:79-85.
56. Hinsen, K. 1998. Analysis of domain motions by approximate normal mode calculations. Proteins 33:417-429.
57. Ma, J. 2004. New advances in normal mode analysis of supermolecular complexes and applications to structural refinement. Curr Protein Pept Sci 5:119-123.
58. Tirion, M. M. 1996. Large Amplitude Elastic Motions in Proteins from a Single-Parameter, Atomic Analysis. Phys Rev Lett 77:1905-1908.
59. Chen, Y., and N. V. Dokholyan. 2006. Insights into allosteric control of vinculin function from its large scale conformational dynamics. J Biol Chem 281:29148-29154.
60. Lu, M., and J. Ma. 2005. The role of shape in determining molecular motions. Biophys J 89:2395-2401.
61. Cohen, D. M., H. Chen, R. P. Johnson, B. Choudhury, and S. W. Craig. 2005. Two distinct head-tail interfaces cooperate to suppress activation of vinculin by talin. J Biol Chem 280:17109-17117.
62. Johnson, C. P., H. Y. Tang, C. Carag, D. W. Speicher, and D. E. Discher. 2007. Forced unfolding of proteins within cells. Science 317:663-666.

63. Mierke, C. T., P. Kollmannsberger, D. P. Zitterbart, J. Smith, B. Fabry, and W. H. Goldmann. 2008. Mechano-coupling and regulation of contractility by the vinculin tail domain. Biophysical journal 94:661-670.
64. Buehler, M. J., and Y. C. Yung. 2009. Deformation and failure of protein materials in physiologically extreme conditions and disease. Nat Mater 8:175-188.
65. Liu, M., K. Oberg, and Y. Zhou. 2007. Expression and function of vinculin in neuroendocrine tumors. Tumour Biol 28:196-204.
66. Wohl, Y., I. Goldberg, A. Gat, O. Ron-Tal, and S. Brenner. 2008. Expression of vinculin in autoimmune cutaneous diseases. Skinmed 7:63-66.
67. Jaalouk, D. E., and J. Lammerding. 2009. Mechanotransduction gone awry. Nat Rev Mol Cell Biol 10:63-73.
68. Huveneers, S., and E. H. Danen. 2009. Adhesion signaling - crosstalk between integrins, Src and Rho. J Cell Sci 122:1059-1069.
69. Golji, J., R. Collins, and M. R. Mofrad. 2009. Molecular mechanics of the alpha-actinin rod domain: bending, torsional, and extensional behavior. PLoS Comput Biol 5:e1000389.
70. Chen, H. S., K. S. Kolahi, and M. R. Mofrad. 2009. Phosphorylation facilitates the integrin binding of filamin under force. Biophys J 97:3095-3104.
71. Kolahi, K. S., and M. R. Mofrad. 2008. Molecular mechanics of filamin's rod domain. Biophys J 94:1075-1083.
72. Mofrad, M. R., J. Golji, N. A. Abdul Rahim, and R. D. Kamm. 2004. Force-induced unfolding of the focal adhesion targeting domain and the influence of paxillin binding. Mech Chem Biosyst 1:253-265.

Figures

Figure 1. Structure of full-length vinculin.
(A) Vinculin has 5 structural domains: D1, D2, D3, D4, and Vt. The proline-rich linker region is shown in yellow. (B)Vinculin is suggested to bind talin at its D1 region and F-actin at its Vt region once activated. In its inactive conformation vinculin is autoinhibited: D1 of the Vh region sterically inhibits interaction of F-actin with Vt (Arrow points to region of steric hindrance). (C) There are fourteen salt bridges between Vt and Vh stabilizing the autoinhibitory conformation. Of those only three are between D1 and Vt, whereas eleven are between Vt and the other Vh domains.

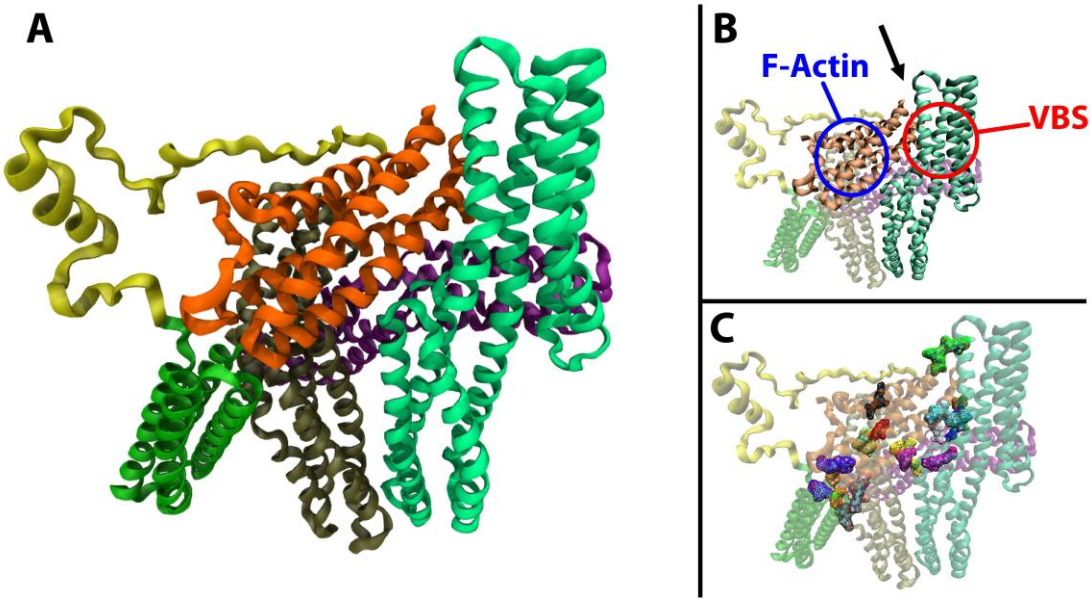

Figure 2. Suggested models of vinculin activation in the cell.
Two competing hypothesis have been presented for the method of vinculin activation. (A) Simultaneous interaction of actin and talin with the two binding sites on vinculin would induce activation, possibly through a stretching force. (B) Talin VBS interacts with vinculin via a helical bundle conversion mechanism. Subsequently vinculin is activated and its Vt domain can interact with actin. Molecular dynamics is used to simulate conformational changes due to stretching of vinculin as suggested by the simultaneous interaction hypothesis, and to simulate conformational changes due to helical bundle conversion. Both sets of simulations are compared to see which is consistent with structural changes needed for vinculin activation.

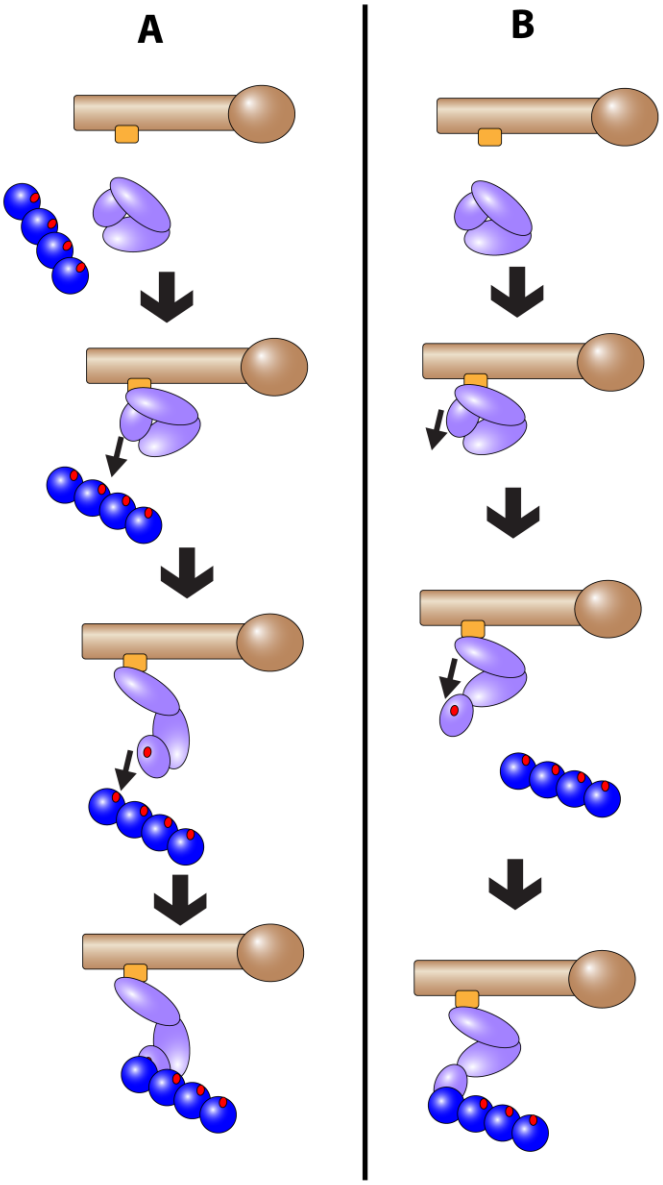

Figure 3. Simulation of vinculin activation by simultaneous interaction.
To simulate the stretching of vinculin due to simultaneous interaction with actin and talin force was applied to Vt (binds to actin) away from the VBS binding region of Vh. (A) The direction of force is shown with the arrow. Four residues nearest the center of mass of the VBS binding region of Vh were constrained (triangle) while 50 pN and 100 pN of constant force was applied to the four residues nearest the center of mass of Vt (residues shown in wire-mesh). (B) After over 300 ps of simulation the VBS binding region of Vh was moved away from Vt. This conformational change involved bending of helical regions in domain 1. As the simulation progressed the VBS binding region moved further away from Vt. Shown here is the conformation of vinculin with the VBS binding region ~120 Å away. At this conformation the steric hindrance preventing Vt interaction with actin is removed and vinculin is likely activated.

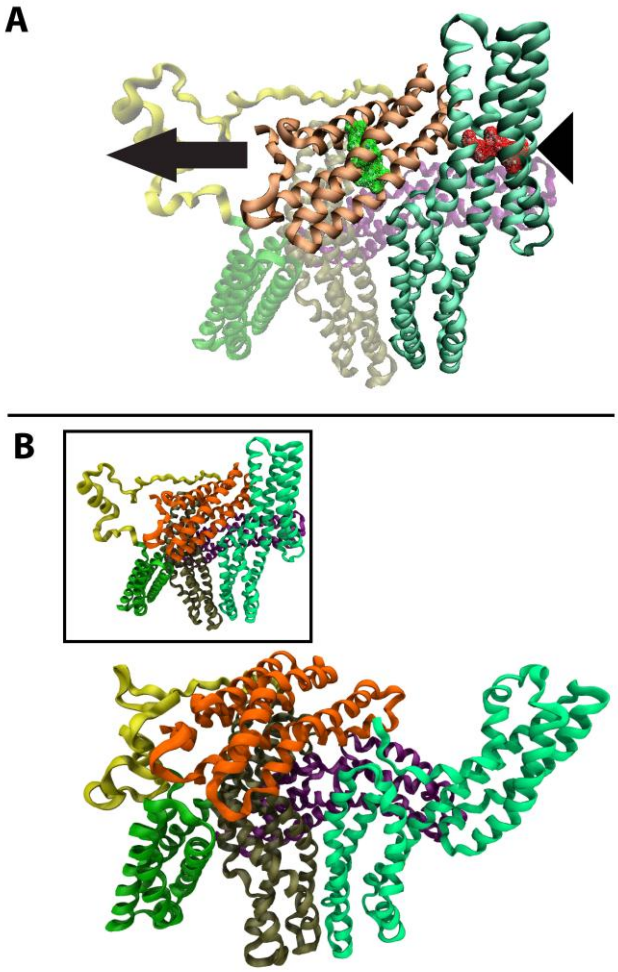

Figure 4. Helical bundle conversion in full-length vinculin.
(A) Vinculin-VBS complex that was formed using structural information from PDB 1TR2 and PDB 1T01. Binding to VBS causes local conformational changes in D1. Two helical regions in D1 are pushed apart while VBS is inserted in between. Three sets of electrostatic interactions exist between D1 and Vt: set 1, E29-R945 and E31-R1008, set 2, E14-K996, set 3, R7-E986. Insertion of VBS causes changes in the electrostatic interactions mainly in set 1. (B) Electrostatic interactions in set 1 prior to VBS binding: E29 interacts with R945, E31 interacts with R1008. (C) Set 1 after VBS complex formation and minimization. After rearrangement from VBS binding E31 interacts with R945 and E29 interacts with R1008. (D) The interaction in set 1 rearranges once again after an equilibration for 100ps. The E29 now interacts with both R945 and R1008 while E31 is no longer paired.

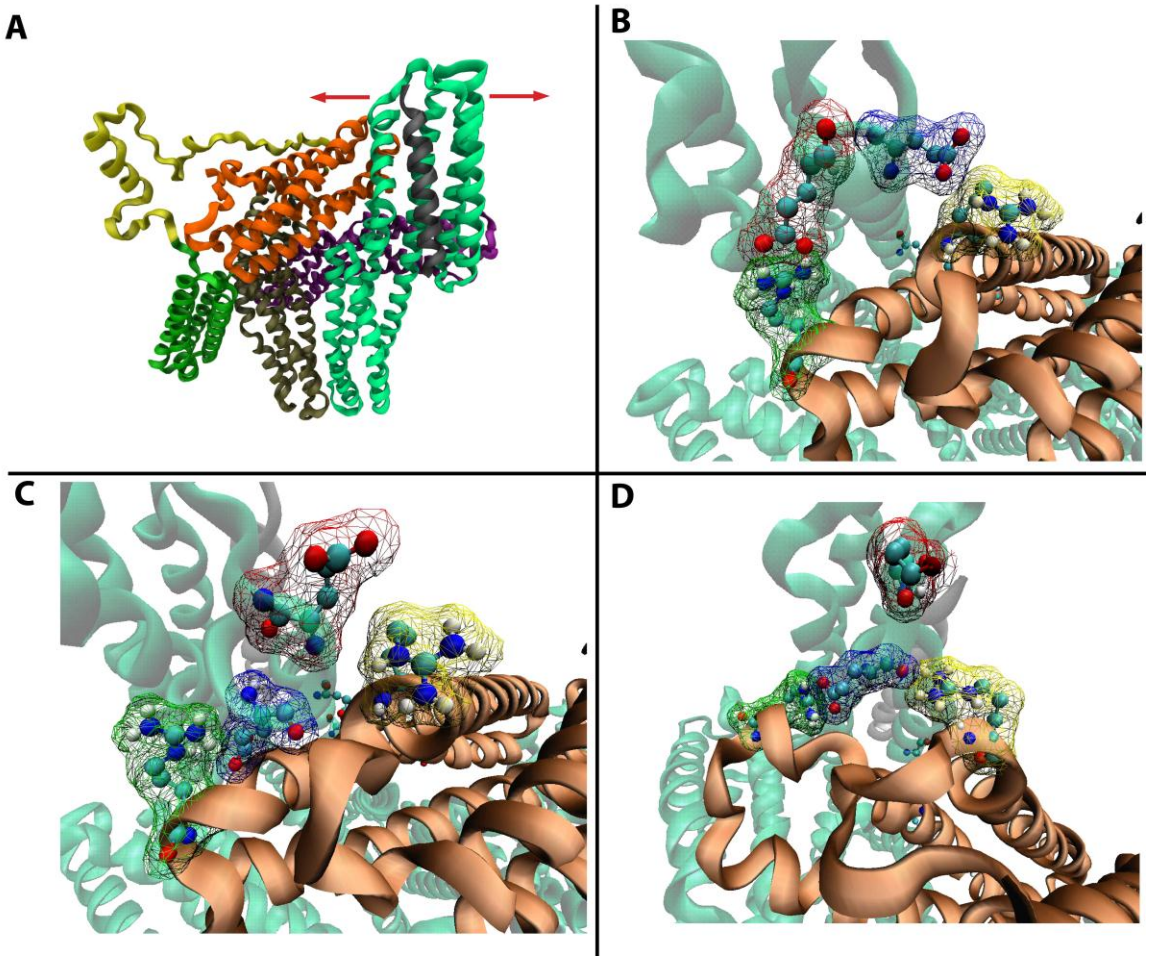

Figure 5. Potential activation of vinculin after exposure to external force.
Forces ranging from 50 pN to 200 pN were used in simulations of vinculin with various molecular dynamics parameters. (A) Results from representative trials show 100 pN of force was needed to alter vinculin while 125pN over 800 ps was needed to alter vinculin with VBS bound. (B) Simulation of vinculin activation with 100pN of force showed that in 8 of the 9 trials 100pN of force over 800ps was sufficient to move domain 1 away from Vt. (C) 100pN is insufficient to move domain 1 away from Vt once it is bound to VBS in any of 5 trials. (D) 125pN of stretching force is necessary to cause domain 1 bound to VBS to move away from Vt in all 5 trial simulations. Together the data suggests that VBS binding increases the force needed to activate vinculin.

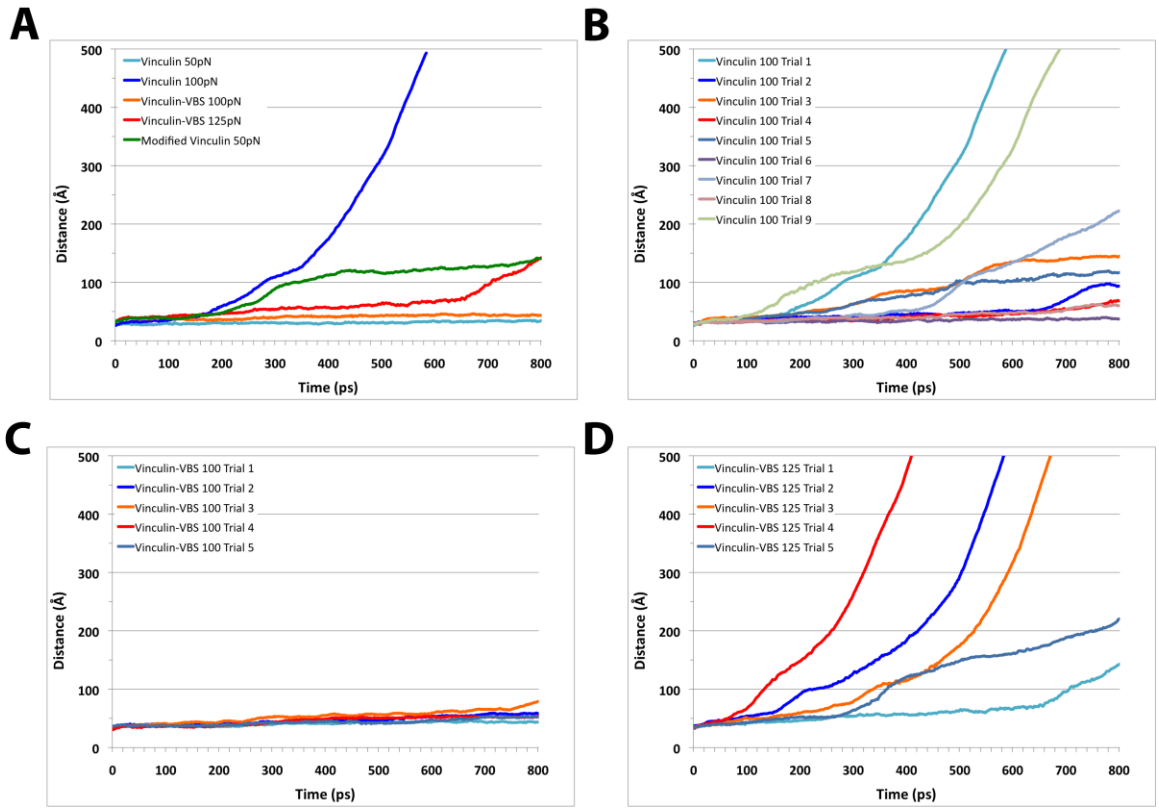

PIP2 Links Vinculin To the Cell Membrane

Abstract

Linkage between vinculin and the cell membrane can be critical to regulating focal adhesion formation. Phosphatidylinositol 4,5-bisphosphate (PIP2) is a membrane embedded acidic phospholipid suggested to interact with basic residues on vinculin. This study evaluates the linkage of vinculin to the cell membrane via PIP2 using molecular dynamics simulations. First, the C-terminus segment of vinculin – a 21 residues segment with several basic residues – was simulated interacting with PIP2 and the lipid membrane. R1049, R1057, and R1060 formed salt-bridges with PIP2 to stabilize the complex. Second, the vinculin tail (Vt) domain was simulated in interaction with PIP2 embedded in the membrane. The R1057 salt-bridge persisted but Vt occluded the other basic C-terminus residues. Third, the interaction of the full-length vinculin structure with PIP2 was simulated. Basic residues on the vinculin head, such as K881, R341, R780, and K784, interacted favorably with PIP2 but the C-terminus and Vt residues were occluded from PIP2. Several polar and basic residues also linked with POPC. The interactions with PIP2 are shown to be more stable and favorable than interactions with POPC. These simulations suggest that the prerequisite for linking to the cell membrane is the presence of exposed basic residues. Linkage of Vt or the C-terminus to the lipid membrane would be unlikely in the absence of conformational changes that would isolate Vt from the vinculin head domains.

Introduction

Focal adhesions are formed at the interface between the cell and its substrate as a means of providing mechanical linkage to the substrate (1). The formation and presence of the mechanical link allows for cell movement, wound healing, and other critical cellular functions (2-8). The focal adhesion itself is a conglomerate of molecules interacting with themselves, with extracellular matrix bound integrins (9, 10), and with cytoskeletal actin filaments (11-13). Talin (14) and vinculin (15) are two focal adhesion-forming molecules critical to the initial formation and the subsequent maturation of focal adhesions (16, 17). Several other proteins and compounds are also critical for facilitating the formation of focal adhesions by talin and vinculin (8, 18). Of particular interest is the compound phosphatidylinositol 4,5-bisphosphate (PIP2) (19), an acidic phospholipid normally embedded within the cellular membrane. The interaction of vinculin with PIP2 and the cellular membrane could play a crucial role in the formation and regulation of focal adhesions.

Vinculin consists of 1066 residues together weighing 117kDa (15). It can exist in either an auto-inhibited closed conformation or an activated open conformation (20). In the cytoplasm, removed from focal adhesions, vinculin exists in its auto-inhibited closed conformation (21). Vinculin consists of 5 domains: domain 1 (D1), domain 2 (D2), domain 3 (D3), domain 4 (D4), and the vinculin tail domain (Vt). D1-

D4 together form the vinculin head and are connected to Vt by a flexible linker region (21, 22). In addition, Vt is linked to the vinculin head domains by a number of salt-bridges and hydrophobic surfaces (23, 24). At focal adhesions, Vt is suggested to bind actin filaments and D1 is suggested to bind to talin, whilein its closed conformation, D1 occludes Vt from binding to actin filaments (25). This closed conformation is stabilized by the multiple interactions linking Vt to the vinculin head (23). Previous molecular dynamics simulations have suggested that the open conformation of vinculin is formed by movement of D1 away from Vt, allowing for interaction of Vt with the actin filaments (24). The activation of vinculin is necessary for its incorporation into focal adhesions (26, 27) and for the growth and maturation of focal adhesions (28).

It has been proposed that an interaction of vinculin with PIP2 could result in its activation (17, 29). PIP2 could effect vinculin activation either directly by inducing conformational changes in vinculin to remove the auto-inhibition, or indirectly by facilitating its activation through another mechanism. The vinculin tail has three distinct patches of charged arginine and lysine residues known as the 'basic collar' (residues 935-978), the 'basic ladder' (residues 1020-1040), and the 'C-terminus' (residues 1052-1066) (30). PIP2 is known to interact with these sites (19) and the interaction could either directly or indirectly lead to vinculin activation. Humphries et al. (17) have shown that cells lacking PIP2 are defective in spreading and migration, and that its presence is therefore essential in regulating focal adhesion dynamics (17), possibly through regulation of vinculin activation. The proposed role of PIP2 in activating vinculin is a typical one ; PIP2 is known to aid in the activation of several other proteins including transmembrane channels, anchoring proteins, and membrane signaling proteins (31).

It has also been proposed that an interaction between vinculin and the cellular membrane could play a part in activation of vinculin and formation of focal adhesions (32). Diez et al. (2) have shown that vinculin can bind to lipids *in vivo and in vitro,* and that such binding is key to cell adhesion and migration. Their study highlights residues 935-978, 1020-1040 and 1052-1066 of Vt (the basic collar, the basic ladder, and the C-terminus basic residues) as critical to interaction with the lipid membrane (2). PIP2 is normally embedded in the lipid membrane (33). Vinculin activation by interaction with PIP2 could be distinct from vinculin activation by interaction with the lipid membrane alone, or these two proposals could effectively be the same mechanism. It is clear that vinculin interacts with both the lipid membrane and with PIP2, but it is uncertain whether these interactions are distinct.

Other proposals concerning mechanisms of vinculin activation and focal adhesion maturation include: activation by interaction with talin (34), activation by co-incidence of talin and actin filaments (35), activation by force and mechanical exposure (24, 36), and activation by phosphorylation (37). These proposals have been widely evaluated both experimentally and computationally (24, 26, 38-46). Investigation of the interaction between vinculin and the lipid membrane, or

vinculin and PIP2 are more limited, however (17, 29, 47, 48). One computational study has investigated the interaction between the last 21 residues of vinculin with the lipid membrane (19). Their simulations showed an interaction and insertion of the C-terminus of vinculin into the lipid membrane. The impact of PIP2 and other regions of vinculin on this interaction, however, have not been evaluated.

This study assessed the impact of PIP2 on the interaction between the last 21 residues of vinculin and the lipid membrane, the impact of other regions of vinculin on the interaction with PIP2 or other regions of the membrane, and the possibility of an interaction between residues outside the vinculin tail with PIP2 or other regions of the membrane. The potential interactions were simulated using the molecular dynamics technique in the absence of any external guiding constraints. These simulations reported the dynamic stability, energetic favorability, and physical nature of these interactions.

Methods

Initial Structure and Configuration

PDB ID 1ST6 was used to build a structure of full-length vinculin (21). The missing proline rich linker region (residues 843-877) was created via homology modeling using the SWISSMODEL toolkit (49), as previously described (24). The structure of open full-length vinculin was taken from a previously published simulation (24). The structure for PIP2 and the associated additional topology data were obtained with the help of Professor Ramone Latorre and Daniel Aguayo from the Center for Bioinformatics & Molecular Simulation at Talca University in Chile. A POPC lipid membrane was created using the *Membrane Builder* feature in VMD (50) with specified dimensions of 200 x 200 Å to accommodate the vinculin proteins. For each simulation, PIP2 was placed at the center of the membrane, and inserted at the position and angle relative to the membrane specified by Li et al. (51). Vinculin was placed within 10Å of the membrane. The entire system was solvated with 12Å of padding at each end of the simulation box. A 0.1M concentration of NaCl was added to the solvent for each simulation configuration.

Eight configurations were set up, each containing a distinct vinculin structure or orientation in complex with a PIP2 embedded membrane: (1) last 21 residues of vinculin with the C-terminus oriented towards the membrane, (2) last 21 residues of vinculin with a second orientation of the vinculin residues, (3) Vt with the C-terminus oriented towards the membrane, (4) full-length vinculin in a closed conformation with the C-terminus oriented towards the membrane, (5) full-length vinculin in an open conformation with the C-terminus oriented towards the membrane, (6) full-length vinculin with K35 oriented towards the membrane, (7) full-length vinculin with R341 oriented towards the membrane, (8) full-length vinculin with K781 and R780 oriented towards the membrane.

Molecular Dynamic Simulation

Simulations were carried out using the NAMD Scalable Molecular Dynamics program (52). Periodic boundary conditions were used along with a Langevin piston Nose-Hoover (53) mechanism for pressure control at 1 Atm. Constant temperature of 310K was maintained using a Langevin damping coefficient of 5/ps. Rigid bonds were enforced between hydrogen atoms and their bound larger atoms (54). The CHARMm 27 force fields were used (55, 56). Simulation timesteps of 1fs were used for all molecular dynamics.

Each configuration was first minimized for 1000 steps using the conjugate gradient and line search algorithm implemented in NAMD (52). Following minimization each configuration was simulated for 10ns or until equilibration. Several trials were produced for each configuration to observe consistency. For each trial the molecular dynamics of the structure was re-initiated with a new minimization, randomized initial velocity , and equilibration, ensuring stochastic differences were preserved between the trials. All simulation results were visualized and analyzed using VMD (50).

Results

The interaction of vinculin with the lipid membrane and PIP2 was simulated with three molecular systems: (1) residues 1046-1066 (last 21) along with a PIP2 embedded lipid membrane, (2) residues 896-1066 (Vt) along with a PIP2 embedded lipid membrane, and (3) residues 1-1066 (full-length vinculin) along with a PIP2 embedded lipid membrane (Figure 1). Each system was arranged with the vinculin residues initially placed within 10Å of the PIP2 embedded lipid membrane and then simulated with no external constraints using the molecular dynamics methodology. Each of these simulations was repeated several times using the same initial arrangement and also several times using different initial arrangements (Table S1). The resulting molecular translations, conformational changes, and intermolecular connections that were exhibited in each simulation were governed by (a) non-specific stochastic movements of all the atoms in the system and (b) specific intermolecular forces acting between the vinculin residues and the PIP2 embedded lipid membrane.

Interaction between PIP2 and the last 21 residues of vinculin

In the first set of simulations a structure of the last 21 residues from vinculin (residues 1046-1066) was placed near (within 10Å) a PIP2 embedded in a POPC lipid membrane. Studies have suggested interaction between residues 1052-1066 and acidic phospholipids (19), thus the last 21 residues were arranged such that these residues were oriented towards the nearby PIP2. Arrangement of vinculin with its binding residues oriented towards PIP2 reduced the entropic barrier to binding and allowed for simulation of their interaction within the nano-second timescale. Two arrangements were used in these sets of simulations. In three simulation trials (trial 1-3) the last 21 residues of vinculin were arranged such that residues 1052-1066 were oriented towards PIP2 only. In the other three simulation

trials (trial 4-6) the last 21 residues of vinculin were arranged such that residues 1052-1066 weree oriented towards both PIP2 and nearby POPC lipids.

In trial 1 residues R1049 and R1057 of vinculin formed a stable intermolecular interaction with PIP2 of the lipid membrane (Figure 2 A). As the simulation progressed, the distance between both R1049 and R1057 and the PIP2 phospholipid decreased to within 2Å (Figure S1 A). The two arginine residues are positively charged and formed a salt-bridge with the negatively charged phosphate group of PIP2 reducing the potential energy of the molecular system and stabilized the complex. The salt-bridge between PIP2 and R1049 stored 150 Kcal/mol of electrostatic potential energy (Figure 3 A) and the salt-bridge between PIP2 and R1057 storee 175 Kcal/mol of electrostatic potential energy (Figure 3 B). In trial 2 and trial 3 the salt bridge between PIP2 and R1057 were again formed (Figure S1 BC) and were able to store 175 Kcal/mol of electrostatic potential energy (Figure 3 B). In trial 2 an additional interaction was formed between a POPC nearby to PIP2 and T1062 (Figure S1 B). This interaction was between a polar threonine residue and the POPC lipid. Calculation of the potential energy changes during interaction between POPC and T1062 (Figure 3 E) showed no significant change. Although the POPC and T1062 were interacting, their interaction did not contribute to stabilizing the linkage between the last 21 residues and the lipid membrane.

Simulation of the last 21 residues oriented towards both PIP2 and nearby POPC lipids resulted in close interaction of R1060, Y1065, or Q1066 with either PIP2 or POPC: in trial 4, R1060 linked with PIP2 and Q1066 linked with POPC (Figure 2 B and S1 D); in trial 5, T1065 linked with POPC (Figure S1 E); and in trial 6, Q1066 linked with PIP2 (Figure S1 F). Of these interactions, the interaction between R1060 with PIP2 resulted in a significant reduction in electrostatic potential energy (175 Kcal/mol) (Figure 3 CDF). Other interactions were between the charged PIP2 and polar residues, whereas the interaction between R1060 and PIP2 resulted in formation of a stable salt-bridge. Although orienting the last 21 residues towards both PIP2 and the nearby POPC encouraged interaction between vinculin and POPC, these resulting interactions were less stabilizing than the salt-bridges that were formed with PIP2 alone.

Interaction between PIP2 and the Vt domain of vinculin

In simulation of the interaction between PIP2 and the last 21 residues of vinculin R1049, R1057, and R1060 formed strong stabilizing electrostatic interactions with the phosphates on PIP2. These positively charged residues have also previously been predicted to bind the lipid membrane (2). Although there was an affinity for PIP2 and the lipids by these arginine residues, it remained possible that nearby residues from the vinculin tail could prevent their interaction. To evaluate this possibility, a second set of simulations were arranged with the Vt domain of vinculin within proximity of PIP2. The Vt structure was oriented such that the last 21 residues, including R1049, R1057, and R1060, were oriented towards PIP2. Three trials with this configuration were simulated.

In all three trials a stable interaction formed between R1057 and PIP2 (Figure 4 A). The interaction was stable for 8ns of simulation in trial 1 (Figure S2 A). In trial 2 and 3, the interaction was initially formed and then the link was stochastically dissociated (Figure S2 BC). In all three trials, the salt-bridge that was formed was stabilizing and reduced the total electrostatic potential energy by at least 125 Kcal/mol (Figure 4 B). The energetic gain from this interaction was smaller than the 175 Kcal/mol from simulations of the last 21 residues with PIP2 (Figure 3 B). Although in both simulations R1057 was interacting with PIP2, in simulation with the Vt structure the nearby Vt residues limited the closeness of the link between R1057 and PIP2: the distance between the residues was 4Å throughout most of the simulation (Figure S2 A). In trial 3 an additional interaction was formed between POPC and R945 (Figure S2 C), but this interaction lacked the stabilizing electrostatic energy change seen with interaction of R1057 with PIP2. These results suggest the Vt structure does limit the efficacy of a PIP2 interaction with R1049, R1057, or R1060. Nevertheless, in all three simulations a significant interaction was formed and Vt is likely to be linked to the lipid membrane.

Interaction between PIP2 and the Vt domain with the full-length vinculin structure
Vinculin is a multi-domain protein with four domains (D1-D4) making up its head region and Vt making up its tail region (21). The protein can adopt either a closed conformation or an open conformation. Recently, a model of the open conformation of vinculin has been suggested (24). In both the closed conformation and the suggested open conformation, head region residues were near to R1049, R1057, R1060 and other PIP2 interacting residues. To evaluate if these nearby residues impacted the interaction between PIP2 and charged residues in Vt, a third set of simulations were produced. In three simulations, full-length vinculin in its closed conformation was arranged with the last 21 residues oriented towards PIP2 and in three simulations full-length vinculin in its suggested open conformation was arranged with the last 21 residues oriented towards PIP2. In one simulation with closed vinculin the vinculin moved away from PIP2 and was discounted from analysis.

In one trial with full-length vinculin in its closed conformation placed near PIP2, an interaction was formed between E857, G868, and POPC (Figure 5 A and S3 A). This link brought nearby E879 into close proximity of PIP2. Since both the glutamate and the phosphate group were negatively charged, this proximity increased the potential energy of the system by more than 100 Kcal/mol (Figure 6 A), and likely reduced the stability of the complex. In the second trial, also using the closed conformation, K881 formed a stable link with PIP2 (Figure S3 B) and the proximity of its positive charge to the phosphate of PIP2 reduced the system's potential energy by 175 Kcal/mol (Figure 6 A). In both trials the residues from the loop region would link to the lipid membrane and not residues from Vt (Figure 5 A). In the full-length vinculin structure the residues from the loop region occluded the last 21 residues and were thus more likely to interact with the nearby lipid membrane.

Three trials (trial 3-5) were also simulated using a full-length vinculin structure in the suggested open conformation (24). In all three trials vinculin was oriented with the last 21 residues towards PIP2, but in only one of the trials (trial 5) did a residue link with PIP2. K731 linked with PIP2 after simulation in trial 5 (Figure 5 B and S3 E). Although the lysine's positive charge was stabilizing, the linkage also brought negatively charged E727 in close proximity of PIP2 (Figure S3 E). The combined electrostatic potential energy loss from interaction of K731 with PIP2 and the electrostatic potential energy gain from interaction of E727 with PIP2 resulted in a volatile total potential energy change for the system (Figure 6 A). Aside from linkage to PIP2, residues R341, G342, Q343, A742, Q745, and E884 all showed linkage to POPC (Figure 5 B and S3 E). Also in trials 3, residues Q1066, Y1065, R547, and P347 linked to POPC (Figure S3 C), and in trial 4, residues S346, K738, and R853 linked to POPC (Figure S3 D). None of these interactions with POPC however significantly changed the potential energy of the system (Figure 6 B-E).

As with simulation of full-length vinculin in its closed conformation, the vinculin head residues were more likely to interact with PIP2 than Vt residues. The suggested open conformation of vinculin has D1 of the head region translated away from Vt. This conformational change however was not sufficient to allow Vt residues to bind the lipid membrane. In six trial simulations with full-length vinculin, only trial 2 displayed a stable, energetically favorable, salt-bridge from between vinculin and PIP2. The interaction between the last 21 residues and the lipid membrane seemed less likely when considering the impact of the nearby vinculin head residues.

Interaction of PIP2 with other basic residues on vinculin

A final possibility concerning the interaction between vinculin and PIP2 is the presence of stable lipid interaction sites at other vinculin regions away from Vt. To investigate this possibility seven additional simulations were produced with different vinculin orientations. In one trial the charged residue K35 was oriented towards PIP2, in two trials R341 was oriented towards PIP2, and in the remaining 4 trials R780 and K784 were oriented towards PIP2 (Figure 7).

Simulation with K35 initially oriented towards PIP2 did not result in linkage between K35 and PIP2. Instead, two nearby residues, V32 and D33, linked with the nearby PIP2 and became closer to the lipid membrane (Figure S4 A). This resulting complex was energetically unstable, as the negative charge of D33 interacted unfavorably with the negative charge of the phosphate group from PIP2, resulting in an increase in the potential energy of the complex by 100 Kcal/mol (Figure 8 A). In contrast, simulations with R341, or K784 and R780 oriented towards PIP2 resulted in favorable interactions that stabilize the complex (Figure 8 BC). In two trials with R341 oriented towards PIP2 a linkage was formed between R341 and PIP2 (Figure S4 BC) and each linkage stabilized the complex by reducing the potential energy by 175 Kcal/mol (Figure 8 B).

In four trials with K784 and R780 oriented towards PIP2 a linkage between PIP2 and K784 was formed in two trials (Figure S4 DG) and a linkage between PIP2 and R780 was formed in the other two trials (Figure S4 EF). Both K784 and R780 are positively charged residues and their interaction with PIP2 was predicted to be stabilizing. Calculation of the changes in potential energy of the complex following interaction with PIP2 confirmed that these interactions were favorable and could stabilize the complex (Figure 8 C). In one particular simulation, trial 5, PIP2 was interacting with both K784 and R780, resulting in a reduction in the potential energy of the complex by 325 Kcal/mol (Figure 8 C). In trial 4 PIP2 interacted with the charged K784 and a nearby polar residue 792. In trial 6 PIP2 interacted with the charged residue R780 and a nearby polar residue P777. In both trial 4 and trial 6 the potential energy reduced by the interaction was less than the reduction from trial 5 (Figure 8 C). In trial 7, the interaction between PIP2 and K784 brought E781 near to PIP2. This negatively charged residue reduced the energetic benefit of the linkage and the interaction never reduced the potential energy of the complex by more than 100 Kcal/mol (Figure 8 C).

Discussion

The interaction between vinculin and the lipid membrane has been well documented (32, 48, 57). Both experiments and simulations (2, 19) have suggested that the last 21 residues of the vinculin tail are especially likely to interact with the lipid membrane. Furthermore, a body of evidence has suggested an interaction between the membrane associated PIP2 and vinculin (17). The simulations from this study probe the structural mechanisms underlying the interaction between vinculin and the lipid membrane to determine (i) the likelihood of an interaction between the last 21 residues and the membrane, and (ii) the likelihood of a specific interaction with PIP2.

Three sets of simulations were produced. The first set simulated the linking of a vinculin structure with only the last 21 residues to the membrane. Residues R1049, R1057, and R1060 were shown to form favorable and stable salt-bridges with PIP2 of the membrane (Figure 2). The second set simulated the linking of a structure with only the Vt domain to the membrane. Although the Vt residues nearby to the last 21 residues did prevent interaction of PIP2 with some of those residues, R1057 maintained a strong and favorable interaction with PIP2 (Figure 4). The third set of simulations evaluated the impact of the full-length vinculin structure on the interaction of vinculin with the membrane. Simulation of full-length vinculin with the last 21 residues of vinculin oriented towards PIP2 showed an interaction between PIP2 and the last 21 residues to be less likely with vinculin head residues nearby to the vinculin tail (Figure 5). Although K881 did form a stable interaction with PIP2 in one simulation, in the remaining 4 simulations of full-length vinculin binding, no significant favorable interactions were formed between the vinculin head residues and PIP2. The simulations of full-length vinculin with either R341, or R780 and K784 oriented towards PIP2 did link to the lipid membrane, and

especially in the case of the linkage between R780 and K784, they formed favorable interactions with PIP2.

Taken together, the results from the three sets of simulations suggest a simple prerequisite for binding to the membrane: that there be surface exposed charged residues on vinculin. R341, R780, K784, and K881 were the surface exposed charged residues on the full-length vinculin structure and formed stable linkages with PIP2 of the lipid membrane. K35 and R853 were also surface exposed positively charged residues, but nearby to them were D33 and D865, respectively, both of which are negatively charged residues and would interact unfavorably with PIP2. In the simulations with a structure of the last 21 residues only, or with a structure of Vt only, the surface exposed charged residues were R1049, R1057, and R1060. These residues were no longer as exposed in the full-length vinculin structure, and were less likely to bind the membrane.

The suggested prerequisite for binding to the membrane is the existence of an exposed basic residue – also isolated from any nearby negatively charged residues. These conditions are consistent with the suggestions that residues 1052-1066 are likely to bind the lipid membrane (30) as a number of residues near the C-terminus are positively charged: K1061, R1060, R1057, and R1049. Other residues near the C-terminus are polar residues that can also contribute to stabilizing the electrostatic link between vinculin and PIP2 embedded in the membrane: Q1066, T1065, T1062, and T1055. The concentration of charged and polar residues near the C-terminus can account for the observed affinity of this region for the membrane, consistent with the findings of Saunders et al. (58) and Ziegler et al. (59). These studies show that the C-terminal region is essential in PIP2 binding, and residues specific to binding include the clusters of arginine and lysine residues within that region. In both their previous studies, and in our study, these acidic residues are shown to be phospholipid binders.

The results from simulations with full-length vinculin do challenge the suggested importance of the last 21 residues for linkage of vinculin to the lipid membrane. One possibility is that the body of evidence supporting this role for the residues near the C-terminus has fundamentally overlooked the impact of vinculin's structure and has only considered regions of vinculin, such as these residues, in isolation from other regions of vinculin. Another possibility is that these regions are indeed critical to the linkage, but only after significant vinculin conformational change that would expose them for binding to PIP2. The suggested conformation of full-length vinculin in its open conformation (24) has considered movement of D1 that would allow binding between Vt and actin, however, it is possible that further conformational changes would be needed to allow for binding between Vt and the lipid membrane.

What of the impact of PIP2 on vinculin and its association with the membrane? In none of the simulations did vinculin undergo significant conformational changes within the 10ns simulation window as a result of the linkage to PIP2. However, in each of the simulations the interactions between PIP2 and arginine or lysine

residues on vinculin resulted in a reduction of the potential energy of the molecular complex by over 150 Kcal/mol (Figure 3 and 8). The interaction of arginine, lysine, or other charged vinculin residues with POPC from the membrane showed minimal impact on the potential energy of the complex. These results suggest that PIP2 can impact the strength of the linking of vinculin to the lipid membrane significantly, but is not likely to cause major conformational changes in vinculin itself.

Our suggestion is similar to a model of vinculin activation presented by Ziegler et al (59). In their model, vinculin is recruited to the lipid membrane as well as PKC. The ensuing proximity between vinculin and PKC would reduce the entropic barrier to vinculin phosphorylation by PKC and would likely result in a phosphorylation event. This phosphorylation could then impact vinculin activation, a topic worthy of future consideration. One possible site of vinculin phosphorylation is at Y1065 (48). If possible, phosphorylation at that site would then lead directly to dissociation of vinculin from PIP2 and the lipid membrane as the proximity of the negative charge to PIP2 would not be favorable. Also, considering the impact of the full-length vinculin structure on the linkage of PIP2 to Vt, it is possible that the initial linkage of vinculin with PIP2 involves R341, R780, K784, K881, or some other already exposed charged residue. In this case, PIP2 would link Vt at some later stage, perhaps after vinculin activation and conformational changes in vinculin that would isolate Vt for PIP2 binding.

Previous molecular dynamics simulations from Diez et al. (2) showed that the C-terminal residues of vinculin interact with and insert into the lipid membrane. From their study it is unclear how this interaction would change in the presence of PIP2 phospholipid embedded in the membrane. This study has shown that the same 21 residues near the C-terminus are able to interact with the membrane embedded PIP2 and the POPC membrane itself. No lipid insertion was seen in the 10ns of simulation, and interactions with the POPC lipid membrane were inconsistent and short-lived. These interactions were also not energetically favorable as they failed to significantly change the potential energy of the bound complex. In contrast, interactions with PIP2 were energetically favorably, resulting in the potential energy of the complex to be reduced by 175 Kcal/mol. These interactions were consistently sustained throughout the 10ns of simulation and can be characterized as stable.

Acidic phospholipids such as PIP2 have been suggested to be crucial for the process of focal adhesion turnover (30, 58). The results from this study highlight the affinity of vinculin arginine and lysine residues for PIP2, and how its presence permits the association of vinculin with the lipid membrane. Perhaps this association can play a role both in the formation of focal adhesions by allowing for PKC interaction with vinculin, as suggested by Zeigler et al. (59), and in the turnover of focal adhesions. In mature focal adhesions vinculin is bound to F-actin residues through its Vt domain (15). Basic residues within the Vt domain also demonstrate affinity for PIP2. If PIP2 were to supplant F-actin in association with the basic residues of Vt, it could contribute to the removal of vinculin from mature focal adhesions and facilitate

focal adhesion turnover. An initial vinculin conformational change resulting in movement of D1 away from Vt (24, 26) would allow vinculin activation for incorporation into growing focal adhesions. Perhaps a second conformational change would result from residence in focal adhesions, and this change would expose C-terminus Vt residues for interaction with PIP2. Such a suggestion is intriguing and worthy of future investigation.

The linkage of vinculin to the lipid membrane is a critical process in formation and potentially turnover of focal adhesions (30). Simulation of the interaction of vinculin with the lipid membrane, and with PIP2 embedded within the lipid membrane has illuminated some of the mechanisms by which this linkage could occur. The electrostatic attraction of exposed basic vinculin residues for the acidic phospholipid PIP2 has proven to be effective in driving this linkage. It is clear that arginine and lysine residues are to be involved in linking vinculin to PIP2 and the membrane, but which arginine and lysine residues are dominant, and which vinculin domain is dominant in interacting with PIP2 is not clear. If association of vinculin with the lipid membrane occurs at two different stages of the focal adhesion life cycle, then perhaps distinct regions of basic vinculin residues are dominant at these different stages. Understanding the dynamics of the vinculin-PIP2 association as a function of the focal adhesion life cycle is the critical next step in understanding the role of the lipid membrane in focal adhesions.

References

1. Puklin-Faucher, E., and M. P. Sheetz. 2009. The mechanical integrin cycle. J Cell Sci 122:179-186.
2. Diez, G., F. List, J. Smith, W. H. Ziegler, and W. H. Goldmann. 2008. Direct evidence of vinculin tail-lipid membrane interaction in beta-sheet conformation. Biochem Biophys Res Commun 373:69-73.
3. Parsons, J. T., A. R. Horwitz, and M. A. Schwartz. 2010. Cell adhesion: integrating cytoskeletal dynamics and cellular tension. Nat Rev Mol Cell Biol 11:633-643.
4. Nagano, M., D. Hoshino, T. Sakamoto, N. Kawasaki, N. Koshikawa, and M. Seiki. 2010. ZF21 protein regulates cell adhesion and motility. J Biol Chem 285:21013-21022.
5. Koestler, S. A., K. Rottner, F. Lai, J. Block, M. Vinzenz, and J. V. Small. 2009. F- and G-actin concentrations in lamellipodia of moving cells. PLoS One 4:e4810.
6. Lopez, J. I., J. K. Mouw, and V. M. Weaver. 2008. Biomechanical regulation of cell orientation and fate. Oncogene 27:6981-6993.
7. Fraley, S. I., Y. Feng, R. Krishnamurthy, D.-H. Kim, A. Celedon, G. D. Longmore, and D. Wirtz. 2010. A distinctive role for focal adhesion proteins in three-dimensional cell motility. Nat Cell Biol 12:598-604.
8. Zamir, E., and B. Geiger. 2001. Components of cell-matrix adhesions. J Cell Sci 114:3577-3579.

9. Anthis, N. J., and I. D. Campbell. 2011. The tail of integrin activation. Trends in biochemical sciences.
10. Katsumi, A., A. W. Orr, E. Tzima, and M. A. Schwartz. 2004. Integrins in mechanotransduction. Journal of Biological Chemistry 279:12001-12004.
11. Patla, I., T. Volberg, N. Elad, V. Hirschfeld-Warneken, C. Grashoff, R. Fässler, J. P. Spatz, B. Geiger, and O. Medalia. 2010. Dissecting the molecular architecture of integrin adhesion sites by cryo-electron tomography. Nat Cell Biol 12:909-915.
12. Wolfenson, H., Y. I. Henis, B. Geiger, and A. D. Bershadsky. 2009. The heel and toe of the cell's foot: a multifaceted approach for understanding the structure and dynamics of focal adhesions. Cell Motil Cytoskeleton 66:1017-1029.
13. Choi, C. K., M. Vicente-Manzanares, J. Zareno, L. A. Whitmore, A. Mogilner, and A. R. Horwitz. 2008. Actin and alpha-actinin orchestrate the assembly and maturation of nascent adhesions in a myosin II motor-independent manner. Nat Cell Biol 10:1039-1050.
14. Critchley, D. R., and A. R. Gingras. 2008. Talin at a glance. J Cell Sci 121:1345-1347.
15. Ziegler, W. H., R. C. Liddington, and D. R. Critchley. 2006. The structure and regulation of vinculin. Trends in Cell Biology 16:453-460.
16. Jiang, G., G. Giannone, D. R. Critchley, E. Fukumoto, and M. P. Sheetz. 2003. Two-piconewton slip bond between fibronectin and the cytoskeleton depends on talin. Nature 424:334-337.
17. Humphries, J. D., P. Wang, C. Streuli, B. Geiger, M. J. Humphries, and C. Ballestrem. 2007. Vinculin controls focal adhesion formation by direct interactions with talin and actin. J Cell Biol 179:1043-1057.
18. Sarkar, S. 1999. Focal adhesions. Curr Biol 9:R428.
19. Palmer, S. M., M. P. Playford, S. W. Craig, M. D. Schaller, and S. L. Campbell. 2009. Lipid binding to the tail domain of vinculin: specificity and the role of the N and C termini. J Biol Chem 284:7223-7231.
20. Cohen, D. M., B. Kutscher, H. Chen, D. B. Murphy, and S. W. Craig. 2006. A conformational switch in vinculin drives formation and dynamics of a talin-vinculin complex at focal adhesions. J Biol Chem 281:16006-16015.
21. Bakolitsa, C., D. M. Cohen, L. A. Bankston, A. A. Bobkov, G. W. Cadwell, L. Jennings, D. R. Critchley, S. W. Craig, and R. C. Liddington. 2004. Structural basis for vinculin activation at sites of cell adhesion. Nature 430:583-586.
22. Borgon, R. A., C. Vonrhein, G. Bricogne, P. R. J. Bois, and T. Izard. 2004. Crystal structure of human vinculin. Structure 12:1189-1197.
23. Cohen, D. M., H. Chen, R. P. Johnson, B. Choudhury, and S. W. Craig. 2005. Two distinct head-tail interfaces cooperate to suppress activation of vinculin by talin. J Biol Chem 280:17109-17117.
24. Golji, J., and M. R. Mofrad. 2010. A molecular dynamics investigation of vinculin activation. Biophys J 99:1073-1081.
25. Critchley, D. R. 2004. Cytoskeletal proteins talin and vinculin in integrin-mediated adhesion. Biochem Soc Trans 32:831-836.
26. Golji, J., J. Lam, and M. R. Mofrad. 2011. Vinculin activation is necessary for complete talin binding. Biophys J 100:332-340.

27. Izard, T., G. Evans, R. A. Borgon, C. L. Rush, G. Bricogne, and P. R. J. Bois. 2004. Vinculin activation by talin through helical bundle conversion. Nature 427:171-175.
28. Mierke, C. T. 2009. The role of vinculin in the regulation of the mechanical properties of cells. Cell Biochem Biophys 53:115-126.
29. Janssen, M. E., E. Kim, H. Liu, L. M. Fujimoto, A. Bobkov, N. Volkmann, and D. Hanein. 2006. Three-dimensional structure of vinculin bound to actin filaments. Mol Cell 21:271-281.
30. Chandrasekar, I., T. E. Stradal, M. R. Holt, F. Entschladen, B. M. Jockusch, and W. H. Ziegler. 2005. Vinculin acts as a sensor in lipid regulation of adhesion-site turnover. Journal of cell science 118:1461-1472.
31. McLaughlin, S., and D. Murray. 2005. Plasma membrane phosphoinositide organization by protein electrostatics. Nature 438:605-611.
32. Diez, G., P. Kollmannsberger, C. T. Mierke, T. M. Koch, H. Vali, B. Fabry, and W. H. Goldmann. 2009. Anchorage of vinculin to lipid membranes influences cell mechanical properties. Biophys J 97:3105-3112.
33. Czech, M. P. 2000. PIP2 and PIP3: complex roles at the cell surface. Cell 100:603-606.
34. Bois, P. R., B. P. O'Hara, D. Nietlispach, J. Kirkpatrick, and T. Izard. 2006. The vinculin binding sites of talin and alpha-actinin are sufficient to activate vinculin. J Biol Chem 281:7228-7236.
35. Chen, H., D. M. Choudhury, and S. W. Craig. 2006. Coincidence of actin filaments and talin is required to activate vinculin. J Biol Chem 281:40389-40398.
36. Grashoff, C., B. D. Hoffman, M. D. Brenner, R. Zhou, M. Parsons, M. T. Yang, M. A. McLean, S. G. Sligar, C. S. Chen, T. Ha, and M. A. Schwartz. 2010. Measuring mechanical tension across vinculin reveals regulation of focal adhesion dynamics. Nature 466:263-266.
37. Kupper, K., N. Lang, C. Mohl, N. Kirchgessner, S. Born, W. H. Goldmann, R. Merkel, and B. Hoffmann. 2010. Tyrosine phosphorylation of vinculin at position 1065 modifies focal adhesion dynamics and cell tractions. Biochem Biophys Res Commun 399:560-564.
38. Golji, J., R. Collins, and M. R. Mofrad. 2009. Molecular mechanics of the alpha-actinin rod domain: bending, torsional, and extensional behavior. PLoS Comput Biol 5:e1000389.
39. Mofrad, M. R., J. Golji, N. A. Abdul Rahim, and R. D. Kamm. 2006. Force-induced unfolding of the focal adhesion targeting domain and the influence of paxillin binding. Mechanics & chemistry of biosystems : MCB 1:253-265.
40. Chen, Y., and N. V. Dokholyan. 2006. Insights into allosteric control of vinculin function from its large scale conformational dynamics. J Biol Chem 281:29148-29154.
41. Kolahi, K. S., and M. R. Mofrad. 2010. Mechanotransduction: A major regulator of homeostasis and development. Wiley Interdisciplinary Reviews: Systems Biology and Medicine. IN PRESS.

42. Mofrad, M. R., and R. D. Kamm. 2009. Cellular Mechanotransduction: Diverse Perspectives From Molecules to Tissues. Cambridge University Press, New York.
43. Kolahi, K. S., and M. R. Mofrad. 2008. Molecular mechanics of filamin's rod domain. Biophys J 94:1075-1083.
44. Lee, S. E., R. D. Kamm, and M. R. Mofrad. 2007. Force-induced activation of talin and its possible role in focal adhesion mechanotransduction. Journal of biomechanics 40:2096-2106.
45. Lee, S. E., S. Chunsrivirot, R. D. Kamm, and M. R. Mofrad. 2008. Molecular dynamics study of talin-vinculin binding. Biophys J 95:2027-2036.
46. del Rio, A., R. Perez-Jimenez, R. Liu, P. Roca-Cusachs, J. M. Fernandez, and M. P. Sheetz. 2009. Stretching Single Talin Rod Molecules Activates Vinculin Binding. Science 323:638.
47. Mierke, C. T., P. Kollmannsberger, D. P. Zitterbart, J. Smith, B. Fabry, and W. H. Goldmann. 2008. Mechano-coupling and regulation of contractility by the vinculin tail domain. Biophys J 94:661-670.
48. Goldmann, W. H. 2010. Correlation between the interaction of the vinculin tail domain with lipid membranes, its phosphorylation and cell mechanical behaviour. Cell Biol Int 34:339-342.
49. Arnold, K., L. Bordoli, J. Kopp, and T. Schwede. 2006. The SWISS-MODEL workspace: a web-based environment for protein structure homology modelling. Bioinformatics 22:195-201.
50. Humphrey, W., A. Dalke, and K. Schulten. 1996. VMD: visual molecular dynamics. J Mol Graph 14:33-38, 27-38.
51. Li, Z., R. M. Venable, L. A. Rogers, D. Murray, and R. W. Pastor. 2009. Molecular dynamics simulations of PIP2 and PIP3 in lipid bilayers: determination of ring orientation, and the effects of surface roughness on a Poisson-Boltzmann description. Biophysical journal 97:155-163.
52. Phillips, J. C., R. Braun, W. Wang, J. Gumbart, E. Tajkhorshid, E. Villa, C. Chipot, R. D. Skeel, L. Kale, and K. Schulten. 2005. Scalable molecular dynamics with NAMD. J Comput Chem 26:1781-1802.
53. Hoover, W. G. 1985. Canonical dynamics: Equilibrium phase-space distributions. Phys Rev A 31:1695-1697.
54. Kraeutler, V., W. F. Gunsteren, and P. H. Huenenberger. 2001. A fast SHAKE algorithm to solve distance constraint equations for small molecules in molecular dynamics simulations¶. J. Comput. Chem. 22:501-508.
55. MacKerell, A. D. J., D. Bashford, M. Bellot, J. R. L. Dunbrack, J. D. Evanseck, M. J. Field, S. Fischer, J. Gao, H. Guo, S. Ha, D. Joseph-McCarthy, L. Kuchnir, K. Kuczera, F. T. K. Lau, C. Mattos, S. Michnick, T. Ngo, D. T. Nguyen, B. Prodhom, I. W. E. Reiher, B. Roux, M. Schlenkrich, J. C. Smith, R. Stote, J. Straub, M. Watanabe, J. Wiorkiewicz-Kuczera, D. Yin, and M. Karplus. 1998. All-Atom Empirical Potential for Molecular Modeling and Dynamics Studies of Proteins. J. Phys. Chem. B 102:3586-3616.
56. Mackerell, A. D. 2004. Empirical force fields for biological macromolecules: overview and issues. Journal of Computational Chemistry 25:1584-1604.

57. Wirth, V. F., F. List, G. Diez, and W. H. Goldmann. 2010. Vinculin's C-terminal region facilitates phospholipid membrane insertion. Biochem Biophys Res Commun 398:433-437.
58. Saunders, R. M., M. R. Holt, L. Jennings, D. H. Sutton, I. L. Barsukov, A. Bobkov, R. C. Liddington, E. A. Adamson, G. A. Dunn, and D. R. Critchley. 2006. Role of vinculin in regulating focal adhesion turnover. Eur J Cell Biol 85:487-500.
59. Ziegler, W. H., U. Tigges, A. Zieseniss, and B. M. Jockusch. 2002. A lipid-regulated docking site on vinculin for protein kinase C. J Biol Chem 277:7396-7404.

Figure Legends

Figure 1. Three sets of molecular dynamic simulations were produced to evaluate the linkage of vinculin with PIP2 embedded in the membrane. (A) The last 21 residues of vinculin were placed within 10Å of PIP2 embedded in the membrane. The orientation of these last 21 residues relative to PIP2 is shown. The vinculin residues are in purple, PIP2 colored by atom type, and the POPC membrane is shown in gray (transparent). (B) The vinculin tail isolated from the vinculin head domains was arranged with its last 21 residues oriented towards PIP2, as shown. The last 21 residues are shown in purple, the vinculin tail in orange, and PIP2 is shown colored by atom type. The POPC membrane is shown in gray (transparent). (C) Full-length vinculin was simulated along with PIP2 embedded in the lipid membrane. Vinculin was oriented such that its last 21 residues were oriented towards PIP2, as shown. The last 21 residues are shown in purple. The Vt domain in orange, the flexible loop region in yellow, and the vinculin head domains in green. PIP2 is colored by atom type, and the POPC is shown in gray (transparent).

Figure 2. The last 21 residues of vinculin were simulated near PIP2 in two arrangements. (A) In the first orientation last 21 residues were oriented towards PIP2 only. The final stable vinculin-PIP2 complex is shown after simulation with this orientation. The two basic residues R1049 and R1057 formed a stable interaction with PIP2. Results from trial 1 of the set of simulations using the last 21 residues are shown. (B) In the second orientation the last 21 residues were oriented towards both PIP2 and POPC. With this orientation both the basic residues such as R1060 linked with PIP2 and other polar residues such as Y1065 and Q1066 linked with POPC. Results from trial 4 of the set of simulations using the last 21 residues are shown. The last 21 residues are shown in purple, the membrane in gray (transparent), PIP2 colored by atom type, and the interacting POPC in cyan.

Figure 3. Changes in the potential energy of the last 21 residue structure complexed with PIP2 and the membrane were calculated throughout the 10ns duration of the simulation. (A) The potential energy between PIP2 and R1049 was calculated throughout the simulation (red plot). Once the two linked at 5ns into the simulation the potential energy was reduced by 175 Kcal/mol. (B) The potential energy between PIP2 and R1057 was calculated throughout the simulations. Results from

trial 1 are shown in blue, from trial 2 in green, and from trial 3 in purple. In each of the trials when PIP2 and R1057 linked the potential energy of the complex was reduced by 175 Kcal/mol. (C) The potential energy between PIP2 and R1060 was plotted throughout the simulation. In trial 4 (green) PIP2 linked with R1060 at 1ns of simulation and the potential energy of the system was reduced by 175 Kcal/mol. (D) The potential energy between POPC and Q1066 from trial 4 (green) and between POPC and Q1066 from trial 6 (blue). No stable change in the potential energy was seen for this interaction. (E) The potential energy change between POPC and T062 was calculated from trial 2 (red). There was no significant change in the potential energy as a result of their interaction. (F) The potential energy change between POPC and Y1065 from trial 5 (red) is plotted. There was no significant energy change from this interaction.

Figure 4. A structure of the Vt isolated from the head domains was simulated near PIP2. (A) After 10ns of simulation R1057 linked with PIP2 in all three trials with this configuration. The final structure after simulation in trial 1 is shown. The last 21 residues are colored purple, the other Vt residues in orange, PIP2 colored by atom type, and the membrane in gray (transparent). (B) The potential energy between PIP2 and R1057 was calculated for all three trials of the simulations using the Vt structure: trial 1 in blue, trial 2 in red, and trial 3 in green. When R1057 and PIP2 linked, the potential energy of the complex was reduced by 125 Kcal/mol. In simulation 1 the potential energy between the two was further reduced to 200 Kcal/mol after they moved closer together.

Figure 5. Simulations of full-length vinculin interacting with PIP2 and the membrane were produced using both the closed and open conformation of vinculin. (A) Simulation with the closed conformation showed less stable interactions with PIP2 than simulation of isolated Vt. Shown here is the final structure after simulation in trial 2 of the set of simulations with full-length vinculin. E879 was in close proximity of PIP2. Both are acidic in nature and this proximity was unfavorable. POPC linked with E867 and the polar G868. (B) Simulation with the suggested open conformation showed little difference in the ability for Vt to interact with the membrane. Results from trial 5 of the simulations using full-length vinculin is shown. POPC linked with Q745, R341, R853, and E884. There was an interaction between K731 and PIP2, but this brought E727 in proximity of PIP2, an unfavorable interaction. POPC interacting residues are shown in cyan, PIP2 colored by atom type, vinculin head domain residues in green, Vt in orange, loop region residues in yellow, and the last 21 residues in purple.

Figure 6. Simulations using the full-length vinculin structure resulted in interaction with both PIP2 and POPC. Changes in the potential energy between interacting residues were calculated throughout the simulation and plotted here. (A) The potential energy was reduced by 175 Kcal/mol from interaction of PIP2 with K881 in trial 2 (red). The potential energy was reduced by 125 Kcal/mol from interaction of PIP2 with E272 and K731 in trial 5 (purple). This reduction was unstable as the proximity of E272 increased the potential energy. The potential energy was

increased by 100 Kcal/mol by the interaction of PIP2 with E879 in trial 1 (green), another unfavorable interaction. (B) The potential energy was unchanged by the interaction of POPC with P347 in trail 3 (orange), or of POPC with S346 in trial 4 (purple). The potential energy was slightly reduced by 75 Kcal/mol by the interaction of POPC with R341, G342, Q343 in trial 5 (green). (C) The potential energy was unchanged by interaction of POPC with E884 in trial 5 (orange), or POPC with E867 and G868 in trial 1 (green). The potential energy was increased by the interaction of POPC with R853 and R865 in trial 5 (purple), and the potential energy was reduced by 100 Kcal/mol by the interaction of POPC with R853 in trial 4 (blue). (D) The potential energy was largely unchanged by interaction of POPC with R547 in trial 2 (orange), POPC with K738 in trial 4 (purple), or POPC with A742 and Q745 in trial 5 (green). (E) No significant change in potential energy was seen form interaction of POPC with Y1065 and Q1066 in trial 3 (green).

Figure 7. Full-length vinculin was also simulated interacting with PIP2 with residues outside Vt oriented towards PIP2. In one simulation (trial 1 of this set) K35 was oriented towards PIP2, in two simulations (trial 2 and 3) R341 was oriented towards PIP2, and in four of the simulations (trial 4 to 7) R780 and K784 were oriented towards PIP2. K35 did not interact favorably with PIP2 as D33 was nearby to PIP2 and its negative charge was unfavorable. R341, R780, and K784 each formed stable links to PIP2. PIP2 is shown colored by atom type, the cell membrane colored in gray (transparent), vinculin head domains in green, Vt in orange, the loop region in yellow, and the last 21 residues in purple.

Figure 8. The potential energy changes between interacting residues in simulations with full-length vinculin oriented with various basic vinculin head residues oriented towards PIP2 were calculated and plotted here. (A) The interaction between PIP2 and D33, V32, and K35 in trial 1 (purple) resulted in an increase in the potential energy by 100 Kcal/mol and was unfavorable. (B) The interaction of PIP2 with R341 was favorable in both trial 3 (green) and trial 2 (red). In both trials the potential energy was reduced by 175 Kcal/mol. (C) The interaction between PIP2 and R780 and K784 in trial 5 (blue) was very favorable and reduced the potential energy of the complex by 325 Kcal/mol. The interaction of PIP2 with R780 and K784 in trial 4 (green) was also favorable, reducing the potential energy of the complex by 175 Kcal/mol. The interaction of PIP2 with K784 and E781 in trial 7 (purple) initially reduced the potential energy of the complex by 125 Kcal/mol, but as E781 was brought in proximity of PIP2 the potential energy change was nullified at around 8ns of simulation. The interaction between PIP2 and K784 in trial 4 (red) was less favorable and the potential energy of the complex was never reduced more than 75 Kcal/mol.

Figure 1

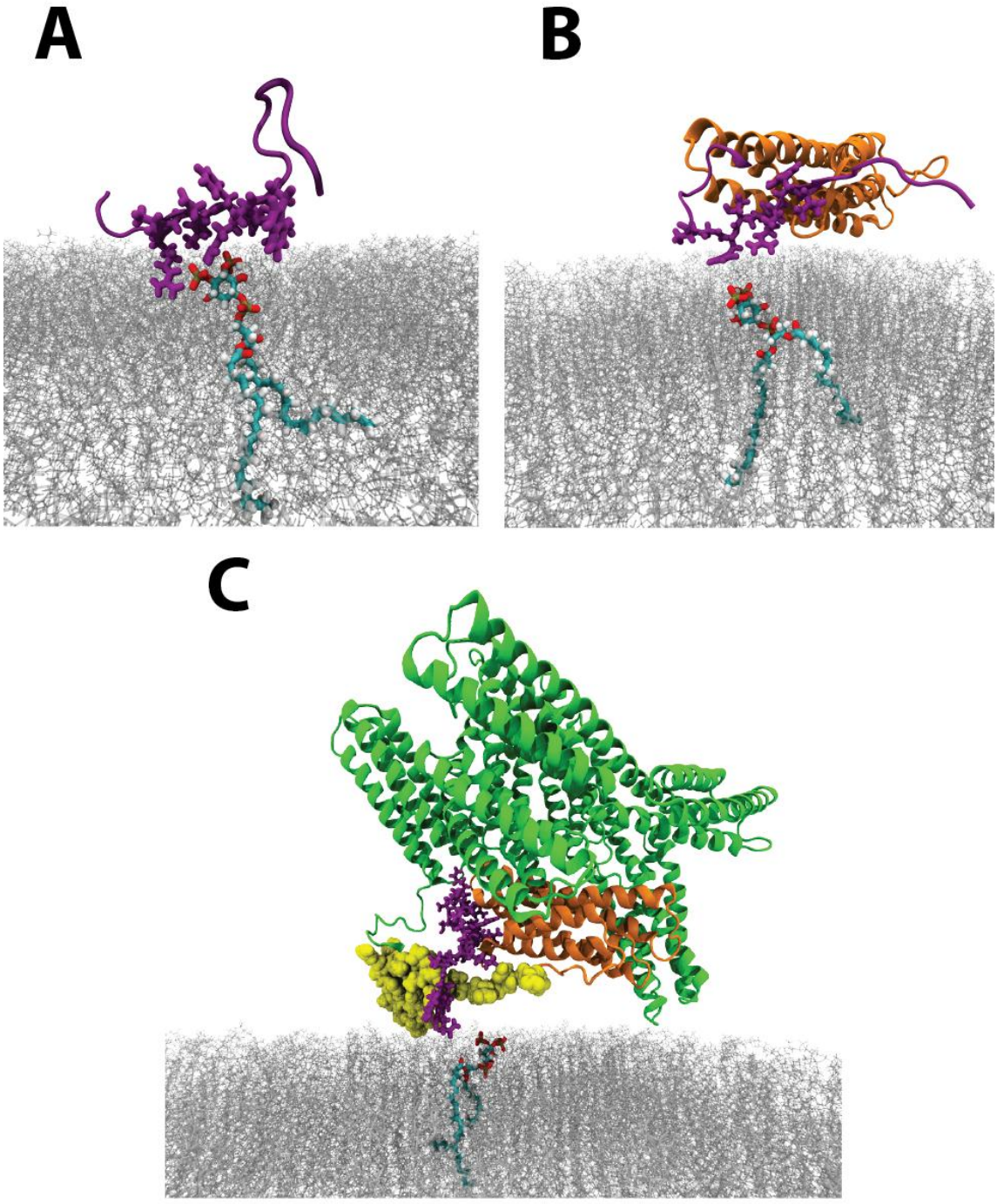

Figure 2

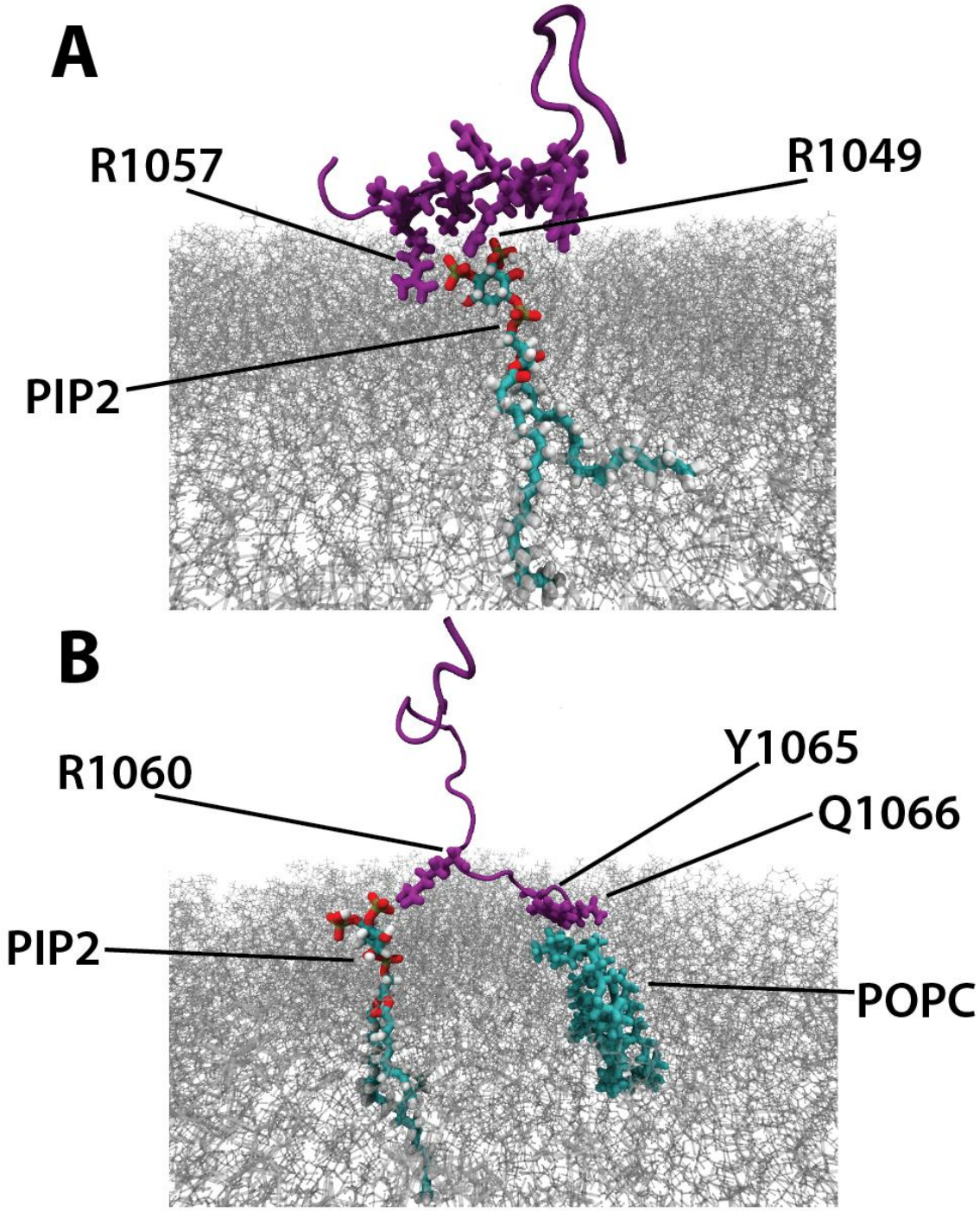

Figure 3

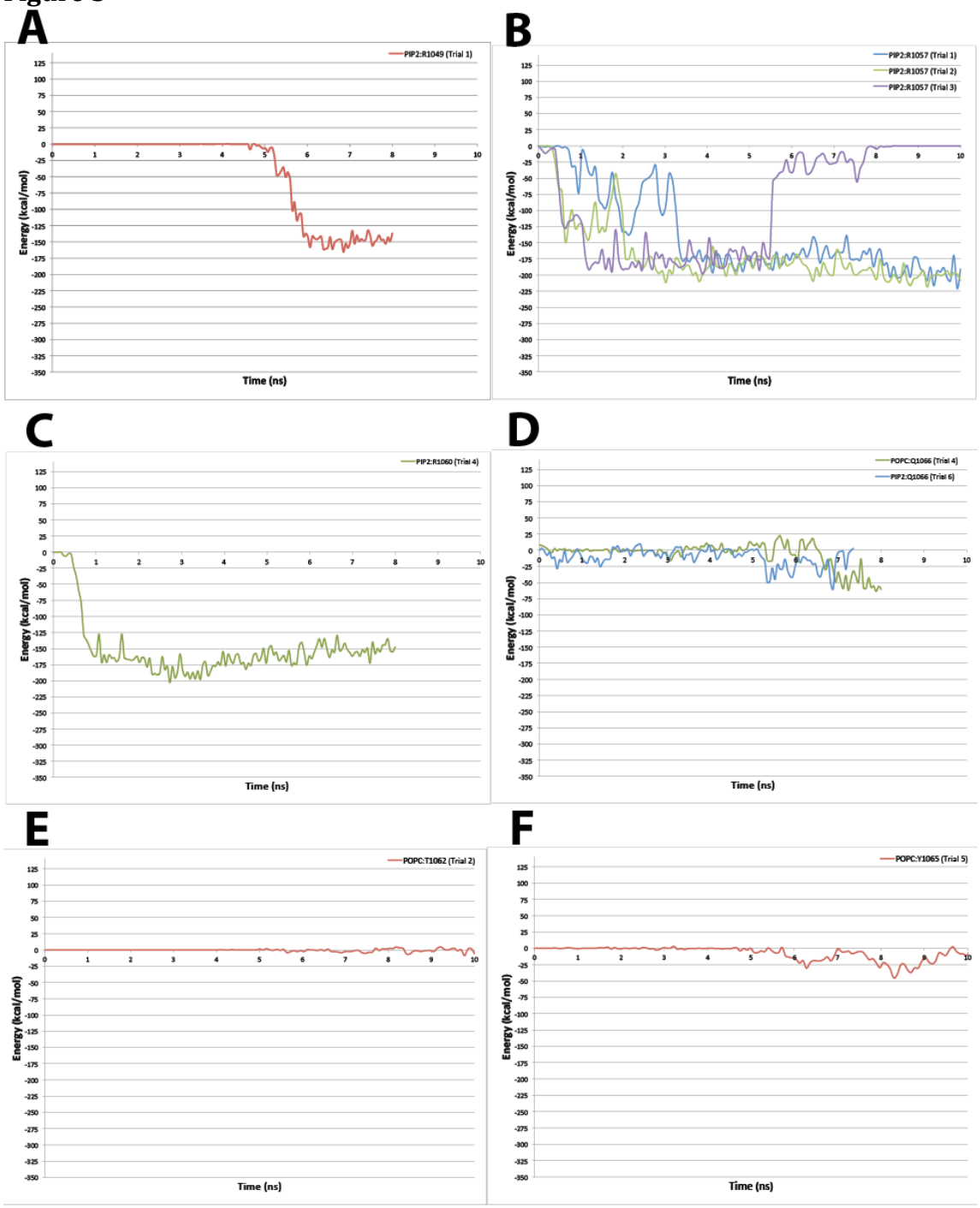
A
PIP2:R1049 (Trial 1)
Energy (kcal/mol)
Time (ns)
B
PIP2:R1057 (Trial 1)
PIP2:R1057 (Trial 2)
PIP2:R1057 (Trial 3)
Energy (kcal/mol)
Time (ns)
C
PIP2:R1060 (Trial 4)
Energy (kcal/mol)
Time (ns)
D
POPC:Q1066 (Trial 4)
PIP2:Q1066 (Trial 6)
Energy (kcal/mol)
Time (ns)
E
POPC:T1062 (Trial 2)
Energy (kcal/mol)
Time (ns)
F
POPC:Y1065 (Trial 5)
Energy (kcal/mol)
Time (ns)

Figure 4

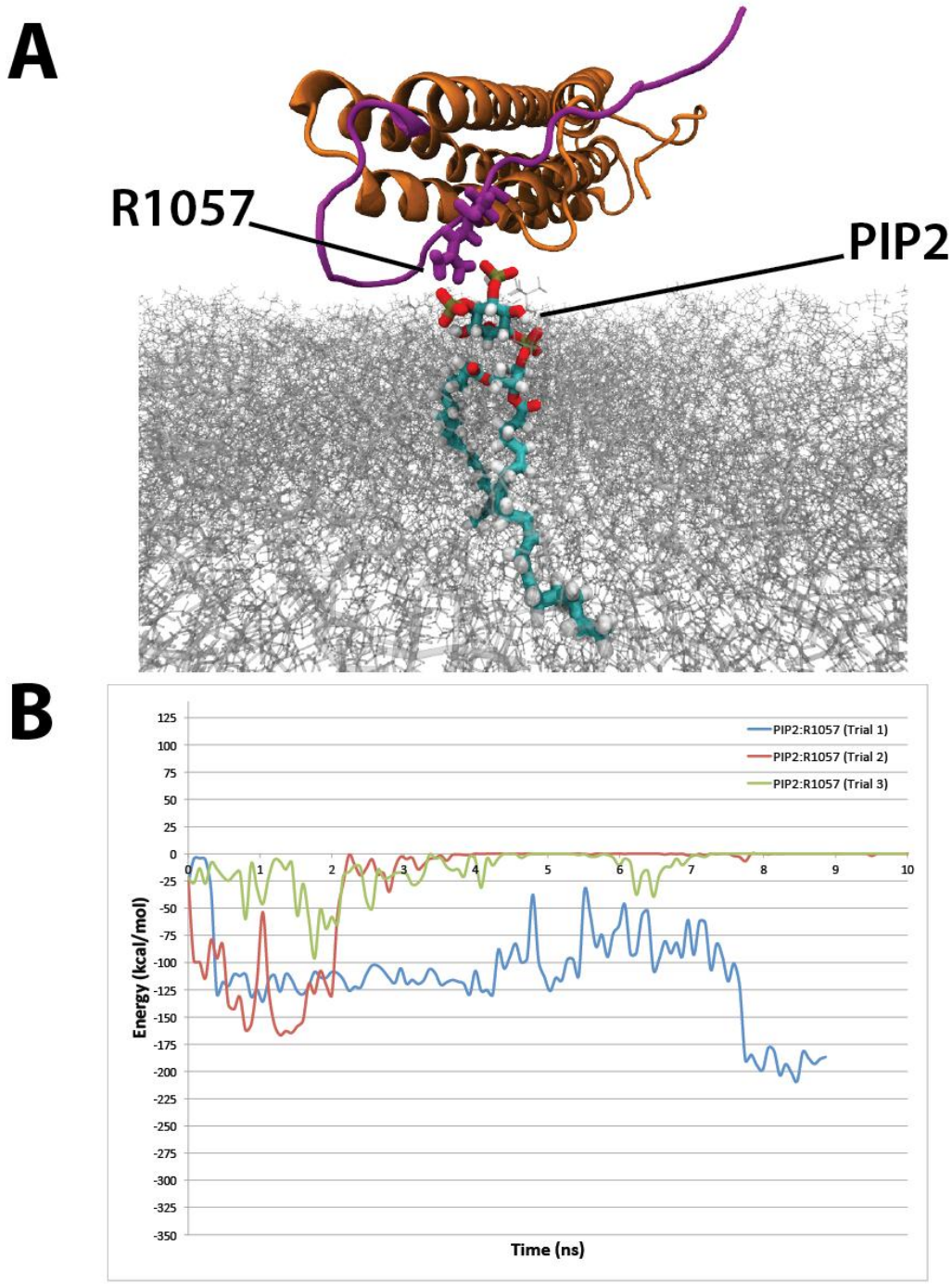
A
R1057
PIP2
B
PIP2:R1057 (Trial 1)
PIP2:R1057 (Trial 2)
PIP2:R1057 (Trial 3)
Energy (kcal/mol)
Time (ns)
125
100
75
50
25
0
-25
-50
-75
-100
-125
-150
-175
-200
-225
-250
-275
-300
-325
-350
0
1
2
3
4
5
6
7
8
9
10

Figure 5

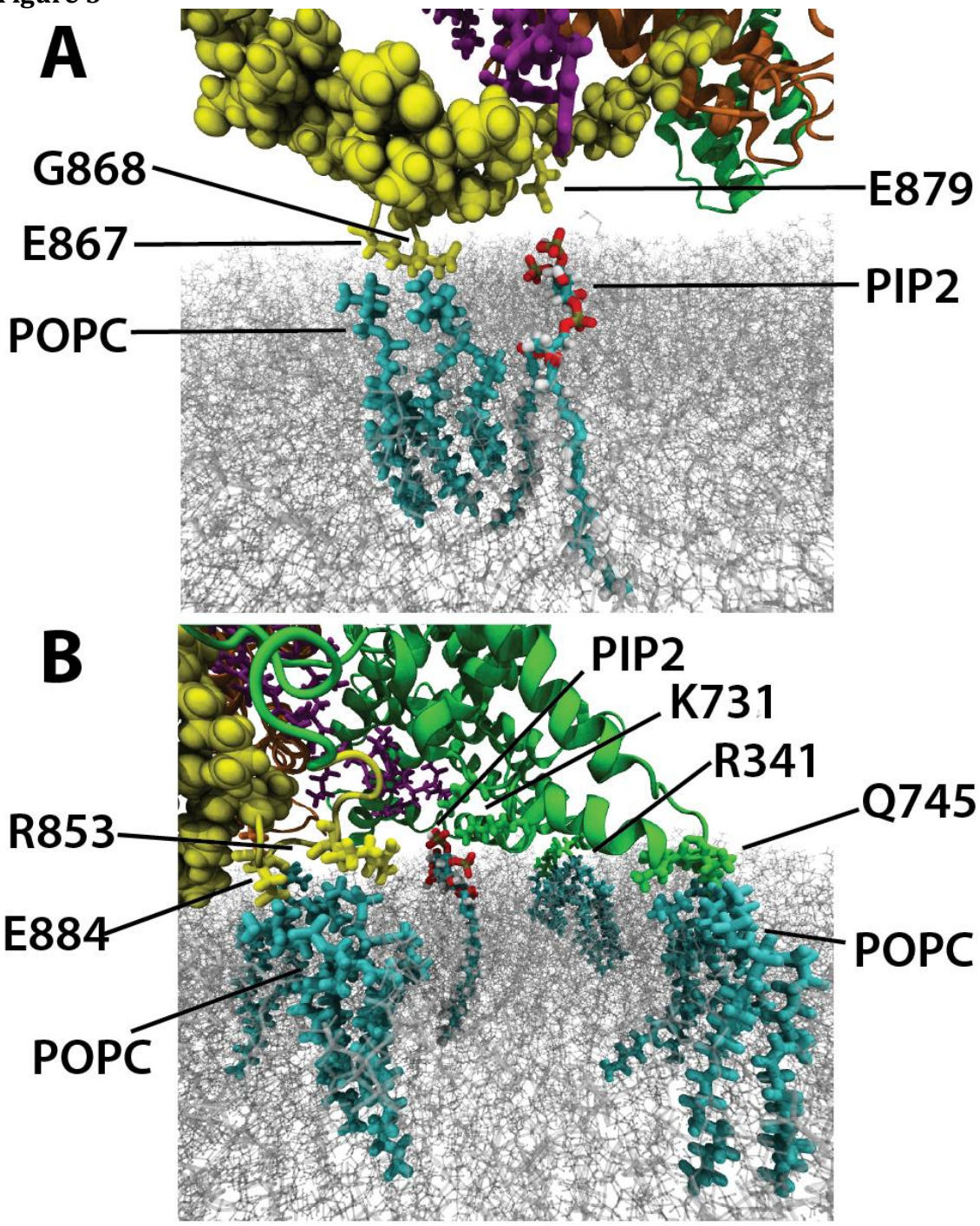
A
G868
E867
POPC
E879
PIP2
B
PIP2
K731
R341
Q745
R853
E884
POPC
POPC

Figure 6

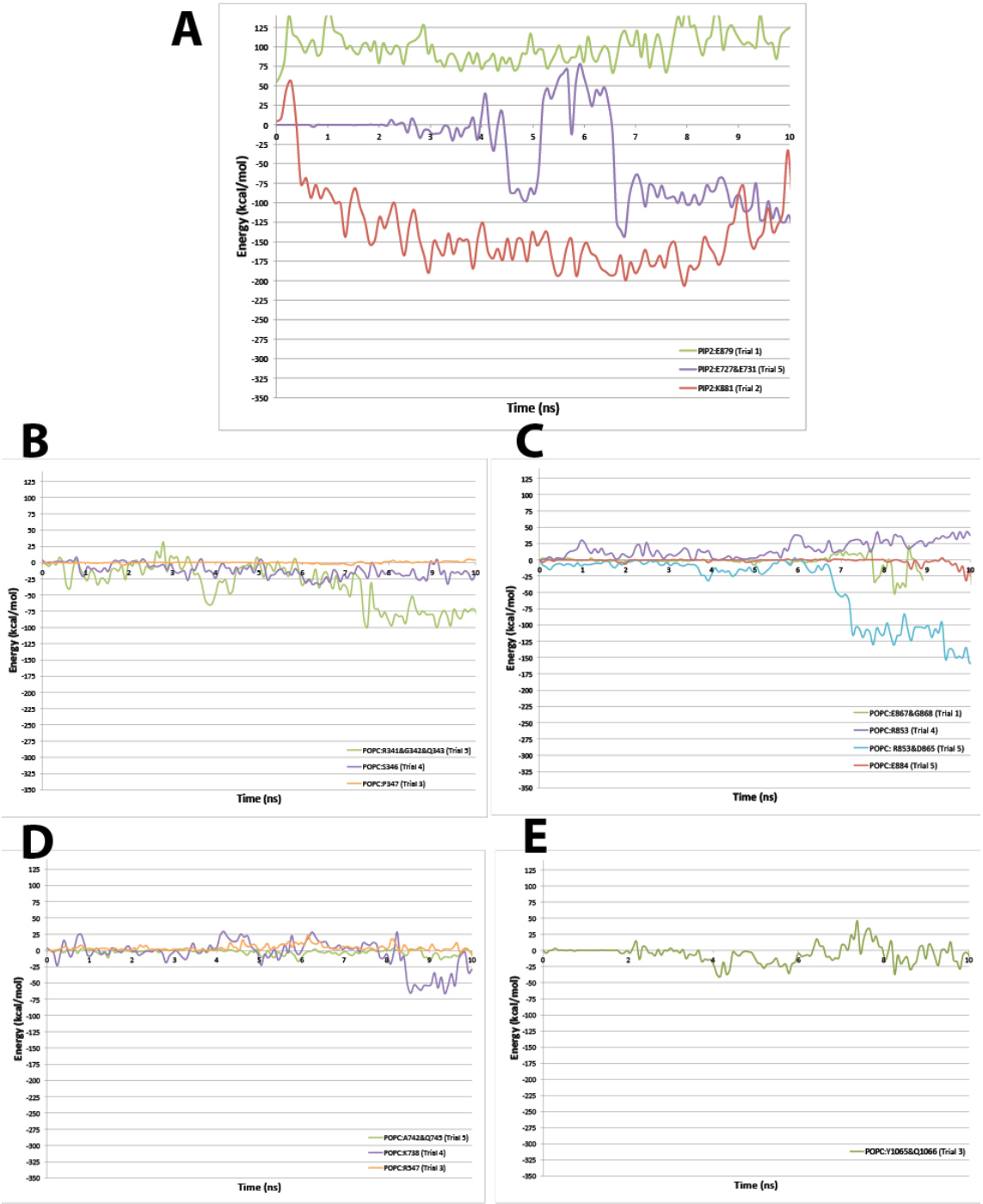
A
Energy (kcal/mol)
Time (ns)
PIP2:E879 (Trial 1)
PIP2:E727&E731 (Trial 5)
PIP2:K881 (Trial 2)
B
Energy (kcal/mol)
Time (ns)
POPC:R341&G342&Q343 (Trial 5)
POPC:S346 (Trial 4)
POPC:P347 (Trial 3)
C
Energy (kcal/mol)
Time (ns)
POPC:E867&G868 (Trial 1)
POPC:R853 (Trial 4)
POPC: R853&D865 (Trial 5)
POPC:E884 (Trial 5)
D
Energy (kcal/mol)
Time (ns)
POPC:A742&Q745 (Trial 5)
POPC:K738 (Trial 4)
POPC:R547 (Trial 3)
E
Energy (kcal/mol)
Time (ns)
POPC:Y1065&Q1066 (Trial 3)

Figure 7

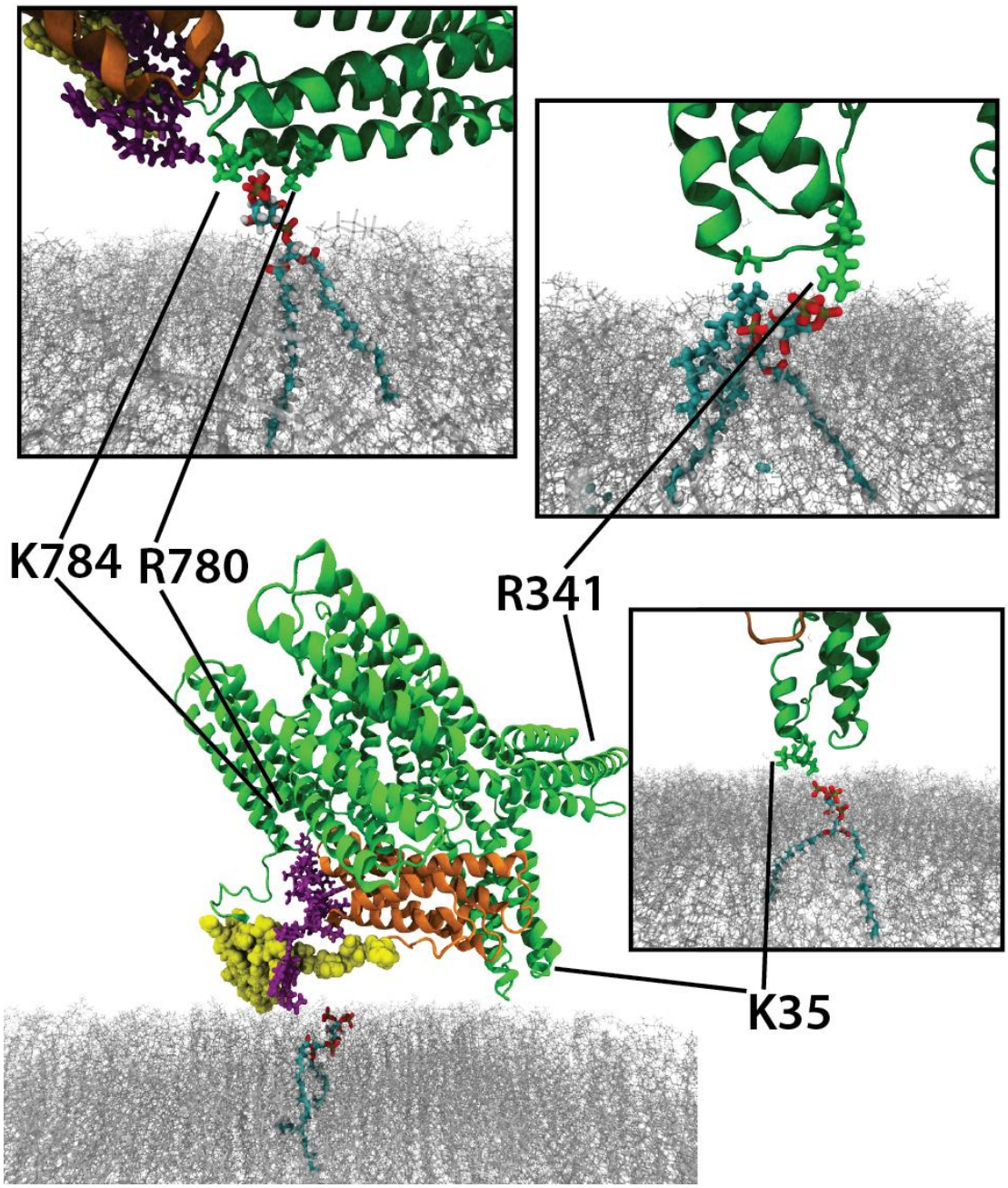

Figure 8

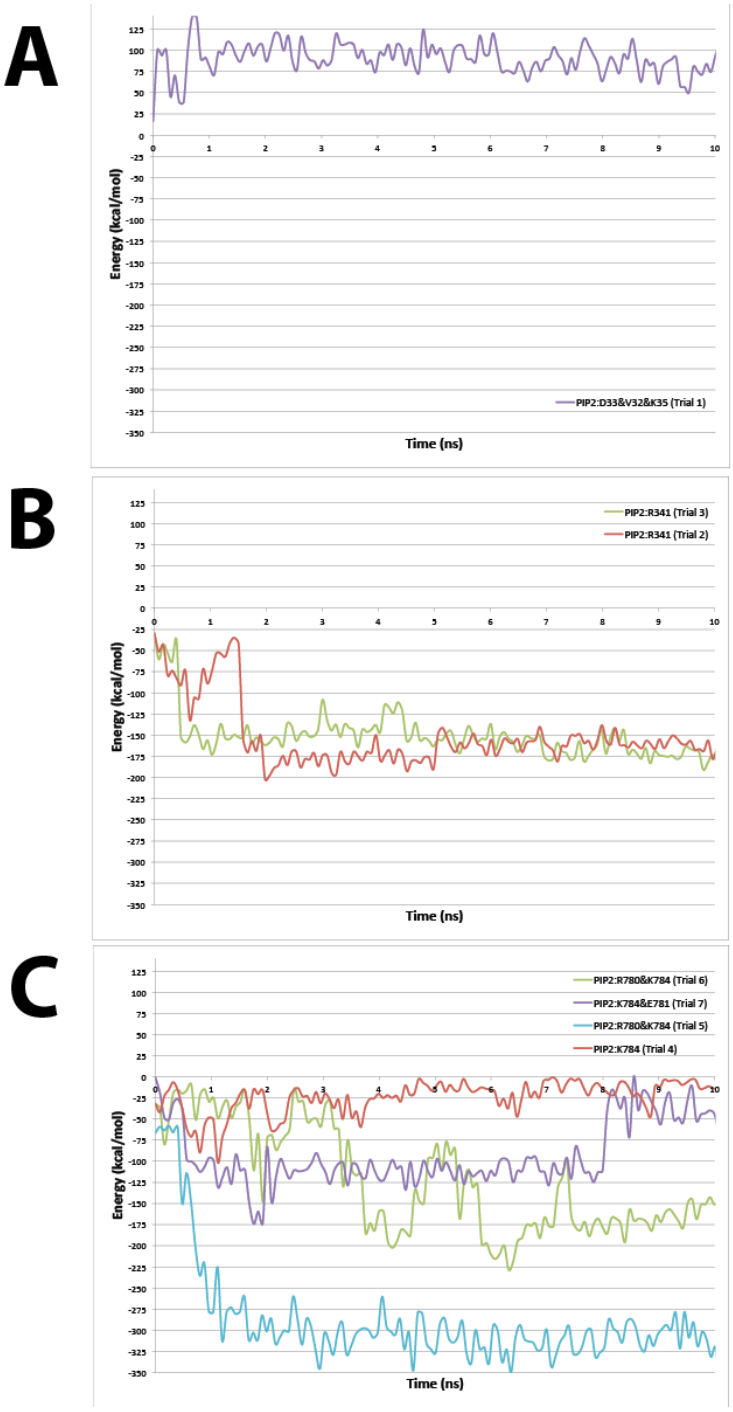
A
Energy (kcal/mol)
Time (ns)
PIP2:D33&V32&K35 (Trial 1)
B
Energy (kcal/mol)
Time (ns)
PIP2:R341 (Trial 3)
PIP2:R341 (Trial 2)
C
Energy (kcal/mol)
Time (ns)
PIP2:R780&K784 (Trial 6)
PIP2:K784&E781 (Trial 7)
PIP2:R780&K784 (Trial 5)
PIP2:K784 (Trial 4)

Phosphorylation Primes Vinculin for Activation

Abstract

Vinculin phosphorylation has been implicated as a potential mechanism for focal adhesion growth and maturation. Four vinculin residues – Y100, S1033, S1045, and Y1065 – are phosphorylated by kinases during focal adhesion maturation. In this study, phosphorylation at each of these residues is simulated using molecular dynamics models. The simulations demonstrate that once each phosphorylated vinculin structure is at equilibrium significant local conformational changes result that may impact either vinculin activation or vinculin binding to actin and PIP2. Simulation of vinculin activation after phosphorylation shows that the added phosphoryl groups can prime vinculin for activation, but do not directly cause vinculin activation. Furthermore phosphorylation at S1033 is especially needed for effective vinculin priming. Vinculin phosphorylation is not sufficient for activation, but may increase the likelihood of an activation event.

Introduction

To understand how a cell senses and responds to its physical environment, it is imperative to understand the signaling logic of the adhesome, the set of structural, mechanical, and biochemical proteins associated with integrin mediated signals and response (1). Adhesion complexes impact a vast and divergent set of cellular and physiological behaviors including such cell migration dependent processes as blood coagulation, leukocyte extravasation, tissue differentiation and repair, bone resorption, and cancer metastasis (2-6). The adhesion complex, initiated through integrin and extracellular matrix (ECM) contact, propagates and matures through mechano-induced scaffold formation, and mechano-induced biochemical signal transduction (2, 7, 8). While individual modes of action are understood for a number of these structural and biochemical signals, the integrated mechanism by which the initial integrin-ECM contact develops into a mature focal adhesion remains uncertain. Following integrin-ECM interaction, the scaffolding protein talin links integrin to F-actin filaments, constituting the initial focal contact (9). Continued maturation, however, requires the force-induced recruitment of vinculin to the focal contact (10). Understanding the mechanism and regulation of vinculin recruitment is thus essential to understanding the signaling dynamics by which focal adhesions are formed.

Vinculin, a 1066 residue globular protein, consists of a head region (Vh), comprised of four helical bundle domains (D1, D2, D3 and D4), which is connected by a proline rich flexible linker region (PRR) to a fifth helical bundle domain known as the tail region (Vt or D5) (11). Vinculin's direct role in focal adhesion maturation is a crosslinking event where vinculin acts to reinforce an initial weak talin-actin filament linkage (12). Upon activation, the vinculin binding domain (VBS) of talin inserts into the hydrophobic core of D1, and Vt binds 2 subunits of F-actin(13-

15). In addition, vinculin interacts with many of the other FA and actin cytoskeleton scaffolding proteins such as α-actinin, paxillin, and VASP, and Arp2/3 (11). These interactions compete, however, with a strong auto-inhibitory binding (Kd < 10^{-9} M) of Vt to D1-D4 in a manner which sterically occludes the F-actin and talin-VBS binding and intermolecular binding of vinculin in general (12, 16). For vinculin to bind its partners it must undergo a conformational change – vinculin activation – that renders actin-binding sites in Vt accessible to F-actin. Vinculin's role in focal adhesion maturation is therefore highly dependent on a process of vinculin activation.

Molecular dynamics modeling offers a valuable approach to understanding the mechanisms of vinculin activation. In previous studies from our group, molecular dynamics simulations of vinculin activation have investigated the trajectory of vinculin conformational changes leading to activation and the impact of interaction with talin on the activation process (12, 17). These simulations suggested a cooperative binding model for vinculin activation, consistent with experimental observations (18). Similarly, talin was shown to bind vinculin only after the vinculin activation process, not before (12). Together these studies illustrate a principle of cooperation between multiple focal adhesion forming molecules in facilitating the focal adhesion maturation process. Furthermore, the molecular dynamics approach suggests a specific activation mode for vinculin in which D1 is moved away from Vt (17) allowing for binding of both actin and talin to vinculin.

One aspect not considered in previous molecular dynamics simulations of vinculin activation is the effect of potential phosphorylation modifications of vinculin by kinases downstream of the mechanical stimuli that lead to focal adhesion maturation. Experimental studies have linked phosphorylation of vinculin residues Y1065 and Y100 with Src family kinases, and S1033 and S1045 as substrates, at least *in vitro,* of protein kinase C (PKC) (19-21). Y822 is also implicated as a phosphorylation target, though unlike Y1065 and Y100 this Y822 modification has not been detected in studies using antibodies to phosphorylated tyrosine (19, 20, 22, 23). Though direct effects of mutating either S1033 or S1045 to a constitutive mimic of the phosphorylated or unphosphorylated form remain untested, activation of PKC stimulates cell adhesion and migration; while, down-regulation of PKC stymies spreading, migration and adhesion, and models have been put forward as to how this phosphorylation may effect recruitment (24). Studies downregulating Src kinases or testing mutations of Y100 and Y1065 to constitutive phosphorylation or dephosphorylation mimics have linked their phosphorylation to cell spreading, the force cells apply to surfaces, lamipodial spreading, and wound healing behavior, as well as abolishing interaction with Arp2/3. Y1065 phosphorylation has been specifically linked to increased exchange dynamics with nacent focal adhesions, promoting their growth (20, 25). On a molecular level, the phosphorylation of Y1065 decreases insertion of the vinculin C-terminal residues into lipid membranes, and both mutation of this residue and deletion of the vinculin C-terminal residues yielded similar decreases in cell traction and force generation (26, 27). Thus each of these phosphorylation events appear to impact the cellular behaviors of focal

adhesion maturation, with a specific role in regulating the C-terminal lipid anchor implied for Y1065.

The connection between vinculin phosphorylation and maturing focal adhesions does not elucidate the effect of these modifications on the molecular state of vinculin, nor how such effects lead to observed cellular force generation. Perhaps specific phosphorylation events modify intramolecular affinities sufficiently to cause a conformational change into the active state, a mode of phosphorylation action classically seen in protein kinase activation for instance (28-30). Alternatively, phosphorylation may increase affinity to certain vinculin binding partners, allowing these partners to better compete with the auto-inhibited state. Or perhaps, in the case of vinculin, phosphorylation could impact focal adhesion development via a novel mechanism.

In this study, we develop molecular dynamics models to determine local and global conformational effects of each vinculin phosphorylation event. Furthermore, we simulate vinculin activation with the inclusion of these phosphorylation events and evaluate directly the impact of vinculin phosphorylation on vinculin activation.

Methods

Phosphorylation of Vinculin model

CHARMm topology patches and force field parameters for pSer and pTyr were used to build models of vinculin with Y100, Y1065, S1033 or S1045 modified to their phosphorylated forms (31). The dianionic form of pSer and pTyr were used in each modification, as the pKa for the second de-protonation of each residue typically occurs at pH ~ 5.7 to 5.9, well below physiological pH (32, 33). Using the crystal structure of unphosphorylated vinculin (PDB ID=1ST6) (34) a model of the missing proline rich linker (residues 843-877) was added using a homology model built by SWISSMODEL (35) as previously described(17). Several different structures were created: with Y100 modified to pTyr, with Y1065 modified to pTyr, with S1033 to pSer, with S1045 to pSer, and with both Y100 modified to pTyr and S1033 modified to pSer. Phosphorylation at both Y100 and S1033 was produced as both of these residues are at the interface between Vt and D1, an interface critical to vinculin auto-inhibition.

Molecular Dynamics of Each Phosphorylation Model

NAMD (36) was used for subsequent simulations of each of the created vinculin models. Each model was immersed in a water box with minimum 12 Å of padding surrounding the molecule, using more than 60,000 water molecules for each simulation. Additional layers of water were added to regions of vinculin known to undergo conformational change during activation to ensure vinculin remains within the periodic cell. Solvent padding was as high as 35Å in these regions of vinculin. The water box measured 99Å by 145Å by 157Å (Figure S1). Each model was minimized for 1000 steps followed by molecular dynamics simulation of over 50ns, and the RMSD of the molecule were calculated (see Figure S2) to ensure equilibration of the phosphorylated structures. CHARMm 27 protein force fields

were used (37, 38). PME method was used for electrostatic interactions, non-bonded interactions were cutoff at 12Å, and a Langevin damping coefficient of 5/ps was used for temperature control. Rigid bonds between hydrogen atoms and associated larger atoms (39) were used in conjunction with 2fs timesteps. Simulations were produced in the NPT ensemble using the Langevin piston Nose-Hoover (40) method for pressure control and a Langevin dynamics for temperature control. Temperature was set to 310K and pressure at 1 Atm.

Simulation of Activation

Following equilibration, models of phosphorylated vinculin that were to be investigated for their impact on vinculin activation (pY100 model, pS1033 model, and model with both pY100 and pS1033) were subjected to a conformational change consistent with previous studies of vinculin activation (12, 17). pY1065 and pS1045 are not likely to affect the movement of D1 away from Vt as they do not lie near the interface between D1 and Vt (Figure 1). D1 of vinculin was pulled away from Vt, simulating vinculin activation. The center of mass of Vt (residues 926, 958, 988, and 1031) was constrained fixed while the center of mass of D1 (residues 15, 51, 81, and 115) was pulled away from Vt. The direction of pull was defined as the vector direction from the constrained residues (mass center of Vt) to the pulled residues (mass center of D1). Pulling simulations were carried out using a dummy atom pulled away at a constant velocity of 0.01 Å/ps (.1 m/s) and connected to the mass center of D1 with a spring constant of 868 pN/Å using the SMD package of NAMD. Simulation of vinculin activation here was set up to be similar to previous molecular dynamics simulations of vinculin activation (12, 17).

Results

Phosphorylation Induced Local Conformational Changes

Four residues in vinculin have been implicated as possible sites of phosphorylation by a kinase: Y100, S1033, S1045, and Y1065 (Figure 1)(20, 21, 25). To simulate the local conformational changes that would result in vinculin from each of these potential phosphorylation events, a structure of full-length vinculin with each of these residues modified to their phosphorylated form were produced. Molecular dynamics simulations of each phosphorylated vinculin molecule were run to test for structural changes that would occur within the nano-second timescale. Evaluation of whether these phosphorylation events could activate vinculin directly would require millisecond simulations, beyond feasible computational time if one wants to explore a useful number of conditions. The simulations presented in this study evaluate the local conformational changes that result from the phosphorylation events.

Phosphorylation of Y100, producing pY100, caused rearrangement of some charged residues at the interface between Vt and D1 (Figure 2). Phosphorylated Y100 forms an electrostatic interaction with the ammonium group of K35, also in D1. This newly formed interaction is sustained through a large part of the 50ns simulation as

quantified by the reduced distance between pY100 and K35. Y100 is located in the turn between helix 3 and 4 of D1, and K35 between helix 1 and 2. The impact of this new interaction is to remove K35 from a long chain of electrostatic interactions at the Vt D1 interface – R1008, E106, R105, E31, and K35 are linked together through interactions between their gaunidinium group and their ammonium group respectively. Once pY100 is introduced, K35 swings away from the E31 carboxyl group toward the Y100 phosphate moving at least 5Å away from E31 and disrupting the hydrogen bond network contributing to the Vt-D1 interface. One possible outcome of Y100 phosphorylation, then, is weakening of Vt-D1 binding. The interaction between Vt and D1 is critical to vinculin auto-inhibition (17) and its degradation could affect vinculin activation, these possibilities are explored in the next section.

Phosphorylation of S1033 also affects the interface between Vt and D1 (Figure 3). A new electrostatic interaction is formed between the phosphate on pS1033 and the R987 gaunidinium group. This breaks a previous interaction between the R987 guanidinium group and the E186 carboxyl group causing the distance between the two residues to increase by 7Å over the 50ns simulation. After introduction of the phosphoryl group and rearrangement of the electrostatic interactions, the hydration of E186 and its nearby residues at the interface between Vt and D1-D3 is increased by 15,000 $Å^2$ (Figure S3). The increased hydration weakens the link between Vt and D1 by both decreasing the surface area of hydrophobic contacts between Vt and D1 in the region, and by shielding the strength of the electrostatic interactions between Vt and D1 in the region. Y100 and S1033 lay on opposite ends of a series of interactions that stabilize the interface between Vt and D1 in the auto-inhibited form. Breaking of these interactions is necessary to reach the activated state (17). To test the impact of these phosphorylation events on the transition to the activated state, we simulated vinculin activation in the presence of these phosphoryl groups as discussed in the next section.

The two other phosphorylation sites do not lie at the interface between Vt and D1. Yet, phosphorylation of both S1045 and Y1065 leads to noticeable local conformational changes (Figures 4 and 5). Phosphorylation of S1045 to pS1045 leads to the formation of a new salt-bridge between the pS1045 phosphate and the guanidinium groups of R1057 and R1060, seen by a decrease in the distance between R1057 and pS1045 of more than 10Å that is sustained throughout the 50ns simulation (Figure 4). This interaction causes the N-terminal of the proline-rich loop region to move away from Vt during simulation. Residue Q851 in the loop region moves more than 20Å away from R1057; the previous interaction between Q851 and R1057 had stabilized the association of the loop region with this section of Vt. Phosphorylation of Y1065 to pY1065 leads to the formation of a new interaction between the pY1065 phosphate and the ammonium group of K881 in the loop region. The newly formed interaction reduced the distance between K881 and its nearby loop region and pY1065 and its nearby Vt region by 3Å (Figure 5). This new interaction links the N-terminal strap if the loop domain to Vt. Although not suggested to play a direct role in vinculin activation, the N-terminal strap has been

implicated in both vinculin binding to actin and to recruitment to the cell membrane through PIP2 binding (41). Furthermore, pS1045 lies near an electrostatic actin-binding region of Vt (14) and pY1065 lies on the C-terminal hairpin, a region more likely to be involved in association of vinculin with PIP2. The proximity of pS1045 and pY1065 to actin and PIP2 binding sites, and the impact of both phosphorylated residues on the loop domain suggests phosphorylation of S1045 and Y1065 would impact focal adhesion development not by affecting vinculin activation, but by affecting the intermolecular binding between vinculin and either PIP2 or F-actin. The results from simulation with each vinculin model are summarized in Table S1.

A shift in the D4 domain with respect to the D3 domain in the head was observed during simulation of the pY1065 phosphorylation. This initially appeared to be a conformational change triggered by phosphorylation. To control if the domain shift was truly a result of the phosphorylation, a control simulation was produced of non-phosphorylated vinculin at equilibrium. A similar shift was found to occur in the non-phosphorylated vinculin simulation, suggesting the shift to be a result of the molecular flexibility. Indeed, previous normal mode analysis of vinculin (17) found a normal mode of D4 shifting with respect to D3. These phosphorylation events seem only to cause local conformational changes and not to impact the global domain conformations in vinculin. Vinculin remained in the auto-inhibitory state in all equilibrium simulations, with stable overall RMSD for at least the last 15 ns of simulation (Figure S2).

Impact of phosphorylation on Vinculin Activation

The local conformational changes induced by phosphorylation of vinculin at Y100 or S1033 suggest that these events could affect vinculin activation. To evaluate this potential effect, vinculin activation was simulated after residue modification to the phosphorylated form. Vinculin activation was simulated using a constant velocity pull of D1 away from Vt, reflecting the mechanism of vinculin activation explored previously (17). Four simulations were produced using this activation scheme, using: a vinculin model with pY100, a model with pS1033, a model with both modifications, and a model with no phosphorylation.

In these simulations, the maximum level of force needed to achieve the activation is reduced only after phosphorylation at pS1033 (Figure 6). The conformational changes seen during each set of vinculin activation simulations illuminates the impact of phosphorylation at pS1033 on vinculin activation (Figure 7). In previously published molecular dynamic investigation of vinculin activation (17) three sets of electrostatic interactions were described as stabilizing the auto-inhibited vinculin conformation. Similarly, in the simulations of activation here, two critical steps towards activation can be described: (A) the separation of Vt and D1 in regions near S1033 (Figure 7A), and (B) the breakage of the electrostatic chain of interactions involving residues R1008, E106, R105, E31, and K35 (Figure 7B). These interactions are consistent with those previously described (17). In simulating activation of non-phosphorylated vinculin, 800pN of force is supplied to D1 within 10ns of simulation.

This force is enough to allow for both (A) and (B) to occur without the need for any subsequent peaks in supplied force. In simulation of vinculin with only pS1033 there is less force needed for (A) as the phosphorylation has already rearranged the electrostatic interactions and weakened the link in this region. The force needed only increases to about 700pN at 30ns of simulation. After hydration of the residues near pS1033 the separation of D1 from Vt near pS1033 (~10ns of simulation) requires ~600pN of force. The separation of D1 from Vt in this region makes separation near Y100 with less force possible at 30ns of simulation. In contrast, simulation of vinculin with only pY100 shows no initial separation of D1 from Vt at the residues near pS1033 and shows an increase in the force peak required to separate charged residues in D1 from R1008. This increased force can be attributed to an interaction between pY100 and R1008 that is formed during the pulling simulation. This interaction was not seen during the equilibrium simulation. Simulation of vinculin with both pY100 and pS1033 shows the same trajectory to activation as phosphorylation with only pS1033 and activation after ~35ns of simulation. The additional time is likely required due to the interaction between pY100 and R1008. The peak force required is 700pN, similar to activation of vinculin with pS1033 only, and less than activation of vinculin without pS1033.

An increased level of force needed for activation in these simulations (more than 700pN) to the level of force reported in our previous simulations (less than 200pN) (17) arises from viscosity induced by water collisions in the explicit solvent treatment and frictional dampening from the temperature control. In the previous simulations (17) the EEF1 implicit solvent model (43) was used, where as in these simulations the TIP3 (44) solvent model is used. Even with the higher levels of force needed in the explicit solvent simulations, the trajectory to activation was the same as the previous simulations with the implicit solvent. Even though the forces seen here are much larger and the time scale much shorter than would be expected *experimentally*, the decrease in force needed to activate vinculin should still hold true *in vivo*. To test this possibility and to compare the impact of the vinculin phosphorylation on vinculin activation at different pulling speeds, vinculin was activated at a faster speed, 1 m/s (Figure S4). The results show an even higher level of force (~1200pN) needed to achieve the activation, but a similar impact of vinculin phosphorylation. Phosphorylation of S1033 to pS1033 is consistently seen as being critical to reducing the force needed to achieve vinculin activation.

Discussion

Vinculin phosphorylation has been repeatedly suggested as one of the mechanisms by which focal adhesions mature; Vinculin phosphorylation has even been linked with vinculin activation and its recruitment to focal adhesions (20, 21, 25). Yet little evidence exists showing the molecular mechanism by which vinculin phosphorylation would impact these cellular processes. Using molecular dynamics, this study has illustrated one mechanism by which vinculin phosphorylation could impact vinculin activation: by priming vinculin for activation. Vinculin priming considers the phosphorylation increasing the chances that vinculin would become

activated by reducing the stability of the auto-inhibition with respect to the pulling trajectory needed for force activation.

Phosphorylation has an impact on the function of a multitude of molecules, and is used as a regulatory mechanism throughout the cell. Primarily, phosphorylation regulates cellular processes either by altering inter-molecular binding or by directly causing activating conformational changes by changing intra-molecular binding (29, 30, 45, 46). In the case of vinculin, involved in mechanotransduction, we suggest a third mode, priming. A priming phosphorylation would not alter binding affinities to the extent to directly cause domain scale conformation change and activation, but would instead modulate a vinculin molecule's susceptibility to activation by]p-'force, specifically the cooperative pulling interaction with talin and actin (17, 18). It remains possible that vinculin phosphorylation could activate vinculin in the absence of a cooperative pulling interaction. Evaluating that possibility with molecular dynamics would require simulation of events on the millisecond timescale.

Two of the phosphorylation sites on vinculin lie at the interface between Vt and D1 and two of the phosphorylation sites lie on Vt near its binding sites for actin and PIP2 (Figure 1). The equilibrium structure of vinculin with each of its potential phosphoryl-groups suggests that phosphorylation S1033 affects vinculin activation (Figure 2-3), while phosphorylation at Y1065 or S1045 could affect Vt binding to actin or PIP2 (Figure 4-5). The impact of phosphorylation on Vt binding to its partners is a topic worthy of consideration in future studies. One possibility is that phosphorylation at multiple sites, for example at Y100 and at Y1065, could enhance vinculin activation by modulating the strength of the auto-inhibited conformation and modulating the binding affinity of Vt for PIP2. Any future study considering the impact of phosphorylation on PIP2 binding should also investigate this possible joint mechanism. Furthermore, the interface between Vt and D4 has been cited as relevant to vinculin activation (47). If so, then investigation of the impact of phosphorylation at S1045 on the strength of this interface is worthy of future study. Phosphorylation at S1045 and S1033 has been suggested by *in vitro* studies, but has yet to be demonstrated *in* vivo (20). Therefore, both the impact of phosphorylation of S1033 on the D1-Vt interface studied here and the impact of phosphorylation of S1045 on the D4-Vt interface that could be studied in the future could prove to be conjecture. Corroborating *in vivo* experimental evidence is needed to solidify the role of these phosphorylation events in focal adhesion formation.

The impact of phosphorylation on vinculin activation was considered here, and simulation of vinculin activation with phosphorylation showed that the combined phosphorylation of Y100 and S1033 decrease the force needed to activate vinculin (Figure 6). Phosphorylation at Y100 alone had minimal impact on reducing the force needed for vinculin activation, and in fact increased the force needed as a result of its interaction with R1008. Phosphorylation of S1033 then is critical to vinculin priming and one must consider that PKC would need to access S1033 in order for this priming to occur. Although in a number of other proteins it has been shown

that phosphorylation is sufficient to induce activation (29, 30, 45, 46), this study shows that in the case of vinculin a cooperative binding event involving actin and talin is still necessary for vinculin activation.

While each phosphorylation altered specific side-chain interactions, none of the phosphorylation events caused major domain shifts. Vinculin's resilience to activation from only phosphorylation is consistent with its cellular role as a reinforcing agent (11). Vinculin has been implicated in both reinforcement of the talin-actin linkage (12) and the α-actinin-actin linkage(48). That phosphorylation can prime vinculin for activation but not completely cause vinculin activation means that vinculin can only be activated under a condition in which its binding partners are present, and perhaps there is some activating tension, i.e. vinculin is only activated when reinforcement is needed. The priming reduces the threshold to reinforcement, but maintains its discipline as a reinforcing agent. In a force induced activation model, vinculin phosphorylation would then modulate sensitivity to tension inputs.

Our simulation of vinculin activation has employed a stretching force between D1 and Vt. Although it is hypothesized this stretch is due to the simultaneous binding of D1 to talin and Vt to actin (12) (17) the stretching force could also result from a tension across vinculin when recruited to the cell membrane or to focal adhesions. A recent experimental investigation (49) showed the presence of a mechanical tension across vinculin *in vivo*. It is unclear whether vinculin was phosphorylated prior to the measured tension in their experiment; our results suggest this is possible, and the phosphorylation could have reduces the level of tension needed to cause a strain in vinculin. Perhaps an experiment could address this by considering the level of tension across vinculin in cells with PKC knocked-out. One possibility is that the reduced barrier to vinculin activation by vinculin phosphorylation increases the frequency of vinculin activation within the cell *in vivo* only after priming by phosphorylation.

One phosphorylation target not considered in this study has been phosphorylation at Y822. Although some investigations point to phosphorylation at Y822 (22), other studies fail to detect phosphorylation at Y822 by Src Kinases [19]. Furthermore, investigation of the impact of phosphorylation at Y822 on the growing focal adhesion has demonstrated that the phosphorylation event has no affect on focal adhesion formation (19), whereas the phosphorylation sites investigated in this study have not only been demonstrated to be possible, but are also suggested to impact the mechanotransduction response. Previous experimental studies (20, 21, 24, 25) have demonstrated an overlap between the effects of vinculin and PKC in focal adhesion maturation, potentially caused by phosphorylation of vinculin by PKC. Phosphorylation of vinculin by SFKs has been shown *in vivo* and our study illustrates one mechanism by which these kinases could be contributing to focal adhesion growth: their phosphorylation of vinculin could be priming vinculin for activation. After phosphorylation by PKC or SFKs, vinculin becomes more susceptible to activation either by simultaneous interaction or by stretch. It is not

likely however, that vinculin activation would result directly from phosphorylation in the absence of some other activating interaction or stimuli. Zeigler (11) suggests a model to vinculin activation in which vinculin is recruited to the lipid membrane along side PKC. Our model suggests that this would allow for S1033 phosphorylation and prime vinculin for later force-induced activation.

This study has explored the impact of phosphorylation on vinculin specifically. Yet a number of focal adhesion forming molecules have been implicated in regulation by phosphorylation (2, 50). It would be interesting to see an investigation of how phosphorylation may regulate other molecules involved in focal adhesion maturation. Perhaps priming, where chemical modifications increase susceptibility to a specific forcing stimulus is a phenomenon associated with many molecules involved in mechanotransduction, not just vinculin.

References

1. Zaidel-Bar, R., S. Itzkovitz, A. Ma'ayan, R. Iyengar, and B. Geiger. 2007. Functional atlas of the integrin adhesome. Nat Cell Biol 9:858-867.
2. Huveneers, S., and E. H. Danen. 2009. Adhesion signaling - crosstalk between integrins, Src and Rho. J Cell Sci 122:1059-1069.
3. Moore, S. W., P. Roca-Cusachs, and M. P. Sheetz. 2010. Stretchy proteins on stretchy substrates: the important elements of integrin-mediated rigidity sensing. Dev Cell 19:194-206.
4. Kumar, S., and V. M. Weaver. 2009. Mechanics, malignancy, and metastasis: the force journey of a tumor cell. Cancer Metastasis Rev 28:113-127.
5. Zhao, J., and J. L. Guan. 2009. Signal transduction by focal adhesion kinase in cancer. Cancer Metastasis Rev 28:35-49.
6. Gardel, M. L., I. C. Schneider, Y. Aratyn-Schaus, and C. M. Waterman. 2010. Mechanical integration of actin and adhesion dynamics in cell migration. Annu Rev Cell Dev Biol 26:315-333.
7. Geiger, B., J. P. Spatz, and A. D. Bershadsky. 2009. Environmental sensing through focal adhesions. Nat Rev Mol Cell Biol 10:21-33.
8. Vogel, V. 2006. Mechanotransduction involving multimodular proteins: converting force into biochemical signals. Annu Rev Biophys Biomol Struct 35:459-488.
9. Izzard, C. S. 1988. A precursor of the focal contact in cultured fibroblasts. Cell Motil Cytoskeleton 10:137-142.
10. Galbraith, C. G., K. M. Yamada, and M. P. Sheetz. 2002. The relationship between force and focal complex development. The Journal of cell biology 159:695-705.
11. Ziegler, W. H., R. C. Liddington, and D. R. Critchley. 2006. The structure and regulation of vinculin. Trends Cell Biol 16:453-460.
12. Golji, J., J. Lam, and M. R. Mofrad. 2011. Vinculin activation is necessary for complete talin binding. Biophys J 100:332-340.

13. Humphries, J. D., P. Wang, C. Streuli, B. Geiger, M. J. Humphries, and C. Ballestrem. 2007. Vinculin controls focal adhesion formation by direct interactions with talin and actin. The Journal of cell biology 179:1043-1057.
14. Janssen, M. E., E. Kim, H. Liu, L. M. Fujimoto, A. Bobkov, N. Volkmann, and D. Hanein. 2006. Three-dimensional structure of vinculin bound to actin filaments. Mol Cell 21:271-281.
15. Izard, T., G. Evans, R. A. Borgon, C. L. Rush, G. Bricogne, and P. R. J. Bois. 2004. Vinculin activation by talin through helical bundle conversion. Nature 427:171-175.
16. Cohen, D. M., H. Chen, R. P. Johnson, B. Choudhury, and S. W. Craig. 2005. Two distinct head-tail interfaces cooperate to suppress activation of vinculin by talin. J Biol Chem 280:17109-17117.
17. Golji, J., and M. R. Mofrad. 2010. Molecular-Dynamics Investigation of Vinculin Activation. Biophysical Journal 99:1073-1081.
18. Chen, H., D. M. Choudhury, and S. W. Craig. 2006. Coincidence of actin filaments and talin is required to activate vinculin. J Biol Chem 281:40389-40398.
19. Moese, S., M. Selbach, V. Brinkmann, A. Karlas, B. Haimovich, S. Backert, and T. F. Meyer. 2007. The Helicobacter pylori CagA protein disrupts matrix adhesion of gastric epithelial cells by dephosphorylation of vinculin. Cell Microbiol 9:1148-1161.
20. Zhang, Z., G. Izaguirre, S. Y. Lin, H. Y. Lee, E. Schaefer, and B. Haimovich. 2004. The phosphorylation of vinculin on tyrosine residues 100 and 1065, mediated by SRC kinases, affects cell spreading. Mol Biol Cell 15:4234-4247.
21. Ziegler, W. H., U. Tigges, A. Zieseniss, and B. M. Jockusch. 2002. A lipid-regulated docking site on vinculin for protein kinase C. Journal of Biological Chemistry 277:7396-7404.
22. Subauste, M. C., O. Pertz, E. D. Adamson, C. E. Turner, S. Junger, and K. M. Hahn. 2004. Vinculin modulation of paxillin-FAK interactions regulates ERK to control survival and motility. J Cell Biol 165:371-381.
23. Goldmann, W. H., R. Galneder, M. Ludwig, W. Xu, E. D. Adamson, N. Wang, and R. M. Ezzell. 1998. Differences in elasticity of vinculin-deficient F9 cells measured by magnetometry and atomic force microscopy. Exp Cell Res 239:235-242.
24. Ziegler, W. H., U. Tigges, A. Zieseniss, and B. M. Jockusch. 2002. A lipid-regulated docking site on vinculin for protein kinase C. J Biol Chem 277:7396-7404.
25. Kupper, K., N. Lang, C. Mohl, N. Kirchgessner, S. Born, W. H. Goldmann, R. Merkel, and B. Hoffmann. 2010. Tyrosine phosphorylation of vinculin at position 1065 modifies focal adhesion dynamics and cell tractions. Biochem Biophys Res Commun 399:560-564.
26. Diez, G., P. Kollmannsberger, C. T. Mierke, T. M. Koch, H. Vali, B. Fabry, and W. H. Goldmann. 2009. Anchorage of vinculin to lipid membranes influences cell mechanical properties. Biophys J 97:3105-3112.

27. Wirth, V. F., F. List, G. Diez, and W. H. Goldmann. 2010. Vinculin's C-terminal region facilitates phospholipid membrane insertion. Biochem Biophys Res Commun 398:433-437.
28. Vuori, K., and E. Ruoslahti. 1993. Activation of protein kinase C precedes alpha 5 beta 1 integrin-mediated cell spreading on fibronectin. J Biol Chem 268:21459-21462.
29. Johnson, L. N. 1992. Glycogen phosphorylase: control by phosphorylation and allosteric effectors. Faseb J 6:2274-2282.
30. Nolen, B., S. Taylor, and G. Ghosh. 2004. Regulation of protein kinases; controlling activity through activation segment conformation. Mol Cell 15:661-675.
31. Feng, M., M. Phillippopoulos, A. D. J. MacKerell, and C. Lim. 1996. Structural Characterization of the Phosphotyrosine Binding Region of a High-Affinity SH2 Domain−Phosphopeptide Complex by Molecular Dynamics Simulation and Chemical Shift Calculations. Journal of the American Chemical Society 118:11265-11277.
32. Domchek, S. M., K. R. Auger, S. Chatterjee, T. R. Burke, Jr., and S. E. Shoelson. 1992. Inhibition of SH2 domain/phosphoprotein association by a nonhydrolyzable phosphonopeptide. Biochemistry 31:9865-9870.
33. Errington, N., and A. J. Doig. 2005. A phosphoserine-lysine salt bridge within an alpha-helical peptide, the strongest alpha-helix side-chain interaction measured to date. Biochemistry 44:7553-7558.
34. Bakolitsa, C., D. M. Cohen, L. A. Bankston, A. A. Bobkov, G. W. Cadwell, L. Jennings, D. R. Critchley, S. W. Craig, and R. C. Liddington. 2004. Structural basis for vinculin activation at sites of cell adhesion. Nature 430:583-586.
35. Arnold, K., L. Bordoli, J. Kopp, and T. Schwede. 2006. The SWISS-MODEL workspace: a web-based environment for protein structure homology modelling. Bioinformatics 22:195-201.
36. Humphrey, W., A. Dalke, and K. Schulten. 1996. VMD: visual molecular dynamics. J Mol Graph 14:33-38.
37. MacKerell, A., D. Bashford, M. Bellot, J. R. L. Dunbrack, J. Evanseck, M. Field, S. Fischer, J. Gao, H. Guo, S. Ha, D. Joseph-McCarthy, L. Kuchnir, K. Kuczera, F. Lau, C. Mattos, S. Michnick, T. Ngo, D. Nguyen, B. Prodhom, I. W. E. Reiher, B. Roux, M. Schlenkrich, J. Smith, R. Stote, J. Straub, M. Watanabe, J. Wiorkiewicz-Kuczera, D. Yin, and M. Karplus. 1998. All-Atom Empirical Potential for Molecular Modeling and Dynamics Studies of Proteins. J. Phys. Chem. B 102:3586-3616.
38. Mackerell, A. D. 2004. Empirical force fields for biological macromolecules: overview and issues. Journal of Computational Chemistry 25:1584-1604.
39. Kräutler, V., W. F. v. Gunsteren, and P. H. Hünenberger. 2001. A fast SHAKE algorithm to solve distance constraint equations for small molecules in molecular dynamics simulations. Journal of Computational Chemistry 22:501-508.
40. Hoover, W. 1985. {Canonical dynamics: Equilibrium phase-space distributions}. Physical Review A 31:1695-1697.

41. Palmer, S. M., M. P. Playford, S. W. Craig, M. D. Schaller, and S. L. Campbell. 2009. Lipid binding to the tail domain of vinculin: specificity and the role of the N and C termini. J Biol Chem 284:7223-7231.
42. Golji, J., and M. R. Mofrad. 2010. A molecular dynamics investigation of vinculin activation. Biophys J 99:1073-1081.
43. Lazaridis, T. 2003. Effective energy function for proteins in lipid membranes. Proteins 52:176-192.
44. Jorgensen, W. L., J. Chandrasekhar, J. D. Madura, R. W. Impey, and M. L. Klein. 1983. Comparison of simple potential functions for simulating liquid water. The Journal of Chemical Physics 79:926-935.
45. Russo, A. A., P. D. Jeffrey, and N. P. Pavletich. 1996. Structural basis of cyclin-dependent kinase activation by phosphorylation. Nat Struct Biol 3:696-700.
46. Machida, K., and B. J. Mayer. 2005. The SH2 domain: versatile signaling module and pharmaceutical target. Biochim Biophys Acta 1747:1-25.
47. Cohen, D., H. Chen, R. Johnson, and B. Choudhury. 2005. Two Distinct Head-Tail Interfaces Cooperate to Suppress Activation of Vinculin by Talin. Journal of Biological Chemistry.
48. Golji, J., R. Collins, and M. R. Mofrad. 2009. Molecular mechanics of the alpha-actinin rod domain: bending, torsional, and extensional behavior. PLoS Comput Biol 5:e1000389.
49. Grashoff, C., B. D. Hoffman, M. D. Brenner, R. Zhou, M. Parsons, M. T. Yang, M. A. McLean, S. G. Sligar, C. S. Chen, T. Ha, and M. A. Schwartz. 2010. Measuring mechanical tension across vinculin reveals regulation of focal adhesion dynamics. Nature 466:263-266.
50. Shattil, S. J., C. Kim, and M. H. Ginsberg. 2010. The final steps of integrin activation: the end game. Nat Rev Mol Cell Biol 11:288-300.

Figure Captions

Figure 1. A cartoon representation of molecular vinculin in the auto-inhibited state, with phosphorylation sites circled and labeled. The domain 1 (D1) helix bundle is colored in green, with the remaining helix bundles (D2-4) in the head domain colored in grey. The proline rich linker region is colored in yellow and the tail domain (Vt) helix bundle is colored in orange. Talin would bind vinculin at D1 while Vt is suggested to interact with actin filaments. Movement of D1 away from Vt allows for Vt to potentially interact with actin. Phosphorylation of vinculin at each of the labeled residues has been implicated in regulating the growth and maturation of focal adhesions (20, 25). Two of these, pY100 and pS1033, are at the interface between Vt and D1 and likely impact vinculin activation. Two of these, pS1045 and pY1065, are near Vt binding sites for actin or PIP2 and likely impact Vt binding.

Figure 2. (A) D1 of vinculin is shown in green while Vt of vinculin is shown in orange. Phosphorylation of Y100 at the top of the D1 helix bundle domain introduces a new electrostatic interaction between K35 and pY100. This new interaction removes K35 from a chain of electrostatic interactions stabilizing the

auto-inhibited vinculin conformation, potentially reducing the strength of binding between Vt and D1. Other residues involved in the chain of electrostatic interactions include E31, R105, E106, and R1008. (B) As the vinculin with pY100 is simulated for 50ns K35 moves and reorients itself towards vinculin. The red plot shows the increase in distance between K35 and E31 throughout the 50ns simulation as a result of the interaction with pY100, and the green plot captures the decrease in distance between pY100 and K35 for nearly 15ns (between 8ns of simulation and 23ns of simulation) due to their association.

Figure 3. (A) Phosphorylation of S1033 causes a shift of R987 and E186 towards to the new phosphoryl group. This in turn removes the electrostatic link between E186 and R7, an interaction critical to maintaining the auto-inhibited conformation of vinculin. After this structural rearrangement the hydration of vinculin is increased through penetration of the D1-Vt interface. D1 is shown in green, Vt in orange, and D2-D4 in gray. (B) The separation of R987 from E186 (red plot) and the association of R987 with pS1033 (green plot) is captured throughout the 50ns of simulation.

Figure 4. (A) Phosphorylation of S1045 releases the loop region near D4. After phosphorylation pS1045 interacts with both R1057 and R1060 releasing Q851 and the loop region from association with R1057. The flexible loop region is shown in yellow, the Vt domain in orange, D1 in green, and D2-D4 in gray. (B) Four distances were tracked throughout the 50ns simulation. The distance between R1057 and Q851 increases early in the simulation (red plot) and remains separated. The R1057 then associates with pS1045 (purple plot) along with R1060 (blue plot). The released Q851 has intermittent association with a nearby loop region residue D841.

Figure 5. (A) Phosphorylation of Y1065 introduces a new interaction between Vt and the loop region near Vt. K881 forms an interaction with pY1065. Vt is shown in orange, D2-D4 in gray, and the loop region in yellow. (B) The new linkage between K881 and pY1065 is formed early and is maintained throughout the 50ns simulation.

Figure 6. Four models of vinculin were simulated with an activating force applied to D1: unphosphorylated vinculin (red), vinculin with pY100 (green), vinculin with pS1033 (purple), and vinculin with both pS1033 and pY100 (blue). Activation of unphosphorylated vinculin and vinculin with pY100 required over 800pN of force, whereas activation of vinculin with pS1033 and with both pS1033 and pY100 required 700pN of force. The reduced level of force required results from significant local conformational changes introduced by pS1033 that prime vinculin for force-induced activation.

Figure 7. Two critical events are necessary for vinculin to activate: (a) D1 regions near residue S1033 need to separate from Vt and (b) The chain of electrostatic interactions involving R1008, E106, R105, E31, and K35 needs to be broken. (A) Simulation of vinculin with pS1033 showed rearrangement of residues near pS1033 allowed for separation of D1 from Vt near pS1033 even before (b) occurs. pS1033

also increased the hydration of the interface between D1 and Vt (arrow). D1 is shown in green, Vt is shown in orange, and D2-D4 is shown in gray. (B) Simulation of vinculin with pY100 showed increased resilience to activation. Part of this increased stability of the auto-inhibited conformation resulted form an interaction between pY100 and R1008 of Vt (arrow).

Figure 1:

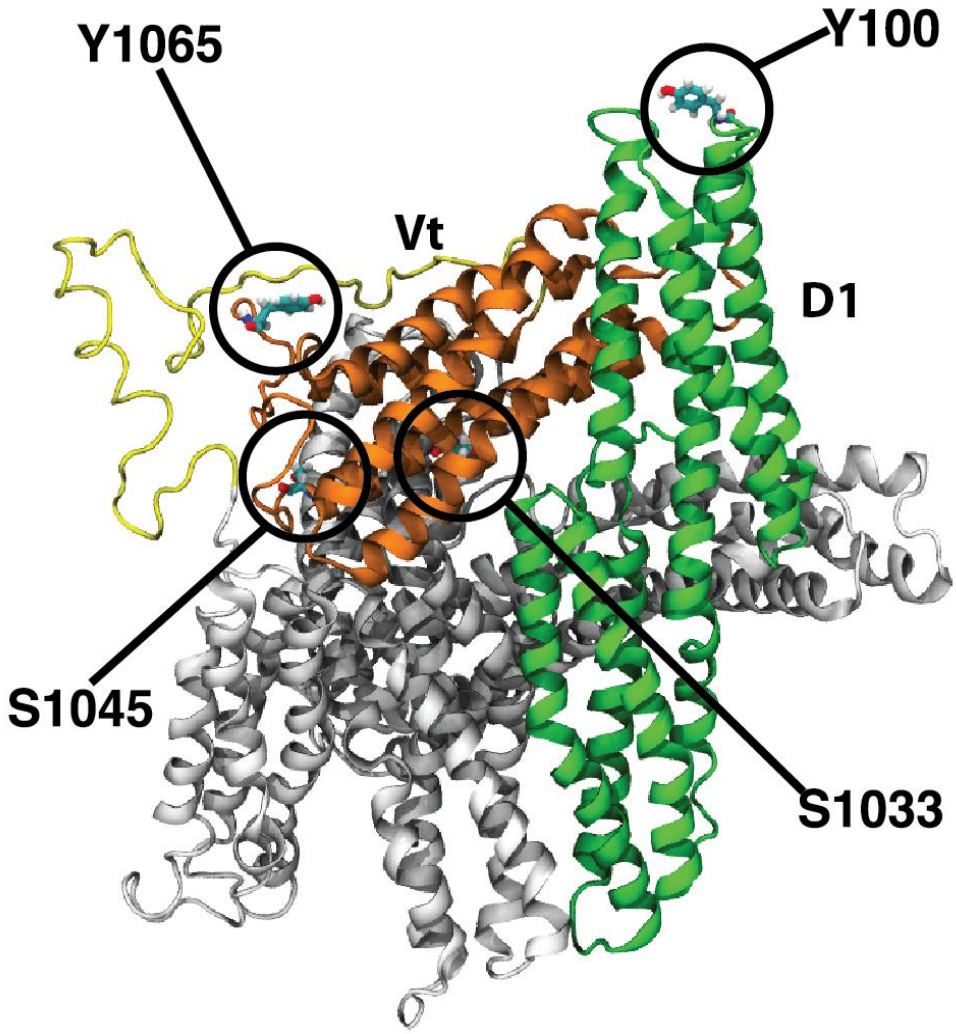

Figure 2:

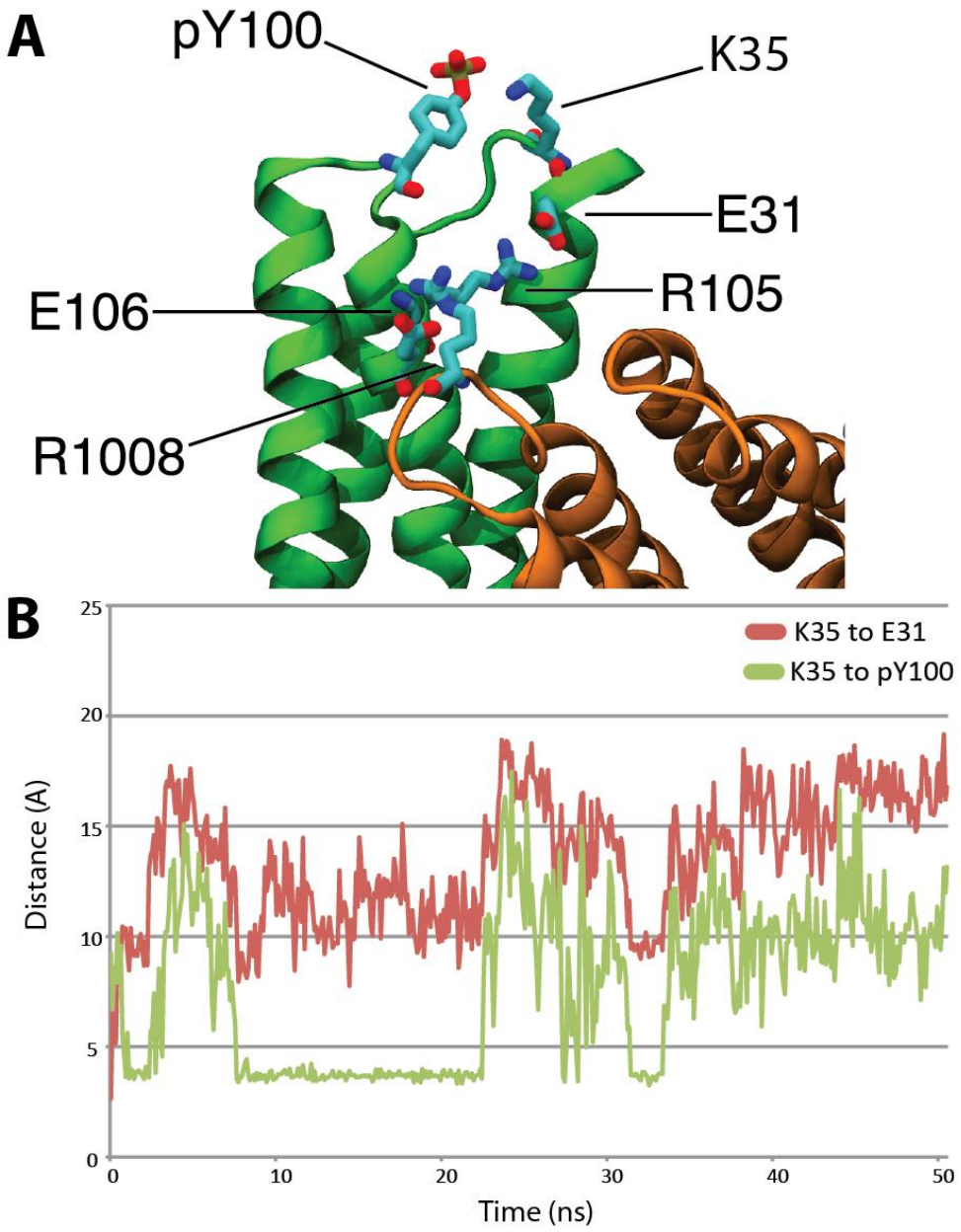
A
pY100
K35
E31
R105
E106
R1008
B
K35 to E31
K35 to pY100
Distance (A)
Time (ns)
0
5
10
15
20
25
0
10
20
30
40
50

Figure 3:

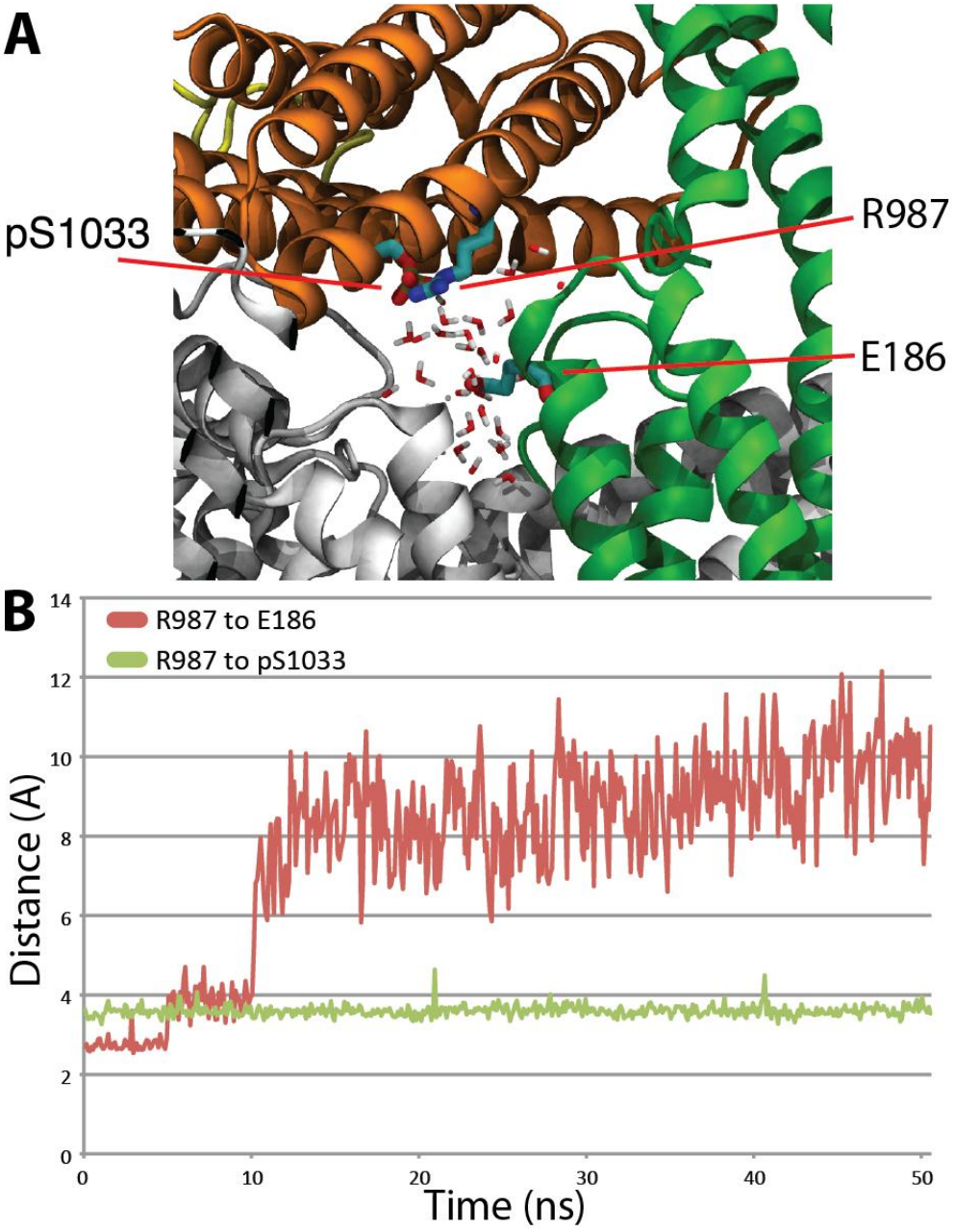
A
pS1033
R987
E186
B
R987 to E186
R987 to pS1033
Distance (A)
Time (ns)
0
2
4
6
8
10
12
14
0
10
20
30
40
50

Figure 4:

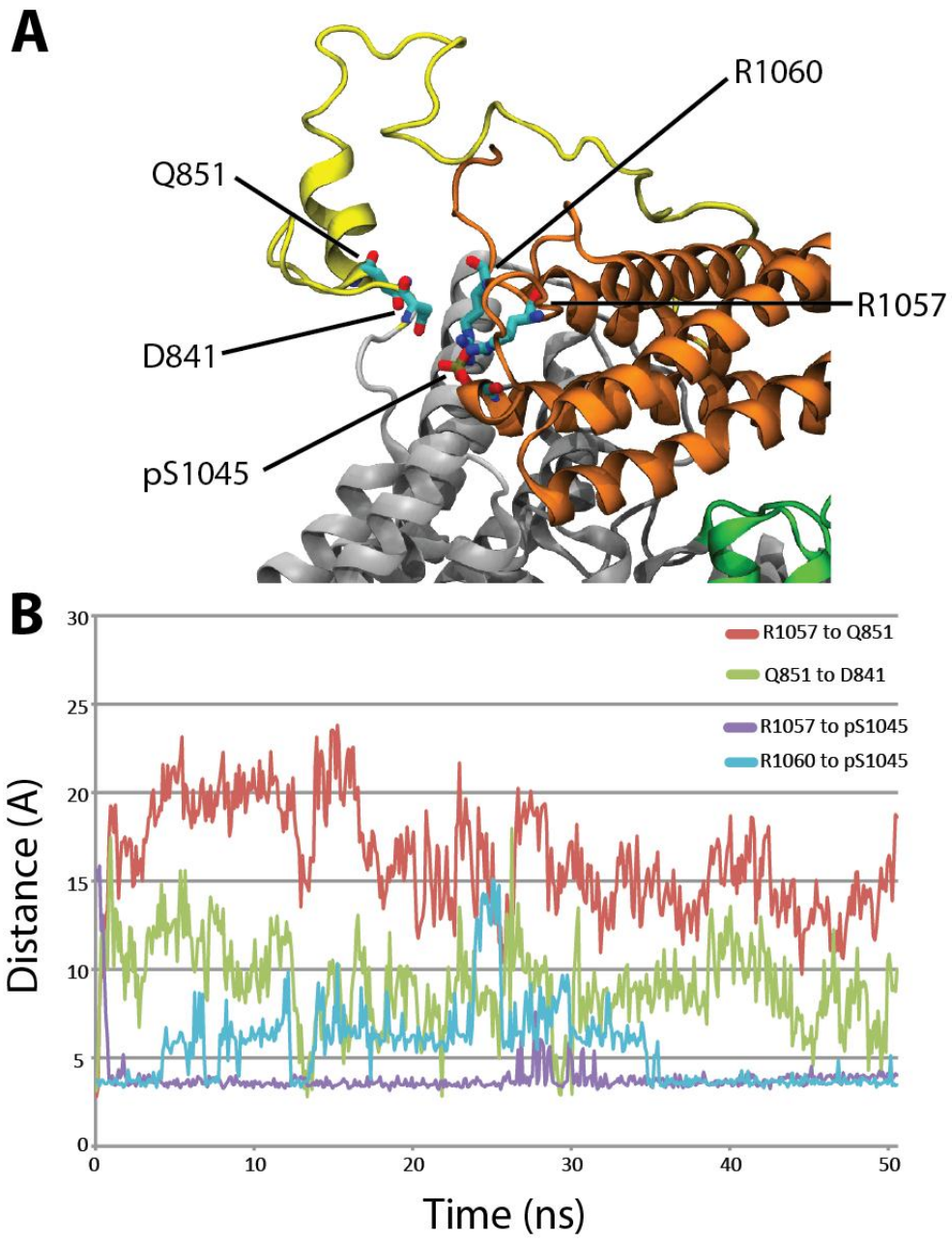
A
R1060
Q851
R1057
D841
pS1045
B
R1057 to Q851
Q851 to D841
R1057 to pS1045
R1060 to pS1045
Distance (A)
Time (ns)
0
5
10
15
20
25
30
0
10
20
30
40
50

Figure 5:

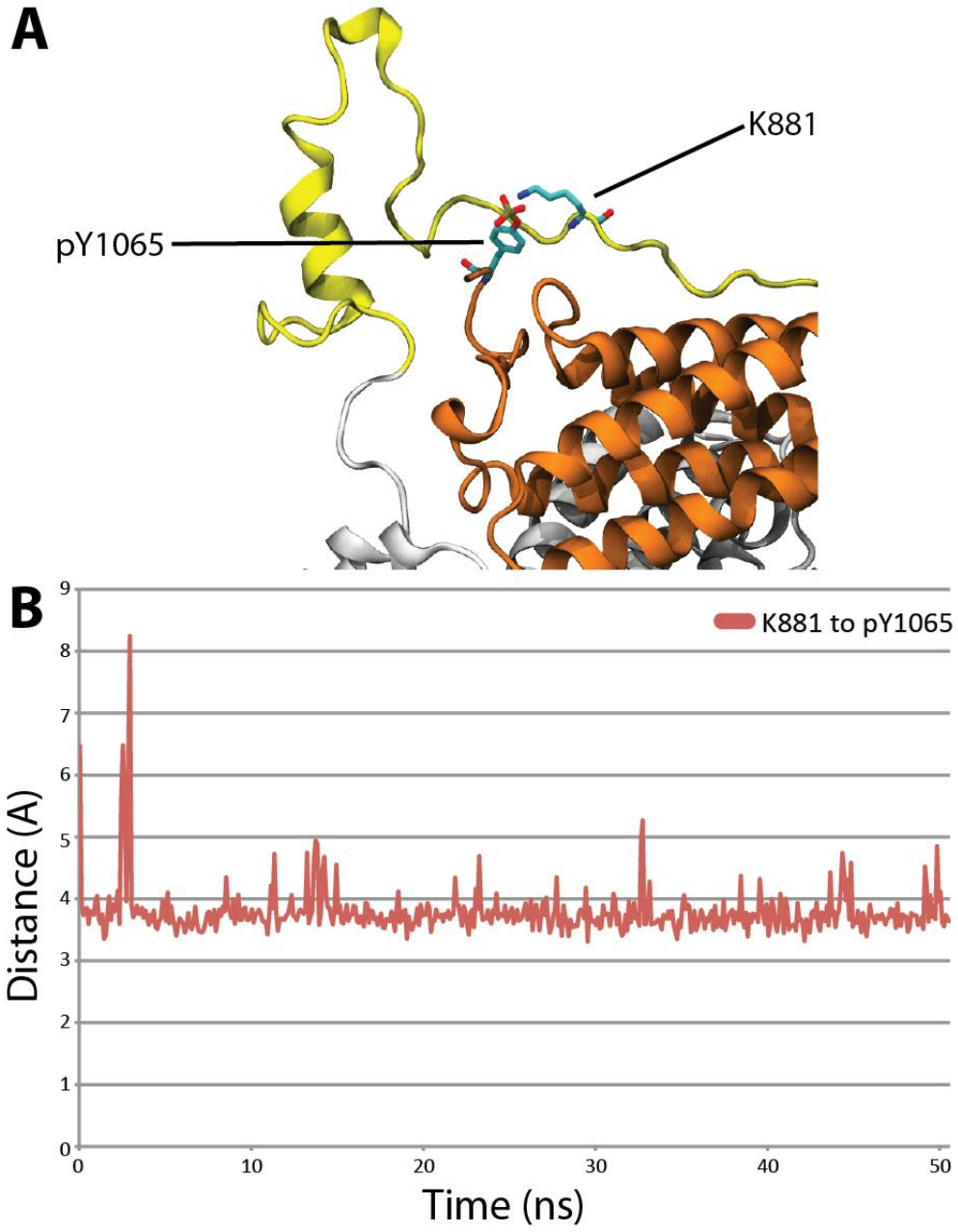
A
K881
pY1065
B
K881 to pY1065
Distance (A)
0
1
2
3
4
5
6
7
8
9
0
10
20
30
40
50
Time (ns)

Figure 6:

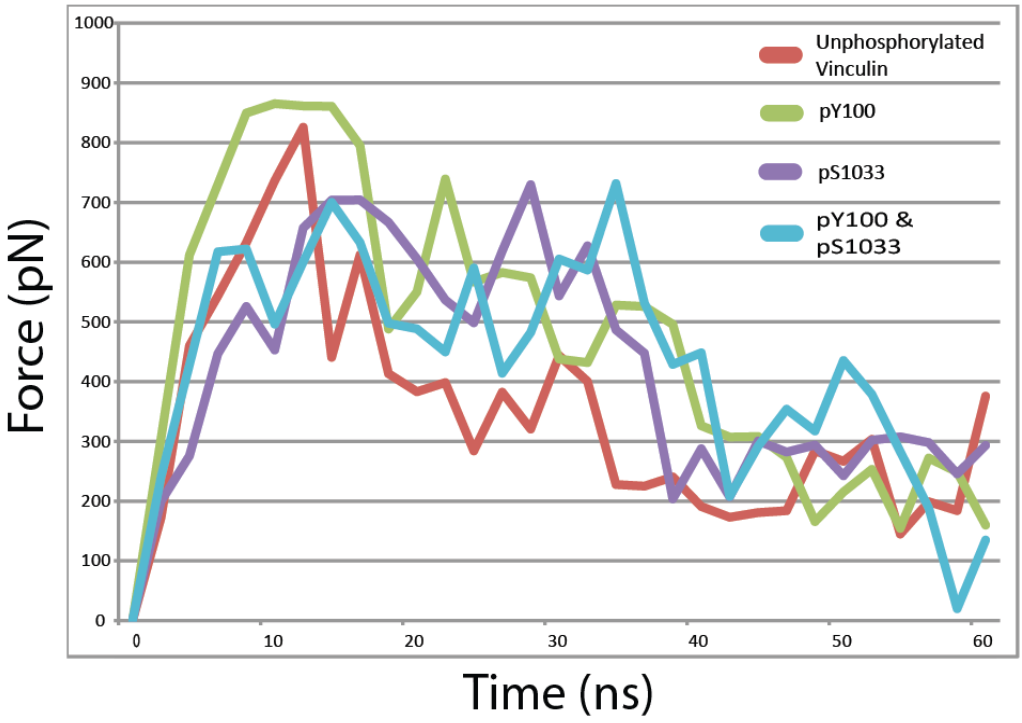
Force (pN)
1000
900
800
700
600
500
400
300
200
100
0
0
10
20
30
40
50
60
Time (ns)
Unphosphorylated Vinculin
pY100
pS1033
pY100 & pS1033

Figure 7:

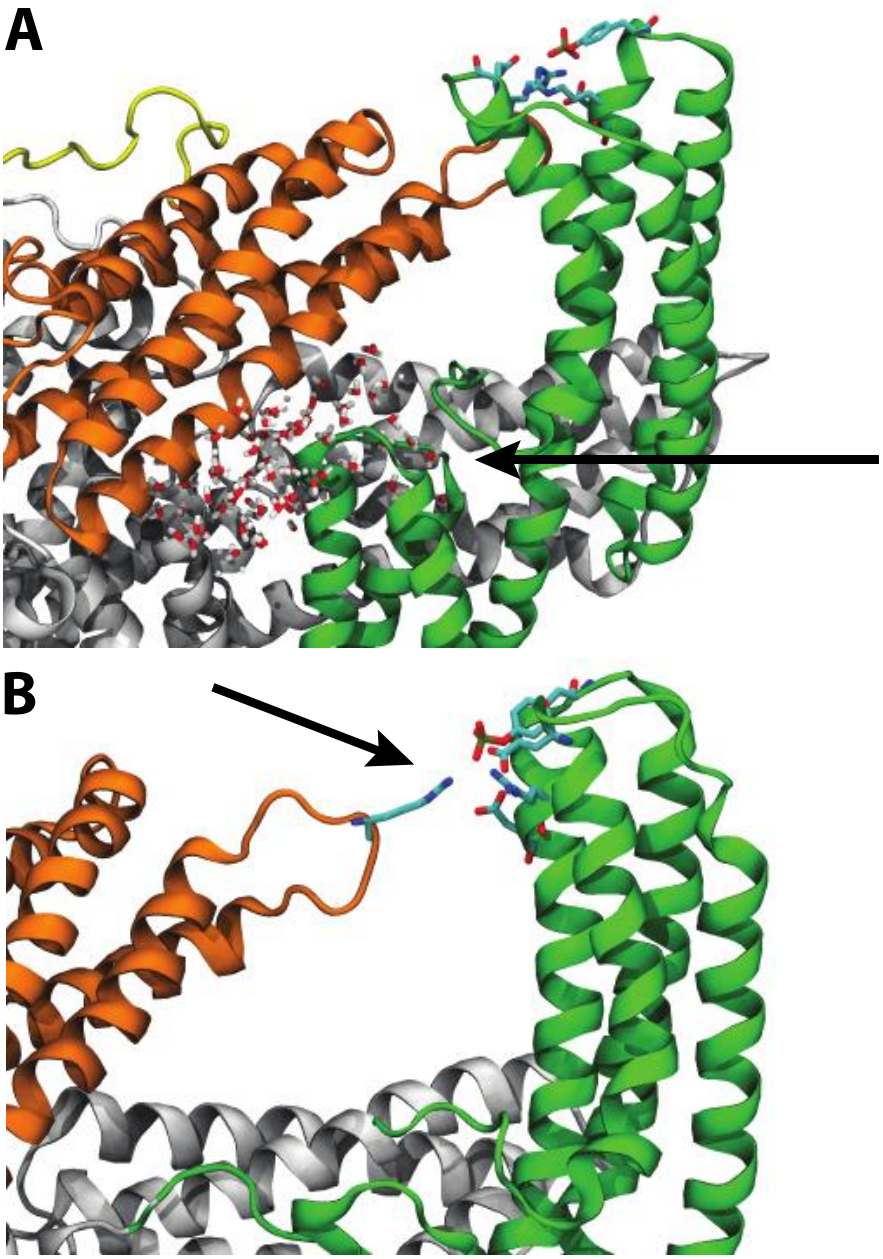

Section III:

The Interaction of Vinculin with Talin and Actin

Vinculin activation is necessary for complete talin binding

Abstract

Focal adhesions are critical to a number of cellular processes that involve mechanotransduction and mechanical interaction with the cellular environment. The growth and strengthening of these focal adhesions is dependent on the interaction between talin and vinculin. This study investigates this interaction and how vinculin activation impacts it. Using molecular dynamics, the interaction between talin's vinculin binding site (VBS) and vinculin's domain 1 (D1) is simulated both before and after vinculin activation. The simulations of VBS binding to vinculin prior to activation suggest the proximity of the vinculin tail to D1 prevents helical movement in D1 and thus prevents binding of VBS. In contrast, interaction of VBS with activated vinculin shows the possibility of complete VBS insertion into D1. In the simulations of both activated and auto-inhibited vinculin where VBS fails to fully bind, VBS demonstrates significant hydrophobic interaction with surface residues in D1. These interactions link VBS to D1 even without its proper insertion into the hydrophobic core. Together these simulations suggest VBS binds to vinculin with the following mechanism: (1) VBS links to D1 via surface hydrophobic interactions, (2) vinculin undergoes activation and D1 is moved away from the vinculin tail, (3) helices in D1 undergo conformational change to allow VBS binding, and (4) VBS inserts itself into the hydrophobic core of D1.

Introduction

Cellular survival, differentiation, migration, and other cellular processes are dependent upon the mechanical coupling of cells to their surroundings (1-9). The mechanical interaction of cells with the extracellular matrix (ECM) is typically mediated by membrane-bound integrin molecules and the focal adhesion complexes that form at sites of mechanical linkage(9-15). Focal adhesion complexes can best be described as a molecular-glue comprising of an array of molecules binding to each other, to the ECM-bound integrins, and to the actin cytoskeleton. A number of studies have demonstrated that the formation of focal adhesions can be induced via an externally applied force (1, 7, 10, 16-18). Furthermore, recruitment of several molecules, such as talin and vinculin, to focal adhesions is directly correlated with mechanical stimulus applied at the site of the focal adhesion formation (1, 9, 11, 19-24). Taken together, these studies suggest mechanical sensation by talin and vinculin and motivate the study of mechanisms of their recruitment and activation.

Talin binds integrin directly and is recruited at the formation of nascent adhesions that later mature into focal adhesions (21). Talin has a head domain that binds integrin, and a larger tail domain that can bind at least one actin filament directly and up to eleven additional actin filaments indirectly via binding to vinculin (23, 25-28). Of the eleven vinculin binding sites (VBS) a number are known to be cryptic and

require activation to bind vinculin (11, 21, 29, 30). A number of both computational and experimental studies have demonstrated the force-induced activation of these cryptic VBSs (11, 31-33). Once activated, VBS will interact with vinculin. Computational simulations have suggested that VBS and vinculin interact via hydrophobic residues (34). Vinculin itself has 5 helical domains named: domain 1 (D1), domain 2 (D2), domain 3 (D3), domain 4 (D4), and the vinculin tail domain (Vt) (35)(Fig. 1 A). Talin's VBS binds to vinculin's D1 while actin filaments bind vinculin's Vt (27, 35). Studies have also suggested a number of other binding partners for vinculin, including α-actinin, PIP2, and paxillin (1, 35, 36). The binding of vinculin to talin and actin can function to multiply the number of actin filaments linked to focal adhesions. Similarly, the binding of vinculin to any of its numerous suggested binding partners can serve to multiply the number of focal adhesion forming molecules that have been recruited. However, vinculin's role as an agent to multiply and strengthen focal adhesions is critically dependent upon vinculin activation; in its native cytoplasmic state vinculin adopts an auto-inhibited conformation (37) in which the proximity of Vt to D1 can prevent binding to vinculin's binding partners (38, 39)(Fig. 1 A). The actin binding site is at Vt and in its closed conformation vinculin is unable to bind actin.

A number of studies have attempted to address vinculin activation and reveal how it is that vinculin transitions from an auto-inhibited to an activated conformation (1, 35, 37, 40-45). One study by Bois et al. (43) suggests that talin and α-actinin can bind D1 of auto-inhibited vinculin and this binding can then lead directly to vinculin activation. In contrast, Chen et al. (42) suggest that vinculin activation occurs only after a simultaneous binding event involving the co-incidence of both actin and talin with vinculin. More recently, molecular dynamic simulations of vinculin activation (46) suggest mechanical tension could play a role in activating vinculin, and even suggest a structure for activated vinculin (Fig. 1 B). Recently, a number of experimental data have emerged that vinculin is important in cellular force generation and transduction, for example experiments by Grashoff et al. (47) using a FRET mechanosensor report mechanical tension across activated vinculin, further supporting the suggestion born from the molecular dynamics simulations (46) that vinculin can be activated by a stretching force. Furthermore, other studies have suggested a phosphorylation event would be necessary to achieve vinculin activation (48-50). The hypothesis of vinculin activation by phorphorylation is not necessarily a competing hypothesis to vinculin activation by a stretching force. It is conceivable that phosphorylation enhances the ability of vinculin to be activated by a stretching force, or perhaps a stretching force enhances the ability of vinculin to be activated by phosphorylation. It is likely that each event enhances the probability of activation and together lead to vinculin activation. Considering the controversy surrounding the mechanism for vinculin activation, it is important to evaluate these hypotheses and refine our understanding of the process of focal adhesion growth via vinculin activation and recruitment.

In this study we evaluate the influence of talin binding to D1 on the activation of vinculin using molecular dynamics simulation. The binding of talin VBS to D1

involves the insertion of VBS into the hydrophobic patch formed by the four helices of D1 (34). Upon binding of talin, D1 is suggested to undergo helical bundle conversion (51). Using molecular dynamics, Lee et al. (34) have simulated the binding of VBS to D1 alone and elaborated a three step binding process: (1) insertion of the VBS helix between helices 1 and 2 of D1, (2) movement of helices 1 and 2 away from VBS, (3) rotation of hydrophobic residues on VBS into the hydrophobic patch of D1. In this study, we expand on the previous simulations and evaluate the influence of the full-length vinculin structure on the VBS binding event.

In our approach, we first simulate the binding of VBS to full-length vinculin in its auto-inhibited conformation. We then simulate binding of VBS to full-length vinculin in an activated conformation. Simulation of binding to auto-inhibited vinculin will evaluate (a) if helical bundle conversion and insertion of VBS into D1 is possible with the close proximity of Vt to D1, and (b) if binding of VBS to D1 can subsequently cause conformational changes in vinculin leading to activation. For simulation of VBS binding to activated vinculin we use the suggested structure of activated vinculin from the previous molecular dynamics study (46), and simulate the interaction of VBS with D1 of vinculin in this conformation. Simulation of VBS binding to an activated vinculin will evaluate the validity of that conformation being activated. An activated vinculin would bind each of its binding partners, including Talin.

Methods

Simulation of VBS near full-length vinculin

To explore the interaction between talin and vinculin in its auto-inhibited conformation (Fig 1 A) molecular dynamics simulations are utilized. The crystal structure of full-length vinculin (PDB ID: 1TR2) (39) is used as the auto-inhibited vinculin structure and the VBS structure from the crystal structure of D1 bound to talin VBS (PDB ID: 1T01) (52) is used after alignment. Swiss-PDB (53) is used to structurally align D1 bound to VBS with D1 from full-length vinculin, effectively establishing the correct VBS orientation needed for binding. Once aligned, VBS is translated 12 Å away from D1 while remaining in the orientation needed for binding. Structural rotation and translations are done with VMD (54). The system is minimized with 3000 steps of the steepest descent method followed by the Adopted Basis Newton Raphson method and then heated to 310K over 80ps. Once heated, harmonic constraints are placed on the center of mass of vinculin – residues E186, W258, A490, and E569 – to prevent its stochastic translation. Initially no other constraints are applied and the two molecules are simulated in the NPT ensemble for 30ns in each trial. The SHAKE algorithm (55) is used to constrain bond lengths between heavy atoms and hydrogen atoms, hence allowing the use of a 2fs timestep. The CHARMM19 force fields (56) are used in conjunction with an implicit solvent model, the Effective Energy Function (EEF1) (57). An implicit solvent model is an appropriate approximation of solvent effects for this simulation since the driving interaction between VBS and D1 of vinculin is hydrophobic. Implicit solvent models,

including EEF1, have been extensively validated by experimental results (58) and have been used numerous times in similar simulations (59). Implicit solvent models lack electrostatic shielding effects, but these shielding effects should have minimal impact on our results considering the hydrophobic nature of the VBS and D1 interaction. The implicit solvent model also lacks accurate viscous solvent effects, which in these simulations allows for binding events to occur within our 30ns simulations window. To track the binding event we monitor both the distance between the center of the VBS helix and the center of the fourth helix in D1 as a reported of the distance between D1 and VBS, and we monitor the distance between helix 1 and helix 2 as a reporter of the helical bundle conversion in D1. All post-simulation calculations, visualizations, and analyses are carried out using VMD (54).

To increase the possibility of binding events between VBS and D1 of auto-inhibited vinculin the molecular dynamics are repeated using an initial nudging force on VBS. Following minimization and heating, a nudging force of 15 pN is applied to VBS at residues Q610, L615, G617, and E621 for a duration of 1 ns in the direction of D1. The short application of the nudging force gives VBS an initial velocity towards D1, increasing the possibility of a binding event. Following the nudge, the VBS and auto-inhibited vinculin system is simulated for an additional 30ns with the absence of any externally applied force. As before, the center of mass of vinculin is harmonically constrained to prevent its stochastic translation. Both simulation of the brief nudging of VBS and the subsequent simulation of the binding of VBS to D1 are carried out as before, with the EEF1 implicit solvent model (57), the CHARMM19 force fields (56), and the SHAKE algorithm (55). All simulations are run with the CHARMm software package (60).

Simulation of VBS near an activated vinculin

To simulate the interaction of talin's VBS with vinculin in an activated conformation (Fig. 1 B), the suggested structure for activated vinculin from our previous molecular dynamics investigation (46) was used along with the structure of VBS from the crystal structure of VBS bound to D1 (PDB ID: 1T01)(52). VBS bound to D1 was aligned with D1 of the activated vinculin structure using Swiss-PDB (53). VBS in its aligned orientation is then used for simulation along with the activated vinculin structure. The aligned VBS is translated 12 Å away from D1, using VMD (54), before the start of the molecular dynamics simulations. Prior to the start of simulation, the activated vinculin structure is minimized with Adopted Basis Newton Raphson for 3000 steps and then equilibrated for 2ns. The additional equilibration is to allow the activated vinculin structure to reach an equilibrium in its new conformation. To prevent stochastic translation harmonic constraints are placed on the center of mass of vinculin. To prevent a conformational switch back to the auto-inhibited conformation weak harmonic constraints (K = 1.0 kcal/mol/Å^2) are placed along helix 4 of domain 1. Previous results from binding of VBS to domain 1 alone (34) showed helix 4 of domain 1 to act as a scaffold for VBS binding with no movement during the binding event, thus application of these weak harmonic constraints on helix 4 should not affect results from our binding simulations using the activated

vinculin conformation. VBS should interact with D1 hydrophobicaly, allowing the use of an implicit solvent treatment without significant artifacts (34). The EEF1 (57) implicit solvent model is used for solvent effects, the SHAKE algorithm (55) is used to constrain hydrogen atoms to heavy atoms, and CHARMM19 force fields (56) are used for the physics definitions. 2fs timesteps are used for each step of the molecular dynamics. Following alignment of VBS, and preparation of activated vinculin, the two molecules are minimized together and then heated to 310K over 80ps. For simulation of the binding event the two molecules are simulated together for 30ns. Results from all simulations were visualized using VMD; trajectory data was also recorded using VMD (54).

As with binding of VBS to the auto-inhibited vinculin conformation, simulation of VBS binding to the activated vinculin conformation are further simulated after the application of initial brief nudging forces of 5 pN, 12.5 pN, or 15 pN are applied to VBS, at residues Q610, L615, G617, and E621, for a duration of 1 ns. The brief nudging force is applied to accelerate VBS towards domain 1 and to increase the possibility of binding. For both simulation of the initial brief nudging of VBS and the subsequent binding of VBS to D1 the same simulation parameters as above are used: weak harmonic constraints are applied to helix 4 of D1 to prevent conformational switch back to the auto-inhibited vinculin conformation, harmonic constraints are applied to the center of mass of vinculin to prevent stochastic translation, the SHAKE algorithm (55) is used to allow 2fs timesteps, and the EEF1 implicit solvent model (57) is used along with CHARMM19 (56) force fields for efficient simulation.

Results

VBS fails to bind auto-inhibited vinculin

Simulation of VBS binding to D1 isolated from other parts of vinculin showed binding of VBS to D1 following movement of helixes 1 and 2 of D1 and hydrophobic insertion of VBS (34). In extension of that study, binding of VBS to D1 is simulated with inclusion of all domains of vinculin in the auto-inhibited conformation. To allow for binding within a reasonable simulation time, VBS is aligned with D1 of full-length vinculin in the orientation predicted by the crystal structure of VBS bound to D1 (61). While maintaining this correct orientation, VBS is then translated away from D1 to be 12 Å away from D1, ensuring a layer of solvation between vinculin and VBS. Twelve simulations, 30ns each, are produced with this setup. These simulations produce two possible outcomes: (1) VBS demonstrates hydrophobic contact with regions of D1 but fails to undergo hydrophobic insertion (Fig. 2), or (2) VBS fails to initiate any hydrophobic contact with D1 and drifts away from D1. It has been predicted that talin binds vinculin by insertion of its hydrophobic residues into the hydrophobic core of D1 (34), therefore we define a complete binding event as any event resulting in complete insertion of VBS into the hydrophobic core of D1. None of the 12 trials show complete binding and hydrophobic insertion of VBS to D1 during the 30ns simulation window.

In 8 out of 12 trials (66%) VBS initiates hydrophobic contact with regions of D1. On average, VBS migrates towards D1 and forms contact with D1 within 5ns of simulation. These initial intermolecular forces link VBS of talin to D1 of vinculin. Initially, P607 and L608 of VBS form hydrophobic interactions with V62, V57, I12, and L54 of D1 (Fig. 3 A). Following these interactions I615 and A616 proceed to interact with P15 and A50 of D1. Together these interactions prevent the drift of VBS away from D1 for the remaining 25ns of simulation. Despite this prolonged link of VBS to D1 at the surface of helix 1 and helix 2, VBS fails to insert into the hydrophobic core of D1. For full binding, the distance between helix 1 and helix 2 needs to increase; yet in each of these trials the distance between these helices remains relatively unchanged (Fig. S1).

In one particular trial, helix 2 of D1 begins to separate from helix 1 (Fig. S1) as VBS forces its way into the hydrophobic core. The separation between helix 1 and helix 2 continues for 10 ns. In the end, VBS fails to insert and is eventually forced out of the gap between the two helices. Contact between helix 1 of D1 and Vt prevents the necessary separation between the helices and prevents the hydrophobic insertion of VBS into D1 (Fig. 4).

In 4 out of 12 trials (33%), VBS forms no contact with D1 and drifts away from its binding site on vinculin. Interaction with and binding to D1 requires (a) VBS maintain the correct orientation necessary for binding, (b) that it stochastically moves towards vinculin, (c) that it forms interactions with D1 that stabilize it and reduce its movement away from D1, and (d) that it proceeds to force its way into the hydrophobic patch in D1. In the trials where VBS drifts away from D1, VBS fails at achieving (b), and stochastically moves in other directions. In the trials where VBS interacts with D1 yet fails to bind, VBS fails to achieve (d). In none of the trials does VBS achieve all the steps and fully bind vinculin.

VBS binds the activated vinculin conformation

Previous molecular dynamics simulation of vinculin activation (46) has produced a suggested conformation for activated vinculin. In this suggested activated conformation D1 has been moved away from Vt, removing the contact between D1 and Vt (Fig. 1 B). To further test the impact of the Vt contact with D1, the binding of VBS to vinculin in this activated conformation is simulated. These simulations also serve to evaluate if this suggested conformation will be consistent with the expected binding behavior of activated vinculin; vinculin should bind its binding partners, namely talin and actin, in its activated conformation. Although it would be more informative to simulate vinculin activation and VBS binding simultaneously, limitations in computing power limit us to simulation of VBS binding before and after vinculin activation. Simulation of activation and binding could report the impact of VBS binding on the rate of vinculin activation, whereas our present simulations will contrast the binding of VBS to vinculin in its inactive, and its suggested active conformation. VBS is simulated interacting with D1 of this activated conformation using only one harmonic constraint to prevent translation of

vinculin, and a second weak harmonic constraint to hold vinculin in the suggested activated conformation. Out of 15 trial of 30ns simulations, 2 simulations show binding of VBS with insertion of VBS into the hydrophobic core of D1 (Fig. 5) and 13 simulations show partial binding of VBS to D1 with incomplete insertion (Fig. 5). These results are comparable to simulation results from a previous study of VBS binding to an isolated D1 (34), where VBS inserted into an isolated D1 in only 1 simulation when no nudging force was used. The use of an initial nudging force reduces the possible translational movements of VBS to those that are towards D1, thereby reducing the sampling necessary to evaluate binding. In both the previous study of binding to an isolated D1 and in our simulations with an activated vinculin coformation a nudging force greatly increases the number of binding events (see below).

In the 13 simulations lacking complete VBS insertion, residues closer to the N-terminus of VBS (lower-VBS) show partial insertion of VBS in between helix 1 and helix 2 of D1 (Fig. 5). At these D1 regions with VBS insertion, helix 1 and helix 2 of D1 are forced apart while D1 regions interaction with VBS residues near the C-terminus of VBS (upper-VBS) show no separation between the helices (Fig. S2). Separation of helix 1 and helix 2 by at least 20.5 Å at all regions of D1 interacting with lower-VBS and upper-VBS is necessary for complete insertion of VBS (34). After complete insertion, VBS should be within 13 Å of helix 4 (34). Insertion of lower-VBS into D1 helices is stabilized by hydrophobic interactions. VBS residues P607, L608, I615, and A616 interact with D1 residues V57, V62, P15, I12, A50, and L54 (Fig. 3 B); VBS interacts with auto-inhibited vinculin at the same residues (see above).

Simulations resulting in the complete insertion of VBS into the hydrophobic core of D1 initially show the same interaction between residues in lower-VBS and D1. The partial insertion of lower-VBS anchors VBS to vinculin allowing upper-VBS to force itself in between helix 1 and helix 2 of D1 (Fig. 5). The results show that regions of D1 nearest lower-VBS show helical separation before regions of D1 nearest upper-VBS (Fig. S2). Insertion of upper-VBS into D1 within the 30ns simulation window occurs in only 2 of the trials. In these trials VBS insertion occurs, after at least 20ns of simulation, following interaction of VBS residues V619, L622, and L623 with D1 residues L23 and P43 (Fig. 3 B). Removal of the contact between helix 1 and Vt allows for insertion of both lower-VBS and upper-VBS into D1.

Acceleration of VBS towards D1 only enhances VBS complete insertion in the activated vinculin conformation

To enhance the binding and full insertion of VBS into D1, the 30ns binding simulations are repeated with the additional application of an initial small nudging force on VBS, applied over 1ns. The nudging force is applied to VBS because of its smaller size as compared to vinculin. The nudging force accelerates VBS towards its binding groove between helix 1 and helix 2 in D1. 12 trials simulate the binding of VBS to vinculin in the auto-inhibited conformation following a 15 pN nudge, and 12

trials simulate the binding of VBS to the activated conformation following an initial nudge – 4 trials with a 15pN nudge, 4 trials with a 12.5 pN nudge, and 4 trials with a 5 pN nudge. Application of the nudging force accelerates VBS towards D1 yet no binding interactions occur within the 1ns window during which the nudge is applied.

Application of the initial accelerating nudge force enhances binding of VBS to the activated vinculin conformation, but none of the simulations of VBS binding to the auto-inhibited vinculin conformation following a nudging force show complete binding (Table S1). VBS inserts into D1 in 25% of the trials with a 5 pN initial nudging force, in 25% of the trials with a 12.5 pN initial nudging force, and in 75% of the trials with a 15 pN initial nudging force. The insertion of VBS following an initial nudge follows the same trajectory as insertion of VBS in the previous sections; first, lower-VBS inserts between helix 1 and helix 2, then, upper-VBS inserts between helix 1 and helix 2, and finally, VBS rotates into the hydrophobic core in D1. The initial force increases the rate of binding of VBS to the activated vinculin structure, within the 30 ns simulation window, yet, the mechanism of binding is unchanged. The contact between Vt and D1 prevents VBS binding to auto-inhibited vinculin, even after the initial nudge.

Discussion

Simulation of the interaction between talin and vinculin in each of its two conformations – auto-inhibited and activated – suggests that a prior vinculin activation event is necessary to allow for full binding of talin to D1 of vinculin. Talin interacts with D1 via the insertion of VBS into the hydrophobic core of D1 (34, 35, 40, 45, 62). The insertion of VBS into D1 while vinculin is in its auto-inhibited conformation (Fig. 1 A) fails to occur in simulation, even after an initial nudge of VBS towards D1 (Table S1 and Fig. 2) because D1 cannot undergo the necessary conformational change to accommodate VBS insertion while in close proximity to Vt (Fig. 4). In contrast, the insertion of VBS into D1 of vinculin in its activated conformation (Fig. 1 B) occurs in simulation following first, separation of D1 helices near lower-VBS, second, separation of D1 helices near upper-VBS, and third, rotation of VBS into the hydrophobic core (Fig. 5). This binding to the activated vinculin conformation is enhanced by an initial nudge of VBS towards D1 (Table S1). Vinculin activation prior to talin binding could reduce the proximity of D1 and Vt (46) allowing for helix 1 and helix 2 to separate and for VBS to follow these steps to activation.

The trajectory suggested here for the binding of VBS to D1 can be compared to the trajectory for VBS binding to D1 in that absence of other vinculin domains (34). Simulation of VBS binding to D1 alone described the binding event as comprising of three essential steps: (1) insertion of VBS into the groove between helix 1 and helix 2, (2) separation of helix 1 from helix 2, and (3) rotation of VBS into the hydrophobic core of D1. The results presented here expand these steps to account for effects of the other vinculin domains; VBS binding to D1 can now be described with the following steps: (1) insertion of lower-VBS into the groove between helix 1

and helix 2 in D1, (2) separation of helix 1 and helix 2 at regions near lower-VBS, (3) insertion of upper-VBS into the groove between helix 1 and helix 2 in D1, (4) separation of helix 1 and 2 at regions near upper-VBS, (5) rotation of VBS hydrophobic residues into the hydrophobic core of D1. The steps suggested here are similar to and confirm the steps suggested by Lee et al. (34). In the previous simulations, VBS from α-actinin and other talin VBSs all bound vinculin D1 with the same mechanism. Simulation of VBS from α-actinin in Lee et al. (34) however suggested α-VBS binds with an inverted orientation. The results presented here demonstrate a significant difference between binding to lower-VBS and upper-VBS, therefore it is unclear if α-VBS would bind D1 of full-length vinculin as it did D1 in the previous simulations. The nature of α-actinin binding to full-length vinculin should be a topic for future investigations.

The suggestion that vinculin activation is required for full talin binding extends the current understanding of vinculin auto-inhibition. Vinculin in its native conformation is defined as being auto-inhibited mainly because the interaction of Vt with actin is not possible in this conformation (38). It has been suggested that actin binding to Vt is inhibited by the proximity of D1 to Vt; D1 would stericly clash with any nearby actin filaments that would otherwise bind Vt. The results from these simulations suggest that vinculin is also auto-inhibited in its native conformation because this proximity between Vt and D1 also prevents the complete binding of talin to D1. Although talin can form a weak hydrophobic link to D1 via interaction at the lower-VBS residues, it is important to recognize that this differs from the mechanisms of talin binding to vinculin previously described (35, 43, 45). The conformation of vinculin can regulate the strength of the talin-vinculin linkage; talin and vinculin would likely link with the greatest strength only after a transition of vinculin to an activated conformation. This observation can lead us to two specific assertions concerning vinculin recruitment to focal adhesions: (1) it is possible that talin is not the only mechanosensor at focal adhesions but vinculin might also be dependent on a mechanical environment for its activation, and (2) vinculin reinforcement at focal adhesions and mechanosensitive focal adhesion growth is a holistic event that depends on a coordinated set of events between numerous molecules. The cooperative nature of focal adhesion growth accounts for the abundance of a number of different molecules at focal complexes.

In the simulations that failed to show full VBS insertion into D1, hydrophobic residues in lower-VBS interact with hydrophobic residues in D1 (Fig. 3). Although these interactions are a weaker intermolecular bond than the full insertion of VBS into the hydrophobic core would have been, they link talin to vinculin and prevent the drifting of VBS away from D1. Considering that the suggested mechanism for vinculin activation is that actin and talin cooperatively interact with vinculin to cause its activation (42, 46), this proximity of talin to vinculin by the weaker hydrophobic interaction at lower-VBS could allow for vinculin activation. Furthermore, phosphorylation of vinculin could also contribute to vinculin activation by enhancing the cooperative binding of actin and talin to vinculin. With D1 weakly interacting with lower-VBS, an electrostatic interaction of Vt with actin

(38) could then stretch vinculin and cause its activation (46). The stretching of vinculin can lead to a conformational change in which D1 moves away from Vt and vinculin becomes activated [Fig. 1 B]. Then, after vinculin activation by movement of D1 away from Vt, talin's VBS would be able to fully insert into D1 to solidify and strengthen the talin-vinculin link (Fig. 6). In this way vinculin can serve as an intermediary for actin binding to talin. The strengthening of the interaction between vinculin and talin after vinculin activation allows for vinculin to take a larger mechanical load at focal adhesions, reflecting its role as a reinforcing agent. With vinculin activation by this mechanism, it is possible that the number of actin filaments linked to each talin rod can be multiplied via vinculin, although there is currently no experimental evidence supporting this hypothesis. The expansion of actin filaments linked to integrin-bound talin molecules is essential to focal adhesion growth and maturation. In force induced focal adhesion formation, as the load on the developing focal complex increases we would expect more vinculin activation and recruitment of activated vinculin to crosslink talin and actin filaments.

That vinculin becomes activated by a stretching force, and furthermore, that after its stretch and activation vinculin strengthens its link to at least one of its binding partners, talin, is entirely consistent with vinculin's role as a linker molecule. Vinculin recruitment to focal adhesions serves to strengthen and reinforce the cytoskeletal link to the ECM (1, 11, 27, 31); vinculin is a reinforcing agent. The ability of vinculin to strengthen its binding upon stretch is a feature that enables its reinforcement. Recent *in vivo* experiments using a FRET probe to measure mechanical tension across single molecules reports that vinculin is under 2.5 pN of tension *in vivo* when reinforcing focal adhesions (47). It is likely that this tension stretches vinculin to a conformation similar to the one tested here (46)(Fig. 1 B), and also that it strengthens the link of vinculin to talin. Mechanosensation at focal adhesions is not limited to talin and vinculin. Other critical components of focal adhesions, such as membrane bound integrins are also involved in mechanosensation by focal adhesions: the process of integrin clustering at focal adhesions can be force induced, and the binding of integrin to ECM can be mechanosensititve (63).

The results reported here are limited to the structures used in simulation. Just as including other regions of vinculin aside from D1 in these simulations demonstrated an impact of those regions on the conformational changes D1 is able to make during binding to VBS, we expect that including other regions of talin near VBS in simulation would investigate the impact of those nearby regions on the ability of VBS to bind to and interact with D1. To further expand on the results presented in this study, and further investigate the mechanisms of this critical interaction between talin and vinculin, it would be important explore the impact of the talin rod on the binding of talin to vinculin. In doing so, one challenge that would need to be addressed is the consistency of conformation of the talin rod with VBS activation. Some studies have reported a talin conformation in which VBS is rotated out of its hydrophobic grove in the rod domain during VBS activation (31), while other studies have suggested an unraveling of the rod domain during talin-VBS activation

(32, 33). Of course both conformations assume talin VBS activation by exposure to an external stress, whereas it is entirely possible that talin mechanosensation is a result of external strain: movement of the integrin binding head domain from each talin monomer would cause a talin dimer to shift in its arrangement of rod domains from parallel to elongated, effectively doubling the number of actin filaments that could be cross-linked by vinculin.

Here we have investigated the interaction of activated vinculin with talin and contrasted it with the interaction of auto-inhibited vinculin with talin. The other significant binding partner of vinculin is the actin filament. It is essential to understand the mechanisms to actin-vinculin binding. It has been suggested that electrostatic forces might play a significant role in driving the binding of vinculin to actin (38). The interactions between Vt and actin filaments that drive this binding event should be studied and characterized. Is the suggested conformation of activated vinculin (46) – which removes the proximity of D1 to Vt via movement of D1 – sufficient to allow Vt to interact with actin? Will there be a clash between an actin filament aiming to bind vinculin and a talin rod domain aiming to bind D1? If so, what are the additional conformational changes in vinculin that would prevent this clash? The results presented here evaluate the activated vinculin conformation for binding to talin, but numerous significant questions remain to be evaluated.

References

1. Mierke, C. T., P. Kollmannsberger, D. P. Zitterbart, J. Smith, B. Fabry, and W. H. Goldmann. 2008. Mechano-coupling and regulation of contractility by the vinculin tail domain. Biophysical journal 94:661-670.
2. Schwarz, U. S., T. Erdmann, and I. B. Bischofs. 2006. Focal adhesions as mechanosensors: the two-spring model. BioSystems 83:225-232.
3. Critchley, D. R. 2000. Focal adhesions - the cytoskeletal connection. Current Opinion in Cell Biology 12:133-139.
4. Bershadsky, A. D., C. Ballestrem, L. Carramusa, Y. Zilberman, B. Gilquin, S. Khochbin, A. Y. Alexandrova, A. B. Verkhovsky, T. Shemesh, and M. M. Kozlov. 2006. Assembly and mechanosensory function of focal adhesions: experiments and models. Eur J Cell Biol 85:165-173.
5. Shen, T. L., A. Y. Park, A. Alcaraz, X. Peng, I. Jang, P. Koni, R. A. Flavell, H. Gu, and J. L. Guan. 2005. Conditional knockout of focal adhesion kinase in endothelial cells reveals its role in angiogenesis and vascular development in late embryogenesis. J Cell Biol 169:941-952.
6. Wu, M. H. 2005. Endothelial focal adhesions and barrier function. J Physiol 569:359-366.
7. Zamir, E., and B. Geiger. 2001. Components of cell-matrix adhesions. Journal of cell science 114:3577-3579.
8. Ingber, D. E. 2003. Mechanobiology and diseases of mechanotransduction. Ann Med 35:564-577.
9. Critchley, D. R. 2004. Cytoskeletal proteins talin and vinculin in integrin-mediated adhesion. Biochemical Society transactions 32:831-836.

10. Geiger, B., J. P. Spatz, and A. D. Bershadsky. 2009. Environmental sensing through focal adhesions. Nat Rev Mol Cell Biol 10:21-33.
11. Ziegler, W. H., A. R. Gingras, D. R. Critchley, and J. Emsley. 2008. Integrin connections to the cytoskeleton through talin and vinculin. Biochemical Society transactions 36:235-239.
12. Xiong, J. P., T. Stehle, S. L. Goodman, and M. A. Arnaout. 2003. New insights into the structural basis of integrin activation. Blood 102:1155-1159.
13. Hynes, R. O. 2002. Integrins: bidirectional, allosteric signaling machines. Cell 110:673-687.
14. Huveneers, S., and E. H. Danen. 2009. Adhesion signaling - crosstalk between integrins, Src and Rho. J Cell Sci 122:1059-1069.
15. Wang, Y. L., L. M. McNamara, M. B. Schaffler, and S. Weinbaum. 2007. A model for the role of integrins in flow induced mechanotransduction in osteocytes. Proc Natl Acad Sci U S A 104:15941-15946.
16. Galbraith, C. G., K. M. Yamada, and M. P. Sheetz. 2002. The relationship between force and focal complex development. The Journal of cell biology 159:695-705.
17. Kamm, R. D., and M. R. Kaazempur-Mofrad. 2004. On the molecular basis for mechanotransduction. Mech Chem Biosyst 1:201-209.
18. Mofrad, M. R., J. Golji, N. A. Abdul Rahim, and R. D. Kamm. 2006. Force-induced unfolding of the focal adhesion targeting domain and the influence of paxillin binding. Mechanics & chemistry of biosystems : MCB 1:253-265.
19. Zhang, X., G. Jiang, Y. Cai, S. J. Monkley, D. R. Critchley, and M. P. Sheetz. 2008. Talin depletion reveals independence of initial cell spreading from integrin activation and traction. Nat Cell Biol 10:1062-1068.
20. Le Clainche, C., and M. F. Carlier. 2008. Regulation of actin assembly associated with protrusion and adhesion in cell migration. Physiol Rev 88:489-513.
21. Critchley, D. R., and A. R. Gingras. 2008. Talin at a glance. Journal of cell science 121:1345-1347.
22. Moes, M., S. Rodius, S. J. Coleman, S. J. Monkley, E. Goormaghtigh, L. Tremuth, C. Kox, P. P. van der Holst, D. R. Critchley, and N. Kieffer. 2007. The integrin binding site 2 (IBS2) in the talin rod domain is essential for linking integrin beta subunits to the cytoskeleton. J Biol Chem 282:17280-17288.
23. Gingras, A. R., N. Bate, B. T. Goult, L. Hazelwood, I. Canestrelli, J. G. Grossmann, H. Liu, N. S. Putz, G. C. Roberts, N. Volkmann, D. Hanein, I. L. Barsukov, and D. R. Critchley. 2008. The structure of the C-terminal actin-binding domain of talin. The EMBO journal 27:458-469.
24. Chen, H., D. M. Cohen, D. M. Choudhury, N. Kioka, and S. W. Craig. 2005. Spatial distribution and functional significance of activated vinculin in living cells. The Journal of cell biology 169:459-470.
25. Brett, T. J., V. Legendre-Guillemin, P. S. McPherson, and D. H. Fremont. 2006. Structural definition of the F-actin-binding THATCH domain from HIP1R. Nat Struct Mol Biol 13:121-130.
26. Hemmings, L., D. J. Rees, V. Ohanian, S. J. Bolton, A. P. Gilmore, B. Patel, H. Priddle, J. E. Trevithick, R. O. Hynes, and D. R. Critchley. 1996. Talin contains

three actin-binding sites each of which is adjacent to a vinculin-binding site. J Cell Sci 109 (Pt 11):2715-2726.
27. Humphries, J. D., P. Wang, C. Streuli, B. Geiger, M. J. Humphries, and C. Ballestrem. 2007. Vinculin controls focal adhesion formation by direct interactions with talin and actin. The Journal of cell biology 179:1043-1057.
28. Critchley, D. R., and A. R. Gingras. 2008. Talin at a glance. J Cell Sci 121:1345-1347.
29. Critchley, D. R. 2005. Genetic, biochemical and structural approaches to talin function. Biochemical Society transactions 33:1308-1312.
30. Gingras, A. R., W. H. Ziegler, R. Frank, I. L. Barsukov, G. C. Roberts, D. R. Critchley, and J. Emsley. 2005. Mapping and consensus sequence identification for multiple vinculin binding sites within the talin rod. J Biol Chem 280:37217-37224.
31. Lee, S. E., R. D. Kamm, and M. R. Mofrad. 2007. Force-induced activation of talin and its possible role in focal adhesion mechanotransduction. Journal of biomechanics 40:2096-2106.
32. Hytonen, V. P., and V. Vogel. 2008. How force might activate talin's vinculin binding sites: SMD reveals a structural mechanism. PLoS Comput Biol 4:e24.
33. del Rio, A., R. Perez-Jimenez, R. Liu, P. Roca-Cusachs, J. M. Fernandez, and M. P. Sheetz. 2009. Stretching single talin rod molecules activates vinculin binding. Science 323:638-641.
34. Lee, S. E., S. Chunsrivirot, R. D. Kamm, and M. R. Mofrad. 2008. Molecular dynamics study of talin-vinculin binding. Biophys J 95:2027-2036.
35. Ziegler, W. H., R. C. Liddington, and D. R. Critchley. 2006. The structure and regulation of vinculin. Trends in Cell Biology 16:453-460.
36. Diez, G., F. List, J. Smith, W. H. Ziegler, and W. H. Goldmann. 2008. Direct evidence of vinculin tail-lipid membrane interaction in beta-sheet conformation. Biochem Biophys Res Commun 373:69-73.
37. Cohen, D. M., H. Chen, R. P. Johnson, B. Choudhury, and S. W. Craig. 2005. Two distinct head-tail interfaces cooperate to suppress activation of vinculin by talin. J Biol Chem 280:17109-17117.
38. Janssen, M. E., E. Kim, H. Liu, L. M. Fujimoto, A. Bobkov, N. Volkmann, and D. Hanein. 2006. Three-dimensional structure of vinculin bound to actin filaments. Mol Cell 21:271-281.
39. Borgon, R. A., C. Vonrhein, G. Bricogne, P. R. Bois, and T. Izard. 2004. Crystal structure of human vinculin. Structure 12:1189-1197.
40. Cohen, D. M., B. Kutscher, H. Chen, D. B. Murphy, and S. W. Craig. 2006. A conformational switch in vinculin drives formation and dynamics of a talin-vinculin complex at focal adhesions. J Biol Chem 281:16006-16015.
41. Chen, Y., and N. V. Dokholyan. 2006. Insights into allosteric control of vinculin function from its large scale conformational dynamics. J Biol Chem 281:29148-29154.
42. Chen, H., D. M. Choudhury, and S. W. Craig. 2006. Coincidence of actin filaments and talin is required to activate vinculin. J Biol Chem 281:40389-40398.

43. Bois, P. R., B. P. O'Hara, D. Nietlispach, J. Kirkpatrick, and T. Izard. 2006. The vinculin binding sites of talin and alpha-actinin are sufficient to activate vinculin. J Biol Chem 281:7228-7236.
44. Izard, T., and C. Vonrhein. 2004. Structural basis for amplifying vinculin activation by talin. J Biol Chem 279:27667-27678.
45. Nhieu, G. T., and T. Izard. 2007. Vinculin binding in its closed conformation by a helix addition mechanism. The EMBO journal 26:4588-4596.
46. Golji, J., and M. R. Mofrad. 2010. Molecular-Dynamics Investigation of Vinculin Activation. Biophysical Journal 99.
47. Grashoff, C., B. D. Hoffman, M. D. Brenner, R. Zhou, M. Parsons, M. T. Yang, M. A. McLean, S. G. Sligar, C. S. Chen, T. Ha, and M. A. Schwartz. 2010. Measuring mechanical tension across vinculin reveals regulation of focal adhesion dynamics. Nature 466:263-266.
48. Kupper, K., N. Lang, C. Mohl, N. Kirchgessner, S. Born, W. H. Goldmann, R. Merkel, and B. Hoffmann. 2010. Tyrosine phosphorylation of vinculin at position 1065 modifies focal adhesion dynamics and cell tractions. Biochem Biophys Res Commun 399:560-564.
49. Zhang, Z., G. Izaguirre, S. Y. Lin, H. Y. Lee, E. Schaefer, and B. Haimovich. 2004. The phosphorylation of vinculin on tyrosine residues 100 and 1065, mediated by SRC kinases, affects cell spreading. Mol Biol Cell 15:4234-4247.
50. Ziegler, W. H., U. Tigges, A. Zieseniss, and B. M. Jockusch. 2002. A lipid-regulated docking site on vinculin for protein kinase C. J Biol Chem 277:7396-7404.
51. Izard, T., G. Evans, R. A. Borgon, C. L. Rush, G. Bricogne, and P. R. J. Bois. 2004. Vinculin activation by talin through helical bundle conversion. Nature 427:171-175.
52. Papagrigoriou, E., A. R. Gingras, I. L. Barsukov, N. Bate, I. J. Fillingham, B. Patel, R. Frank, W. H. Ziegler, G. C. Roberts, D. R. Critchley, and J. Emsley. 2004. Activation of a vinculin-binding site in the talin rod involves rearrangement of a five-helix bundle. The EMBO journal 23:2942-2951.
53. Arnold, K., L. Bordoli, J. Kopp, and T. Schwede. 2006. The SWISS-MODEL workspace: a web-based environment for protein structure homology modelling. Bioinformatics 22:195-201.
54. Humphrey, W., A. Dalke, and K. Schulten. 1996. VMD: visual molecular dynamics. J Mol Graph 14:33-38, 27-38.
55. Kräutler, V., W. F. v. Gunsteren, and P. H. Hünenberger. 2001. A fast SHAKE algorithm to solve distance constraint equations for small molecules in molecular dynamics simulations. Journal of Computational Chemistry 22:501-508.
56. Neria, E., S. Fischer, and M. Karplus. 1996. Simulation of activation free energies in molecular systems. J. Chem. Phys. 105:1902-1921.
57. Lazaridis, T. 2003. Effective energy function for proteins in lipid membranes. Proteins 52:176-192.
58. Best, R. B., J. Clarke, and M. Karplus. 2005. What contributions to protein side-chain dynamics are probed by NMR experiments? A molecular dynamics simulation analysis. J Mol Biol 349:185-203.

59. Feig, M., and C. L. Brooks, 3rd. 2004. Recent advances in the development and application of implicit solvent models in biomolecule simulations. Curr Opin Struct Biol 14:217-224.
60. Brooks, B. R., R. E. Bruccoleri, B. D. Olafson, D. J. States, S. Swaminathan, and M. Karplus. 1983. Charmm - a Program for Macromolecular Energy, Minimization, and Dynamics Calculations. Journal of Computational Chemistry 4:187-217.
61. Izard, T., and C. Vonrhein. 2004. Structural basis for amplifying vinculin activation by talin. J Biol Chem 279:27667-27678.
62. Patel, B., A. R. Gingras, A. A. Bobkov, L. M. Fujimoto, M. Zhang, R. C. Liddington, D. Mazzeo, J. Emsley, G. C. Roberts, I. L. Barsukov, and D. R. Critchley. 2006. The activity of the vinculin binding sites in talin is influenced by the stability of the helical bundles that make up the talin rod. J Biol Chem 281:7458-7467.
63. Friedland, J. C., M. H. Lee, and D. Boettiger. 2009. Mechanically activated integrin switch controls alpha5beta1 function. Science 323:642-644.

Figures

Figure 1. Vinculin can adopt an auto-inhibited conformation or an activated conformation. (A) In its native state vinculin is in an auto-inhibited conformation. Vinculin has five helical domains: D1, D2, D3, D4, and Vt. Vt contains binding sites for F-actin while D1 contains binding sites for VBS. In its native conformation the proximity of D1 to Vt prevents the binding of Vt to F-actin. The proximity of Vt to D1 could also impact the binding of D1 to VBS. (B) A suggested conformation of activated vinculin. Investigation of vinculin activation by a stretching force (46) using molecular dynamics has suggested that during activation D1 of vinculin undergoes a conformational change and rotates away from Vt. In this conformation the proximity of Vt and D1 is reduced, potentially allowing for interaction of those domains with binding partners.

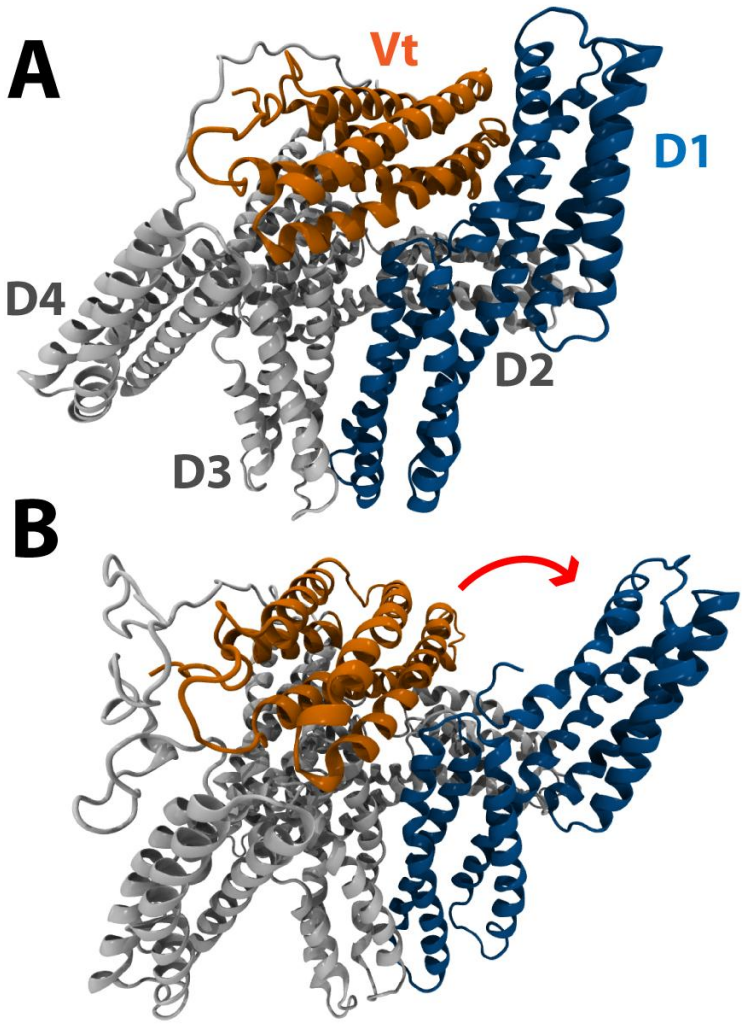

Figure 2. VBS does not bind auto-inhibited vinculin. Simulation of the binding of VBS to D1 of vinculin in its auto-inhibited conformation suggests that VBS can interact with hydrophobic residues on the surface of D1 between helix 1 and helix 2, but it cannot insert into the hydrophobic core of D1. For VBS to insert into D1, helix 1 and helix 2 of D1 need to separate. VBS is linked to D1 by the surface interactions but without helical separation it fails to fully insert into D1.

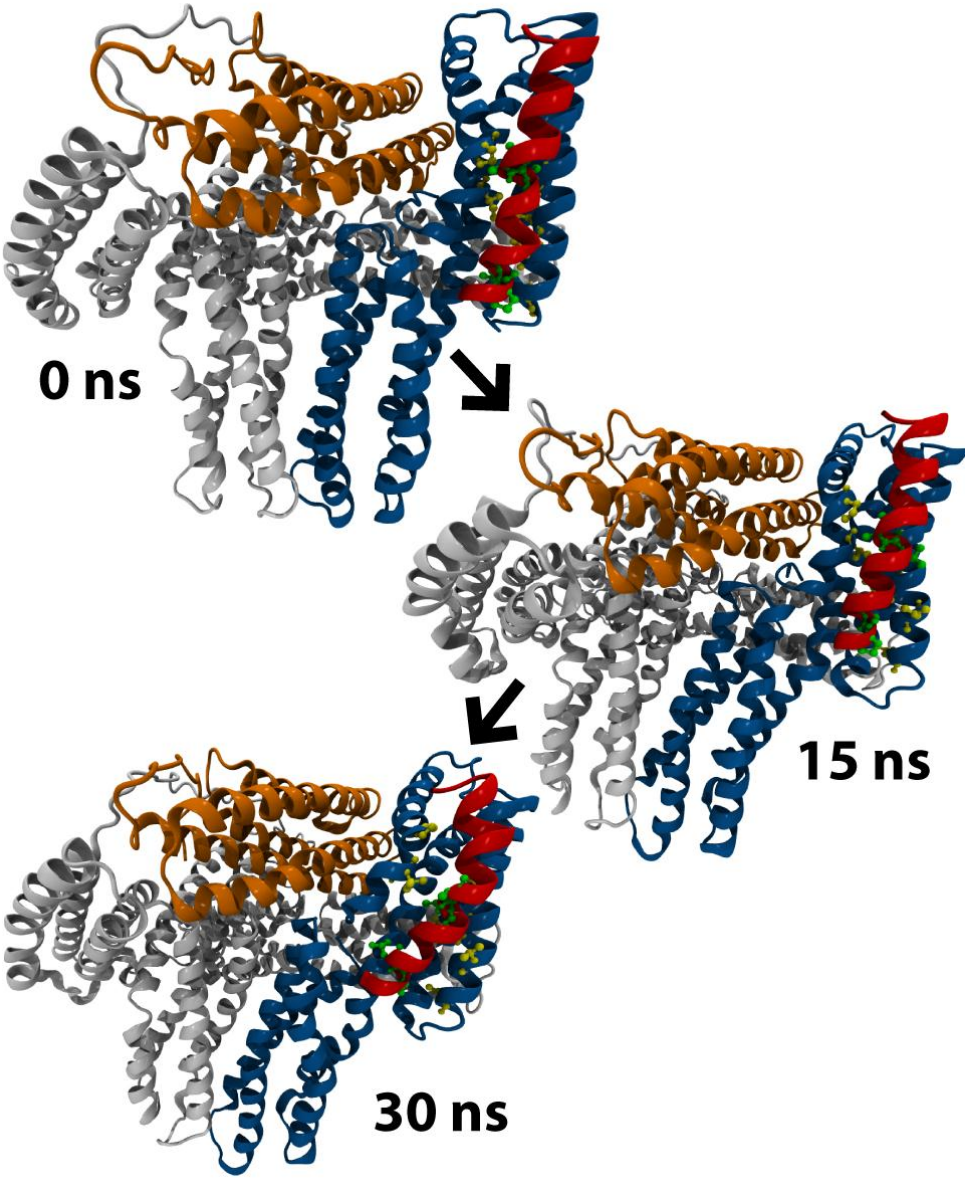

Figure 3. Hydrophobic interactions link VBS to D1. (A) Interaction between VBS residues P607, L608, I615, and A616 with D1 residues I12, P15, A50, L54, V57, and V62 link lower-VBS to D1. Lower-VBS links to D1 by these interactions in simulation with auto-inhibited vinculin (shown here) and with activated vinculin. (B) In addition to the lower-VBS interactions, a second set of surface hydrophobic interactions link upper-VBS to D1 in simulations with activated vinuclin. Residues V619, L622, and L623 of VBS interact with residues L23 and P43 of D1. D1 Helical separation near lower-VBS allows interaction of these residues near upper-VBS.

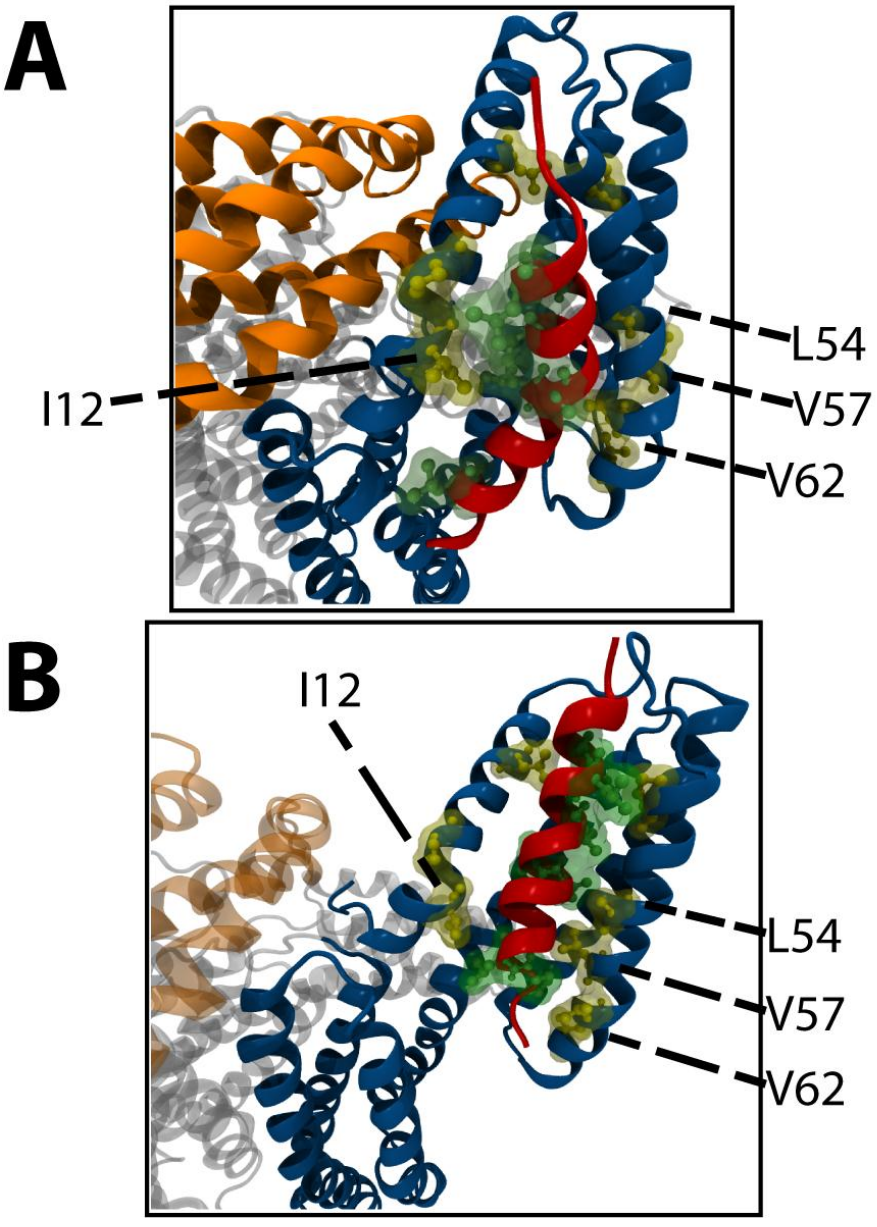

Figure 4. Contact between D1 and Vt prevents VBS binding to auto-inhibited vinculin. VBS insertion into D1 requires separation of helix 1 and helix 2. Helix 1 is near Vt and can stericaly contact Vt residues during separation. The proximity of Vt to D1 limits helix 1 movement; residues R7, E10, Q18, I20, S21, V24, and I25 clash with residues G940, S941, T943, R945, A946, P989, T993, K996, and I997. Separation of Vt and D1 by vinculin activation removes these clashes allowing for helix 1 movement and VBS insertion.

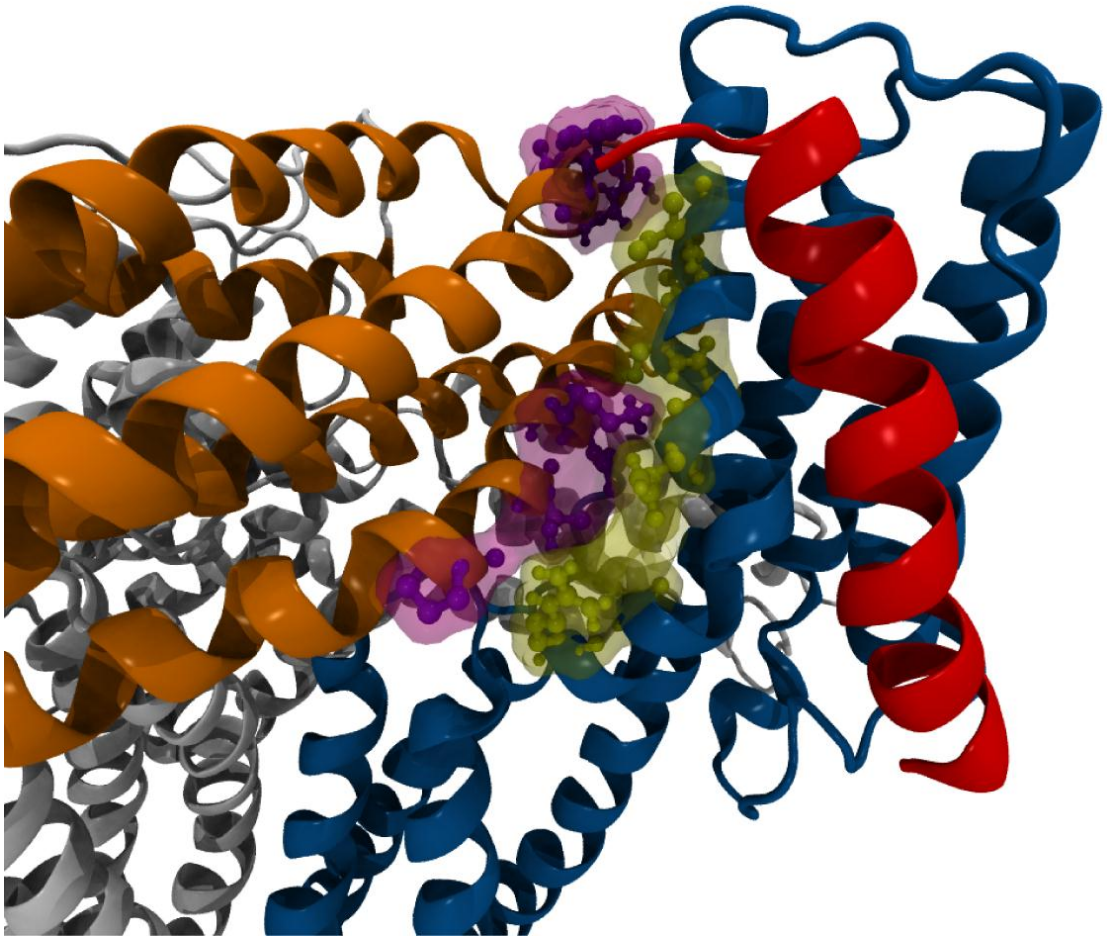

Figure 5. VBS can bind activated vinculin. (A) Interaction between hydrophobic residues in VBS and D1 links lower-VBS to D1. Separation of Vt from D1 in activated vinculin allows for helix 1 movement and insertion of lower-VBS after linking to D1. (B) Upper-VBS can link D1 after lower-VBS insertion. Following surface interactions between upper-VBS and D1, if D1 helices continue to separate, upper-VBS can also insert into D1. (C) VBS inserts into activated vinculin, first, by inserting lower-VBS, followed by insertion of upper-VBS, and finally, rotation of VBS hydrophobic residues into the hydrophobic core of D1. D1 is shown with a view looking down its helices.

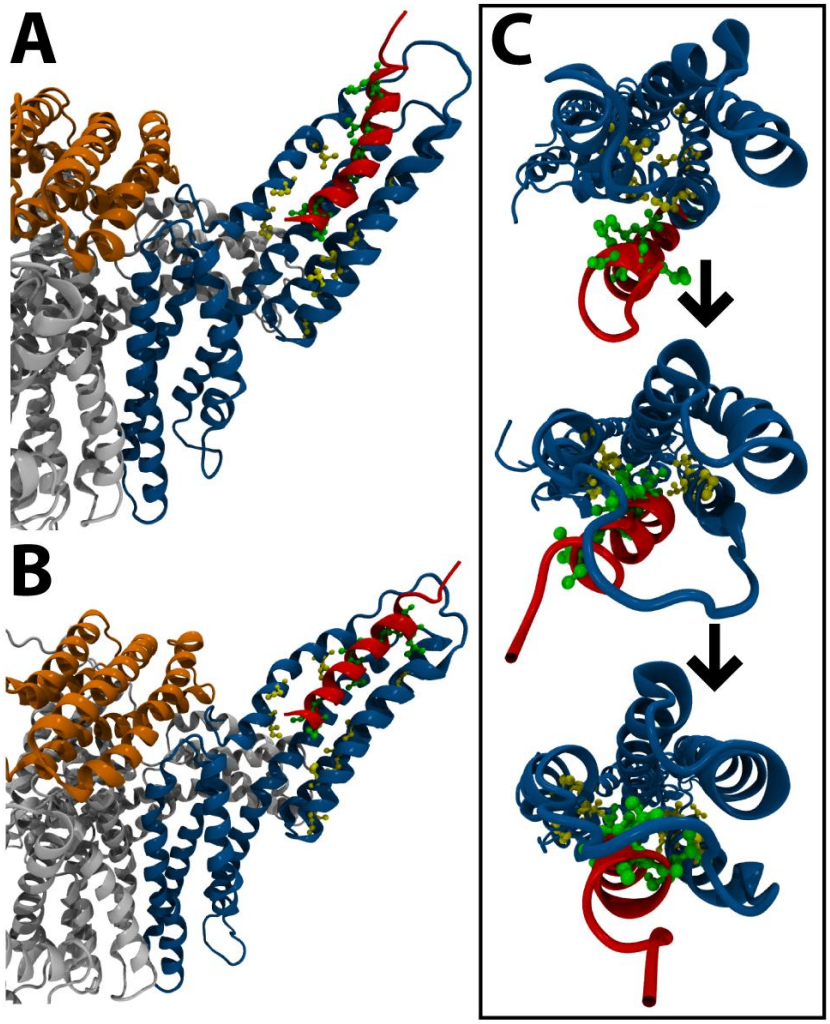

Figure 6. A mechanism for vinculin activation: VBS linking followed by binding. Simulation of VBS interaction with auto-inhibited vinculin suggests that VBS can link to D1 but cannot insert into D1 with Vt in close proximity. Simulation of VBS interaction with activated vinculin suggests that VBS can link to and insert into D1 after the proximity of Vt is removed. Together, these results suggest the following mechanism for vinculin activation: (I) lower-VBS links to D1, (II) vinculin is stretched (by simultaneous interaction with talin and actin perhaps), (III) VBS fully inserts into D1.

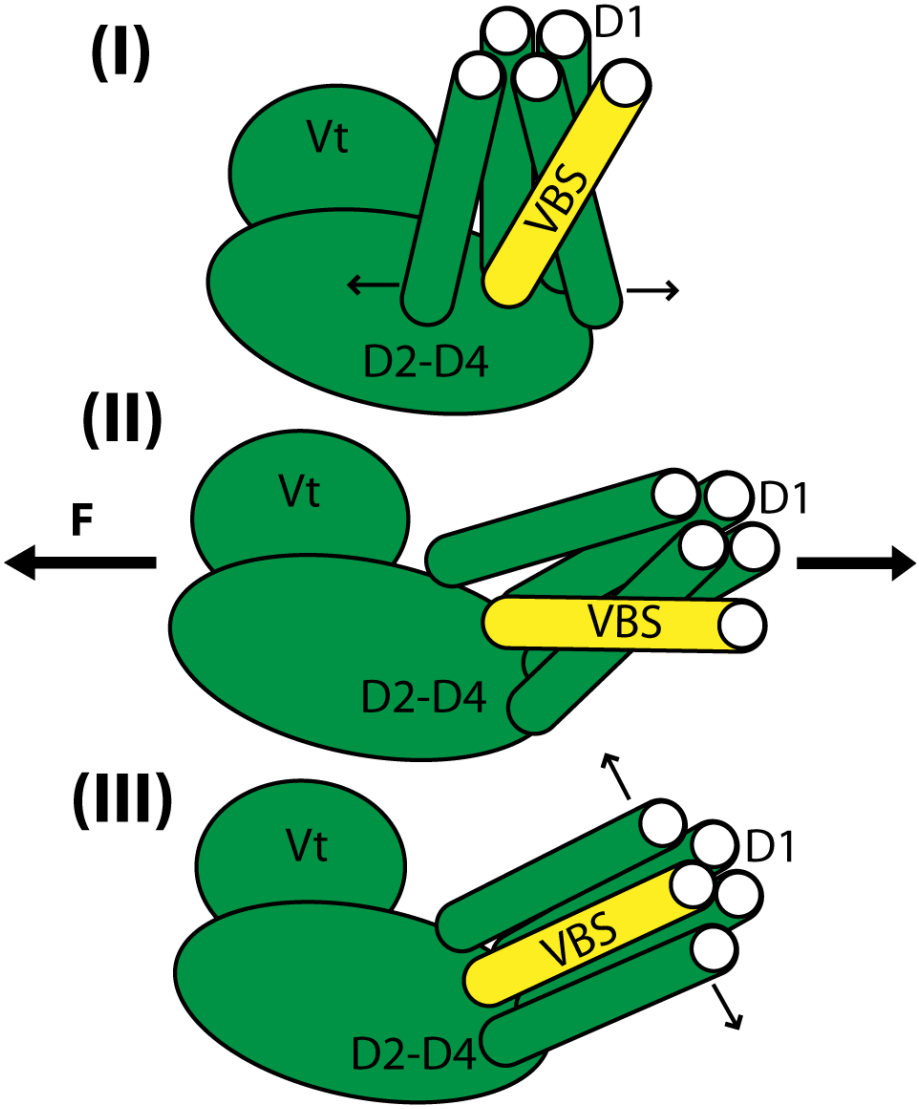

The Interaction of Vinculin with Actin

Abstract
Vinculin can interact with F-actin both in recruitment of actin filaments to the growing focal adhesions and also in capping of actin filaments to regulate actin dynamics. Using molecular dynamics both interactions are simulated using different vinculin conformations. Vinculin is simulated either with only its vinculin tail domain (Vt) , with all residues in its closed conformation, with all residues in an open I conformation, and with all residues in an open II conformation The open I conformation results from movement of domain 1 away from Vt, the open II conformation results from complete dissociation of Vt from the vinculin head domains. Simulation of vinculin binding along the actin filament showed that Vt alone can bind along the actin filaments, that vinculin in its closed conformation cannot bind along the actin filaments, and that vinculin in its open I conformation can bind along the actin filaments. The simulations confirm that movement of domain 1 away from Vt in formation of vinculin 1 is sufficient for allowing Vt to bind along the actin filament. Simulation of Vt capping actin filaments probe six possible bound structures and suggest that vinculin would cap actin filaments by interacting with both S1 and S3 of the barbed-end using the surface of Vt normally occluded by D4 and nearby vinculin head domain residues. Simulation of D4 separation from Vt after D1 separation formed the open II conformation. Binding of open II vinculin to the barbed-end suggests this conformation allows for vinculin capping. Three binding sites on F-actin are suggested as regions that could link to vinculin. Vinculin is suggested to function as a variable switch at the focal adhesions. The conformation of vinculin and the precise F-actin binding conformation is dependent on the level of mechanical load on the focal adhesion.

Introduction

The focal adhesion is imperative for a mechanical linkage between the cell and its substrate [1]. Cell movement [2,3], wound healing [4], cancer cell metastasis [5,6], and other processes rely on the mechanical linkage to a substrate [7-9]. The actin filaments of the cellular cytoskeleton are linked to the extra-cellular membrane (ECM) of the substrate through the focal adhesion [4]. Once linked, both mechanical forces originating from within the cell – such as myosin induced contraction of the actin filaments [10] during cell migration – can act on the ECM and the substrate, and, mechanical forces originating from outside the cell – such as flow induced cyclic stress in the case of endothelial cells [11] – can be transduced to the cellular machinery [12]. Without the focal adhesion the cell could effectively become mechanically isolated from its surroundings.

Formation of the focal adhesion involves linkage of focal adhesion proteins to ECM bound integrins [13], linkage of focal adhesion proteins to each other [14], and linkage of the ECM-focal adhesion complex to actin filaments [15]. Linkage to integrin results from either inside-out [16,17] or outside-in [17,18] activation of

integrin, and likely involves an initial connection between talin and integrin [16]. Many molecules make up the focal adhesion [19] and the molecular composition of the focal adhesion is dynamic; vinculin [20] and talin are likely early recruits to focal adhesions, where as α-actinin [21] and zyxin [22,23] are likely late recruits to a maturing focal adhesion. The simplest focal complex structure would consist of a talin molecule bound to integrin via its head domain and bound to actin via its tail domain [24]. Talin has 11 cryptic binding sites for vinculin [25,26] and activation of these binding sites along with subsequent recruitment of vinculin to the growing focal adhesion correlates with the strengthening of the focal adhesion [27]. Vinculin, in the right conformation, can crosslink an actin filament to the talin molecule [28]. The focal adhesion is strengthened subsequent to vinculin recruitment by the resulting multitude of actin filament linkages. Binding of the focal adhesion to actin filaments, by vinculin or other focal adhesion forming molecules, is a critical step in completing formation of a mechanical link between the cell and its substrate.

The actin filament is composed of numerous individual actin subunits bound together to form a polar double-stranded filament [29]. Both the actin subunits and the actin filament are polar, with a barbed-end (+) and a pointed-end (-). In this paper, the actin subunit at the barbed-end is referred to as subunit *n,* with the next subunit towards the pointed-end referred to as subunit *n+1*, and the subsequent subunit to *n+1* is referred to as *n+2*, and so on (Figure 1). Polymerization of the actin filament can occur at both ends of actin, but occurs with much higher efficiency at the barbed-end [30]. Each actin subunit has 4 subdomains: S1, S2, S3, and S4 [29]. The S2 subdomain contains a DNase-I-binding loop (D-loop) that can interact with a neighboring actin subunit [29]. Recently, it was shown that polymerization of F-actin at the pointed-end is slower than polymerization at the barbed-end because of an interaction between the D-loop at *n+1* with a hydrophobic patch of *n+2* (at the pointed-end) [31]. Any actin subunit that would add to the pointed-end would need to bind the *n+1* subunit, and the D-loop of *n+1* has been shown to interact critically with hydrophobic residues on what would be *n+3* [29]. In contrast, addition of an additional subunit, *n-1*, would more easily be achieved as long as the D-loop of *n-1* can access key hydrophobic residues on *n+1*. Any subsequent additional actin subunits, i.e. subunit *n-2*, polymerizing to the barbed-end would bind subunit *n* via interaction of their D-loop with the key hydrophobic patch on subunit *n.* The hydrophobic patch at the barbed-end resides between S1 and S3.

Vinculin is a globular protein much smaller than actin and with 5 helical domains: domain 1 (D1), domain 2 (D2), domain 3 (D3), domain 4 (D4), and the vinculin tail domain (Vt) [32]. D1-D4 together form the vinculin head domains. These vinculin head domains are linked to Vt in several ways: (i) covalently through a flexible linker region between D4 and Vt, (ii) electrostatically through a number of salt-bridges between Vt and multiple regions of the vinculin head domains, and (iii) entropicly through hydrophobic patches buried between Vt and the vinculin head domains [33]. With Vt fully linked to each of the vinculin head domains, vinculin is considered to be in a closed conformation. Vt contains the likely binding sites for an actin filament [34], while D1 contains the likely binding sites for talin [35]. Other

proteins have been suggested to interact with vinculin [32], but the interaction of vinculin with talin and actin is well characterized as critical to the formation of focal adhesions [36]. In its closed conformation vinculin is unable to bind both F-actin at Vt and talin at D1 [37], and the closed conformation is often referred to as the auto-inhibited conformation [38]. D1 of the vinculin head inhibits the linkage of Vt with F-actin. Several hypotheses have been explored concerning the mechanism of vinculin activation [39,40]. It is clear that a vinculin conformational change is necessary to allow for binding of vinculin to both F-actin and talin [41]. A recent computational study has proposed a conformational change that could activate vinculin: D1 of the vinculin head could move away from Vt and towards its talin binding partner [42]. The movement of D1 leading to vinculin activation could result from a force-induced stretching of vinculin [40,43]. It is well established that vinculin is recruited to mechanically stressed focal adhesions [43]. Vinculin could be described as a cellular reinforcing agent that reinforces mechanically stressed adhesion structures.

Activation of vinculin binding sites (VBS) within the talin rod is a force-induced process [44,45]. The VBS are hydrophobic in nature and buried within the helical structure of talin in the absence of force [46]. Initial computational investigation [47,48] and later experimental investigation [44] as demonstrated the exposure of the buried hydrophobic VBS only after force induced stretch of the talin rod. Once activated, the VBS can bind D1 of vinculin. Recent computational simulation suggests the interaction of D1 with VBS is completed, again, after force-induced activation of vinculin [49]. Both talin activation and vinculin activation are potentially force-induced events. In fact, formation of focal adhesions has also been demonstrated to be force-induced [50]. Perhaps it is the activation of talin and vinculin under stress that can regulate the formation of focal adhesion under stress. The focal complex serves to link ECM-bound integrin to actin filaments: force-induced activation of talin and activation of vinculin are effective only if the activated vinculin can bind along the actin filament and link it to the focal adhesion. Binding of vinculin to F-actin is the final step to complete this structure.

Vinculin-actin binding is necessary for focal adhesions to be mechanically resilient [51], and the interaction is crucial to the strengthening of the focal adhesion [36]. What features of the vinculin tail and F-actin allow for this crucial interaction? Using a combination of experimental electron microscopy and computational protein docking methods Janssen et al. [37] have addressed the Vt interaction with F-actin. They suggest two patches of basic residues on the surface of Vt link with two patches of acidic residues on the surface of F-actin. One of the actin acidic patches is on the *n+2* subunit and the other is on the *n* subunit. Their study also suggests that full-length vinculin in its closed conformation would be unable to bind along the actin filament as D1 would stericly clash with regions of the actin filament. It is unclear dynamically how D1 would inhibit the link to F-actin, which of the acidic patches on F-actin are more critical to linking Vt, and whether the suggested conformation of activated vinculin [42] would allow for Vt to link these acidic

patches. Section 1 of this study on the binding of vinculin along the actin filament will address these issues.

It has also been suggested that interaction of Vt with F-actin can inhibit actin polymerization [52]. During cell movement actin filaments in the lamellipodia will polymerize at their barbed-ends [30]. The polymerization is involved in membrane protrusion at the leading edge of a migration cell [53]. As the filaments in the lamellipodia expand the cell membrane at the lamellipodia will also expand causing protrusion of the cell membrane. Actin polymerization also can play a significant role in the plasticity of the cell membrane in the neuronal dendritic spine [54], in the transduction of acoustic signals into electrical nerve signals [55], and in the metastasis of cancer cells [56]. One line of evidence supporting the notion that Vt can inhibit actin polymerization comes from studies of the bacterial effector IpaA [52,57]. IpaA can stop polymerization of actin filaments of its target cell and can even cause depolymerization of the actin filaments. The direct effect of IpaA is to activate vinculin for capping of F-actin at the barbed-end. Although the mechanisms of vinculin activation for F-actin capping by IpaA are not clear, it is clear from these studies that vinculin can cap the actin filament and prevent its polymerization. Further lines of evidence for vinculin capping of actin filaments come from studies showing that Vt (isolated form other vinculin residues) can catalyze G-actin nucleation through interaction with the barbed-end of G-actin [58]. Most recently, Le Clainche et. al. [59] have explored capping of F-actin by vinculin *in vitro*. They used pyrenyl-labeled actin fluorescence [60,61] to assay the polymerization of G-actin into F-actin before and after introduction of Vt *in vitro*. Introduction of Vt prevents polymerization of F-actin. Their results suggest that residues 1044-1066 of Vt are critical to capping of F-actin by vinculin. Several questions arise concerning this capping of actin filaments by vinculin that section 2 of this study will address: what is the structure of F-actin capped by Vt? What residues and surface regions of the barbed-end are critical to interaction with Vt? How favorable or stable are these interactions between the barbed-end of F-actin and Vt?

The interaction between vinculin and actin is clearly of importance not only to efforts aimed at understanding focal adhesion formation via talin and vinculin, but also to efforts aimed at understanding the role of vinculin in regulating actin dynamics. Perhaps even, vinculin at the focal adhesion is regulating actin polymerization through capping of the barbed-end. This study investigates both the interaction of vinculin along the actin filament and the capping interaction of vinculin with the barbed-end of F-actin. In section 1 molecular dynamics simulations are used to probe the interaction of vinculin along the actin filament using: (a) a structure of only Vt interacting with actin subunits *n* and *n+1*, (b) a structure of vinculin is its closed conformation, and (c) a structure of vinculin in its suggested activated conformation [42]. In section 2 a similar molecular dynamics approach is used to determine the likely structure, dynamics, and energetics of the interaction between Vt and the capping end of F-actin. In the final section of the study, section 3, computational techniques are used to evaluate an additional conformational change in full-length vinculin (beyond the suggested activation of

vinculin at D1) and explore the possibility of an interaction between the barbed-end of the actin filaments and vinculin in this second open structure.

Results/Discussion

Section 1: Vinculin binding along the actin filament

Linkage to actin filaments is important for formation of stable focal adhesion structures [36]. At the focal adhesion, the reinforcing agent vinculin binds talin through D1 and is suggested to bind actin through Vt. Molecular dynamics was used to simulate the interaction between Vt and the actin filament. A structure of the actin filament was used with 3 subunits, each in their F-actin conformation (as opposed to the G-actin conformation)[62]. Vt was initially oriented to approach F-actin for binding along the filament (Figure 2). Actin subunits *n* and *n+2* together form the filament surface that Vt would approach. Vt is initially placed more than 15Å away from F-actin. A small nudging force was used briefly (less than 1ns) to accelerate Vt towards the actin filament. Nudging Vt towards actin reduces the entropic barrier to an interaction between Vt and actin, and had been used previously for simulation of binding events [49,63]. Following the brief nudge, the two-molecule system – with Vt and F-actin – was simulated with no external forces or constraints for 15ns. A final complex was formed with Vt linked along the actin filament (Figure 3).

Two interfaces were formed between Vt and F-actin: an interface between Vt and actin subunit *n+*2, and an interface between Vt and actin subunit *n*. Vt interacted with the S3 subdomain of *n+2*. There are four interactions between polar and charged residues stabilizing this interaction (Figure 3): T1004 with K328, T1000 with R147, K996 with S145, and R963 with S350. K996 and R963 are basic residues on Vt and have previously been suggested to link with F-actin [37]. Vt also interacted with S1 of *n*. At this interface three salt-bridges are formed: E986 with R28, K996 with D51, and R978 with E93. There were an additional two interactions at the S1-Vt interface between polar and charged groups: K996 with G48, and T973 with R95(Figure S1). Both the interactions with *n+2* and with *n* contribute to stabilizing the Vt-actin linkage. The existence of salt-bridges between *n* and Vt suggest this interface to be more dominant.

To compare the influence of the two interfaces on the stability of the Vt-F-actin complex, the potential energy of the interacting residues at both interfaces were calculated throughout both simulations. Molecular complexes will likely adopt conformations and arrangements that reside in local potential energy minima [64]. Of the two interfaces, whichever is contributing more towards reducing the potential energy of the system is likely more dominant in effecting the formation of the molecular complex. The calculations showed that the interactions between Vt and F-actin at the interface with S1 of *n* store 150 Kcal/mol of potential energy, considerably more than the interaction of Vt with *n+2* (Figure 4). This would be expected given the absence of salt-bridges at the Vt-*n+2* interface.

The two interfaces, one between Vt and *n* and the other between Vt and *n+2*, are comparable to the two acidic patches on the F-actin surface previously predicted to be involved in linking Vt to F-actin [37]. What was previously described as the upper Vt binding site on F-actin is the interface between Vt and *n+2* seen in our molecular dynamics simulations. And the previously described lower Vt binding site on F-actin is the interface between Vt and *n*. The molecular dynamics simulation of Vt interacting with F-actin confirms the predictions of Janssen et al [37]. Evaluation of the potential energy changes resulting from each set of interactions predicts that of the two sites, the lower binding site, or the interaction between Vt and S1 of *n* is more favorable and more important to linking F-actin to focal adhesions.

Numerous studies have described the vinculin head domains as being auto-inhibitory and preventing the linkage between Vt and F-actin [33,38-41,65]. The study by Janssen et al [37] also predicted that D1 of the vinculin head would stericly clash with F-actin and prevent linkage between Vt and F-actin. To evaluate the impact of D1 and other vinculin head domain residues on the interaction with F-actin, molecular dynamics simulations were run with full-length vinculin oriented towards the two Vt binding sites along the filament. Full-length vinculin was simulated with both its closed conformation and with the suggested open conformation [42]. The vinculin structures were initially placed 15Å away from F-actin and accelerated towards the F-actin binding sites using a small force for less than 1ns [49]. In simulation with both structures, after the initial nudge the system is simulated for 15ns in the absence of any external forces or constraints. The simulation of vinculin in a closed conformation did not result in formation of a complex between vinculin and F-actin (Figure 5) and the simulation of vinculin with the predicted open conformation resulted in formation of a complex between vinculin and F-actin (Figure 6).

Two residues on the surface of F-actin along the filament made contact with the closed conformation of vinculin during the 15 ns simulation (Figure 5): P333 and R147. These residues contact residues Q93, Q96, S97, A42, A45, and A44 of vinculin in the closed conformation. The contact was not favorable and vinculin moved away from F-actin following the contact (Figure S2). The failure of vinculin in the closed conformation to bind F-actin was expected [37]. The molecular dynamics simulations confirmed that a conformational change is necessary for binding along the F-actin filament and have demonstrated a trajectory of the steric repulsion between D1 and F-actin.

In the simulation of open vinculin with the actin filament three interfaces were formed between vinculin and F-actin (Figure 6). K956 linked with R51 and G48, and K952 linked with G48 at one interface – between vinculin domain Vt and S2 of *n*. E967 linked with R95, R978 linked with E93, K970 linked with E93, Q971 linked with E100 and R978 linked with D2 at the second interface – between vinculin domain Vt and S1 of *n*. And interestingly, H27, E29, and E28 of vinculin domain D1 linked with S323, K326, and K328 of *n+2* (subdomain S3). This third interface is unique to the simulation with an open vinculin conformation. The first and second

interface are similar in location to the lower binding site previously described for interaction of Vt (isolated from the vinculin head domains) with F-actin. No interface was formed between Vt and the upper binding site on F-actin. The absence of an interface with the upper binding site is consistent with our prediction that the lower binding site, at S1 of *n*, is more critical to an interaction between F-actin and vinculin. All interactions persisted throughout most of the 15ns simulation (Figure S3)

It remains possible that stochastically, if further simulations between open vinculin and F-actin were performed an interaction between vinculin and the upper binding site would present itself. This simulation points out the consistency of an S1-Vt interface. The third interface that linked vinculin to F-actin was formed between D1 and Vt. Previous studies had not considered a possible interaction between Vt and F-actin. In the closed conformation, the charged residues of D1 that interact with F-actin – E29 and E28 – are linking D1 to Vt. Any study of vinculin in its closed conformation binding to F-actin would fail to recognize and interaction between these acidic residues and their basic counterparts on *n+2* because the acidic residues would be linked to R1008 of Vt. In the open conformation however, D1 has separated from Vt, and E28 and E29 are available for linking to basic residues on the F-actin surface. Our simulations demonstrated that the well-characterized interaction between Vt and F-actin would bring these residues in close proximity to *n+2* allowing them to further link vinculin to F-actin. The suggested open conformation of vinculin facilitates the binding of vinculin along the actin filament not only by removing the steric hindrance to a Vt-F-actin interaction, as previously suggested [37], but also through contributing an additional binding interface between D1 and F-actin.

Comparing the potential energy stored in the interaction between D1 and Vt with the potential energy stored in the Vt-F-actin interface (Figure 7), it is clear that as with binding of Vt along the actin filament, the interaction with S1 is more favorable. The D1 interaction does contribute to reducing the potential energy of the system but not to the same level as Vt. Considering the mainly ionic nature of the interactions between Vt and S1 of *n*, it is not surprising that the Vt-S1 interaction is favorable.

Comparing the three simulations of vinculin binding along the F-actin filament (Figure 8) it is evident that Vt does interact favorably with F-actin when isolated from D1 of the vinculin head domain. The suggested conformational change leading to open vinculin [42] is evaluated in these simulations. Only after the movement of D1 away from Vt did vinculin interact favorably with F-actin, and no further conformational changes proved necessary to allow the F-actin interaction. Elsewhere it has been suggested that complete separation of Vt from all vinculin-head domains is necessary to allow for binding of vinculin along the actin filament [32]. Our results contend that D1 movement away from Vt is necessary and sufficient for vinculin activation.

The suggested open vinculin conformation resulted from previous simulations that considered the transient interaction of vinculin with nearby actin filaments while linked to talin [42]. Considering that the S1 binding site on subunit *n* of actin was shown to be the site of primary linkage between Vt and S1, it remains possible that a transient interaction between these two regions coupled with stress transduced to vinculin through its linkage to talin could catalyze the movement of D1 away from Vt. Alternatively, the clash between D1 and F-actin, if coupled with stress transduced to vinculin through its linkage to talin could also catalyze the movement of D1 from Vt. Exploring those possibilities, and exploring the trajectory of vinculin activation through a simultaneous interaction with actin and talin – suggested both by our previous simulations [42] and previous experimental results [40] – would make a valuable future study. The results presented here confirm the D1 movement facilitates F-actin binding, but beg the question of how that D1 movement could be achieved *in vivo*.

Understanding the binding of vinculin along the actin filament is important because of the role of actin filaments at focal adhesions [36]. The actin filament network provides the mechanical stability needed by the cell [9,20,66-71]. At focal adhesions, this network is coupled to the ECM and the external environment. Any forces originated from within the cell or from without the cell can only be mechanically reinforced by the actin network if this coupling is complete. In the motile cell, the actin network forms short parallel actin fibers near to the cell edge [51]. It is to these shorter parallel actin fibers that the newly forming nascent adhesions aim to connect with. Our simulations predict that the vinculin from the maturing nascent adhesion would facilitate the F-actin linkage at the stage of maturation in which mechanical stresses are present. If at the earliest stages of nascent adhesion formation, mechanical stress in the amount necessary to separate D1 from Vt is absent, then the linkage to Vt is likely through other molecules, such as talin itself. As the nascent adhesion matures, and the stress around the maturing nascent adhesion intensifies vinculin becomes activated and linkage to the actin filaments intensify. In this way vinculin can be described as a reinforcing agent.

One possible source of stress that could activate vinculin at the nascent adhesion would be the retrograde flow of the actin fibers within the lamellipodium [72]. The moving actin filaments would brush against focal adhesion proteins. Vinculin in its closed conformation, linked to talin at D1, could collide with the flowing actin filaments, and the collision could bias the population of vinculin to bring about a population-shift from closed vinculin to open vinculin [73]. Further evidence supporting the notion that actin flow at the lamella and the lamellipodium can stress the focal adhesion molecules come from a recent study describing the formation of an actin arc structure [74]. At the leading edge of the migrating cell the actin filaments show polymerization followed by retraction. The polymerizing actin filament will cause protrusion of the cell membrane. The retraction and rearward movement of the actin filaments correlates with retraction of the cell membrane. Interestingly, the actin filaments form arc like structures around adhesions complexes during the retraction stage of the cycle. The arc form as a result of the

actin flow, and can stress the nascent adhesions enough to facilitate vinculin activation followed by linking of the open vinculin to the actin filaments.

During retrograde flow of the actin filaments, at times the focal adhesion or nascent adhesion linked to the actin filament will undergo slippage [75]. One possibility is that although the integrin and other focal adhesion molecules would disconnect from the moving actin filament, vinculin would remain connected. After the movement, the vinculin would reconnect to another adhesion structure preventing further flow of the actin filament. In such a way the focal adhesion proteins would act a molecular clutch providing a variable contact between F-actin and integrin [75]. It is possible the stress on vinculin during the slippage event would surpass the energy barrier needed to activate vinculin and cause further vinculin conformational changes. What role would any second vinculin conformational change play either at the focal adhesion or in regulating the dynamics of actin filaments? One possibility is the second conformational change could regulate the capping of actin filaments by vinculin.

Section 2: Vt Capping of the F-actin Barbed-end

Using pyrenyl-labeled actin to assay F-actin polymerization Le Clainche et al [59] demonstrated *in vitro* that Vt can effectively cap the barbed-end of actin. Capping of the actin filaments by vinculin has been demonstrated in cells affected by IpaA [76]. In such cells the capping of F-actin serves to depolymerize the actin filaments and make the cells compliant for Shigella invasion [52]. It is unclear if capping of actin filaments could play a role at sites of focal adhesions. It is also unclear if vinculin at focal adhesions is able to cap the actin filaments. A step towards clarifying both possibilities is to understand the nature of F-actin capping by vinculin.

The vinculin tail residues implicated in F-actin capping reside in the C-terminus region and have also been implicated in interaction with the lipid membrane [77]. The last 21 residues of vinculin consist of a number of charged and basic residues that are predicted to readily interact with acidic residues at the actin barbed-end or on acidic phospholipids (Figure 9). In its closed conformation vinculin head domains occlude access to most of these residues. With Vt isolated from the vinculin head domains the last 21 residues could interact with the barbed-end of F-actin either through the surface of Vt that would be occluded by vinculin head domains, the occluded surface, or through the surface of Vt already exposed to solvent, the exposed surface of Vt. From the structure of Vt it is predicted that the occluded face of Vt would better link the barbed-end given the higher density of charged residues at this surface (Figure 9).

Newly added actin subunits would interact with the barbed-end of F-actin. Examination of the F-actin structure predicts that the D-loop of subunit *n* interacts favorably with the interface between S1 and S3 of subunit *n+2* (Figure 1). Specifically, residues 283-294, 139, 140, 143, 346, 351, and 374 of the barbed-end are implicating in stabilizing additional actin subunits by interacting with their D-

loop structures [29]. Recent high resolution imaging of the actin filament pointed-end confirms the likely interaction between the D-loop of a newly polymerized actin monomer and the interface between S1 and S3 at the barbed-end of the actin filament [31].

Capping of F-actin by CapZ and other capping proteins prevents actin polymerization by occluding access to S1 or S3 [31]. Capping of F-actin by Vt would then likely result from interaction of Vt with S1 of the barbed-end, S3 of the barbed-end, or both subunits S1 and S3 of the barbed-end (Figure 10). The interaction of Vt with F-actin is evaluated using molecular dynamics. Vt is simulated initially oriented towards the barbed-end towards either (A) S1 only, (B) S3 only, or (C) towards S1 and S3. Each orientation is simulated both with the exposed face of Vt initially oriented towards the barbed-end and with the occluded face of Vt initially oriented towards F-actin (Table S1).

Simulation of Vt interacting with S1 of the barbed-end (Figure 11 and 12) showed formation of a significant link both between the exposed surface of Vt and S1, and between the occluded surface of Vt and S1. The link between the exposed surface and S1 involves the hydrophobic insertion of P863, P864, and L865 into the small hydrophobic patch between S1 and S3 (Figure 11). Additionally, R925 links with E99 and E100, K889 links with D363, E883 links with K359, E880 and E884 link with D882 and Q360, and K881 links with S358. Six salt-bridges and a few polar interactions dominate this interaction and stabilize the linkage between the exposed surface of Vt and S1 (Figure S4). The link between the occluded surface and S1 involves the following stable interactions (Figure 12 and S5): R903 with D2 and D3, K911 with D4, R1060 with E99 and E100, K881 with S350, E879 with Q354, R874 with E361, and E869 with R372. These ionic and polar links are comparable to the links between the exposed face of vinculin and S1. Comparison of the potential energy changes resulting from both interactions (Figure 13) confirms that both are favorable, storing as much as 350 Kcal/mol of potential energy, and are equally likely to occur.

The hydrophobic insertion into the groove between S1 and S3 by Vt is consistent with previous studies examining the structure of CapZ bound to the barbed-end of F-actin [31]. CapZ hydrophobic residues insert in the same hydrophobic patch between S1 and S3. Basic residues on CapZ also interact with acidic residues at the barbed-end. A study of β-thymosin/WH2 capping actin filaments [78] also confirms the role of a hydrophobic insertion between S1 and S3 in capping actin filaments. Our simulations suggest the hydrophobic insertion also plays a role in stabilizing F-actin capping by Vt. Although P863, P864, and L865 were able to bind the barbed-end in simulation with the exposed surface of Vt, these residues lie within the flexible loop region. Whether in a full-length vinculin structure these loop region residues would be available for F-actin capping is unclear.

Simulation of Vt interacting with S3 of the barbed-end (Figure 14 and 15) showed little linkage being formed between Vt and S3. The exposed surface of Vt formed

three salt-bridges between Vt and F-actin (Figure 14 and S6): R1049 with D288, D1051 with R290, and E839 with R290. The occluded surface of Vt formed two salt-bridges between Vt and F-actin (Figure 15 and S7): R1060 and K911 with D288, and D907 with K291. Although more links were formed at the exposed surface of Vt, calculation of the potential energy stored in the interactions shows interaction with the occluded surface of Vt is more favorable (Figure 16). Both sets of salt-bridges have at least 150 Kcal/mol of potential energy stored. Because basic residues of the occluded surface of Vt were able to get closer to the acidic residues of S3, these ionic links were calculated to store a maximum of over 250 Kcal/mol. In comparison to interactions with S1, the interactions with S3 are less profound and likely play less of a role in the capping of F-actin by Vt.

The third set of capping simulations oriented Vt towards both S1 and S3 of the barbed end. In simulation with the exposed surface of Vt only 1 stable salt-bridge was formed with F-actin after 15ns of simulation (Figure 17 and S8): K915 with E364. Two weaker polar interactions were also formed: D848 with H173, and E960 with Q360. The polar interactions likely contribute less to stabilizing the complex. In contrast to capping with the exposed surface, F-actin capping with the occluded surface of Vt was shown to be very stable and likely favorable (Figure S9). A large interface was formed between the occluded surface of Vt and the barbed end of F-actin (Figure 18). Numerous close links were formed: E884 with K328 and R147, D848 with R372, R910 with G146, E879 with T166, T1065 with E167, K1061 with T143 and T148, R1039 with D25, R1060 with Q354, R832 with Q353 and T351, K1047 with D4, R976 with D3, and K1047 with S350. Calculation of the potential energy stored in this large interface confirmed that it is indeed favorable (Figure 19). A total of more than 550 Kcal/mol of potential energy was stored in the large interface between the occluded surface of Vt and F-actin. The interaction between the exposed surface and F-actin only stored 100 Kcal/mol. These results suggest that the occluded surface of Vt is more likely the surface involved in capping of F-actin.

A total of six simulations were run to explore the possible interaction between Vt and the barbed-end of F-actin (Figure 20). Of these simulations, one resulted in the likely structure of Vt capping an actin filament (Figure 18): the occluded surface of Vt bound to S1 and S3. This interaction contained the largest number of ionic and polar links between Vt and the barbed-end, and the highest level of potential energy stored within the linkage. Overall, interactions with S1 were shown to be more favorable than interactions with S3, and interaction with the occluded surface of Vt was shown to be more favorable than interaction with the exposed surface of Vt. Interaction with S3 and interaction with the exposed surface did show favorable linkages, but less favorable than interaction with S1 or interaction at the occluded surface.

S1 of subunit *n* was shown to be significant both to the binding of vinculin along the actin filament and to the capping of the actin filament. The feature of S1 that lends it such a significant role is the prevalence of acidic residues on its surface. The

existence of the acidic residues have previously been recognized elsewhere both for binding along the actin filament [37] and for capping of the actin filament [29,79]. These acidic residues play a role not only in vinculin binding but also in binding to other proteins [80].

The results from simulations of F-actin capping are consistent with the understanding of F-actin capping in general [79]. Two interactions stabilize the subunits that make up an actin filament: (1) hydrophobic interaction between the D-loop of an *n* subunit and the hydrophobic patch between S1 and S3 of an *n+2* subunit, and (2) interactions between acidic residues on S1 and S3 on *n+*2 and basic residues on *n* [29]. In one of the simulations, three hydrophobic residues, P863, P864, and L865, inserted into the hydrophobic patch between S1 and S3. Although these residues are from the loop region and might not be involved with F-actin capping, the interaction demonstrates dynamically the importance of the hydrophobic interaction. The strongest link with the barbed-end of F-actin was formed when interacting with both S1 and S3, consistent with previous notions [81]. In order for an interaction to prevent polymerization the two key mechanisms for stabilizing the new actin subunit should be disrupted. Binding of Vt to the barbed end can disrupt both mechanisms. Vt can be an effective F-actin capping protein.

The capping of F-actin by vinculin has been demonstrated in cells affected by Shigella and its effector IpaA [76]. Can vinculin cap F-actin at focal adhesion, and can this capping play a role in regulating actin dynamics at focal adhesions? The answer is unclear. A hypothesis would be that indeed it could. Considering the role actin network movement and dynamics can play in regulating focal adhesion growth [20], its possible that as a negative feedback loop vinculin could regulate the dynamics of those actin networks. Vinculin would then be acting not as a binary switch, shifting between a closed and an open conformation, but as a variable switch, shifting between a closed, an open I, and an open II conformation. The open I conformation would correspond to the structure of vinculin with D1 moved away from Vt allowing for linking of F-actin to the focal adhesion. The open II conformation would involve a second conformational change that would expose the residues predicted in these simulations to be critical for linking Vt to both S1 and S3 of the F-actin barbed-end.

Section 3: The vinculin open II conformation

An additional conformational change is necessary for vinculin to be able to cap actin filaments. The simulations of Vt capping of actin filaments suggest that the occluded surface of Vt forms the most likely interaction with the interface between S1 and S3. The occluded surface is normally in contact with D4 residues. Movement of D1 away from Vt, which was shown to be sufficient for allowing vinculin to bind along actin filaments, does not result in dissociation of Vt from D4. The occluded surface of Vt, critical to F-actin capping, requires additional conformational changes in vinculin beyond D1 movement. Le-Clainche et al [59,82] also suggest a second vinculin conformational change is necessary to allow for vinculin capping of the actin-filaments.

The interface between D4 and Vt has been implicated elsewhere as critical to Vt activation in general. Chen et al [82] describe a pincer-like mechanism to vinculin activation in which both the interface of D1 with Vt and the interface of D4 with Vt is disrupted to allow Vt to leave the pocket formed by the vinculin head domains and link with F-acitn. In another study, Cohen et al [65] demonstrate that both interactions between Vt and D1 and interactions between Vt and D4 are critical to maintaining an auto-inhibited conformation. The simulations in this study suggests that disruption of the key interactions between Vt and D1 coupled with movement of D1 away from Vt is sufficient to allow binding of vinculin along the actin filament. The interaction between Vt and D4 could however play a critical role in regulating Vt capping of actin filaments.

The separation of D1 from Vt was simulated by assuming a cooperative activation mechanism and introducing stretch of vinculin to be consistent with that mechanism [42]. The source for D4 separation from Vt is less clear. If Vt separates from D4 at the focal adhesions then perhaps the movement of the actin filaments across the developing focal adhesion can supply induce separation of Vt from D4. If however Vt separation from D4 is particular to cells affected by Shigella [76], then D4 separation would result from the interaction with IpaA. Whatever the source allowing fro D4 separation, it is likely that D4 would separate after D1 separation.

In this section of the study, D4 is separated from Vt following separation of D1 from Vt. Vt is pulled at a constant velocity away from D4 and the simulation results in formation of a second open conformation, the open II (Figure 21). Following the separation the new structure is simulated without any external constraints or forces and allowed to relax to its new equilibrium structure (Figure 21 D). In the equilibrated open II conformation Vt has completely separated itself from the vinculin head domains. D1 is under less strain than in the open 1 conformation (Figure 21B). Even with D1 moving towards Vt, Vt remains likely to bind along the actin filament in the open II conformation.

Formation of the open II conformation involves disruption of the interface between Vt and D4 (Figure 22). Five salt-bridges cooperate to maintain the Vt-D4 interface: R1057 with D841, R1060 with D856, R978 with K1047, K975 with E775, and R976 with E 770. Once all of these interactions are broken, then Vt readily moves away from the vinculin head domains and the linker residues begin to stretch. The dissociation of the salt-bridges is shown by calculation of the loss in potential energy stored in the D4-Vt interface (Figure S10). Although other interfaces between Vt and the vinculin head domains exist, these residues along with the residues at the D1-Vt interface are the crucial interactions after which Vt can completely separate from the vinculin head domains. The importance of the Vt-D4 interactions is consistent with previous studies [65,82].

To compare the likelihood of a open II conformation being formed following formation of the open I conformation, the potential of mean force [83] and free

energy difference between the closed vinculin conformation, the open I conformation, and the open II conformation are calculated (Figure 23). About 90 KT of free energy must be supplied to vinculin for D1 to separate from Vt, and an additional 10 KT of free energy must be supplied to separate D4 from Vt. If 90 KT of free energy has been supplied by one of the possible sources – either cooperative binding between Vt and F-actin, or mechanical forces from movement of actin filaments near the focal adhesions – then it is possible that an additional 10 KT of energy would completely remove Vt from the vinculin head.

That vinculin can undergo two conformational changes, and that which change takes place can be regulated by how much energy is supplied to vinculin is consistent with a role for vinculin as a molecular clutch [75]. At the focal adhesion, first a nascent adhesion would begin to form. As the mechanical stress on the nascent adhesion intensifies the talin molecules would begin to become activated for interaction with vinculin [25], and once vinculin links with talin, further mechanical stress of movement of actin filaments could cooperate to cause vinculin to change from its closed to the open I conformation. With the open I conformation vinculin could completely bind F-actin and talin. If at this stage, where the nascent adhesion has matured to a focal complex and is becoming a mature focal adhesion [84], the mechanical stress is even larger or the movement of F-actin is even stronger, then the additional stress could cause vinculin to transform from its open I conformation to an open II conformation and maintain a dynamic link between the moving actin filaments and F-actin. By such a mechanism the open II conformation would not only be significant for potentially allowing for vinculin capping, but also for allowing a dynamic link between F-actin and the focal adhesion. Complete separation of Vt from the vinculin head domains allows for Vt to link moving F-actin more easily.

It is known that the open II conformation, induced by IpaA, can cap actin filaments [57]. However, if open II is achieved at focal adhesion in cells not affected by Shigella, then an interesting question arises: are actin filaments capped at focal adhesions? If it is shown that an open II conformation will readily link the capping end of an actin filament (as predicted) then capping of actin filaments at highly stressed focal adhesions becomes likely.

To evaluate if the open II conformation will bind the barbed-end of F-actin two simulations were produced, one with full-length vinculin in a closed conformation, and one with vinculin in the open II conformation (Figure 24 and 25). Simulation with the closed conformation showed minimal interaction with F-actin (Figure 24). Initially Vt is attracted towards the barbed-end but residues in the vinculin head interacted with the barbed-end and vinculin moved away from F-actin (Figure S11). The brief interaction between the vinculin head and the barbed-end involved: E565 with K328, and Q568with D292 and K291. In contrast, simulation of vinculin in the open II conformation with F-actin resulted in the formation of an interface with many ionic and polar interactions stabilizing the open II vinculin at the barbed-end of actin filaments (Figure 25): E932 with K291, R935 and K889 with D288, N943 with D286, E883 with R147, R925 with E167, K956 with T351, K952 with Q354, and

R945 with Q349. Comparing the potential energy stored in the interface between vinculin and F-actin with the two structures confirms the favorability of the open II conformation for F-actin capping (Figure 26). Interaction of vinculin with the open II conformation with F-actin resulted in reduction of the potential energy of the complex by nearly 300 Kcal/mol. It is likely then that an open II conformation would result in F-actin capping, even at focal adhesion not affected by Shigella.

What role could F-actin capping play at focal adhesions? The open II conformation would form at the focal adhesion when stress levels are high. Perhaps, binding of vinculin even to the barbed-end of F-actin at these highly stressed focal adhesion would allow an additional layer of reinforcement. Alternatively, actin polymerization should occur at the leading edge of the moving cell. If the barbed-end is near to a stressed and maturing focal adhesion, polymerization of the actin filament near the focal adhesion would be unnecessary and the capping of F-actin at the focal adhesions would serve to limit actin polymerization only to the barbed end. The results from these simulation show that vinculin in an open II conformation can cap F-actin. Future experimental investigation is required to validate that this capping could occur at the maturing focal adhesion.

Conclusion

The interaction between vinculin and actin was explored using molecular dynamics simulations in three sections: first, the interaction of vinculin along the actin filament was investigated, then, the interaction of Vt with the barbed-end of the actin filament, and finally, the possible interaction between an open II vinculin conformation and the actin filament. Simulation of the interaction along the actin filament confirmed that although Vt can bind along the actin filament, full-length vinculin in its closed conformation is inhibited from binding along the filament. The open I conformation, previously suggested as a conformation of activated vinculin, was able to bind along the actin filament as Vt had, confirming that it is likely the structure of activated vinculin. Simulation of Vt interacting with the barbed-end of F-actin confirmed that Vt could indeed prevent polymerization of the actin filament. Vt binds to the barbed-end of F-actin similar to other capping proteins [79] and can prevent the association of a new actin subunit with S1 and S3. Simulation of vinculin conformational changes beyond D1 separation and formation of the open I conformation revealed the possibility of an open II conformation. With the open II conformation vinculin could cap actin filaments, even at the focal adhesion.

Putting together the results from all of these simulations, we can predict three potential regions of an actin filament that would bind vinculin (Figure 27). Consistently, the acidic residues in S1 – vinculin binding site A – were shown to be critical for an interaction between Vt and F-actin. These residues stabilized both the binding of vinculin along the actin filament in section 1, and in they were involved in stabilizing Vt capping of the actin filament in section 2. The surface between S1 and S3 of the barbed end – vinculin binding site B – was also consistently shown to stabilize Vt in section 2. Hydrophobic residues in this region would form

hydrophobic cores with nonpolar residues from Vt. Both basic and acidic residues in this region would form salt-bridges with their counterparts on Vt. The interactions between Vt and S1 that were highlighted by our simulations had previously been suggested to be involved in binding of vinculin along the actin filament, and the interactions between S1 and S3 were previously shown to be significant for capping of the actin filament. However, the third region on the surface of the actin filament that is suggested here to be involved in vinculin binding is novel: the residues in S3 of subunit *n+2* – vinculin-binding site C. These residues can interact with charged residues from D1 of vinculin and in doing so contribute to further stabilizing the vinculin actin linkage. With the presence of three binding regions we can predict that vinculin will differentially bind to each of the binding sites depending on the intensity of mechanical stress on the focal adhesion. It is possible that binding site A would interact with vinculin during vinculin activation, and would completely bind vinculin active activation. This interaction would require the least level of mechanical stress. Binding site C would bind vinculin after D1 is separated from Vt and can link it. This would potentially require some level of mechanical stress. And binding of binding site B to vinculin would occur after transition of vinculin to the open II conformation. This would require the most level of mechanical stress. The exact binding interface between vinculin and F-actin, therefore, would be a function of the level of mechanical stress at the focal adhesion. Vinculin would be a variable switch at the focal adhesion, increasing its level of activation and F-actin binding depending on the level of mechanical stress at the focal adhesion.

Previously, it was shown that formation of the vinculin open I conformation allows for the complete insertion of talin VBS in to D1 of vinculin [49]. We can now expand on those results and further state that after complete linking of vinculin to talin via D1, and linking along the actin filament via Vt in the open I conformation, any additional forces from further movement or stress of the actin filament could induce an open II conformation (Figure 28). The formation of an open II conformation would then allow vinculin to remain linked to F-actin even as it moves. In this way vinculin could act both as a molecular clutch and as a variable switch at the focal adhesion.

The question that remains unanswered after our simulations and analysis is whether the actin filaments can be capped at the focal adhesion. The simulations of vinculin in an open II conformation with the barbed-end suggested that F-actin can be capped, but what role would this play at the focal adhesion? The understanding that vinculin is a variable switch is a testable and valuable prediction from the molecular dynamics simulation, but the capping of actin filaments at focal adhesions is really an unanswered question that is posed by our molecular dynamics simulations. Further investigations – both computational and experimental – are sought to address this question.

Methods

Initial Structure and Configuration

PDB ID 1ST6 was used to build a structure of full-length vinculin [33]. The missing proline rich linker region (residues 843-877) was created via homology modeling using the SWISSMODEL toolkit [85], as previously described [42]. Vt was built as residues 895-1066 from the full-length vinculin model. The structure of open full-length vinculin was taken from previously published simulation [42]. PDB ID 3LUE [33] was used to build a structure of F-actin. The 3LUE structure has α-actinin CH domains bound to F-actin. The CH-domains are removed and only 3 of the F-actin subunits are used to build the F-actin structure.

Complex of Vt bound to F-actin was build using Janssen et al [37] to orient Vt towards the two binding pockets along F-actin. Structure of full-length was build using the same Vt orientation but including the vinculin head domain residues. Vinculin was translated to be at least 15 Å away from F-actin. For simulation of Vt interaction with the barbed end, Vt was oriented either with the exposed or the occluded surface oriented towards Vt. Three arrangements of Vt with the barbed-end were simulated: Vt oriented towards S1 of the barbed-end of F-actin, Vt oriented towards S3 of the barbed-end of F-actin, Vt oriented towards both S1 and S3 of the barbed end. Vt was placed within 10 Å of the barbed-end in these structures. For simulation with vinculin in the closed or the open II conformation, additional vinculin head residues are included with maintaining the Vt orientation. Each system was solvated with 12Å of padding at each end of the simulation box.

Molecular Dynamic Simulation

Simulations were carried out using the NAMD Scalable Molecular Dynamics program [86]. Periodic boundary conditions were used along with a Langevin piston Nose-Hoover [87] mechanism for pressure control at 1 Atm. Constant temperature of 310K was maintained using a Langevin damping coefficient of 5/ps. Rigid bonds were enforced between hydrogen atoms and their bound larger atoms [88]. The CHARMm 27 force fields were used [89,90]. Simulation timesteps of 2fs were used for all molecular dynamics.

Each configuration was first minimized for 1000 steps using the conjugate gradient and line search algorithm implemented in NAMD [86]. Following minimization each configuration is simulated for at least 15ns or until equilibration. All simulation results were visualized and analyzed using VMD [91]. For simulations of binding along F-actin the Vt, closed vinculin, and open I vinculin were initially nudged towards F-actin for less than 1ns prior to simulation for 15ns. Use of the nudge reduces the entropic barrier to binding. For simulation of Vt capping actin filaments no initial nudge is used and instead Vt is placed 5 Å closer to the barbed-end. Vt is smaller than full-length vinculin and can have faster translation, thus binding occurred even without an initial nudging force.

Umbrella Sampling

Umbrella sampling of D4 separation from Vt was carried out using GROMACS [92]. The reaction coordinate was defined as the distance between the center of mass of D4 and the center of mass of Vt. Residues in D1 16, 51, 81, and 115 were constrained

with 1000 Kj/mol*nm^2 to maintain an open I conformation throughout the simulation. Residues 926, 958, 988, and 1031 of Vt were defined as the pull group and constrained along the reaction coordinate away from residues 730, 760, 794, and 824 of D4. An umbrella potential of 1000 Kj/mol*nm^2 was used with a reference step of 0.2 Å in order to maximize umbrella overlap. The final potential of mean force was calculated using Grossfield's WHAM code [93].

References

1. Schwartz MA (2009) Cell biology. The force is with us. Science 323: 588-589.
2. Fraley SI, Feng Y, Krishnamurthy R, Kim D-H, Celedon A, et al. (2010) A distinctive role for focal adhesion proteins in three-dimensional cell motility. Nat Cell Biol 12: 598-604.
3. Zaidel-Bar R, Ballestrem C, Kam Z, Geiger B (2003) Early molecular events in the assembly of matrix adhesions at the leading edge of migrating cells. J Cell Sci 116: 4605-4613.
4. Berrier AL, Yamada KM (2007) Cell-matrix adhesion. J Cell Physiol 213: 565-573.
5. Kumar S, Weaver VM (2009) Mechanics, malignancy, and metastasis: the force journey of a tumor cell. Cancer Metastasis Rev 28: 113-127.
6. Guo W, Giancotti FG (2004) Integrin signalling during tumour progression. Nat Rev Mol Cell Biol 5: 816-826.
7. Wang YL, McNamara LM, Schaffler MB, Weinbaum S (2007) A model for the role of integrins in flow induced mechanotransduction in osteocytes. Proc Natl Acad Sci U S A 104: 15941-15946.
8. Liu Z, Tan JL, Cohen DM, Yang MT, Sniadecki NJ, et al. (2010) Mechanical tugging force regulates the size of cell-cell junctions. Proc Natl Acad Sci USA 107: 9944-9949.
9. Kolahi KS, Mofrad MR (2010) Mechanotransduction: a major regulator of homeostasis and development. Wiley interdisciplinary reviews Systems biology and medicine 2: 625-639.
10. Rossier OM, Gauthier N, Biais N, Vonnegut W, Fardin M-A, et al. (2010) Force generated by actomyosin contraction builds bridges between adhesive contacts. EMBO J 29: 1055-1068.
11. Ngu H, Feng Y, Lu L, Oswald SJ, Longmore GD, et al. (2010) Effect of focal adhesion proteins on endothelial cell adhesion, motility and orientation response to cyclic strain. Annals of biomedical engineering 38: 208-222.
12. Parsons JT, Horwitz AR, Schwartz MA (2010) Cell adhesion: integrating cytoskeletal dynamics and cellular tension. Nat Rev Mol Cell Biol 11: 633-643.
13. Shattil SJ, Kim C, Ginsberg MH (2010) The final steps of integrin activation: the end game. Nat Rev Mol Cell Biol 11: 288-300.
14. Dubash AD, Menold MM, Samson T, Boulter E, Garc a-Mata R, et al. (2009) Focal adhesions: new angles on an old structure. International review of cell and molecular biology 277: 1-65.

15. Patla I, Volberg T, Elad N, Hirschfeld-Warneken V, Grashoff C, et al. (2010) Dissecting the molecular architecture of integrin adhesion sites by cryo-electron tomography. Nat Cell Biol 12: 909-915.
16. Anthis NJ, Wegener KL, Ye F, Kim C, Goult BT, et al. (2009) The structure of an integrin/talin complex reveals the basis of inside-out signal transduction. EMBO J 28: 3623-3632.
17. Arnaout MA, Goodman SL, Xiong JP (2007) Structure and mechanics of integrin-based cell adhesion. Curr Opin Cell Biol 19: 495-507.
18. Nieves B, Jones CW, Ward R, Ohta Y, Reverte CG, et al. (2010) The NPIY motif in the integrin beta1 tail dictates the requirement for talin-1 in outside-in signaling. Journal of cell science 123: 1216-1226.
19. Zaidel-Bar R, Geiger B (2010) The switchable integrin adhesome. Journal of cell science 123: 1385-1388.
20. Ziegler WH, Gingras AR, Critchley DR, Emsley J (2008) Integrin connections to the cytoskeleton through talin and vinculin. Biochem Soc Trans 36: 235-239.
21. Choi CK, Vicente-Manzanares M, Zareno J, Whitmore LA, Mogilner A, et al. (2008) Actin and alpha-actinin orchestrate the assembly and maturation of nascent adhesions in a myosin II motor-independent manner. Nat Cell Biol 10: 1039-1050.
22. Yoshigi M, Hoffman LM, Jensen CC, Yost HJ, Beckerle MC (2005) Mechanical force mobilizes zyxin from focal adhesions to actin filaments and regulates cytoskeletal reinforcement. The Journal of cell biology 171: 209-215.
23. Hirata H, Tatsumi H, Sokabe M (2008) Mechanical forces facilitate actin polymerization at focal adhesions in a zyxin-dependent manner. Journal of Cell Science 121: 2795-2804.
24. Jiang G, Giannone G, Critchley DR, Fukumoto E, Sheetz MP (2003) Two-piconewton slip bond between fibronectin and the cytoskeleton depends on talin. Nature 424: 334-337.
25. Izard T, Vonrhein C (2004) Structural basis for amplifying vinculin activation by talin. J Biol Chem 279: 27667-27678.
26. Gingras AR, Ziegler WH, Frank R, Barsukov IL, Roberts GC, et al. (2005) Mapping and consensus sequence identification for multiple vinculin binding sites within the talin rod. J Biol Chem 280: 37217-37224.
27. Mierke CT (2009) The role of vinculin in the regulation of the mechanical properties of cells. Cell biochemistry and biophysics 53: 115-126.
28. Cohen DM, Kutscher B, Chen H, Murphy DB, Craig SW (2006) A conformational switch in vinculin drives formation and dynamics of a talin-vinculin complex at focal adhesions. J Biol Chem 281: 16006-16015.
29. Oda T, Iwasa M, Aihara T, Maeda Y, Narita A (2009) The nature of the globular- to fibrous-actin transition. Nature 457: 441-445.
30. Bugyi B, Carlier MF (2010) Control of actin filament treadmilling in cell motility. Annual review of biophysics 39: 449-470.
31. Narita A, Oda T, Maeda Y (2011) Structural basis for the slow dynamics of the actin filament pointed end. The EMBO journal 30: 1230-1237.
32. Ziegler WH, Liddington RC, Critchley DR (2006) The structure and regulation of vinculin. Trends in Cell Biology 16: 453-460.

33. Bakolitsa C, Cohen DM, Bankston LA, Bobkov AA, Cadwell GW, et al. (2004) Structural basis for vinculin activation at sites of cell adhesion. Nature 430: 583-586.
34. Carisey A, Ballestrem C (2010) Vinculin, an adapter protein in control of cell adhesion signalling. European Journal of Cell Biology.
35. Nhieu GTV, Izard T (2007) Vinculin binding in its closed conformation by a helix addition mechanism. EMBO J 26: 4588-4596.
36. Humphries JD, Wang P, Streuli C, Geiger B, Humphries MJ, et al. (2007) Vinculin controls focal adhesion formation by direct interactions with talin and actin. J Cell Biol 179: 1043-1057.
37. Janssen ME, Kim E, Liu H, Fujimoto LM, Bobkov A, et al. (2006) Three-dimensional structure of vinculin bound to actin filaments. Mol Cell 21: 271-281.
38. Borgon RA, Vonrhein C, Bricogne G, Bois PRJ, Izard T (2004) Crystal structure of human vinculin. Structure 12: 1189-1197.
39. Bois PR, O'Hara BP, Nietlispach D, Kirkpatrick J, Izard T (2006) The vinculin binding sites of talin and alpha-actinin are sufficient to activate vinculin. J Biol Chem 281: 7228-7236.
40. Chen H, Choudhury DM, Craig SW (2006) Coincidence of actin filaments and talin is required to activate vinculin. J Biol Chem 281: 40389-40398.
41. Izard T, Evans G, Borgon RA, Rush CL, Bricogne G, et al. (2004) Vinculin activation by talin through helical bundle conversion. Nature 427: 171-175.
42. Golji J, Mofrad MR (2010) A molecular dynamics investigation of vinculin activation. Biophys J 99: 1073-1081.
43. Mierke CT, Kollmannsberger P, Zitterbart DP, Smith J, Fabry B, et al. (2008) Mechano-coupling and regulation of contractility by the vinculin tail domain. Biophys J 94: 661-670.
44. del Rio A, Perez-Jimenez R, Liu R, Roca-Cusachs P, Fernandez JM, et al. (2009) Stretching Single Talin Rod Molecules Activates Vinculin Binding. Science 323: 638.
45. Patel B, Gingras AR, Bobkov AA, Fujimoto LM, Zhang M, et al. (2006) The activity of the vinculin binding sites in talin is influenced by the stability of the helical bundles that make up the talin rod. J Biol Chem 281: 7458-7467.
46. Bass MD, Smith BJ, Prigent SA, Critchley DR (1999) Talin contains three similar vinculin-binding sites predicted to form an amphipathic helix. Biochem J 341 (Pt 2): 257-263.
47. Lee SE, Kamm RD, Mofrad MR (2007) Force-induced activation of talin and its possible role in focal adhesion mechanotransduction. Journal of biomechanics 40: 2096-2106.
48. Hytönen VP, Vogel V (2008) How force might activate talin's vinculin binding sites: SMD reveals a structural mechanism. PLoS Comput Biol 4: e24.
49. Golji J, Lam J, Mofrad MR (2011) Vinculin activation is necessary for complete talin binding. Biophys J 100: 332-340.
50. Galbraith CG, Yamada KM, Sheetz MP (2002) The relationship between force and focal complex development. J Cell Biol 159: 695-705.

51. Gardel ML, Schneider IC, Aratyn-Schaus Y, Waterman CM (2010) Mechanical integration of actin and adhesion dynamics in cell migration. Annu Rev Cell Dev Biol 26: 315-333.
52. Bourdet-Sicard R, Rudiger M, Jockusch BM, Gounon P, Sansonetti PJ, et al. (1999) Binding of the Shigella protein IpaA to vinculin induces F-actin depolymerization. The EMBO journal 18: 5853-5862.
53. Lai FP, Szczodrak M, Block J, Faix J, Breitsprecher D, et al. (2008) Arp2/3 complex interactions and actin network turnover in lamellipodia. The EMBO journal 27: 982-992.
54. Hotulainen P, Hoogenraad CC (2010) Actin in dendritic spines: connecting dynamics to function. The Journal of cell biology 189: 619-629.
55. Manor U, Kachar B (2008) Dynamic length regulation of sensory stereocilia. Seminars in cell & developmental biology 19: 502-510.
56. Condeelis JS, Wyckoff JB, Bailly M, Pestell R, Lawrence D, et al. (2001) Lamellipodia in invasion. Seminars in cancer biology 11: 119-128.
57. Ramarao N, Le Clainche C, Izard T, Bourdet-Sicard R, Ageron E, et al. (2007) Capping of actin filaments by vinculin activated by the Shigella IpaA carboxyl-terminal domain. FEBS letters 581: 853-857.
58. Wen K-K, Rubenstein PA, DeMali KA (2009) Vinculin nucleates actin polymerization and modifies actin filament structure. J Biol Chem 284: 30463-30473.
59. Le Clainche C, Dwivedi SP, Didry D, Carlier M-F (2010) Vinculin is a dually regulated actin filament barbed end-capping and side-binding protein. J Biol Chem 285: 23420-23432.
60. Kouyama T, Mihashi K (1981) Fluorimetry study of N-(1-pyrenyl)iodoacetamide-labelled F-actin. Local structural change of actin protomer both on polymerization and on binding of heavy meromyosin. European journal of biochemistry / FEBS 114: 33-38.
61. Cooper JA, Pollard TD (1982) Methods to measure actin polymerization. Methods in enzymology 85 Pt B: 182-210.
62. Wang H, Robinson RC, Burtnick LD (2010) The structure of native G-actin. Cytoskeleton (Hoboken) 67: 456-465.
63. Lee SE, Chunsrivirot S, Kamm RD, Mofrad MR (2008) Molecular dynamics study of talin-vinculin binding. Biophys J 95: 2027-2036.
64. Frauenfelder H, Sligar SG, Wolynes PG (1991) The energy landscapes and motions of proteins. Science 254: 1598-1603.
65. Cohen DM, Chen H, Johnson RP, Choudhury B, Craig SW (2005) Two distinct head-tail interfaces cooperate to suppress activation of vinculin by talin. J Biol Chem 280: 17109-17117.
66. Mofrad MRK (2009) Rheology of the Cytoskeleton. Annual Review of Fluid Mechanics 41: 433-453.
67. Mofrad MR, Kamm RD (2009) Cellular Mechanotransduction: Diverse Perspectives From Molecules to Tissues. New York: Cambridge University Press.
68. Chandran PL, Mofrad MR (2010) Averaged implicit hydrodynamic model of semiflexible filaments. Phys Rev E Stat Nonlin Soft Matter Phys 81: 031920.

69. Golji J, Collins R, Mofrad MR (2009) Molecular mechanics of the alpha-actinin rod domain: bending, torsional, and extensional behavior. PLoS Comput Biol 5: e1000389.
70. Chandran PL, Mofrad MR (2009) Rods-on-string idealization captures semiflexible filament dynamics. Phys Rev E Stat Nonlin Soft Matter Phys 79: 011906.
71. Mofrad MR, Kamm RD (2006) Cytoskeletal Mechanics: Models and Measurements. New York: Cambridge University Press. 244 p.
72. Alexandrova AY, Arnold K, Schaub S, Vasiliev JM, Meister JJ, et al. (2008) Comparative dynamics of retrograde actin flow and focal adhesions: formation of nascent adhesions triggers transition from fast to slow flow. PLoS ONE 3: e3234.
73. Okazaki K, Takada S (2008) Dynamic energy landscape view of coupled binding and protein conformational change: induced-fit versus population-shift mechanisms. Proceedings of the National Academy of Sciences of the United States of America 105: 11182-11187.
74. Burnette DT, Manley S, Sengupta P, Sougrat R, Davidson MW, et al. (2011) A role for actin arcs in the leading-edge advance of migrating cells. Nature cell biology 13: 371-381.
75. Hu K, Ji L, Applegate KT, Danuser G, Waterman-Storer CM (2007) Differential transmission of actin motion within focal adhesions. Science 315: 111-115.
76. Ramarao N, Le Clainche C, Izard T, Bourdet-Sicard R, Ageron E, et al. (2007) Capping of actin filaments by vinculin activated by the Shigella IpaA carboxyl-terminal domain. FEBS Lett 581: 853-857.
77. Palmer SM, Playford MP, Craig SW, Schaller MD, Campbell SL (2009) Lipid binding to the tail domain of vinculin: specificity and the role of the N and C termini. J Biol Chem 284: 7223-7231.
78. Hertzog M, van Heijenoort C, Didry D, Gaudier M, Coutant J, et al. (2004) The beta-thymosin/WH2 domain; structural basis for the switch from inhibition to promotion of actin assembly. Cell 117: 611-623.
79. Kim T, Cooper JA, Sept D (2010) The interaction of capping protein with the barbed end of the actin filament. Journal of Molecular Biology 404: 794-802.
80. Wirth VF, List F, Diez G, Goldmann WH (2010) Vinculin's C-terminal region facilitates phospholipid membrane insertion. Biochem Biophys Res Commun 398: 433-437.
81. Narita A, Takeda S, Yamashita A, Maeda Y (2006) Structural basis of actin filament capping at the barbed-end: a cryo-electron microscopy study. The EMBO journal 25: 5626-5633.
82. Chen Y, Dokholyan NV (2006) Insights into allosteric control of vinculin function from its large scale conformational dynamics. J Biol Chem 281: 29148-29154.
83. Torrie G, Valleau J (1977) Nonphysical sampling distributions in Monte Carlo free-energy estimation: Umbrella sampling. Journal of Computational Physics 23: 187-199.
84. Mierke CT (2009) The role of vinculin in the regulation of the mechanical properties of cells. Cell Biochem Biophys 53: 115-126.

85. Arnold K, Bordoli L, Kopp J, Schwede T (2006) The SWISS-MODEL workspace: a web-based environment for protein structure homology modelling. Bioinformatics 22: 195-201.
86. Phillips JC, Braun R, Wang W, Gumbart J, Tajkhorshid E, et al. (2005) Scalable molecular dynamics with NAMD. J Comput Chem 26: 1781-1802.
87. Hoover WG (1985) Canonical dynamics: Equilibrium phase-space distributions. Phys Rev A 31: 1695-1697.
88. Kraeutler V, Gunsteren WF, Huenenberger PH (2001) A fast SHAKE algorithm to solve distance constraint equations for small molecules in molecular dynamics simulations¶. J Comput Chem 22: 501-508.
89. MacKerell ADJ, Bashford D, Bellot M, R. L. Dunbrack J, Evanseck JD, et al. (1998) All-Atom Empirical Potential for Molecular Modeling and Dynamics Studies of Proteins. J Phys Chem B 102: 3586-3616.
90. Mackerell AD (2004) Empirical force fields for biological macromolecules: overview and issues. Journal of Computational Chemistry 25: 1584-1604.
91. Humphrey W, Dalke A, Schulten K (1996) VMD: visual molecular dynamics. J Mol Graph 14: 33-38, 27-38.
92. Van Der Spoel D, Lindahl E, Hess B, Groenhof G, Mark AE, et al. (2005) GROMACS: Fast, flexible, and free. Journal of Computational Chemistry 26: 1701-1718.
93. Kumar S, Rosenberg JM, Bouzida D, Swendsen RH, Kollman PA (1992) THE weighted histogram analysis method for free-energy calculations on biomolecules. I. The method. Journal of Computational Chemistry 13: 1011-1021.

Figure Legends

Figure 1. Structure of an actin filament.
The actin filament is a polar double stranded polymer with individual polar actin subunits. Each subunit has a pointed (-) end and a barbed (+) end [29]. Actin filaments are formed mainly by addition of new actin subunits to the barbed (+) end. (A) The actin filament used in simulation for interacting with vinculin is three subunits in length: subunit *n* (blue), subunit *n+1* (white), and subunit *n+2* (red). The pointed-ends of all the subunits are aligned. An additional subunit *n-1* would add to the barbed-end of the filament. (B) Each actin subunit has four subdomains: S1 (green), S2 (cyan), S3 (pink), and S4 (tan). The S2 subdomain consists mainly of the recognizable DNase-I-binding loop (D-loop) (cyan), and can be used to identify the pointed-end of the actin filament. The subdomains of *n* and *n+2* are shown and are involved in interaction with vinculin. The subdomains of *n+1* are not differentially colored. These *n+1* subdomains are inversely oriented. S2 of *n+1* lies near S3 of *n+2*, S4 of *n+1* lies near S1 of *n+2*, S3 of *n+1* lies near S2 of *n*, and S4 of *n+1* lies near S3 of *n*. (C) View of the actin filament shown in (A) rotated 90 degrees. Actin subunit *n+1* lies behind *n* and *n+2* as viewed from (A). (D) View of the actin filament shown in (B) rotated 90 degrees. Each subunit of the actin filament is rotated relative to its neighboring subunits. This view shows the *n* subunit is rotated relative to the *n+2* subunit.

Figure 2. Vinculin can bind actin filaments both along the filament and at the barbed-end.
Experimental evidence suggests vinculin can interact with actin at two locations: (1) along the actin filament, thus interacting with subunit *n* (blue) and subunit *n+2* (red)[37], or (2) at the barbed-end of the actin filament [59]. Arrows point to do possible locations of vinculin interaction. Binding of actin along the filament allows for recruitment of F-actin to focal adhesion via vinculin and talin [20]. Binding of actin at its barbed-end would result in capping of the actin filament to prevent further proliferation of the filament [79]. Molecular dynamics simulations are produced investigating interaction of vinculin with the actin filament at both possible locations. Subunit *n+1* is shown in white.

Figure 3. Interaction of Vt with actin along the filament.
The interaction between Vt (orange) and the F-actin is simulated using molecular dynamics. A structure of vinculin with only the Vt residues represented is used. Vt is placed in an orientation according to Janssen et al [37]. The final equilibrium bound structure is shown here. Vt forms two sets of interactions with F-actin along the filament: (1) an interaction with S3 of *n+2* (top inset), (2) and interaction with S1 of *n* (bottom inset). Four interactions are formed between Vt and *n+2*: T1004 with K328, T1000 with R147, K996 with S145, and R963 with S350. Each of these interactions are between a polar and a charged residue. Five interactions are formed between Vt and *n*: K996 with G48, E986 with R28, K996 with D51, T973 with R95, and R978 with E93. Of these, three are salt-bridges between charged residues and 2 are interactions between a polar and a charged residue. The interaction between Vt and *n* is likely stronger than the interaction between Vt and *n+2*. Actin subunit *n* is shown in blue, and subunit *n+2* is shown in red.

Figure 4. Potential energy changes resulting from interaction of Vt with F-actin.
Simulation of Vt interacting with F-actin showed the final bound complex consists of two binding regions: (1) the interaction of Vt with actin subunit *n+2*, and (2) the interaction of Vt with actin subunit *n*. The potential energy between the binding residues on Vt and on F-actin are calculated throughout the 15ns simulation. The potential energy between Vt and *n+2* is shown in green and the potential energy between Vt and *n* is shown in red. The interaction of Vt with *n* results in a 150 Kcal/mol reduction in the potential energy of the interacting complex, whereas the interaction of Vt with *n+2* produces negligible change in the potential energy. A loss in potential energy results from interaction between the basic residues on Vt and the acidic residues on F-actin and could represent formation of a stable interaction.

Figure 5. Interaction between vinculin in its closed conformation with F-actin along the filament.
The interaction between full-length vinculin in its closed conformation and F-actin is simulated with molecular dynamics. Initially vinculin is with the same orientation relative to F-actin that was used for simulation of Vt interacting with F-actin. After 15ns of simulation no stabilizing interactions are formed between vinculin in the

closed conformation and F-actin. The closed vinculin makes contact with P333 and R147 of F-actin, as shown in the inset. Q93, Q96, and S97 of vinculin contact P333, and A42, A45, and A44 of vinculin contact R147. The contacts result in steric clashes and are followed by movement of vinculin in its closed conformation away from F-actin. D1 of vinculin (green) prevents interaction of Vt (orange) with actin. Other vinculin residues are shown in black, the *n* subunit of actin is shown in blue, and the *n+2* subunit of actin is shown in red.

Figure 6. Interaction between vinculin in its open conformation with F-actin along the filament.

A structure of vinculin in its open conformation has previously been suggested [42]. Using this structure, the interaction between vinculin in its open conformation and F-actin is simulated using molecular dynamics. The vinculin molecule is initially oriented towards actin with the same orientation that was used for simulation of Vt binding along the actin filament. After 15ns of simulation the open conformation of vinculin has formed three sets of binding interactions along the actin filament: (1) an interaction if Vt (orange) with S2 of subunit *n* (top left inset), (2) and interaction of Vt with S1 of subunit *n* (top right inset), and (3) and interaction of D1 (green) mainly with S3 of subunit *n+2* (bottom right inset). Three interactions are formed between Vt and S2 of *n*: K956 with R51, K952 with G48, and K956 with G48. Five interactions are formed between Vt and S1 of *n*: E967 with R95, R978 with E93, K970 with E93, Q971 with E100, and R978 with D2. Four interactions are formed between D1 and S3 of *n+2*: H27 with S323, E29 with K326, E28 with K326, and E29 with K328. Two interactions are formed between D1 and S4 of *n* (also shown in bottom right inset): H22 with E241, and Q19 with E241. The strongest of these interactions is likely the interaction between Vt and S1 of *n* as there are 4 salt-bridges between the two. There are also 3 salt-bridges between D1 and *n+2*. The open conformation allows for Vt to bind along the actin filament, and further stabilizes the link via an additional interaction between D1 and actin.

Figure 7. Potential energy changes resulting from interaction of full-length vinculin with F-actin.

The potential energy between binding residues on vinculin and on F-actin is calculated for both simulation of binding along the filament using the closed conformation of vinculin and using the suggested open conformation of vinculin. The interaction between vinculin in the closed conformation and F-actin resulted in steric clashes and no binding. The potential energy between clashing residues is plotted in red. Since no binding occurred and the closed vinculin moved away from F-actin no potential energy is reported between the two. Vinculin in a open conformation forms interactions between Vt and the *n* subunit and between D1 and the *n+2* subunit. The potential energy between interacting residues in both sets of interactions is plotted: the energy between D1 and *n+2* is plotted in blue; the energy between Vt and *n* is plotted in orange. Interaction of Vt with *n* resulted in a reduction of potential energy of up to 200 Kcal/mol. In contrast the interaction between D1 and *n+2* resulted in no more than a 50 Kcal/mol reduction in potential

energy. The link between Vt and *n* is the most energetically favorable of the interactions.

Figure 8. Interaction along the actin filament by three vinculin structures.
Three simulations were produced of vinculin interacting with actin along its filament: (A) using the structure of Vt only, (B) using the structure of vinculin in its closed conformation, and (C) using the structure of vinculin in a suggested open conformation. The final arrangement of the molecules is shown from each of the three simulations after 15ns of simulation with the same viewpoint. Only interaction of Vt (A) and interaction vinculin in its open conformation (C) resulted in a stable linkage along the actin filament. Interaction of vinculin in its closed conformation (B) resulted in steric repulsion.

Figure 9. Basic C-terminus residues on the vinculin tail.
Recent experimental evidence suggests Vt can bind the barbed-end of an actin filament [59]. Residues 1044 to 1066 (red) of the C-terminus region of Vt are likely involved in capping of the actin filament. There are several charged residues within the C-terminus region: K1047, R1049, D1051, R1057, R1060, and K1061. These residues would interact with the barbed end of actin either through the surface of Vt that is exposed to solvent and F-actin, or through the surface of Vt that is occluded by the vinculin head domains. The vinculin tail is shown in orange with each of the charged residues colored by atom type. The top view of Vt is rotated by 90 degrees to produce the bottom view of Vt. Interaction through the exposed face of Vt could involve D1051 and R1049, whereas interaction through the occluded face of Vt could involve K1047, R1057, R1069, and K1061 (see bottom view). The interaction of Vt with the barbed-end of actin is simulated with either the exposed surface of Vt oriented towards actin, or the occluded surface of Vt oriented towards actin.

Figure 10. Capping at the barbed-end of actin.
Vinculin could approach the barbed-end of actin for capping from three directions: (A) approaching S1 of the *n* subunit, (B) approaching S3 of the *n* subunit, or (C) approaching S1 and S3 of the *n* subunit. Binding to actin from any of these directions would result in capping of the barbed-end of actin and prevent further polymerization of actin at the barbed-end. S1 is shown in green, S2 in cyan, S3 in pink, and S4 in tan.

Figure 11. Capping of the actin filament at S1 with the exposed surface of Vt.
Vt (orange) is simulated interacting with the barbed-end of actin. The Exposed surface of Vt is initially oriented towards actin, and Vt is arranged to approach S1 of the barbed-end. After 15ns of simulation two binding surfaces are produced: (A) electrostatic linkage between charged Vt residues and S1 (top inset), and (B) hydrophobic insertion of 3 Vt residues into a hydrophobic patch between S1 and S3. The interaction between Vt and S1 consists of: R925 interacting with E99 and E100, K889 with D363, E883 with K359, E880, E884, and D882 with Q360, and K881 with S358. An interaction is also formed between R1008 and D3 late in the simulation. Also, E867 interacts with R147 of S3 from the *n* subunit (seen in bottom inset). The

hydrophobic residues P863, P864, and L865 insert into the hydrophobic patch between S1 and S3. Together there are two salt-bridges and an small hydrophobic insertion that stabilize this interaction. Subunit *n* is shown in blue, and subunit *n+2* is shown in red.

Figure 12. Capping of the actin filament at S1 with the occluded surface of Vt.
Vt (orange) is simulated interacting with the barbed-end of actin with its occluded surface initially oriented towards actin. Vt is arranged such that it is near to S1 of the barbed-end. After 15ns of simulation a binding surface is produced between Vt and S1 of the barbed-end (inset). Several interactions are formed at this interface: R903 interacts with D2 and D3 of S1, K911 with D4, R1060 with E99 and E100, K881 with S350, E879 with Q354, R874 with E361, and E869 with R372. Five of these interactions are salt-bridges contributing to stabilizing this interaction. Subunit *n* is shown in blue, and subunit *n+2* is shown in red.

Figure 13. Comparison of potential energy changes from capping S1 by exposed and occluded Vt.
The potential energy between binding residues on S1 and on Vt is calculated for both simulations with the exposed surface of Vt oriented towards S1 and with the occluded surface of Vt oriented towards S1. In both simulations the potential energy is reduced by as much as 350 Kcal/mol as the simulation progresses and the two molecules are linked together. Changes in the potential energy throughout the 15ns simulation with the exposed surface of vinculin is plotted in blue, and the potential energy throughout the simulation with the occluded surface of vinculin is plotted in red. Binding at both surfaces to S1 are energetically highly favorable.

Figure 14. Capping of the actin filament at S3 with the exposed surface of Vt.
Vt (orange) is simulated with its exposed surface initially oriented towards the S3 subdomain of the barbed-end of F-actin. After 15ns a small interacting interface is formed (inset). There are three interactions at this interface: R1049 with D288, D1051 with R290, and E839 with R290. All three are salt-bridges and can contribute to stabilizing the complex. Subunit *n* is shown in blue, and subunit *n+2* is shown in red.

Figure 15. Capping of the actin filament at S3 with the occluded surface of Vt.
Vt (orange) is simulated with its occluded surface initially oriented towards S3 of the *n* subunit. After 15ns of simulation two interactions are formed between the occluded surface of Vt and S3 of the barbed-end (inset): R1060 and K911 interact with D288, and D907 interacts with K291. These residues form salt-bridges to stabilize the complex. Subunit *n* is shown in blue, and subunit *n+2* is shown in red.

Figure 16. Comparison of potential energy changes from S1 capping by exposed and occluded Vt.
The potential energy between binding residues in Vt and S1 of the capping-end of F-actin is calculated throughout the 15ns simulations of both interaction with the exposed surface of Vt and interaction with the occluded surface of Vt. The potential

energy of the exposed surface's interaction is plotted in green and the potential energy of the occluded surface's interaction is plotted in blue. Interaction with the exposed surface never reduces the potential energy between the binding residues more than 150 Kcal/mol whereas interaction with the occluded surface of Vt reduced the potential energy between the binding residues by as much as 250 Kcal/mol. Both interactions are favorable, but the interaction with the occluded surface is more stabilizing as it reduces the potential energy further.

Figure 17. Capping of the actin filament at S1 and S3 with the exposed surface of Vt.
Vt (orange) with its exposed surface initially oriented towards both S1 and S3 is simulated interacting with the barbed-end of F-actin. After 15ns of simulation a binding interface is formed between the exposed surface of Vt and the barbed-end (inset). D848 of Vt interacts with H173 of S3, while two interactions are formed between Vt and S1: K915 with E364, and E960 with Q360. Interaction of the occluded face of vinculin with S1 and S3 resulted in only one salt-bridge being formed to stabilize the complex. Subunit *n* is shown in blue, and subunit *n+2* is shown in red.

Figure 18. Capping of the actin filament at S1 and S3 with the occluded surface of Vt.
Vt (orange) is simulated with its occluded surface initially oriented towards both S1 and S3. After 15ns of simulation the occluded surface of Vt forms a large interface at the barbed-end of Vt, interacting with both S1 and S3. Both insets together show the interactions at this large interface. The following interactions stabilize the Vt capping of F-actin: E884 with K328 and R147, D848 with R372, R910 with G146, E879 with T166, T1065 with E167, K1061 with T143 and T148, R1039 with D25, R1060 with Q354, R832 with Q353 and T351, K1047 with D4, R976 with D3, and K1047 with S350. There are five salt-bridges at this interface stabilizing the link between Vt and barbed-end. The interface between the occluded face of Vt and both S1 and S3 of the barbed-end is likely the most stable interface investigated. Subunit *n* is shown in blue, and subunit *n+2* is shown in red.

Figure 19. Comparison of potential energy changes from capping S1 and S3 by exposed and occluded Vt.
The potential energy between binding residues from Vt and S1 and S3 of the barbed-end of F-actin is calculated throughout the 15ns simulation for both the interaction of the exposed surface of Vt with S1 and S3 and the interaction of the occluded surface of Vt with S1 and S3. The interaction of Vt using its exposed surface with F-actin reduces the potential energy of the complex by 100 Kcal/mol. The interaction of Vt using it occluded surface with F-actin reduces the potential energy of the complex by over 550 Kcal/mol. The interaction between the occluded surface of Vt and the S1 and S3 subdomains is highly energetically favorable and likely represents the true binding interface between Vt and the barbed-end of F-actin.

Figure 20. F-actin capping by Vt was investigated with six possible arrangements.
A total of six possible arrangements of Vt and F-actin were simulated to investigate the interaction between vinculin and F-actin. Two surfaces of Vt were used, the surface exposed to solvent and F-actin (A), (B), and (C), and the surface normally occluded from F-actin by the vinculin head (D), (E), and (F). Both surfaces were initially arranged such that they were oriented towards S1 (C) and (F), towards S3 (A) and (D), or towards both S1 and S3 (B) and (E); exposed and occluded surfaces respectively. Interaction of Vt with either S1 only or with S1 and S3 was found to be more stable. Interaction with the occluded surface of Vt was found to be more likely than interaction with the exposed surface of Vt. Vt is shown in orange. Subunit *n* is shown in blue, and subunit *n+2* is shown in red.

Figure 21. Formation of a vinculin open II conformation.
In its closed conformation (A) vinculin is not likely to bind actin filament. Separation of D1 from Vt constitutes formation of the open I conformation (B) and molecular dynamics simulations suggest the open I conformation can bind along the actin filament. Another critical link between Vt and the vinculin head domains exists at the interface between D4 and Vt. Separation of Vt from D4 results in formation of an open 2 conformation (C). (D) When the open II conformation is equilibrated after being formed D1 moves towards Vt and the loop region reduces its strain. However, Vt remains detached from the vinculin head and D1 remains removed from Vt. In this open II conformation vinculin could interact with F-actin both along the filament and at its barbed-end.

Figure 22. The interactions between D4 and Vt break to allow for the open II conformation.
To produce the open II conformation, Vt is pulled away from D4. There are 5 salt-bridges between D4 and Vt: R1057 with D847, R1060 with D856, R978 with K1047, K975 with E775, and R976 with E770. The presence of these salt-bridges stabilized Vt near to the vinculin head and likely prevents interaction of Vt with the barbed-end of F-actin. After these interactions are broken and Vt separated from D4 and the rest of the vinculin head domain, then Vt is likely to be able to bind the barbed-end of the actin filaments.

Figure 23. Free energy profile of the open I and open II conformational changes.
Using the umbrella sampling method [83] the potential of mean force for two reaction coordinates were calculated: (A) the distance between D1 and Vt, and (B) the distance between D4 and Vt. Progress along reaction coordinate (A) leads to formation of the open I conformation. Progress along reaction coordinate (B) leads to formation of the open II conformation. Formation of the open I conformation has a free energy barrier of 90 KT and the open I conformation is not likely to stay open without persistant energy input. The formation of the open II conformation following formation of the open I conformation has a smaller free energy barrier of

less than 20 KT. The plateau at the end of reaction coordinate (B) suggests the open II conformation could remain open without external force.

Figure 24. Capping of F-actin by vinculin in its closed conformation.
The surface of Vt (orange) likely to cap F-actin is normally occluded by vinculin head domains (black). D1 of the vinculin head is shown in green and the flexible loop region is shown in yellow. Subunit *n* of actin is shown in blue, and subunit *n+2* of actin is shown in red. Simulation with full-length vinculin in its closed conformation oriented towards S1 and S3 and with the same orientation as used for binding of the occluded surface of Vt to S1 and S3 resulted in formation of a small interface between Vt and the barbed-end of actin (inset). Two interactions are present at this interface: E565 with K328, and Q568with D292 and K291. This single salt-bridge accompanied by an interaction between a polar and a charged residue is the only interaction that could potentially stabilize the complex.

Figure 25. Capping of F-actin by vinculin in a second open conformation.
The occlusion of Vt from F-actin can be removed after a potential conformational change. The structure of this second open conformation with D1 moved away from Vt and subsequently Vt moved away from D4 and the rest of the vinculin head is initially oriented such that Vt is in the same orientation towards S1 and S3 as the previous simulation showing interaction of the occluded surface of Vt with S1 and S3. After 15ns of simulation this full-length vinculin structure with a conformational change has formed an interface between Vt and F-actin (inset). Several interactions stabilize this interface: E932 with K291, R935 and K889 with D288, N943 with D286, E883 with R147, R925 with E167, K956 with T351, K952 with Q354, and R945 with Q349. There are four salt-bridges in this interface. Vt is shown in orange, vinculin head domains are shown in black, D1 of the vinculin head is shown in green and the flexible loop region is shown in yellow. Subunit *n* of actin is shown in blue, and subunit *n+2* of actin is shown in red.

Figure 26. Comparison of the potential energy change after capping by two vinculin conformations.
The potential energy between interacting residues on vinculin and the barbed-end of F-actin are calculated throughout 15ns of simulation for both simulation with the closed conformation and simulation with a conformational change releasing Vt from the vinculin head. The potential energy between interacting residues is never reduced more than 50 Kcal/mol in interaction with the closed conformation of vinculin (blue plot). In contrast, interaction of vinculin after a second conformational change with S1 and S3 reduces the potential energy of the interacting residues by as much as 300 Kcal/mol. This interaction is highly energetically favorable and likely represents the true interface formed by capping of F-actin by full-length vinculin.

Figure 27. The vinculin binding regions on the surface of F-actin.
The surface of F-actin is shown with all residues shown to interact vinculin colored by charge (basic residues in blue, acidic residues in red, and polar residues in

green). The *n* subunit is shown in cyan, the *n+1* subunit in white, and the *n+2* subunit in pink. Three regions on the surface of F-actin are found to be involved in interaction with vinculin: (A) residues in S1 of subunit *n* are involved in both binding of vinculin along the filament and in capping of the filament by vinculin, (B) residues at S1 and S3 of the barbed-end are involved in capping of the filament by vinculin, and (C) residues at S3 of *n+2* and S4 of *n* are involved in binding to D1 of vinculin in its open conformation while binding F-actin along the filament.

Figure 28. The open II conformation allows for dynamic linking to F-actin.
The interaction of talin VBS with D1 of vinculin is regulated by the conformation of vinculin. (I) In its closed conformation vinculin can only link to talin VBS. (II) Transition of vinculin form a closed conformation to an open I conformation would result form interaction of Vt with F-actin combined with partial linking of D1 to talin. (III) Formation of the open I conformation allows for complete talin VBS insertion in to D1. (IV) Following formation of open I vinculin, further forces from F-actin can cause formation of the open II conformation. With the open II conformation vinculin can form a dynamic link to F-actin.

Figure 1

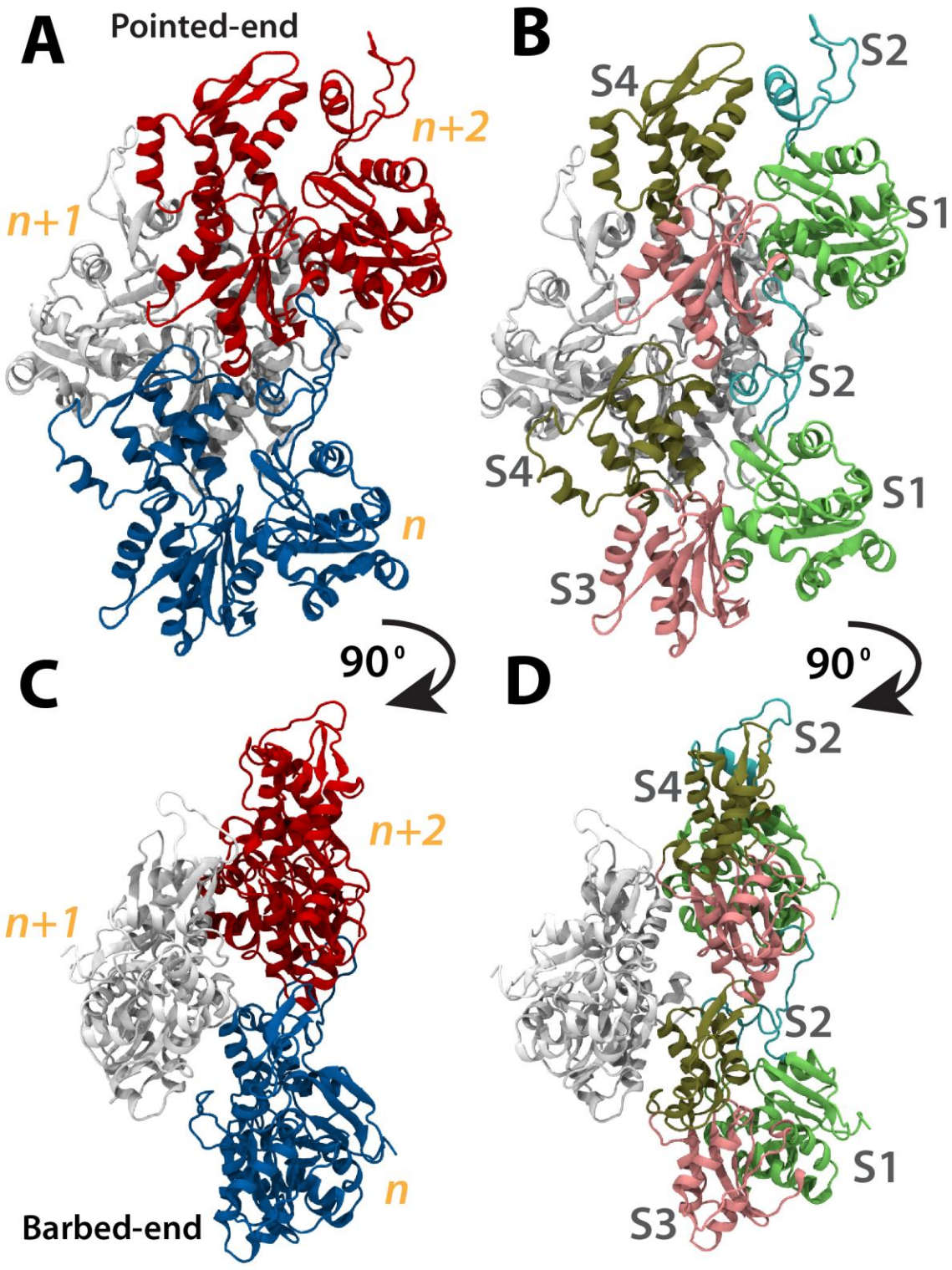
A
Pointed-end
n+2
n+1
n
B
S2
S4
S1
S2
S4
S1
S3
90°
C
n+2
n+1
n
Barbed-end
90°
D
S2
S4
S2
S1
S3

Figure 2

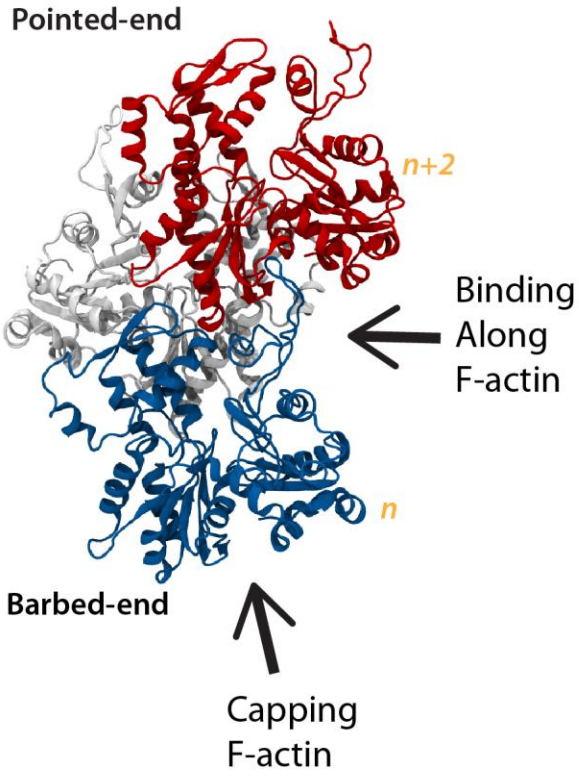
Pointed-end
n+2
Binding
Along
F-actin
n
Barbed-end
Capping
F-actin

Figure 3

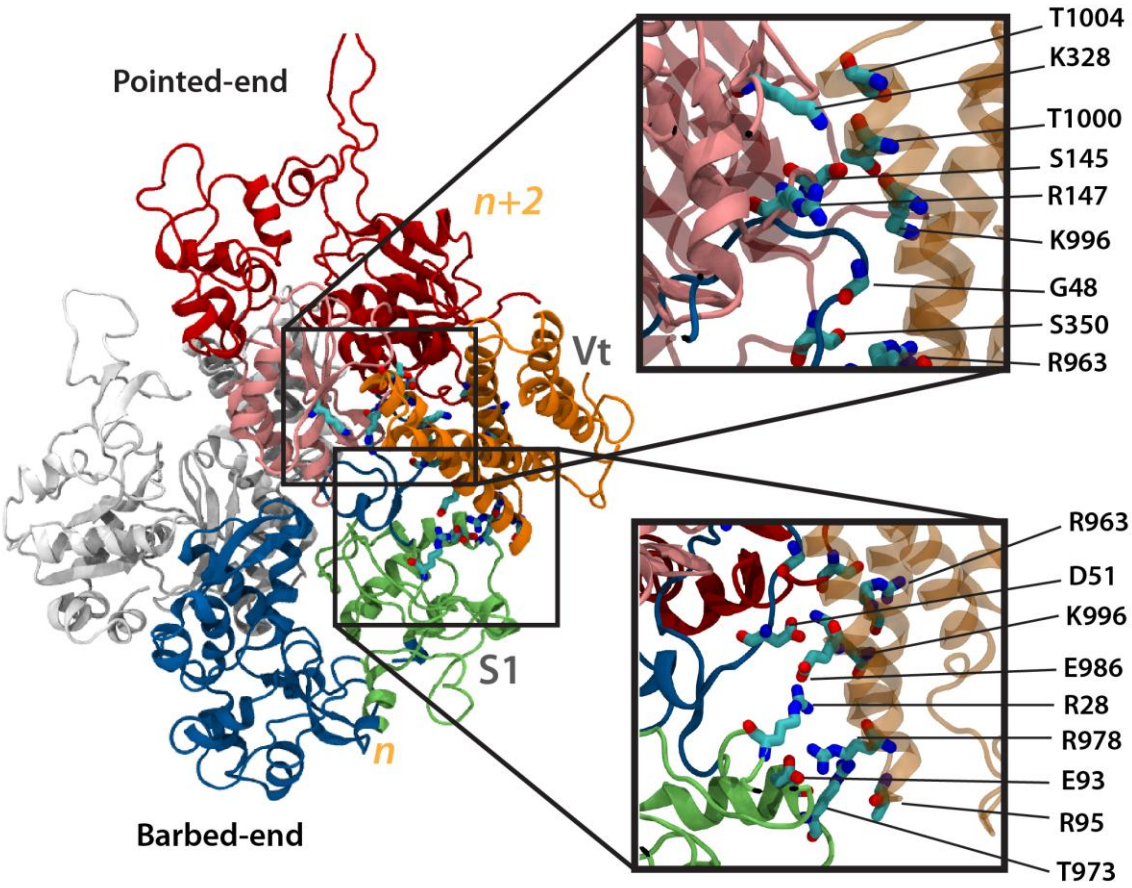
Pointed-end
n+2
Vt
S1
n
Barbed-end
T1004
K328
T1000
S145
R147
K996
G48
S350
R963
R963
D51
K996
E986
R28
R978
E93
R95
T973

Figure 4

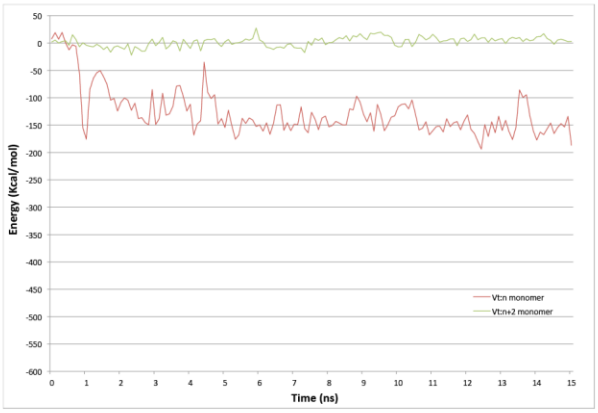

Figure 5

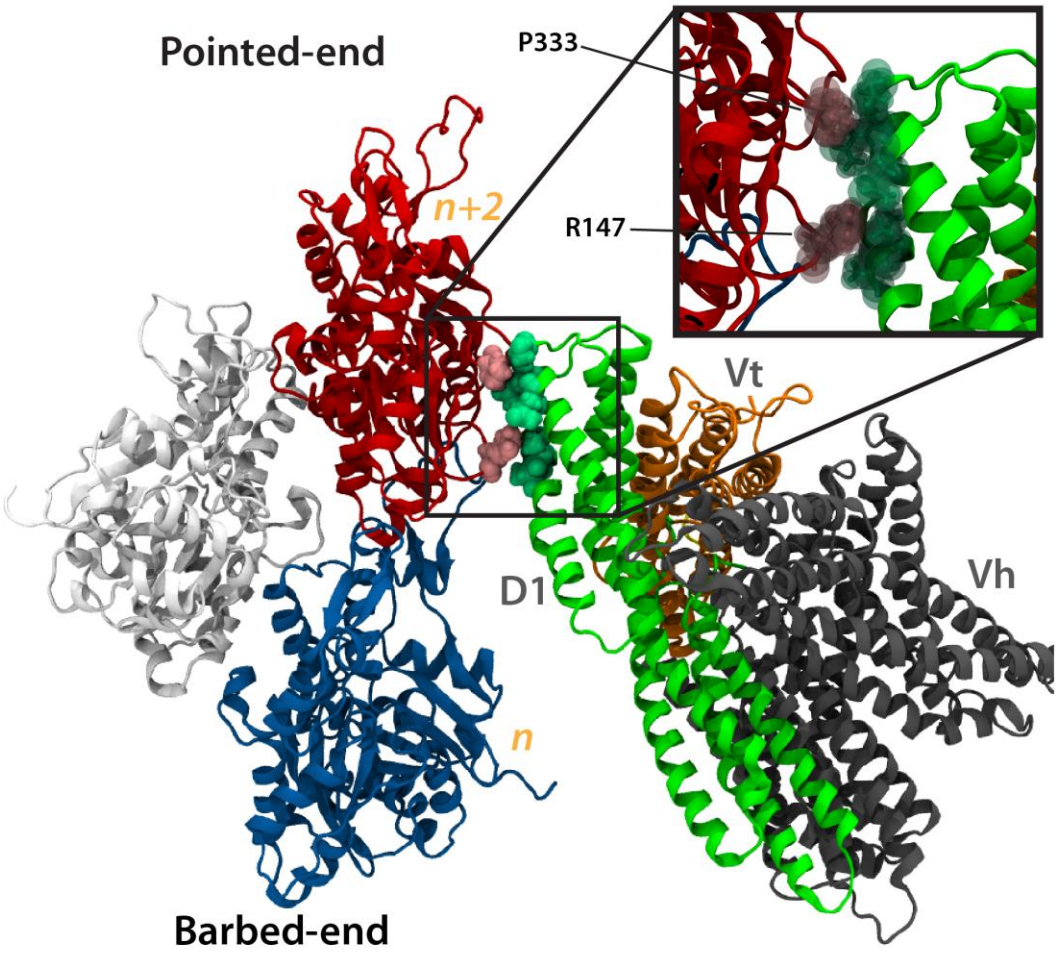

Figure 6

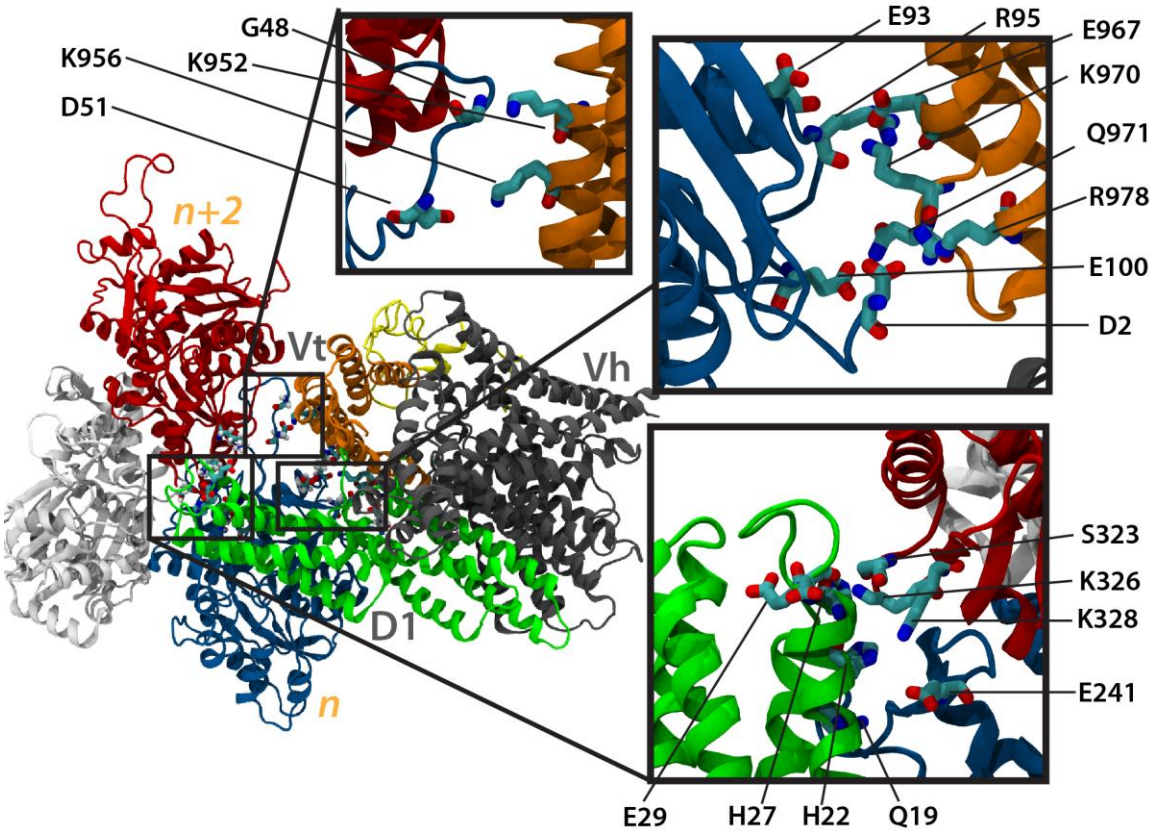
G48
K956
K952
D51
n+2
Vt
Vh
D1
n
E93
R95
E967
K970
Q971
R978
E100
D2
S323
K326
K328
E241
E29
H27
H22
Q19

Figure 7

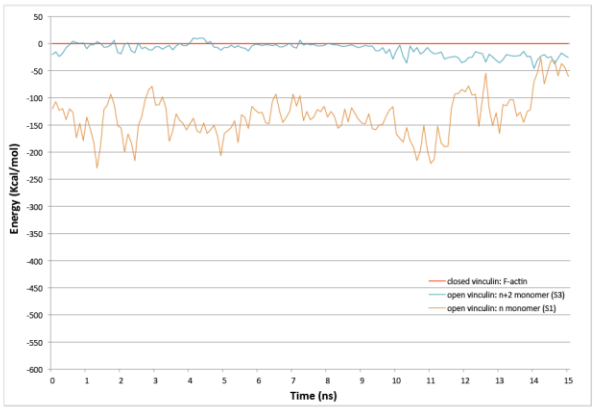
Energy (Kcal/mol)
Time (ns)
closed vinculin: F-actin
open vinculin: n+2 monomer (S3)
open vinculin: n monomer (S1)

Figure 8

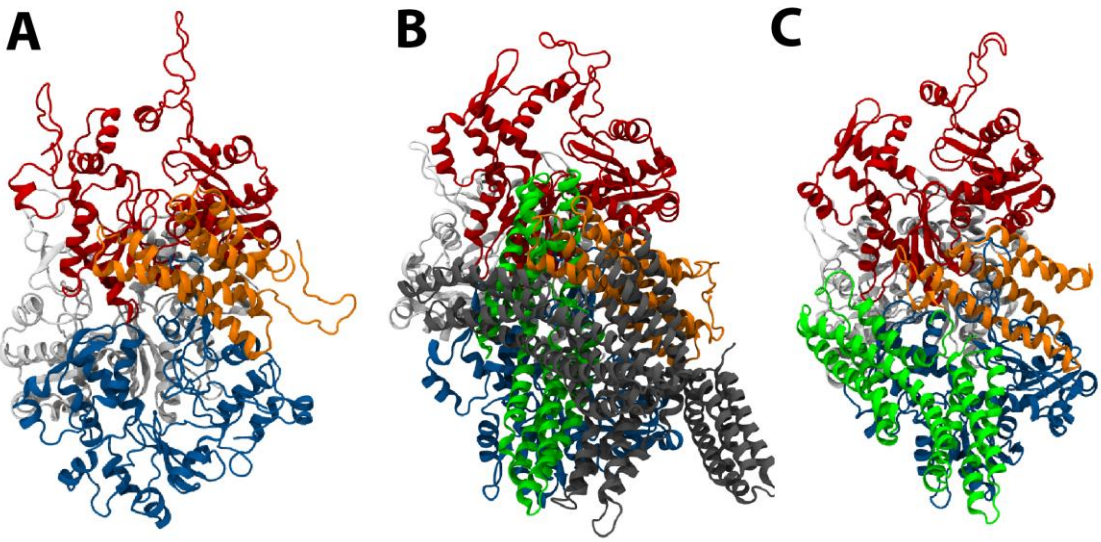

Figure 9

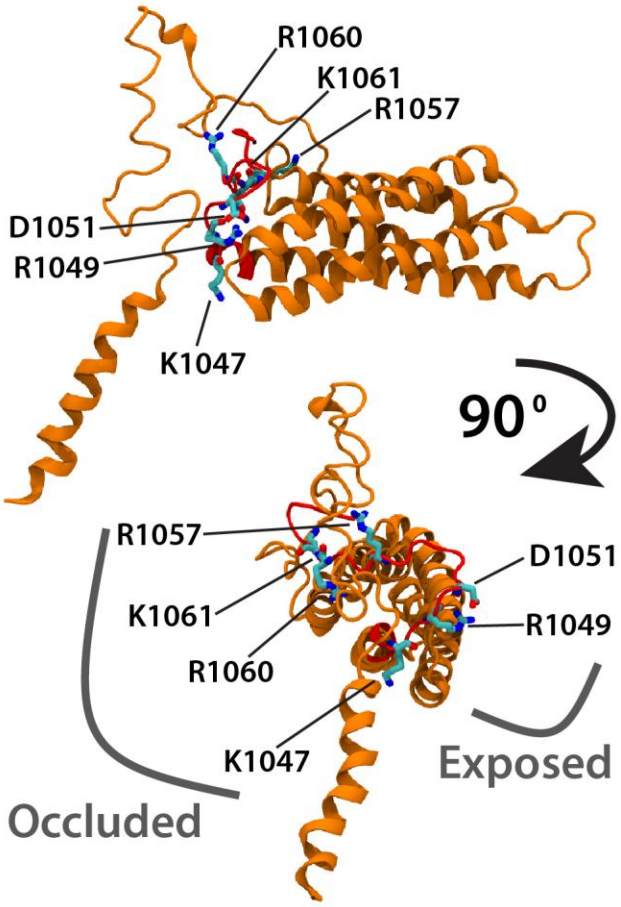
R1060
K1061
R1057
D1051
R1049
K1047
90°
R1057
D1051
K1061
R1049
R1060
K1047
Exposed
Occluded

Figure 10

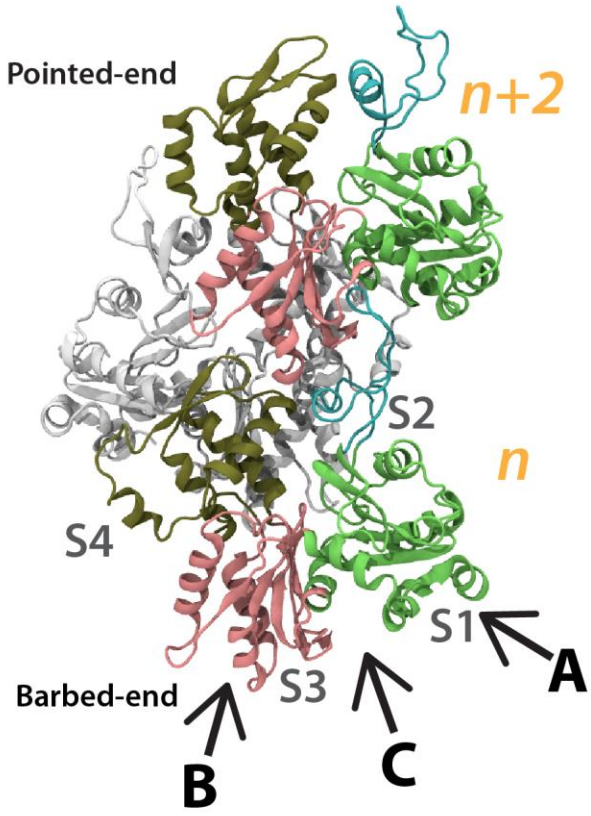

Figure 11

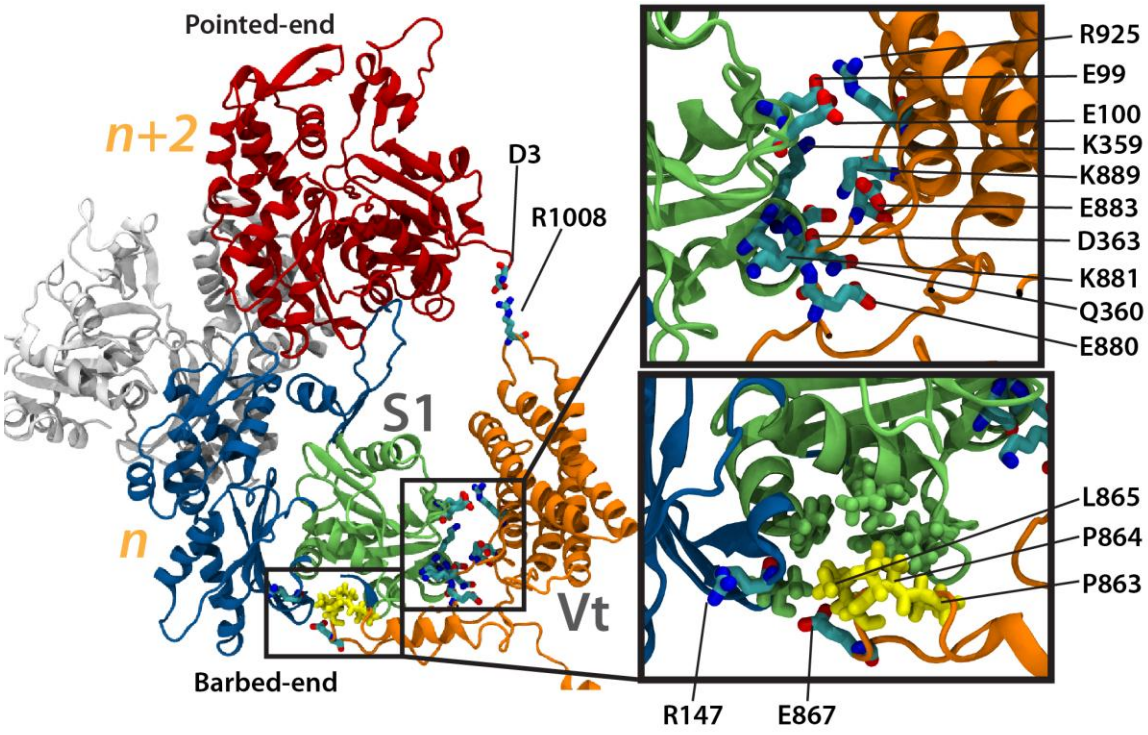
Pointed-end
n+2
D3
R1008
S1
n
Vt
Barbed-end
R925
E99
E100
K359
K889
E883
D363
K881
Q360
E880
L865
P864
P863
R147
E867

Figure 12

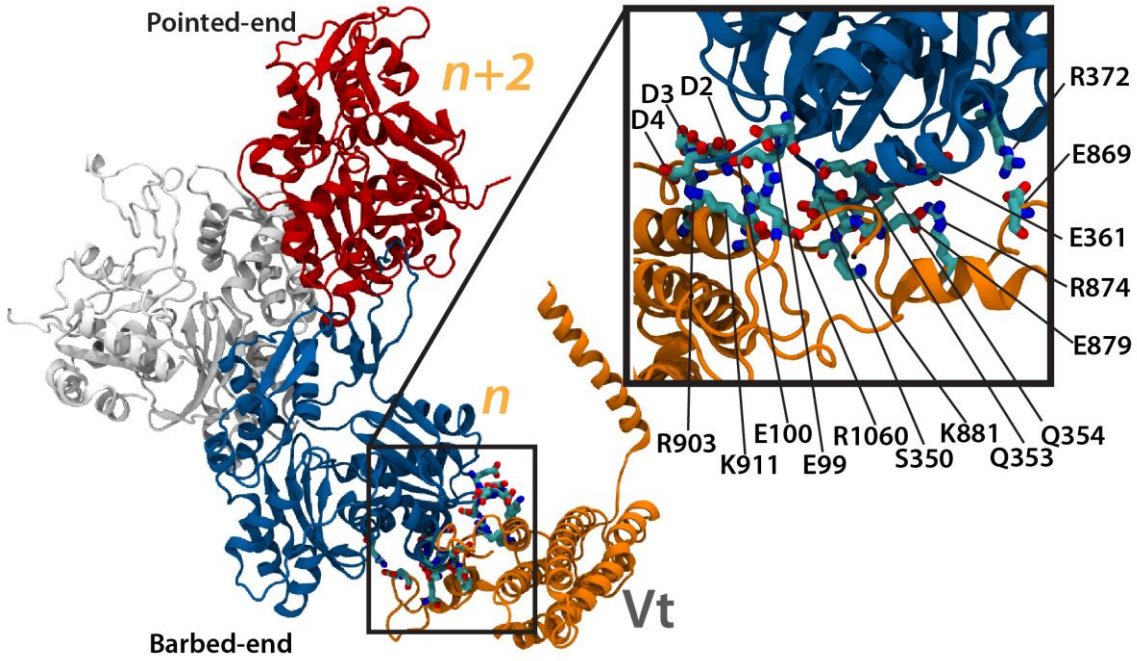
Pointed-end
n+2
n
Barbed-end
Vt
D3
D2
D4
R372
E869
E361
R874
E879
R903
K911
E100
E99
R1060
S350
K881
Q353
Q354

Figure 13

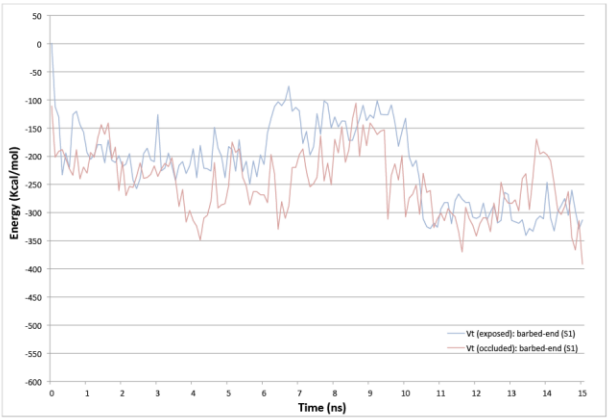
Energy (Kcal/mol)
Time (ns)
Vt (exposed): barbed-end (S1)
Vt (occluded): barbed-end (S1)

Figure 14

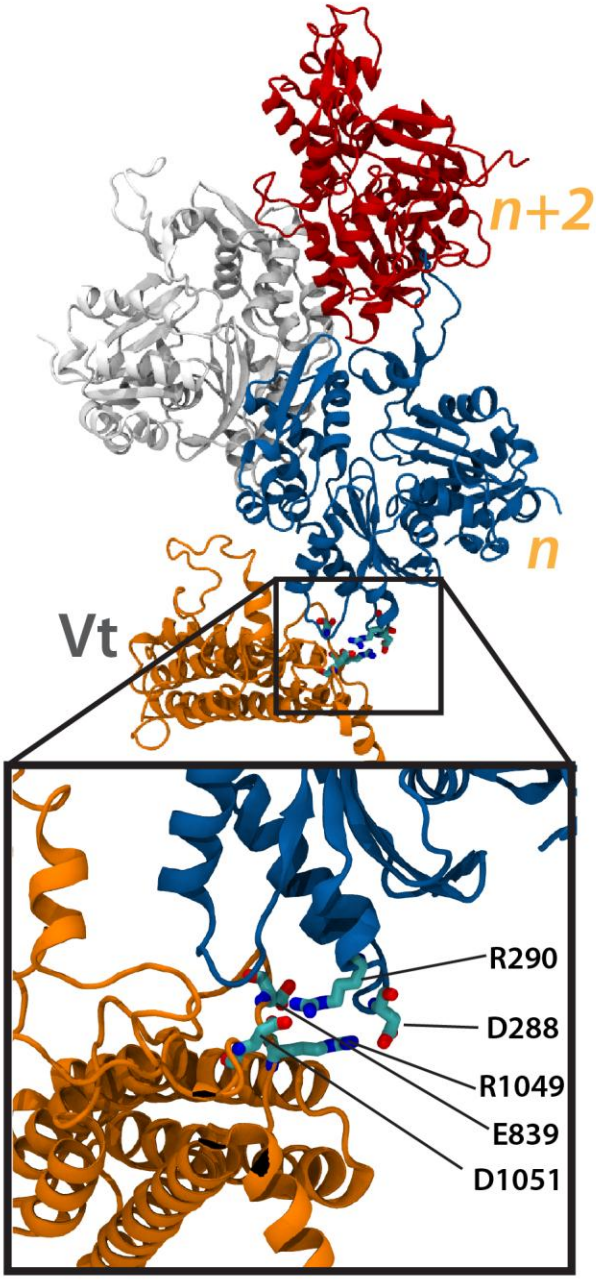

Figure 15

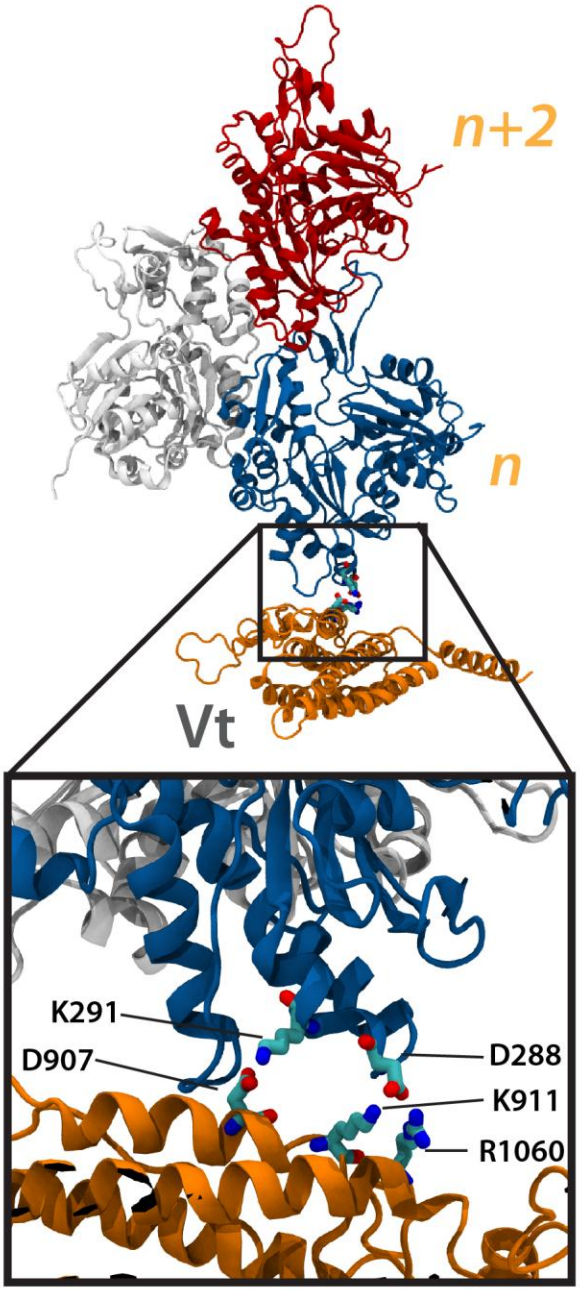

Figure 16

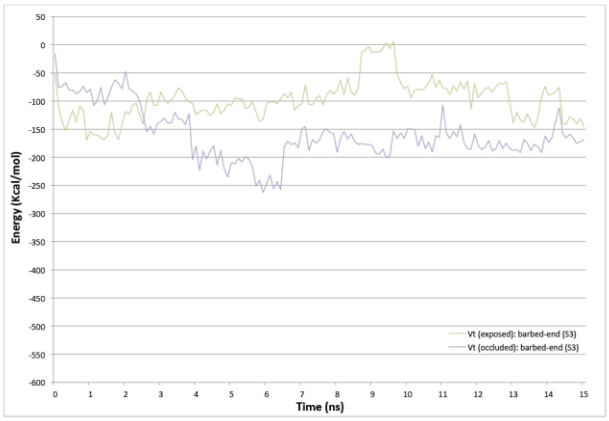
Energy (Kcal/mol)
Time (ns)
Vt (exposed): barbed-end (S3)
Vt (occluded): barbed-end (S3)

Figure 17

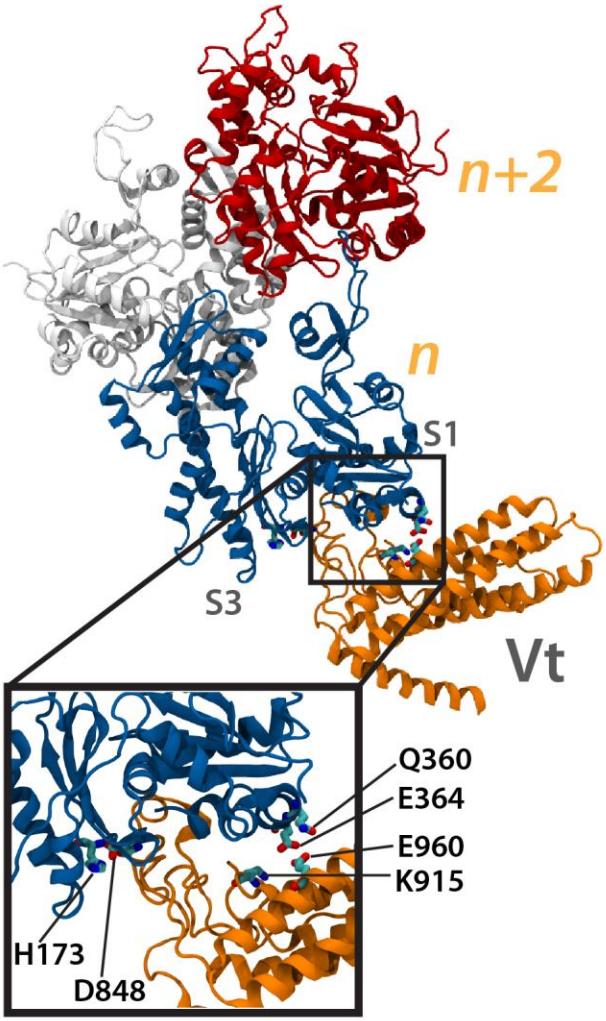

Figure 18

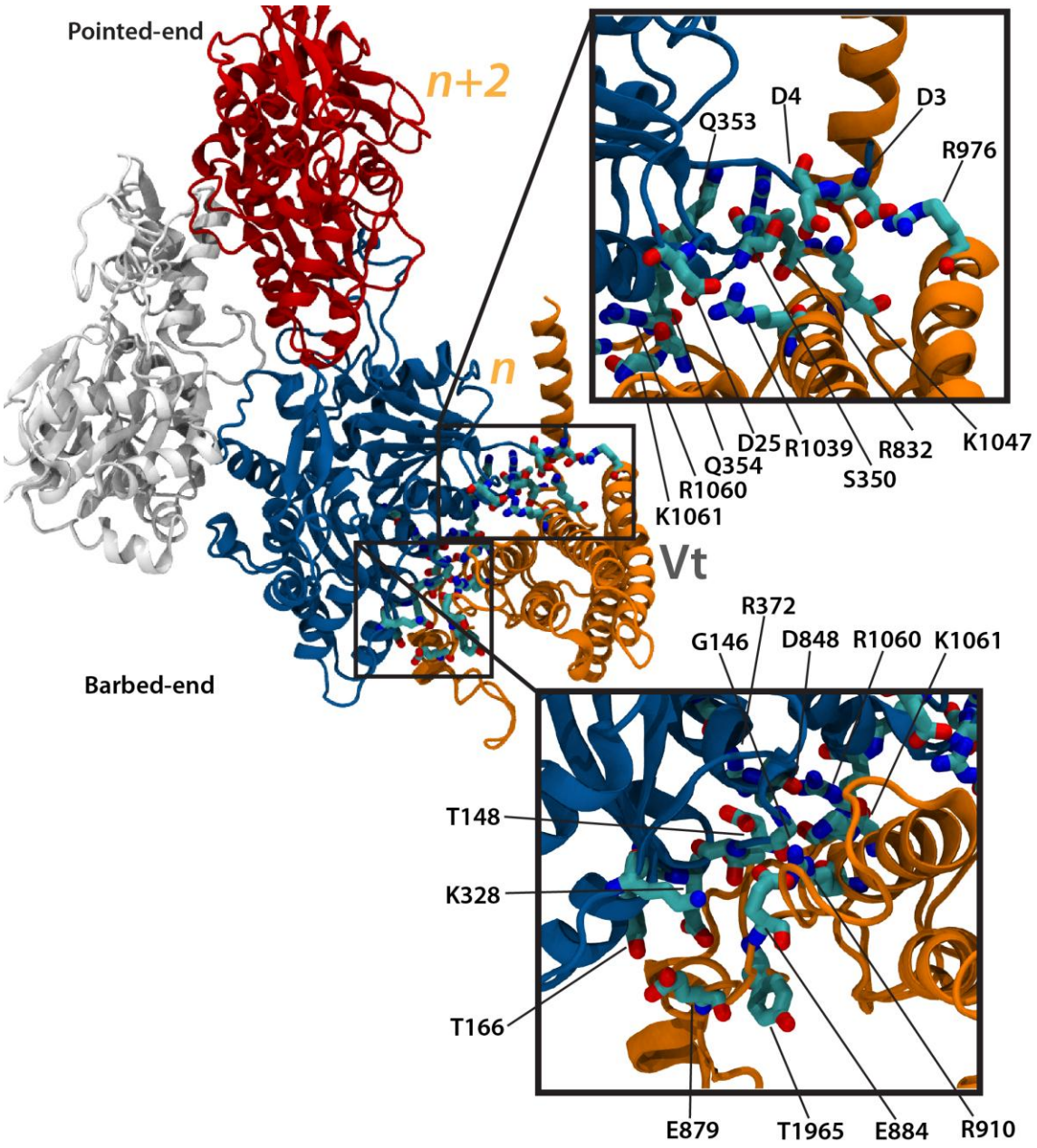
Pointed-end
n+2
n
Barbed-end
Vt
D4
D3
Q353
R976
D25
R1039
R832
K1047
Q354
R1060
S350
K1061
R372
G146
D848
R1060
K1061
T148
K328
T166
E879
T1965
E884
R910

Figure 19

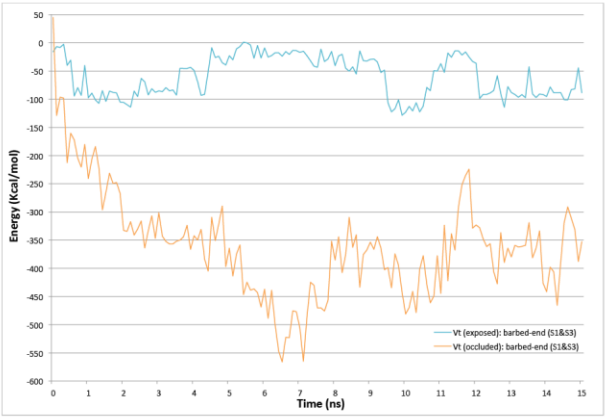
Energy (Kcal/mol)
Time (ns)
Vt (exposed): barbed-end (S1&S3)
Vt (occluded): barbed-end (S1&S3)

Figure 20

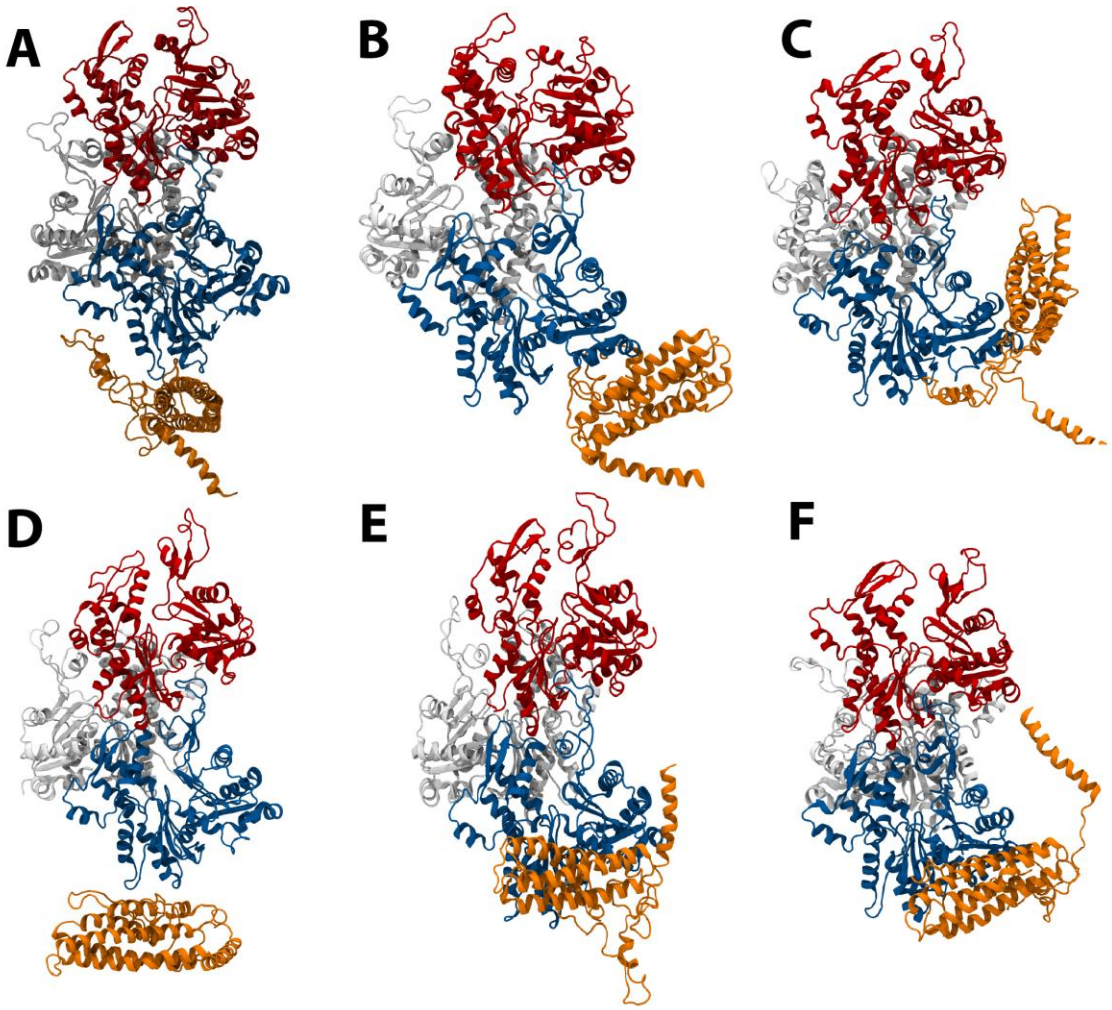

Figure 21

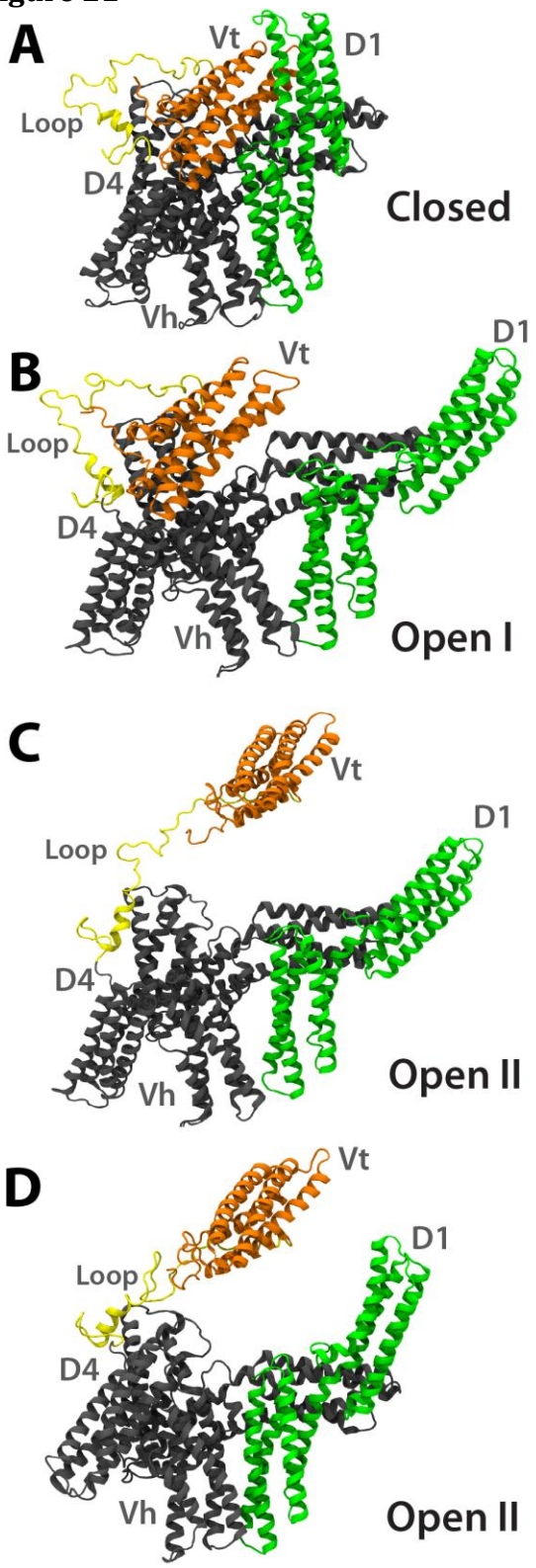
A
Vt
D1
Loop
D4
Closed
Vh
B
D1
Vt
Loop
D4
Vh
Open I
C
Vt
D1
Loop
D4
Vh
Open II
D
Vt
D1
Loop
D4
Vh
Open II

Figure 22

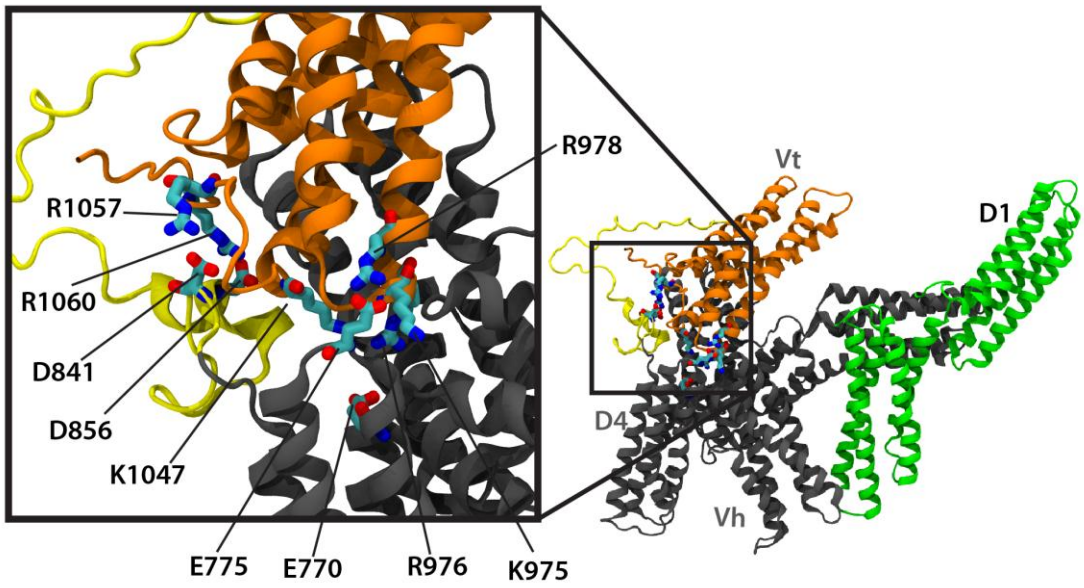
R978
R1057
R1060
D841
D856
K1047
E775
E770
R976
K975
Vt
D1
D4
Vh

Figure 23

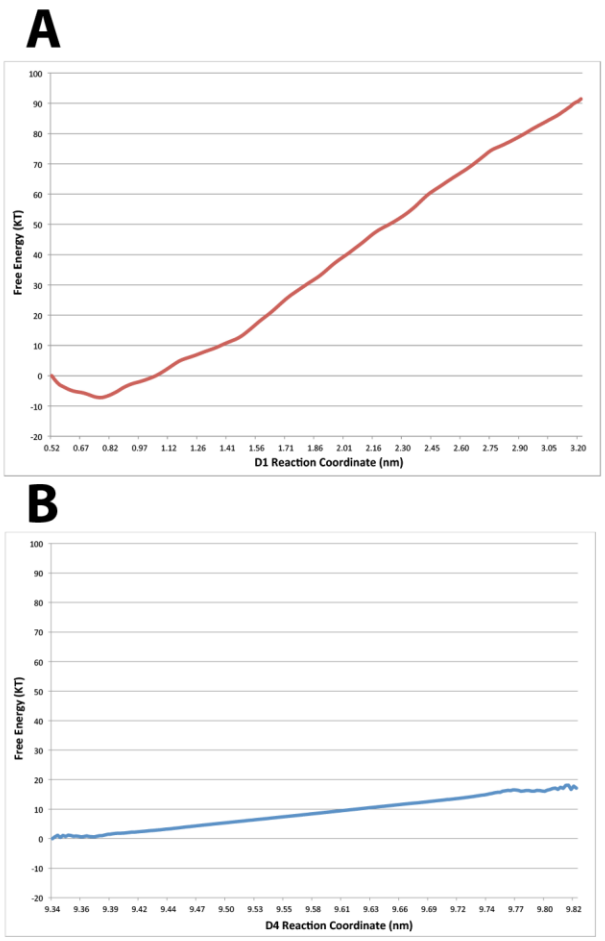
A
Free Energy (KT)
D1 Reaction Coordinate (nm)
B
Free Energy (KT)
D4 Reaction Coordinate (nm)

Figure 24

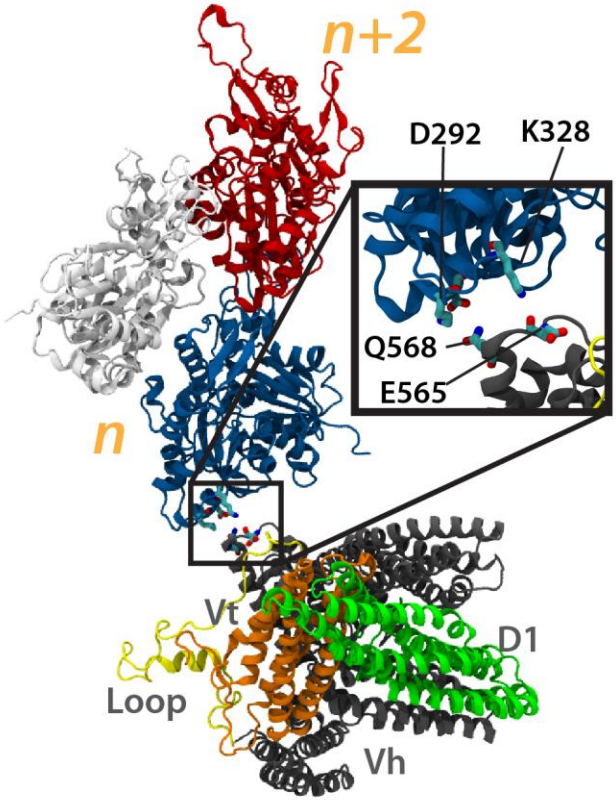

Figure 25

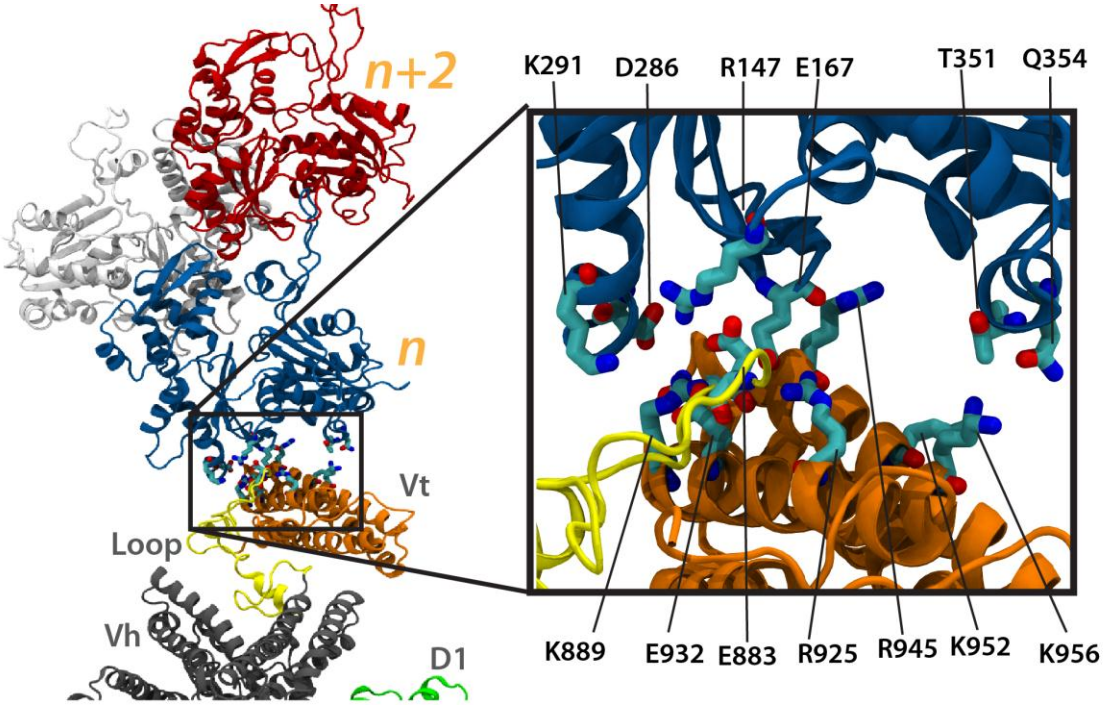
n+2
n
Vt
Loop
Vh
D1
K291
D286
R147
E167
T351
Q354
K889
E932
E883
R925
R945
K952
K956

Figure 26

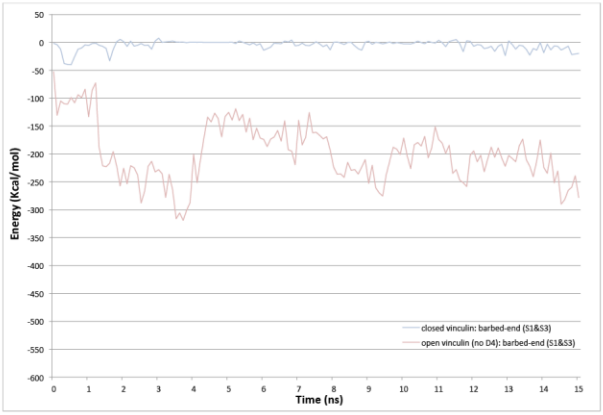
Energy (Kcal/mol)
Time (ns)
closed vinculin: barbed-end (S1&S3)
open vinculin (no D4): barbed-end (S1&S3)

Figure 27

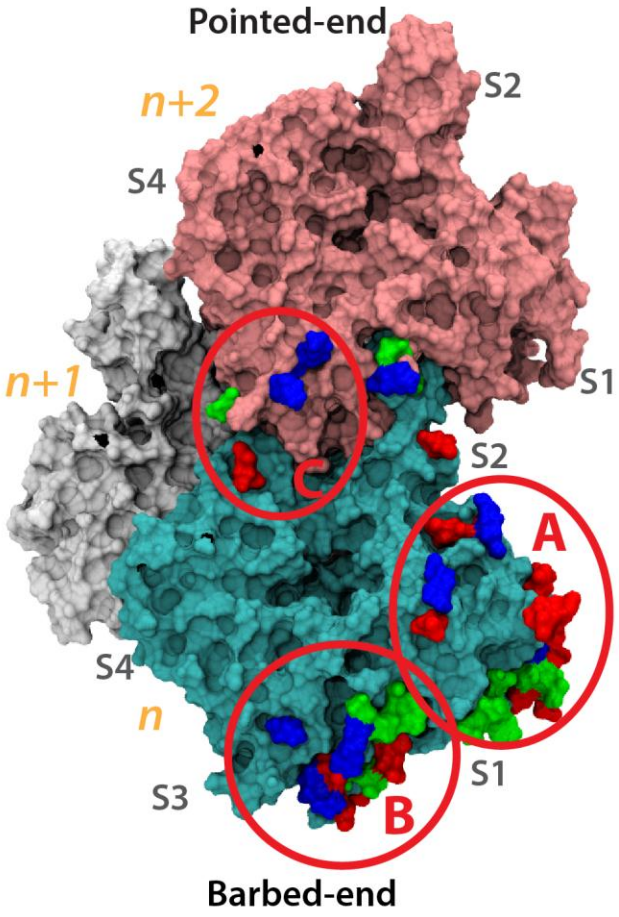

Figure 28

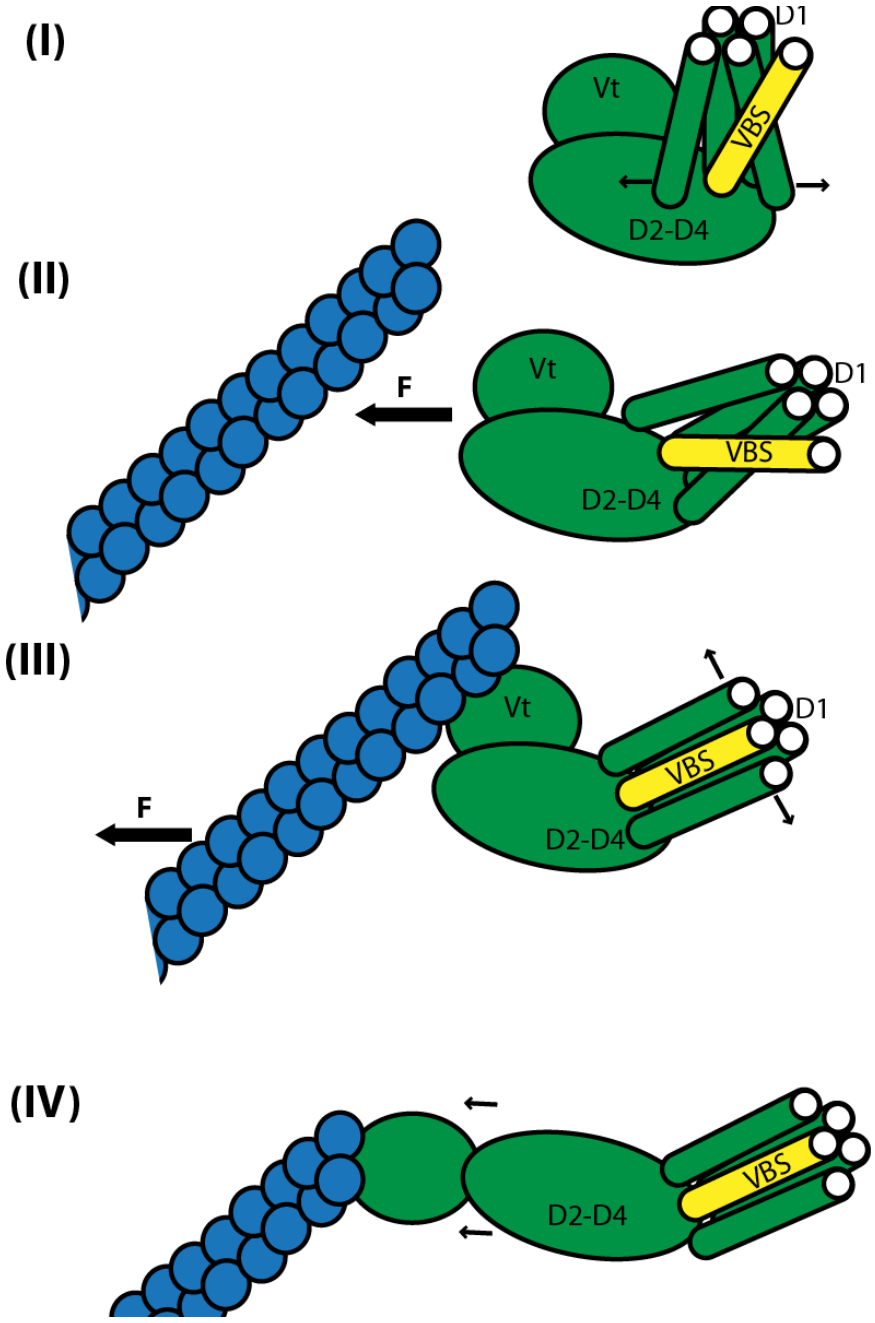
(I)
D1
Vt
VBS
D2-D4
(II)
F
Vt
D1
VBS
D2-D4
(III)
Vt
D1
VBS
F
D2-D4
(IV)
VBS
D2-D4

Conclusion

Summary and Conclusion

This dissertation has addressed the hypothesis that individual proteins at the focal adhesions can exhibit mechanosensing characteristics. The focal adhesion can form in response to an external force (1), it can mitigate the transmission of internal forces to the extra-cellular matrix (2), and it can be a site for mechanotransduction (3) – translating mechanical signals into biochemical signals. The mechanosensing proteins would exhibit force-induced changes in their structure and conformation that would allow the focal adhesion to respond to mechanical stimuli. The basic molecular components of the focal adhesion are talin and vinculin. Together they can link several actin filaments to a single set of integrin proteins. Both can be mechanosensors and together they can lend mechanosensation to the focal adhesion. Using molecular dynamics, the structural and functional characteristics of talin, of vinculin, of the two interacting together, and of vinculin interacting with actin has been explored. The results are interesting and support the notion of molecular mechanosensing. Furthermore, the simulations have revealed new binding sites on F-actin for the focal adhesion protein vinculin, a pathway involving PIP2 and PKC that would ease the growth of the focal adhesion, and a novel mechanism by which the talin dimer could modulate the size of a focal adhesion in response to strain in the ECM.

Talin, the earliest recruit to a growing focal adhesion (4), was shown in Section I to have two characteristic modes of mechanosensing: force-induced movement of its cryptic vinculin-binding sites (VBS) out of the rod domain, and force-induced reorientation of its dimer conformation. The force-induced activation of VBS was a topic of previous investigation (5). Recent experimental evidence solidified the likelihood of the first mechanosensing mode (6). Simulation of the C-terminus region of talin in a dimer conformation established (i) that the linker between the dimerization domain and the nearby actin-binding helical bundle lends significant flexibility to the C-terminus region, and (ii) this flexibility allows for the dimer to adopt different orientations depending on the level and nature of mechanical force it is exposed to. Two scenarios can be described in which talin mechanosensing can play a role in expanding the focal adhesion. In the first scenario, a talin is detached from the actin-filaments and only crosslinking integrins. No focal contact is established, however, the initial stage of the contact – activation of integrin and binding of talin to integrin (7) – has completed. Here, the second mode of talin mechanosensing would allow a talin dimer to respond to changes in the ECM by reorienting the dimer (Figure 1 A). Adoption of an elongated conformation would increase the likelihood of a link between the ECM and actin filaments. In the second scenario, once the focal contact is established and the actin filament is bound to talin at the actin-binding domain, a contraction of the actin filaments would drive separation of the multiple VBS domains from the hydrophobic core of the rod domain (Figure 1 B). This mechanosensing mode would allow talin to respond to mechanical stimulation from the actin filament by increasing the likelihood of

recruitment of further cytoskeletal links via vinculin binding to VBS. The more actin filaments become linked to the focal adhesion the stronger the contact.

Talin mechanosensing in both scenarios will modulate the focal adhesion mechanoresponse via the vinculin-actin interface. Two remaining steps in establishing the link to further actin filaments via vinculin are the activation of vinculin itself, and the interaction of the activated vinculin with its binding partners. In Section II the activation of vinculin was explored and in Section III the interaction of activated vinculin with its binding partners was further explored. In Section II, first, molecular dynamics predicted a trajectory to vinculin activation that would involve separation of domain 1 (D1) from the vinculin tail (Vt). It was predicted that this conformational change would allow Vt to interact with the actin filament without steric limitations imposed by the proximity of D1 to Vt. A movement of D1 was deemed easier than complete disassociation of Vt form all four vinculin head domains. The conformational change and activation of vinculin would require not only interaction of VBS with domain 1, but also a transient interaction of actin with Vt and/or exposure of the closed vinculin conformation to a stretching force – potential imposed by the movement of actin filaments across a focal complex – that would drive the separation of D1 from Vt (Figure 1 DE). A clear activation energy would be needed to cause the predicted conformational change.

Following establishment of the trajectory to vinculin activation, two alternative paths to activation were explored: activation by means of an interaction with PIP2 and activation by means of phosphorylation by a protein kinase. To investigate the interaction between PIP2 and vinculin and its likely impact on vinculin activation several simulations were carried out capturing the mechanisms of PIP2 binding to various regions on the vinculin tail and also on other vinculin head residues. These simulations established that PIP2 is likely acting as a vinculin recruiting agent driving the accumulation of vinculin in the membrane proximal region by exhibiting strong stickiness for any basic residues on the vinculin surface (of which there are plenty). It is suggested that PIP2 binding in itself is not likely to activate vinculin alone, but could contribute to vinculin activation by increasing the likelihood of an activation event occurring. One possibility is that the recruitment of vinculin by PIP2 coincides with the recruitment of PKC and other protein kinases by PIP2, and the two events make a phosphorylation of vinculin highly likely (Figure 1 C). Therefore, we explored the impact of a potential phosphorylation on the vinculin structure and the vinculin activation trajectory. Simulation of four phosphorylation events predicted that one particular phosphorylation event, at residue S1033, would reduce the energy barrier to vinculin activation. Comparison of the activation trajectory and the forces needed to achieve that trajectory *in silico* confirmed the prediction. Phosphorylation of vinculin at S1033 likely primes vinculin for activation. It is unclear if recruitment via PIP2 and phosphorylation of vinculin is necessary in all vinculin activation events. It is likely there are two pathways to vinculin activation: (1) a conformational change is induced in vinculin either by a mechanical stimulation (as in our simulations) or by some other cooperative binding mechanism, and (2) vinculin is first primed for activation by PIP2

recruitment and subsequent phosphorylation then a conformational change is induced in vinculin. The difference between the two pathways lies in the input energy needed to achieve vinculin activation. In (1) there is no prior priming, whereas in (2) the priming has made the likelihood of vinculin activation increased. The priming of vinculin allows for more activated vinculin with any given mechanical stimulation. The trajectory of vinculin activation is modulated by the mechanical environment and can describe a mode of vinculin mechanosensing.

The final step in the formation of the basic focal complex is the interaction of vinculin with its binding partners. In the first part of Section III the interaction of vinculin with talin VBS is explored. Here it was shown that the activation of vinculin via movement of D1 away form Vt would not only likely modulate the ability of Vt to interact with F-actin, but it also modulates the strength of the link between talin and D1. Prior to activation talin VBS was shown to partially insert into D1 but was unable to fully insert due to the proximity of Vt to D1. Following activation of vinculin the VBS was able to achieve full insertion into D1 and complete the link between talin and vinculin. The existence of two stages of the link between vinculin and talin allows for the interaction itself to act as a switch at the focal adhesion. In the absence of a mechanical load a more transient and less complete link is formed between vinculin and talin whereas in the present of a mechanical load talin completely inserts itself into D1 and the link is solidified.

In the second part of Section III the interaction between vinculin and F-actin is explored. Interestingly, vinculin is shown not only to bind along the actin filament, as repeatedly predicted previously (8-10), but it was also shown to very likely bind the capping end of the acting filament. The predicted trajectory of vinculin activation from Section II was evaluated and it was confirmed that movement of D1 away from Vt is necessary and sufficient to allow linkage between F-actin and Vt. The closed conformation failed to bind both the side of F-actin and the barbed-end of F-actin. For capping of the actin filament, it was demonstrated that after a second conformational change and formation of an open II conformation, vinculin is able to link strongly to the barbed-end of F-actin. Although it has been previously suggested that the linking of vinculin the barbed-end could play a role in IpaA depolymerization of a cell's actin filaments (11), it is unclear if F-actin capping plays a role at the focal adhesion. What is clear from the results presented in this dissertation is that the interaction between vinculin and the barbed-end of F-actin represents another mechanoresponsive switch at the focal adhesion. Vinculin conformational switch to the open I conformation – movement of D1 away from Vt – is one mechanoresponsive switch that would solidify the link between vinculin and talin, and allow a link between vinculin and actin. The second conformational change to the open II conformation – complete dissociation of Vt form all four vinculin head domains – would allow for the link between vinculin and F-actin to become further reinforced by introducing an additional vinculin-binding site of F-actin (Figure 1 F). The presence of multiple binding sites, and the regulation of the binding site by mechanical load is itself a method of mechanosensing. Vinculin can be described as acting as a clutch-like contact between F-actin and the focal

adhesion. It is a variable switch whose level of linkage to F-actin reflects the level of tension in the its environment.

These underlying events and molecular mechanisms at the focal adhesion can capture the force-induced behavior seen at the focal adhesion. The presence of a mechanical stimulation from outside the cell will first cause reorientation of the talin dimer, then contribute to activation of vinculin and linkage of actin filaments to talin-vinculin and formation of a focal adhesion. The presence of a mechanical stimulation from inside the cell, potentially from actin filament movement, could cause stretching of the talin rod domain and activation of its VBS regions. Subsequent activation of vinculin and linkage of the activated vinculin to F-actin could cause the formation of focal contacts. And after formation of a contact the exposure of this focal contact to further F-actin movement or stress could cause a second vinculin conformational change that would further reinforce the link and strengthen the focal adhesion. Talin is predicted from these simulations to be critical to the initial formation of focal adhesions – a prediction supported by experimental evidence (12)– and vinculin is predicted from our simulations to be critical to the mechanical reinforcement of focal adhesions – also a prediction supported by experimental evidence (13).

Understanding the mechanisms by which focal adhesion form and can be regulated by mechanical stimulation can be critical to efforts aimed at understanding cell movement (14), cancer cell metastasis (15), stem cell differentiation (16), and endothelial cell function (17). To continue towards that end and build on the work presented here a number of suggestions are made for future investigators to consider: (1) the simulations of talin dimer reorientation presented here consider the reorientation at the C-terminus region of the talin rod only, it would be telling to see how the other regions of the talin rod and also the talin head domain would react to a similar mechanical load and if the dimer reorientation is consistent with behavior at those regions; (2) the trajectory considered here for vinculin activation is one possible trajectory, future studies should consider other possible trajectories and also evaluate the free energy differences between these trajectories; (3) PIP2 has behaved as an agent recruiting the vinculin molecules to the membrane proximal regions, it is possible PIP2 is recruiting other focal adhesion forming molecules as well, and the interaction of PIP2 with these other focal adhesion components should be considered; (4) only 1 of the possible vinculin phosphorylation events was shown to prime vinculin for activation, perhaps the other phosphorylation events impact the likelihood of an interaction between vinculin and a binding partner and this possibility should be further explored; (5) the linkage between activated vinculin and VBS was simulated as well as the linkage between activated vinculin and F-actin, and both were shown to be possible, however, it is not entirely clear that a three-molecule complex between talin, vinculin, and F-actin could form without further steric limitations imposed by the proximity of talin to F-actin and evaluation of these potential limitations could prove to be very interesting, (6) multiple vinculin-binding sites on F-actin are predicted, but it is unclear which is more favorable without evaluation of the free

energy to binding at each site and thus a free energy comparison between the three binding sites is called for; (7) it is predicted from the simulations presented here that vinculin can bind the barbed-end of the actin filaments following formation of the open II conformation and the role of this interaction in potentially capping actin polymerization near focal adhesions should be considered.

The results that have been arrived at thus far are proving valuable to the understanding of focal adhesions, and the results from any of these follow-up investigations should also prove to be noted contributions. The impact of molecular dynamics is steadily increasing, due in large part to improvements to computational methods and resources. As a prediction of *in silico* biological research this author asserts that the use of computational tools in biological research will continue to expand and its impact will continue to accelerate. Similarly, the impact of mechanical phenomena on biological processes will likely continue to be understood and emphasized. If the work presented in this dissertation is of interest and has impacted the understanding of focal adhesions, then future studies are sure to be even more highly impactful.

References

1. Galbraith, C. G., K. M. Yamada, and M. P. Sheetz. 2002. The relationship between force and focal complex development. J Cell Biol 159:695-705.
2. Parsons, J. T., A. R. Horwitz, and M. A. Schwartz. 2010. Cell adhesion: integrating cytoskeletal dynamics and cellular tension. Nat Rev Mol Cell Biol 11:633-643.
3. Geiger, B., J. P. Spatz, and A. D. Bershadsky. 2009. Environmental sensing through focal adhesions. Nat Rev Mol Cell Biol 10:21-33.
4. Critchley, D. R., and A. R. Gingras. 2008. Talin at a glance. J Cell Sci 121:1345-1347.
5. Lee, S. E., R. D. Kamm, and M. R. Mofrad. 2007. Force-induced activation of talin and its possible role in focal adhesion mechanotransduction. Journal of biomechanics 40:2096-2106.
6. del Rio, A., R. Perez-Jimenez, R. Liu, P. Roca-Cusachs, J. M. Fernandez, and M. P. Sheetz. 2009. Stretching Single Talin Rod Molecules Activates Vinculin Binding. Science 323:638.
7. Shattil, S. J., C. Kim, and M. H. Ginsberg. 2010. The final steps of integrin activation: the end game. Nat Rev Mol Cell Biol 11:288-300.
8. Carisey, A., and C. Ballestrem. 2010. Vinculin, an adapter protein in control of cell adhesion signalling. European Journal of Cell Biology.
9. Humphries, J. D., P. Wang, C. Streuli, B. Geiger, M. J. Humphries, and C. Ballestrem. 2007. Vinculin controls focal adhesion formation by direct interactions with talin and actin. J Cell Biol 179:1043-1057.
10. Ziegler, W. H., R. C. Liddington, and D. R. Critchley. 2006. The structure and regulation of vinculin. Trends in Cell Biology 16:453-460.
11. Ramarao, N., C. Le Clainche, T. Izard, R. Bourdet-Sicard, E. Ageron, P. J. Sansonetti, M.-F. Carlier, and G. Tran Van Nhieu. 2007. Capping of actin

filaments by vinculin activated by the Shigella IpaA carboxyl-terminal domain. FEBS Lett 581:853-857.
12. Jiang, G., G. Giannone, D. R. Critchley, E. Fukumoto, and M. P. Sheetz. 2003. Two-piconewton slip bond between fibronectin and the cytoskeleton depends on talin. Nature 424:334-337.
13. Grashoff, C., B. D. Hoffman, M. D. Brenner, R. Zhou, M. Parsons, M. T. Yang, M. A. McLean, S. G. Sligar, C. S. Chen, T. Ha, and M. A. Schwartz. 2010. Measuring mechanical tension across vinculin reveals regulation of focal adhesion dynamics. Nature 466:263-266.
14. Gardel, M. L., I. C. Schneider, Y. Aratyn-Schaus, and C. M. Waterman. 2010. Mechanical integration of actin and adhesion dynamics in cell migration. Annu Rev Cell Dev Biol 26:315-333.
15. Brooks, S. A., H. J. Lomax-Browne, T. M. Carter, C. E. Kinch, and D. M. Hall. 2010. Molecular interactions in cancer cell metastasis. Acta Histochem 112:3-25.
16. Discher, D. E., D. J. Mooney, and P. W. Zandstra. 2009. Growth factors, matrices, and forces combine and control stem cells. Science 324:1673-1677.
17. Ngu, H., Y. Feng, L. Lu, S. J. Oswald, G. D. Longmore, and F. C. Yin. 2010. Effect of focal adhesion proteins on endothelial cell adhesion, motility and orientation response to cyclic strain. Annals of biomedical engineering 38:208-222.

Figures

Figure 1. The mechanoresponse of the focal adhesion can be explained by the mechanosensing of individual protein components of the focal adhesions. Shown here is a schematic capturing the possible mechanosensing events during focal adhesion formation. (A) A talin dimer that is crosslinking to integrins can respond to forces from the ECM that drive integrin separation by reorienting its dimer conformation. This allows for building of a focal adhesion on the elongated scaffold. (B) The stretch of an individual talin rod domain can be induced by forces originating from movement or contraction of an attached actin filament. This stretch would lead to exposure of the vinculin-binding site (VBS) in the rod domain. (C) The interaction of PIP2 with vinculin serves to recruit vinculin to the membrane proximal regions of the cell. This can also coincide with the recruitment of protein kinases to the membrane and can allow for vinculin phosphorylation. The vinculin phosphorylation can impact vinculin activation. (D) Once VBS is activated vinculin can link to VBS. Two possibilities exist, (i) vinculin will can link to VBS before phosphorylation, or (ii) vinculin is first phosphorylated then it links to VBS. Phosphorylation of vinculin primes it for activation. (E) The cooperation of vinculin partially linked to talin an the stimulation of vinculin by a nearby actin filament could lead to formation of the open I vinculin conformation that can then fully link to talin and bind the actin filament. (F) Additional stretching forces from the actin filament can induce further conformational changes to vinculin and it can adopt a open II conformation With the open II conformation vinculin can reinforce moving actin filaments and potentially bind the barbed-end of F-actin. Through these steps the individual force induced structural changes in talin and vinculin allow for focal adhesion to be respond to their mechanical environment.

Figure 1

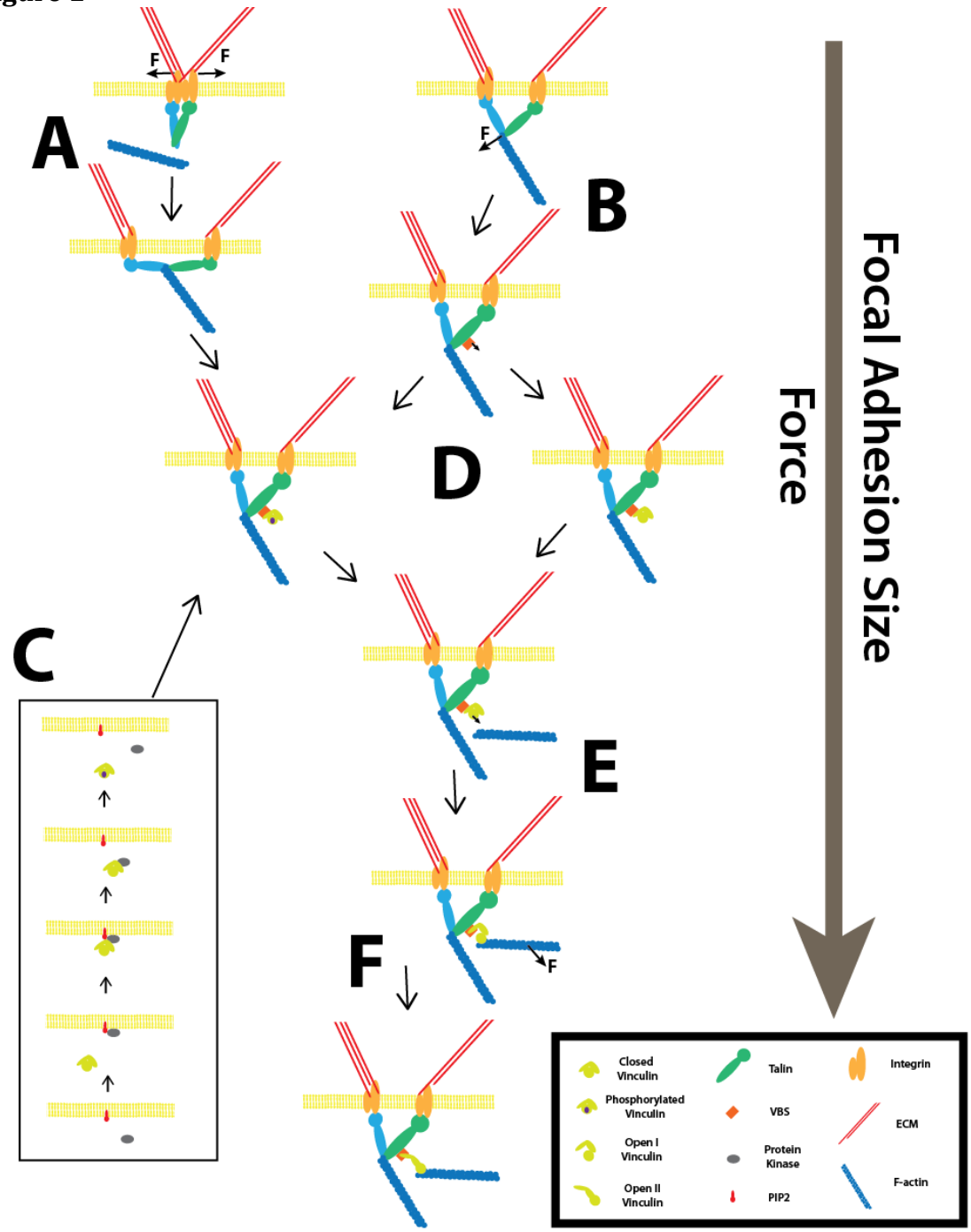
A
B
C
D
E
F
F
F
F
Force
Focal Adhesion Size
Closed Vinculin
Phosphorylated Vinculin
Open I Vinculin
Open II Vinculin
Talin
VBS
Protein Kinase
PIP2
Integrin
ECM
F-actin